

EVALUATION OF SEAT PERFORMANCE CRITERIA FOR REAR-END IMPACT TESTING

Johan Davidsson

Chalmers University of Technology
Sweden

Anders Kullgren

Folksam Research and Chalmers University of Technology
Sweden

Paper Number 11-0373

ABSTRACT

The BioRID II has been recommended to be used in future legislative dynamic rear-end impact seat performance tests. Recommended injury criteria and assessment reference values to be used with the dummy is however still pending. This is mainly due to the incomplete understanding of the injury site and mechanisms responsible for the symptoms presented after such impacts. This lack of biomechanical data limits the possibility to evaluate any proposed injury criteria and associated reference values.

The aim with this study is to address these limitations by comparing crash test dummy parameter values from performed sled tests with real-life accident data. The results are expected to indicate the injury predictability of the complete sled test method, which includes performance criteria, the use of generic sled acceleration pulse, the use of the BioRID II and its current positioning procedure, etc.

Real-life injury risk was calculated for groups with similar seat designs from data provided by Folksam. By introducing grouped data, i.e. by dividing applicable data into groups with similar characteristics, the reliability of the insurance data increased while the dummy measurements remained constant. Two different injury risks were used in this study; those that had documented symptoms for more than 1 month and those that were classified as a permanent impairment as the consequence of a rear-end impact. The injury risks for the groups were compared to single crash test dummy parameter values from sled tests performed with a BioRID II in 16 kph *medium* Euro-NCAP pulse. In the comparison, 12 seat groups were compared with 6665 insurance cases (range from 94 to 1575 cases/group). Regression coefficients (R^2) were calculated.

The analysis of groups with similar seat design provided the most reliable results. The analysis showed that NIC, upper neck shear force, vertical head acceleration and lower neck bending moment were the parameters that best predicted the risk of developing permanent impairment given that the occupant had initial symptoms following a rear-end

impact. Similarly, NIC, vertical head acceleration and lower neck moment were parameters that best predicted the risk of short term (> 1 month) symptoms. These results are supported by recent studies.

INTRODUCTION

A number of studies have compared rear-end crash test results with real life performance in the past with the main target to either recommend new or evaluate existing test methods used to assess risk of symptoms following a rear-end impact. The main focus in many of these studies has been on the preferred choice of criteria. The choice of dummy, handling and instrumentation of the dummy, crash pulse used and so forth has a large effect of the outcome of such study and needs to be taken into account.

One of the first studies to combine dummy and real life data was that by Heitplatz et al. (2003). The study found that lower neck moment recorded in crash test with dummies with rigid or semi flexible spines such as the Hybrid III and RID 2, respectively, in OEM seats correlated with insurance claims data for these seats (data from Gesamtverband der Deutschen Versicherungswirtschaft, also referred to as GDV). The study approach adopted introduces some limitations on the generalization of their results, only three seat models, although these were seats with good, average and poor performance, were included for which the number of crashes per seat model were 79, 152 and 96 respectively. This reduces the generalization of the results to be valid for other types of seats than those tested. In case a normal distributed is adopted the statistical significance of the results can be estimated. It then appears that there was no significant difference (on 95% level) in injury risk, for any duration, between the seats included in the study.

Using whiplash insurance injury claims data from two cars only, the *Saab 900* and *Saab 9-3*, along with corresponding rear-end impact sled tests Kuppa (2004) developed an injury risk curve based on head-to-torso-rotation of the Hybrid III dummy. The author conducted a logistic regression, using only the two

data sets of head-to-torso rotation and insurance injury claims, to establish the injury risk curve. Kuppaa also suggested, based on data by Voo et al. (2003) that for the Hybrid III the peak head-to-torso rotations highly correlate to peak lower neck moments, which earlier have been suggested to correlate to injury risk in rear end impacts (Prasad et al. 1997). Despite incomplete control for vehicle acceleration, and the fact that only data for two seat models were included in the study by Kuppaa in 2004, Kuppaa et al. (2005) used the results to suggest a whiplash injury criterion along with dynamic test with the Hybrid III dummy. The Hybrid III dummy head rotation angle criterion later became the main criterion for the dynamic test option in the current GTR-7.

The injury reducing effect of the *WHIPS* seat, which are seats installed in *Volvo* cars from 1998, on real-life performance have been shown to be significant for both initial and long term symptoms (Farmer et al. 2003, Jakobsson and Norin 2005, Kullgren and Krafft 2010). The former study showed that the short and long term symptoms were reduced in the *WHIPS* seat by 33% and 53%, respectively, compared to a traditional *Volvo* seat. Andersson and Boström (2006) presented results from rear-end impact tests using these two versions of the *Volvo* seats and a Hybrid III dummy. They found very small difference in peak head-to-torso rotation and that none of the seats had acceptable performance according to the dynamic injury criteria suggested by Kuppaa et al. (2005). Those findings were in contradiction to the studies on injury reduction and suggest that the dynamic test procedure suggested by Kuppaa et al. 2005 may not adequately assess risk of symptoms in rear end impacts.

Linder et al. (2004) reconstructed 25 rear-end impacts with known 1 month duration of neck injury symptoms. In the reconstructions the BioRID II was placed in the same type of seat as in the impacted vehicle and the vehicle accelerations were reproduced. The results from the study provided a link between real-world neck injury symptoms and average dummy readings and provided indications of thresholds for a 10% risk of neck injury symptoms persisting for more than 1 month. The parameters suggested to be studied further were:

- The Neck injury Criterion (NIC, Boström et al., 1996) that takes the horizontal relative acceleration and velocity between the head and the neck into account.

- Neck Injury Criteria (N_{km} , Schmitt et al., 2002) that takes the combination of shear forces and flexion/extension moments at the upper region of the neck into consideration.
- Maximum upper neck forces.
- Maximum horizontal T1 acceleration.

Cappon et al. (2005) correlated crash test parameters using the RID3D and the BioRID II dummies with German accident statistics. Only squared correlation coefficients of the linear relation between dummy measurements and acute injury risk was used. In one of the two parts of this study, injury risk for each vehicle model was estimated using insurance data in combination with the number of vehicles in the region for the particular model. The approach used gave a crude estimate of real life risk. The dummy parameters included in the study were NIC, N_{km} , Neck injury Criteria (N_{ij}), Lower Neck Load Criteria (LNL), upper neck shear and compression/tension forces, lower neck shear forces and bending moment, and average x-acceleration of the lower neck-thorax junction and the sled. The study found an acceptable correlation of the lower neck shear force measured in a RID^{3D} with their accident data. The study also found a reasonable correlation between NIC as measured in the BioRID and real life risk.

Kullgren et al. (2003) compared symptom duration of 110 occupants that had been involved in rear-end impacts with parameter values obtained in reconstructions of the impacts using a mathematical model of the BioRID and seats. The study showed that NIC and N_{km} clearly predicted a neck injury with high accuracy; both initial as well as symptoms duration of more than 1 month. The study also presented data that show that, when using a mathematical model of the BioRID, head-to-torso rotation does not correlate with neck injury symptoms. A general concern and weakness of the study was the use of mathematical models of seats and a prototype of BioRID II.

Boström and Kullgren (2007) compared real-life performance of car seats with BioRID II test results for Saab, Volvo and Toyota seats before and after the anti-whiplash systems were introduced. The authors included NIC, N_{km} , upper neck shear and compression loads, rebound and T1 acceleration/head-to-contact time in the analysis. They found a positive correlation between good real-life performance and performance in dynamic tests, but did not suggest criteria to be used in future seat evaluations. Nevertheless, in their comparisons of dummy results in tests with seats with

and without anti-whiplash systems, NIC and upper neck shear loads were found to have been reduced more than the other parameters. The reduction of these two parameters could have contributed to a large degree to the reduced injury risk as observed in the seats with anti-whiplash systems.

Farmer et al. (2008) studied the relationship between seat ratings schemes used by Insurance Institute of Highway Safety (IIHS) and their partner International Insurance Whiplash Protection Group (IIWPG) and the rating schemes used by Swedish Road Administration (SRA) to real-world neck injury rates due to rear-end impacts. The main finding was that seat systems that perform better in dynamic sled tests have lower risk of neck injury than seats that rate poor. This was especially clear for long term injuries (>3 months injury claim). However, the study also concluded that further research is needed in the field of injury criteria, injury threshold and test design to improve the predictability of real-world neck injuries by mechanical tests of seat systems.

Zuby and Farmer (2008) studied the correlation between 26 BioRID II test parameters and seat design injury rates. In total 55 different seat designs were included in the analysis for which more than 30 claims had been filed. The study found that none of the 26 studied parameters was highly correlated with neck injury rates. For some parameters, a higher parameter value even correlated with a lower injury risk. It was identified that variables other than sled test variables, such as state group, crash damage, vehicle price etc, could have reduced the expected correlations.

Ono et al. 2009 used mathematical modelling to reconstructed volunteer and cadaver experiments and rear-end impact accidents with known initial, short and long term risk of neck injury symptoms and known crash pulse and seat characteristics. In total 20 cases were reconstructed for which the velocity change during the rear-end impact ranged from 9 km/h to 28 km/h. The results reveal that displacements between the cervical vertebrae may be responsible for the persistent neck symptoms following rear-end impacts. The study suggested adopting the NIC and neck forces to assess the risk of these injuries. WAD2+ injury risk curves were suggested for NIC values and neck forces (upper M_y , lower F_x and F_z).

In the past, EEVC WG12 (Biomechanics) has evaluated a number of low severity rear impact dummies and associated injury criteria and injury assessment reference values to be used in the WG20

(Whiplash) test procedure (Hynd et al. 2007 and Hynd and Carrol 2008). During the preparation of that report, it was concluded that a thorough understanding of the injury site and mechanisms responsible for the symptoms presented after rear-end collisions and injury threshold were unavailable. The reports concluded that this lack of biomechanical data presents challenges for the possibility to evaluate the proposed injury criteria and suggested reference values. The EEVC working groups have thereafter suggested comparing real-life data with crash test dummy parameter values and injury criteria values from sled tests to evaluate the applicability of crash test methods targeted at assessing the risk of whiplash injury in rear-end impacts.

Objective

The objective of this study is to assess the applicability of seat performance criteria, i.e. crash test dummy parameter values and injury criteria values, for rear-end impact seat-system testing. This will be done by finding a correlation between whiplash injury risks, as calculated from real real-life insurance data, and crash test dummy values. Parameters and injury criteria that correlate with injury risk will be recommended for additional studies in which injury risk functions and reference values are developed.

To serve this objective crash test results with injury claims rates for groups of seats in which the seat design was the same will be compared. An example of such a group would be all cars from Volvo in which only WHIPS seats of the same version were installed.

Such comparisons would be similar to the approach adopted by Heitplatz et al. (2003), Linder et al. (2004), Cappon et al. (2005) and Zuby and Farmer (2008) but the comparison will be carried using grouped data based on seat design and the real-life accident data will be more robust. Further, permanent impairment data have been suggested to be more robust than data on acute symptoms and the use of permanent impairment data, as in the current study, may lead to more reliable results. In addition, Folksam is using insurance data where a uniform compensation policy was used throughout the collection region and collection period, and possible compensation is limited to reimbursement of medical cost and loss of income. This policy will reduce the influence of variables other than collision and car related variables.

MATERIAL AND METHODS

Insurance data

Whiplash injury claims from crashes that occurred between 1995 and 2008 at +/-30 degree from straight rear-end and reported to the insurance company Folksam were used in this study. In total 13 958 reported injuries were included. Insurance claims were used to verify if the reported whiplash injuries led to long-term symptoms. Occupants that had a medical record of injury and claimed compensation for injury symptoms for more than 1 month were defined as *symptoms >1 month* (Equation 4). These claims entitle the occupant to a payment of 2000 SEK (about 210 €). The *symptoms >1 month* category includes those that possibly recovered after 1 month or later and those that later were classified as sustaining a permanent impairment. In total 2 665 occupants that reported whiplash injury sustained symptoms for more than one month.

$$\begin{aligned} > 1 \text{ month} = \frac{\# \text{ occupants with symptoms for } > 1 \text{ month}}{\# \text{ occupants with reported initial symptoms}} \end{aligned} \quad (1)$$

The second injury category is occupants with whiplash symptoms classified as *permanent* (Equation 5). This classification is primarily set after approximately 1 year but it usually takes longer time to set a final degree of impairment. In rare cases it can even take up to three years. Due to the three-year period only data from accidents that occurred between 1995 and 2008 could be used. In total 1543 occupants with permanent whiplash symptoms were included.

$$\begin{aligned} \text{permanent} \\ \text{impairment} = \frac{\# \text{ occupants with permanent symptoms}}{\# \text{ occupants with reported initial symptoms}} \end{aligned} \quad (2)$$

Accuracy of data

All the variables included in this model can be considered as random variables with some associated distribution. Because we do not know the real distribution of the variables, all variables are assumed to be normally distributed. The injury risk utilised in the study is calculated by computing the proportion p_j of recorded crashes leading to a whiplash injury for each seat model j . If N_j crashes are recorded, an estimation of the standard deviation for each calculated proportion is

$$SE_j = \sqrt{\frac{p_j(1-p_j)}{N_j}} \quad (3)$$

The standard error (the estimate of the standard deviation) can be utilised when calculating confidence intervals for the injury risks. If x_j is the measured value for a given parameter, the confidence interval for a 68% confidence is $(x_j - SE_j$ and $x_j + SE_j)$.

For the sled-test parameter values, we cannot compute a standard error because we do not have access to the required number of tests. However, there will still be an uncertainty in the measure of these parameters. In the following sections, we will only plot the confidence intervals for the injury risk and not for the measures parameters.

Grouping based on seat characteristics

To obtain a reliable statistical result regarding the injury risks, insurance claim data were grouped. Different types of groups can be used e.g. based on risk level and principle seat design. Here we have chosen to group seat and corresponding insurance data for seats that have the same design characteristics. By doing this we reduce the scatter in dummy readings that may appear if the groups were based according to risk level. This scatter may be due to the inclusion of seats with different injury reduction measures, which also influence the sled test parameters, and when included in the same group increases parameter value scatter.

The groups analyzed were *Volvo, Saab, Toyota, VW-group (Audi, Seat, VW and Skoda), Opel, Ford and Mercedes* (Table 1). For most of these groups both traditional seats and anti-whiplash seat designs from the same car producer were included. Heavy cars and light cars were excluded in this analysis to reduce the differences in average vehicle weight between the different groups (Table1). Gender distribution was not a reason for exclusion or inclusion in the different groups. The resulting proportion of females in each group is presented in Table 1. Table 2 lists the conditions in the particular sled test used to represent the different groups.

Table 1.

Groups defined in this study; n is the number of insurance cases included in each the group; f is the proportion of females in each group; m is the average vehicle weight of the cars included in the group. The range is the year the car model was produced.

| | | | |
|---|-------|--|-------|
| Ford with STD, n=163, f=57%, m=1397 kg | | Volvo with STD, n=921, f=50%, m=1496 kg | |
| Focus | 99-05 | S40/V40 | 96-99 |
| Galaxy | 96-05 | 850 | 91-97 |
| | | V70 | 97-00 |
| Mercedes with STD, n=227, f=44%, m=1469 kg | | Volvo with WHIPS, n=192, f=50%, m=1524 kg | |
| A-class | 98-04 | S40/V40 | 00-04 |
| C-class | 93-01 | S40/V50 | 04- |
| E-class | 96-01 | V70 | 00-06 |
| | | S60 | 01-99 |
| Opel with STD, n=410, f=52%, m=1363 kg | | S80 | 98-06 |
| Astra | 98-04 | | |
| Meriva | 03- | VW group with STD, n=1575, f=51%, m=1414 kg | |
| Vectra | 96-98 | Audi A3 | 96-03 |
| Zafira | 99-04 | Audi A4 | 95-00 |
| | | Audi A6 | 95-97 |
| Opel with RHR, n=125, f=49%, m=1402 kg | | Audi A6 | 98-05 |
| Signum | 03-04 | Seat Toledo/Leon | 99-04 |
| Tigra | 04- | Skoda Octavia | 97-04 |
| Vectra | 99-01 | Skoda Fabia | 00- |
| Vectra | 02-08 | VW Bora | 99-04 |
| | | VW Golf | 98-04 |
| Saab with STD, n=968, f=49%, m=1462 kg | | VW Passat | 97-05 |
| Saab 900 | 94-98 | VW Polo | 02- |
| Saab 9000 | 85-97 | | |
| | | VW group with RHR, n=94, f=59%, m=1475 kg | |
| Saab with SAHR, n=279, f=51%, m=1597 kg | | Audi A3 | 03-04 |
| Saab 9-3 | 98-02 | Audi A3 | 05-06 |
| Saab 9-5 | 98-09 | Audi A4 | 01-06 |
| | | Audi A6 | 05-06 |
| Toyota with STD, n=735, f=61%, m=1335 kg | | Seat Ibiza | 03- |
| Avensis | 98-02 | Skoda Octavia | 05- |
| Camry | 97-01 | VW Touran | 03- |
| Corolla | 98-02 | VW Golf/Jetta | 04- |
| Picnic | 97-01 | VW Passat | 05- |
| Previa | 00-05 | | |
| RAV4 | 95-99 | | |
| Starlet | 97-99 | | |
| | | | |
| Toyota with WIL, n=976, f=64% m=1309 kg | | | |
| Auris | 07- | | |
| Avensis | 03-08 | | |
| Avensis Verso | 01-05 | | |
| Camry | 01-03 | | |
| Corolla | 02-07 | | |
| Corolla Verso | 02-03 | | |
| Corolla Verso | 04-10 | | |
| Prius | 00-03 | | |
| Prius | 04-09 | | |
| Rav4 | 00-04 | | |
| Rav4 | 05- | | |
| Yaris and Yaris Verso | 99-05 | | |
| Yaris | 05- | | |

All criteria/parameter values used in the analysis were taken from one single seat test from each seat group. In an additional analysis also a median criteria/parameter value for each seat group was also analysed. The former is referred to as representative values and the latter median values.

For the representative values, the seat test that provided the largest number of parameter values that were close to the median values for the studied parameter and appeared to provide reasonable values, including head-to-head restraint distance, was selected and used. In case the most representative test did not provide data for all parameters, e.g. a test that was selected and used in the analysis did not provide proper film data, the most representative parameter value among the available test for a particular parameter was used in the analysis.

The analysis using median values were included to evaluate if the selection of representative values could have introduced the results, i.e. the linear regression r^2 -values. Such r^2 -values were also calculated for all criteria/parameters using the median parameter value of the included test in each seat group (Table 5).

Sled test data

All sled tests that were suitable and available for this study were conducted at Autoliv in Vårgårda, Sweden, during the period 2004 to 2006 and at Thatcham, UK, between 2003 and 2006. Table 2 provides information on the selected sled tests used in the analysis of grouped data. Additional information on the sled tests conditions and insurance data can be found in Davidsson and Kullgren (2011). The sled tests carried out at Autoliv were performed according to the Swedish Road Administration (SRA) and Folksam seat performance rating procedure which was harmonized with the International Insurance Whiplash Protection Group (IIWPG) rating procedure used by Thatcham. In brief, a H-point machine including a Head Restraint Measuring Device (HRMD) was used to adjust seatback angle and determine H-point position. Thereafter the H-point tool was removed and a BioRID II, build level e or g, was installed in the seat.

The main differences between the included test series were the make and build level of the Head Restraint Measuring Device (HRMD), H-point tool and the BioRID II (Table 2).

The sled acceleration used was the median risk - median frequency pulse (Krafft et al. 2005, Krafft et al. 2002), with a velocity change of 16 kph, an

average acceleration of 5.5 g and with a triangular shape with 10 g peak. This pulse is the same as one of the pulses currently used in Euro-NCAP.

The injury parameters measured and calculated were those previously suggested by SRA/Folksam and IIWPG (Table 3). In addition, head relative T1 displacement data expressed in a coordinate system that was attached to the T1 unit were retrieved from film analysis.

The tested seats were mainly new except seats from Volvo V70 97-00, SAAB 900 94-97 and SAAB 9-3 98-02 which were used.

Linear regression

A linear regression model was adopted to provide ideas about how the parameters were correlated with the injury risk. To have a measure of how good the fit of the model a coefficient of determination, r^2 -values, were calculated. The r^2 -value represents the proportion of common variation in the two variables, i.e. the parameter value and the injury risk. In addition a significance level could be calculated for each correlation and will be a measure of the reliability of the correlation. However, the number samples in this study are small and for that reason significance level is not calculated.

The regression line is determined by minimizing the sum of squares of distances of data points from this line. Therefore single outliers have a profound influence on the slope of the regression line and on the value of the correlation coefficient r^2 . For this reason data was plotted and outliers identified.

Table 2.
Car model, type of seat system, year the seat was tested, test facility, BioRID build level, H-point tool, initial horizontal head-to-head-restraint distance (back set).

| Groups | Model | Prod. year | WAD mitigation system ¹ | Year tested | Test facility | BioRID II version | H-point tool ² | Backset (mm) |
|----------|----------------|------------|------------------------------------|-------------|---------------|-------------------|---------------------------|--------------|
| Ford | Focus I | 99-06 | None | 2004 | Autoliv | E | TS | 55 |
| Mercedes | C-class | 93-01 | None | 2004 | Thatcham | G | AA | 55 |
| Opel | Astra | 98-04 | None | 2004 | Thatcham | G | AA | 72 |
| | Vectra | 02-08 | RHR | 2004 | Thatcham | G | AA | 75 |
| SAAB | 900 | 94-97 | None | 2006 | Autoliv | G | AA | 30 |
| | 9-5 | 98-09 | SAHR | 2004 | Autoliv | E | AA | 40 |
| Toyota | Corolla | 98-02 | None | 2005 | Autoliv | E | AA | 65 |
| | Corolla Versio | 04-10 | WIL | 2005 | Autoliv | E | AA | 95 |
| Volvo | V70 | 97-00 | None | 2006 | Autoliv | G | AA | 74 |
| | V/S70 | 00-06 | WHIPS | 2004 | Thatcham | G | AA | 32 |
| VW | Seat Altea | 04- | None | 2004 | Thatcham | G | AA | 65 |
| | Audi A6 | 05-06 | RHR | 2005 | Autoliv | E | TS | 55 |

Note 1 None No system is activated before or during the impact
 RHR Reactive Head Restraints
 SAHR Saab Active Head Restraint, version 1 and 2
 WHIPS Whiplash Protection System
 WIL Whiplash Injury Lessening

Note 2 TS refers to TechnoSports, Inc., USA and AA refers to Automotive Accessories, Ltd., UK

Table 3
Parameters included in the analysis in this study:

- Maximum Neck Injury Criteria (NIC)
- Maximum Neck Force Criteria (N_{km})
- Maximum Lower Neck Loads Criteria (LNL)
- Maximum Head x- and z-acceleration
- Maximum C4 x- and z-acceleration
- Maximum T1 x- and z-acceleration
- Maximum T8 x- and z-acceleration
- Maximum L1 x- and z-acceleration
- Maximum Pelvis x- and z-acceleration
- Maximum and minimum Upper Neck Loads (U. N. F_x , F_z and M_y , before head contact stop)
- Maximum and minimum Lower Neck Loads (L. N. F_x , F_z and M_y , before head contact stop)
- Maximum Occipital condyle rel. T1 x- and z-displacement in the T1 frame (OC-x and OC-z, respectively)
- Maximum Head relative T1 angular displacement (Neck extension)
- Head Contact Time (HCT)
- Maximum Head Rebound Velocity (HRV)

RESULTS

Linear regression for neck injury criteria and other parameters measured in a representative dummy test were performed on the grouped data. The correlations between the parameters and the two categories of injury risks are presented in Table 4 and 5 and plots of the injury risks versus the various parameters are

displayed in Figure 1-3. In addition, the correlations between the median parameter values for each group and the two categories of injury risks are listed in Table 5. Only parameters with correlation coefficients above 0.3 are listed Table 4 and 5 in addition to those included in the current Euro-NCAP protocol.

As can be seen in Table 4, the permanent impairment risk and symptoms longer than one month both

showed correlations with both the maximum NIC and Upper Neck Shear Force. The Lower Neck Flexion Moment and L1 x-acceleration and N_{km} showed a limited correlation. Notably, HCT and HRV showed small or only limited correlation with the injury risk.

Table 4.
Correlation (r^2) between the peak value of the included parameters and the injury risks. Based on analysis of data from one representative sled test per seat group.

| Parameter | Permanent Imp. | Symp. < 1 month |
|-------------------------|-----------------------|---------------------------|
| NIC | <u>0,75</u> | <u>0,78</u> |
| U. N. F_x (head r.w.) | <u>0,53</u> | <u>0,64</u> |
| L. N. M_y (flexion) | 0,37 | <u>0,63</u> |
| L1 x-acceleration | 0,34 | 0,28 |
| N_{km} | 0,32 | 0,39 |
| Neck extension | 0,31 | 0,21 |
| T8 z-acc. | 0,31 | 0,19 |
| L. N. M_y (extension) | 0,26 | 0,29 |
| HCT | 0,20 | 0,37 |
| Head z-acc. | 0,20 | 0,22 |
| LNL | 0,16 | 0,44 |
| T1 x-acc. | 0,11 | 0,34 |
| U. N. F_z (tension) | 0,08 | 0,29 |
| L. N. F_x (head r.w.) | 0,08 | 0,33 |
| OC x-disp. | 0,03 | 0,03 |
| Head x-acc. | 0,03 | 0,21 |
| HRV | 0,09 | 0,19 |

A mathematical method to be used to select the most representative test, when there was more than one test available for each seat group, was not developed or used. The selection of the most representative test, as explained in the Materials and Methods section, could have introduced some bias. Therefore a complimentary analysis was carried out using the median value for each parameter of all available seat tests data for each seat group (Table 5). As can be seen in Table 5, a few additional parameters were found to correlate to injury risk. The additional parameters Head and T1 vertical accelerations and Lower Neck Flexion Moment appear to be more convincing than in the analysis of representative data. One other change, when using median values for each seat group, were that Head Contact Time appeared to correlate even less compared to when representative test were used.

Table 5.
Correlation (r^2) between the peak value of the included parameters and the injury risks. Based on an analysis in which the median values for each parameter from each seat group was used.

| Parameter | Permanent Imp. | Symp. < 1 month |
|-------------------------|-----------------------|---------------------------|
| NIC | <u>0,70</u> | <u>0,74</u> |
| Head z-acc. | <u>0,61</u> | <u>0,73</u> |
| U. N. F_x (head r.w.) | <u>0,57</u> | <u>0,68</u> |
| T8 z-acc. | <u>0,52</u> | 0,42 |
| L. N. M_y (flexion) | 0,47 | <u>0,69</u> |
| Neck extension | 0,46 | 0,33 |
| L1 x-acceleration | 0,44 | 0,45 |
| OC x-disp. | 0,44 | 0,44 |
| N_{km} | 0,37 | 0,47 |
| L. N. M_y (extension) | 0,31 | 0,26 |
| LNL | 0,23 | <u>0,53</u> |
| U. N. F_z (tension) | 0,17 | 0,41 |
| L. N. F_x (head r.w.) | 0,15 | 0,40 |
| HRV | 0,14 | 0,25 |
| Head x-acc. | 0,11 | 0,32 |
| T1 x-acc. | 0,09 | 0,32 |
| HCT | 0,00 | 0,04 |

In Figure 1-3, lines have been drawn between data points for groups for which grouped data were available for seats with and without ant-whiplash systems. These lines were included to enable a comparison between parameter values and injury risk with a reduce influence of factors such chassis design characteristics of the make, car owner characteristics specific for the make, and partly vehicle mass.

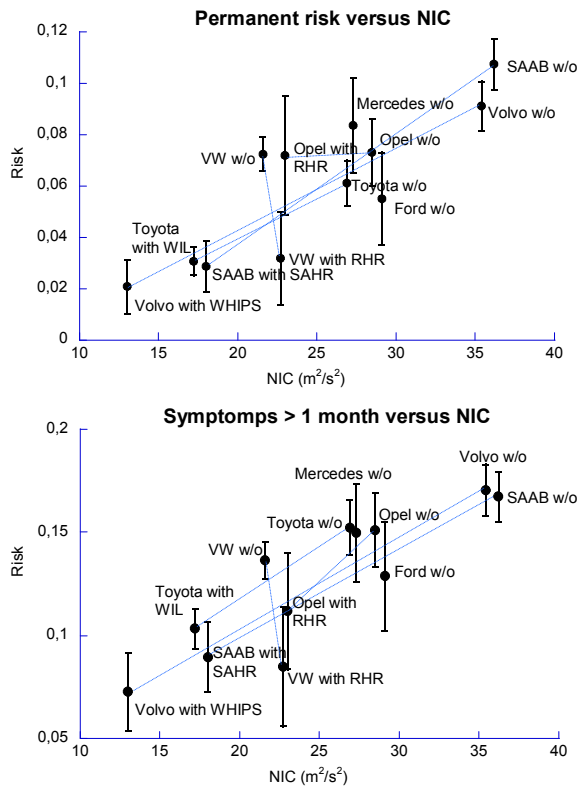


Figure 1. Permanent impairment group and > 1 month symptom limit risks versus the maximum of the parameter NIC for twelve different groups (average ± 1 SE).

By studying Figure 1, it appears that all car producers have reduced the NIC values considerably when anti-whiplash systems were introduced with the exception of the VW group. For the VW group the reduction in injury risk, may have been achieved by a combination of the reduction of other parameters/criteria values. Despite these differences between the seat groups, it appears that seats designs that produces a NIC lower than $25 \text{ m}^2/\text{s}^2$ will result in a risk that is less than approximately 6% to develop permanent neck symptoms following a rear-end with initial symptoms (Figure 1).

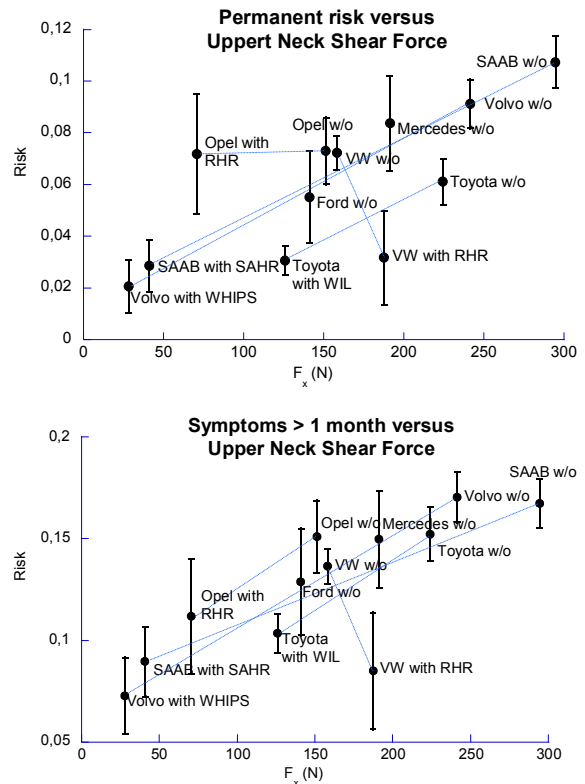


Figure 2. Permanent impairment group and > 1 month symptom limit risks versus the maximum of the parameter Upper Neck Shear Force (F_x) for twelve different groups (average ± 1 SE).

The similar situation appears to be the case for the Upper Neck Shear Force produced when the head moves rearward relative to the upper neck (Figure 2). For this parameter it appears that a 125 N force or less will result in a risk of 6% or less.

There seem to be no relation between Head Contact Time and risk of permanent impairment or symptoms lasting more than one month (Figure 3) following an accident with acute symptoms. The

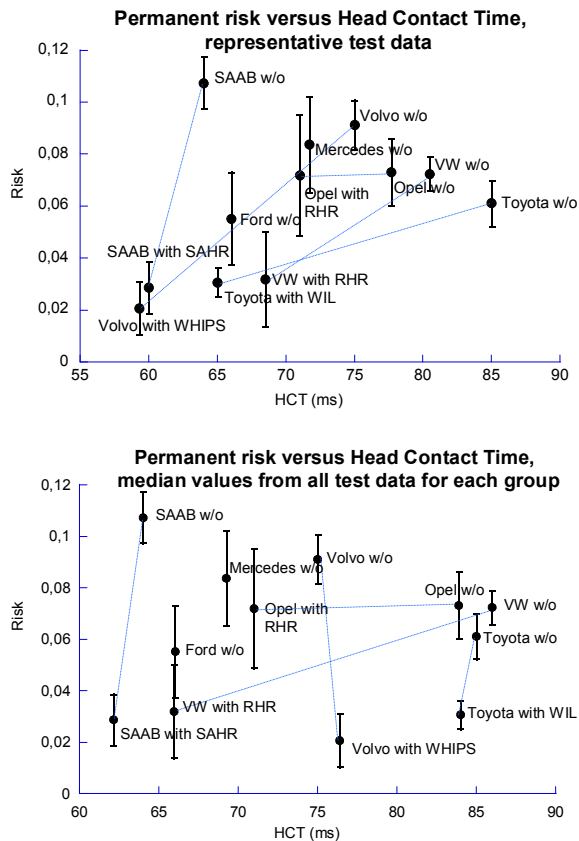


Figure 3. Risk of permanent impairment versus the Head Contact Time for twelve groups (average ± 1 SE). HCT values as presented when a single representative test (top) and median (bottom) were used in the analysis.

DISCUSSION

By pooling seat models without anti-whiplash seat designs in one group, and seat models with anti-whiplash seat designs in another group (for each car manufacturer), it was expected that a better statistical analysis can be made. The injury risks estimate was found to be more reliable than using individual seat data and the vehicle related parameters less influential compared to the use of groups based on similar risk. The reason for the latter was partly due to the inclusion of vehicles with similar mass and vehicle body characteristics for each car manufacturer.

The car manufacturers included in the analysis claim that their systems were designed to reduce head-to-head restraint distance and/or yield/absorb energy in a force controlled manner. Using the insurance data, we can conclude that the anti-whiplash seat designs reduce the risk of sustaining whiplash injuries. *Saab* showed a reduction of approximately 73%, *Toyota* a

reduction of approximately 50% and *Volvo* a reduction of approximately 77% of permanent impairment. Opel have managed to cut the risk of short term injury but it does not appear to have changed the risk of permanent impairment when introducing RHR. By analyzing the figures, one can note that:

- Saab has managed to lower the value for all available parameters by introducing SAHR except Head Contact Time (HCT).
- Toyota managed to lower the value for all available parameters except T1, Upper neck F_z and Head Rebound velocity (HRV).
- Volvo decreased all parameter, including OC-x, except HCT. The HCT remained almost constant when comparing before and after the introduction of WHIPS.
- VW group has managed to reduce some of the upper and lower neck forces, LNL and the HCT while many parameters have remained rather constant e.g. the NIC or HRV.
- Opel has managed to reduce NIC, N_{km} , LNL and some of the neck load parameters.

In summary the analysis of these five car makes showed that a reduction of NIC, Upper Neck Shear Force (F_x) and Lower Neck Compression (increasing the $-F_z$) appear to reduce the injury risk (Figure 1-2). Further, there is no apparent correlation between HCT and injury risks (Figure 3).

For evaluation of the robustness of the analysis, two other groups were included in the analysis. These were Ford and Mercedes and were not fitted with anti-whiplash systems. The regression analysis, including these seats (Table 4) provided that NIC, Upper Neck Shear Force (F_x), and Lower Neck Flexion Moment, predicted the risk of permanent as well as the risk of symptoms for more than one month following a rear-end impact. These findings are in line with other studies on this matter which suggested that NIC and Upper Neck Shear Forces are suitable for assessing seat performance in rear-end impacts (Kullgren and Boström 2007).

Ono et al. (2009) also came to similar conclusions as in this study, but using a different approach than in our study. Ono and co-authors reconstructed a number of rear-end impacts using a detailed mathematical model of the human and combining the

results obtained with results obtained in previous studies in which volunteers were used. The study by Ono et al (2009) also suggested the NIC and neck loads, including upper neck M_y , lower F_x and lower F_z , should be used in the evaluation of seat performance in rear-end impacts.

The findings of this study are, however, not in line with the study by Zuby and Farmer (2008) who found no correlation between dummy measurements and claims rate. The differences between these two studies are difficult to identify and only tentative explanations have been identified. Firstly, in the study by Zuby and Farmer (2008) the number of insurance cases for most of the car models was high. But for some car models included in their analysis, only 30 cases of rear-end impacts were available in the insurance database. For these models the estimated injury risk was uncertain since the outcome of a single accident highly influence the numbers used in the correlation study. Secondly, there are probably differences in the insurance data between the study by Zuby and Farmer and the current study. These differences could be associated with differences in injury coding, differences in compensation for property damage, compensation for injury claims, social welfare system, etc. Thirdly, in the current study the most representative sled test data set was used in the analysis. This data set was selected from a number of available sled tests that had been conducted at either Autoliv or Thatcham (Davidsson and Kullgren 2011). The use of representative data sets in this study means that the analysis was carried out using more robust dummy data than in the study by Zuby and Farmer. These three differences may be small but can in combination with the methods used to assess correlations, in these two studies, which both are known to be very sensitive to outliers, provide very different level of correlation and as such, explain the differences between the two studies.

As mentioned in the previous paragraph, this study used measurements from the most representative test from each seat group. Such a selection could contribute to the fact that we could identify correlations whereas studies in the past could not. This selection approach was adopted since a study of this kind requires, for a proper comparison between real life data and sled test data, that seats used in the sled tests are representative of the seats installed in the cars involved in rear-end collisions and included in the used insurance data base. This does not mean that multiple tests with identical seats should be introduced in future test programs. We rather adopted this approach because it is likely that there were differences between the tested seats in each seat

group. By introducing this selection we facilitated inclusion of the more representative test in the correlation analysis. The differences between the seats within one single seat group could be due to introductions of small differences in design over the time span. These differences could be due to foam thickness, foam properties, fabric selection, etc. In addition to these reasons, other sources for variability were present during the testing and which justify the used selection approach. The largest source was most likely the introduced by the lack of H-point and HRMD tool calibration routines at the time of testing. In this study we used test data which was generated using three different H-point tools which most likely could explain the differences in measured and used head-to-head restraint distances. A second source was the use of two different BioRID II build levels. The differences between these two build levels were mainly the position of the spine in relation to the exterior of the flesh. By selecting the most representative test data set for each seat group the problem using "old" seat test data could be reduced.

The sled test data used in this study was generated in different laboratories using almost identical test conditions. Over the time a few dissimilarities in the test conditions have been identified and could explain some of the observed variability (Davidsson and Kullgren 2011). This variability introduces a noise and it is expected that a better correlation would be obtained if all seat tests were carried out using the latest test protocol. However, using the latest test protocol and dummy build level may not produce more consistent results since some of the seat models included are no longer in production. This assumption is based on the hypothesis that the seat characteristics are more important than complying with the state of the art seating procedure to produce representative seat test results. The analysis carried out by Davidsson and Kullgren (2011, appendix 3) also suggested that the inconsistency level was limited for most of the parameters but was rather inflated for others, such as head rebound velocity, upper neck moments and a few of the lower neck loads, and that this inconsistency could possibly explain the limited correlations found in this study for some of the parameters.

It is unlikely that only one single parameter fully could assess risk of injury to all the different injury mechanisms that have been suggested in a rear-end impact. The results in this study support that several parameters should preferably be used.

One can discuss if the risks used in the current study were based on true injuries or not and if they were a

direct result of the car crashes. Firstly, occupants with permanent symptoms were defined as those that have a classified degree of impairment by physicians. The same procedure is used for all Swedish insurance companies. The whole procedure setting a final degree of impairment may take up to three years after the crash. Symptoms >1 month is defined as those that has obtained a medical record of their symptoms. In these records the injury has most often not been verified as it most often was just a question of pain following a rear-end collision. Secondly, if the injuries/symptoms would only occur randomly or be influenced by factors not linked to the car crash, you would not see any differences in risk between car models. Despite the fact that there might be problems with quality of the risk estimate, large differences in risk can be shown. If the quality would be further improved it is expected that even larger differences in risk would be seen.

The inclusion of both males and females in the insurance data may introduce noise because females load the seat in real life accident differently from the males and this may also be reflected in the seat tests. In case we could compare dummy data and male data separately we expect a better correlation between dummy sled test data and injury risk. Unfortunately the number of cases in the insurance data does not allow comparing dummy data with insurance data for males only.

The injury risk has been reported to be higher for females than for males. In this study we did not compensate for differences in gender distribution between the different seat groups. However, for a majority of the included car groups in this study the numbers of insurance cases were almost identical for males and females (Table 1). For the groups denoted Toyota with standard seat, Toyota with WIL seat and VW group with RHR seat, the proportions of the insurance case in which the occupant was a female was 61%, 64% and 59%, respectively. For these three groups the estimated risks, which were used in the analysis in this study, were most likely somewhat higher than the risk if the female proportion were 50%. The effect of this shift in risk for these three groups on the presented results is expected to be small.

A perfect correlation was not expected since only a single generic crash pulse was included in the analysis. This generic pulse has been found to be representative of the crashes in the insurance data. But adding other pulses and adopting a statistical model that allow a combination of results from a

number of crash pulses may provide a better correlation and further justify the obtained results.

Vehicle mass have been shown to influence injury risk in rear-end accidents. Risk of permanent injury is lower in heavy vehicles as compared to lighter vehicles according to the insurance data (Figure 4). Despite this difference, sled tests are generally carried out using generic crash pulses. In this study only data from a single generic crash pulse was included. Since not the actual vehicle specific pulse was used, including very light and very heavy vehicles could smokescreen any possible correlation between parameter values and injury risk. Therefore, car models with very low or high vehicle mass were excluded in the analysis.

Despite the exclusions of light and heavy vehicles, there were still differences in vehicle mass between the studied seat groups; seats with anti-whiplash systems were in general slightly heavier than those without (Figure 4). It could be hypothesised that the observed injury risk reductions were completely due to increased vehicle mass and not due to installation of anti whiplash systems or improved seat designs. However, the observed risk reductions were mainly due to design changes, as shown in Figure 4, and the observed correlations were therefore a function of measured dummy parameter values rather than just by coincidence.

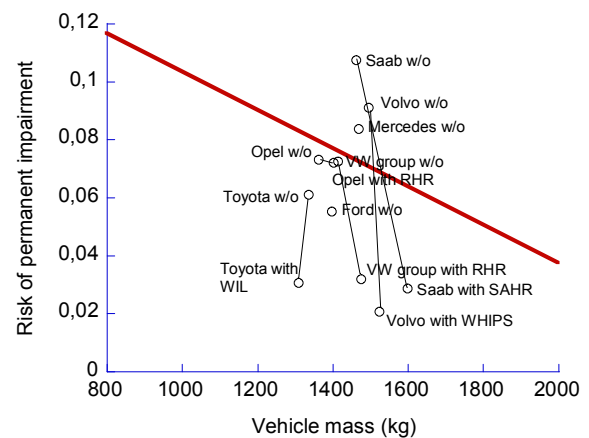


Figure 4: Risk of permanent impairment versus vehicle mass.

For the seat model groups the average risk and weighted representative vehicle mass was calculated and used. For the average car data, the tick line, was generated using all data available in the Folksam data base (n=13958). Note that the average risk also includes anti-whiplash seats and that during the sampling period such systems were more common in

larger and thereby heavier cars than small and light cars.

CONCLUSION

The main finding in this study was that the neck injury criterion, NIC, and upper neck shear force appear to be the best predictors of long term and short term neck injury following a rear-end impact. Head vertical acceleration and Lower neck bending moment (flexion) was also found to correlate to some degree to the injury risks.

Another finding was that grouped insurance data based on characteristics of the seat system was useful since it reduced the uncertainties in the estimated risks.

We also conclude that other parameters may be shown to be useful when a larger data set becomes available and when new seat tests are carried out using the latest test routines, a calibrated H-point machine and the newest dummy version.

REFERENCES

- Andersson, T. and Boström, O. (2006) Test of force controlled yielding seats to draft GTR head restraint dynamic test, Head Restraint Informal Working Group Meeting January 23-26, BAST, Köln, Document HR-5-12 ; <http://www.unece.org/trans/main/wp29/wp29wgs/wp29grsp/head05.html>
- Boström, O., Svensson, M., Aldman, B., Hansson, H., Håland, Y., Lövsund, P., Seeman, T., Suneson, A., Säljö, A., Örtengren, T. (1996) A new neck injury criterion candidate based on injury findings in the cervical spinal ganglia after experimental neck extension trauma, Proceedings of International IRCOBI Conference Biomechanics of Impacts, pp. 123-136.
- Boström, O. and Kullgren, A. (2007) Characteristics of anti-whiplash seat designs with good real-life performance, Proceedings of International IRCOBI Conference Biomechanics of Impacts, pp. 219-232.
- Cappon, H., Hell, W., Hoschopf, H., Muser, M., Wismans, J. (2005) Correlation of accident statistics to whiplash performance parameters using the RID 3D and BioRID dummy, Proceedings of International IRCOBI Conference Biomechanics of Impacts, pp. 229-243.
- Davidsson, J. and Kullgren, A. (2011) EEVC WG12 Interim report: Evaluation of Seat Performance Criteria for Rear-end Impact Testing; http://www.eevec.org/publicdocs/WG12_Interim_Evaluation_of_seat_performance_criteria_2011-02-01.pdf
- Farmer, C. M., Wells, J. K., Lund, A. K. (2003) Effects of head restraint and seat redesign on neck injury risk in rear-end crashes, Traffic Injury Prevention, Vol. 4(2), pp. 83-90.
- Farmer, C. M., Zuby, D. S., Wells, J. K., Hellinga L. A. (2008) Relationship of Dynamic Seat Ratings to Real-World Neck Injury Rates, Traffic Injury Prevention, 9:561–567, 2008.
- Zuby, D. S. And Farmer, C. M. (2008) Relationship between Seat Ratings Test Results and Neck Injury Rates in Rear Crashes. Whiplash – Neck Pain in Car Crashes, November 18-19, 2008, Munich, Germany.
- Heitplatz, F., Sferco, R., Fay, P., Reim, J., Kim, A., Prasad, P., (2003) An evaluation of Existing and Proposed Injury Criteria with Various Dummies to Determine their Ability to Predict the Levels of Soft Tissue Neck Injury Seen in Real World Accidents, Proceedings of 18th International Technical Conference on the Enhanced Safety of Vehicles, no 504-O.
- Hynd, D., Svensson, M., Trosseille, X., van Ratingen, M., Davidsson, J. (2007) EEVC WG12 Report – Document Number 505A: Biofidelity Requirements and Injury Criteria for a Low-speed Rear Impact Whiplash Dummy, On behalf of the European Enhanced Vehicle-safety Committee (EEVC), Working Group 12, September 2007.
- Hynd, D. And Carrol, J. (2008) EEVC WG12 Report – Document Number 505C: Summary Report: Requirements and Assessment of Low-Speed Rear Impact Whiplash Dummies. On behalf of the European Enhanced Vehicle-safety Committee (EEVC), Working Group 12, October 2008.
- Krafft, M., Kullgren, A., Ydenius, A., Tingvall, C. (2002) Influence of Crash Pulse Characteristics on Whiplash Associated Disorders in Rear Impacts--Crash Recording in Real Life Crashes, Traffic Injury Prevention, 3:2, 141 — 149.
- Krafft, M., Kullgren, A., Malm, S., Ydenius, A. (2005) Influence of Crash Severity on Various Whiplash Injury Symptoms: A Study Based on Real-Life Rear-End Crashes with Recorded Crash Pulses.

International Technical Conference on the Enhanced Safety of Vehicles, No. 05-0363.

Kullgren, A., Eriksson, L., Boström, O., Kraft, M. (2003) Validation of Neck Injury Criteria using Reconstructed Real-life Rear-end Crashes with Recorded Crash Pulses, Proceeding of 18th International Technical Conference on the Enhanced Safety of Vehicles, No. 344-O.

Kullgren, A., Kraft, M., Anders Lie, A., Tingvall, C., (2007) The Effect of Whiplash Protection Systems in Real-life Crashes and their Correlation to Consumer Crash Test Programmes, International Technical Conference on the Enhanced Safety of Vehicles, No. 07-0468.

Kullgren, A. and Kraft, M (2010), 'Gender Analysis on Whiplash Seat Effectiveness: Results from Real-world Crashes', *Int. IRCOBI Conf. on the Biomechanics of Injury* (Hannover).

Kuppa, S. (2004) Injury Criteria and Anthropomorphic Test Devices for Whiplash Injury Assessment, NHTSA Docket No. 19807, <http://dmses.dot.gov/docimages/p80/313219.pdf>.

Kuppa, S., Saunders, J., Stammen, J., Ann Mallory (2005). Kinematically Based Whiplash Injury Criterion, Proceeding of 19th International Technical Conference on the Enhanced Safety of Vehicles, No. 05-0211-O.

Jakobsson, L. and Norin, H. (2005) Field Analysis of AIS1 Neck Injuries in Rear-End Car Impacts-Injury Reducing Effect of *WHIPS* Seat, *J. of Whiplash & Related Disorder*, Vol 3(2), pp. 37-53.

Linder, A., Avery, M., Kullgren, A., Kraft, M., (2004). Real-World Rear Impacts Reconstructed in Sled Tests, Proceedings of International IRCOBI Conference Biomechanics of Impacts, 2004.

Ono, K., Inami, S., Kaneoka, K., Gotou, T., Kisanuki, Y., Sakuma, S., Miki, K. (1999) Relationship between Localized Spine Deformation and Cervical Vertebral Motions for Low Speed Rear Impacts using Human Volunteers, Proceedings of International IRCOBI Conference Biomechanics of Impacts, pp 149-164.

Ono, K., Ejima, S., Yamazaki, K., Sato, F., Pramudita, J.A., Kaneoka, K., and Ujihashi S. (2009) Evaluation Criteria for the Reduction of Minor Neck Injuries during Rear-end Impacts Based on Human Volunteer Experiments and Accident Reconstruction Using Human FE Model Simulations, Proceedings of International IRCOBI Conference Biomechanics of Impacts, 381-398.

Prasad, P., Kim, A., Weerappuli, D. (1997) Biofidelity of Anthropomorphic Test Devices for Rear Impact, Proceedings of the 41st Stapp Car Crash Conference, pp. 387-415, SAE No. 973342.

Schmitt, K-U., Muser, M., Walz, F., Niederer, P. (2002): N_{km} — a proposal for a neck protection criterion for low speed rear-end impacts, *Traffic Injury Prevention*, Vol. 3 (2), pp. 117-126

Voo, L., Merkle, A., Shin Sung, C., Kleinberger, M. (2003) Comparison of Three Rotation Measurement Techniques in Rear Impact Application, SAE, 2003.

Study on Impact Response (Injury Value) Variation Factors for BioRID-II Dummies

Taichi Nakajima

Kunio Yamazaki

Koshiro Ono

Japan Automobile Research Institute (JARI)

Japan

Masahide Sawada,

Japan Automobile Manufacturers Association, Inc. (JAMA)

Japan

(on behalf of the JAMA Rear-impact Neck Injury Evaluation Sub-Group)

Paper Number 11-0201

ABSTRACT

The study aims to contribute to discussions for the standardization of BioRID-II dummies as an evaluation test tool, which is underway at the UN ECE/WP29/GRSP Head Restraint gtr Informal Meeting. Since it is important that as a test tool, BioRID-II be able to ensure a high repeatability and reproducibility, BioRID-II's response variations in calibration and sled tests be examined using the following simulation techniques: First, to identify variation factors, a calibration test simulation model (MADYMO 7.2) was developed. In the simulation, three parameters (i.e., bumper characteristics, cable-spring characteristics, and damper characteristics) were varied in such a way that the prescribed corridor was satisfied and the resultant variations in acceleration, load, moment and other readings of BioRID-II were examined. Next, a sled test simulation model was developed, and using this simulation model, a similar parameter study was conducted for sled testing. The dummies' head acceleration, T1 acceleration, neck force and neck moment were measured. In addition, rotations of the head, neck and torso were also measured and analyzed. According to the simulation results, the calibration test generated the following variations in terms of CV values: 2~20% for rotation angle and 2~10% for acceleration, load and moment. On the other hand the sled test generated variations of: 2~15% for rotation angle and 2~15% for acceleration, load and moment. The data proves that the bumper, the cable spring, and the damper influence the impact response of the dummy's rotation angle and injury value. Moreover, injury value variations proved practically identical between calibration and sled tests. Nevertheless clear differences between the two tests were found in the impact responses of respective rotation angles and injury values, also in the peak values and peak times. It was also found that these injury value variations can be minimized by approximation of impact responses and peak values, and by the synchronization of peak times between the two tests. Consequently it was considered necessary to introduce a calibration test method requiring seatback and head restraint conditions closely resembling that of the actual vehicle. This research

compares the results of a calibration test and a $\Delta V16$ km/h sled test. The problem of determining what factors are affected by the calibration method of the BioRID-II dummy can now be defined. Moreover, the variation factor of the test conditions (dummy set, pulse, etc.) was also eliminated, and therefore only the cause of the variation of the dummy was studied. This analysis have yet to be reported until now, which makes such reports indispensable to the study of HR dynamic examination method of the UN ECE/WP29/GRSP.

1. Background

At the UN ECE/WP29/GRSP, an Informal Working Group on development of Global technical regulation No.7 ("Head Restraint gtr Informal Meeting") has been held since February 2005. Phase1 (it regulates as a standard requirement to the headrest about static backset (distance between the back of the head of a seated 3D mannequin and the head restraint)) was manufactured in March, 2008. Then, from December 2009, Phase2 of the Head Restraint gtr Informal Meeting (evaluation by dynamic test) was initiated. At the meeting, established was the evaluation by non geometric requirements called static backset but with a dummy injury value as a target. What was discussed was a target injury, a test method, etc. This currently, study focuses on dummy repeatability and reproducibility for use in regulation.

Japan Automobile Research Institute (JARI) and Japan Automobile Manufacturers Association (JAMA) has been studying ^{(1) - (3)} the test evaluation method which can reduce the neck injury generated during vehicle accident, and this testing method is to be proposed to Japan or other countries. As part of the research, injury value variation generated in evaluation test is examined. Various factors, such as variations in test conditions (impact acceleration, a dummy arrangement, etc.) and the individual differences of dummies or sheet, are included in injury value variation. This research particularly focused on whether or not injury value variation in calibration testing affects dummy responses in rear impact sled test. More specifically, analysis of the simulation of calibration test and Sled test was

similarly performed on the test condition, and the influence of the variation given to a dummy injury value was examined.

2. BioRID-II Dummies

2.1 Issues concerning BioRID-II Dummies

Dummies such as BioRID-II, RID3D and Hybrid-III have been proposed as rear impact dummies. Past research⁽⁴⁾ indicated that BioRID-II (Fig.1) is proven to be the most biofidelic dummy, and test methods using BioRID-II have been adopted by the JNCAP and EuroNCAP. BioRID-II has a spine comprising of 24 vertebrae including not only the cervical but also the thoracic and lumbar vertebrae. With such a structure, BioRID-II now has the characteristic that enables it to reproduce the human spine movements. In additionally, the various body parts of BioRID-II have been given mechanical characteristics that resemble the responses of human body parts in volunteer sled tests. These merits have contributed to the high biofidelity of BioRID-II. On the other hand, because of its having a more structure compared to other dummies, BioRID-II has been reported to have issues of test reproducibility and differences in individual dummies⁽⁶⁾. The major factors responsible for injury value variations have been thought of as (a) individual differences of dummies, (b) dummy adjustment, and (c) dummy setting at the sled test.

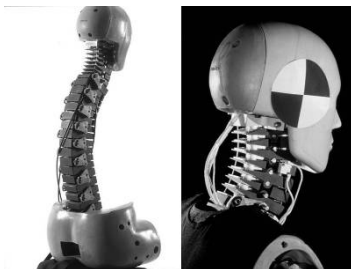


Fig.1 BioRID-II

2.2 Calibration Test Method for BioRID-II

To make sure that a dummy secures its dynamic response characteristics, BioRID-II calibration tests provide corridors⁽⁵⁾ for each of the measurement items listed in Table 1. Regarding the three rotation angles shown in Fig.3, corridors have been set for each head rotation of the occipital condyle (Pot.A), neck link rotation about the first thoracic vertebra (Pot.B), and T1 rotation (Pot.C). In order to place the dummy's response in the corridors at calibration test, various body parts of the dummy need to be adjusted. According to the users' manual on BioRID-II, the bumper, cable spring and damper are mainly what need to be adjusted to put the three rotation angles into their respective corridors⁽⁷⁾ in a calibration test. Moreover, the new calibration test method of BioRID-II is also proposed, but this

research applied the existing method of calibration testing.

Table.1 Measurement Item of Calibration Test

| <i>Measurement Item</i> | |
|---------------------------------------|------------------|
| Pendulum Force | N |
| Sled Acceleration | m/s ² |
| Sled Velocity | m/s |
| T1 Acceleration | m/s ² |
| Head Rotation about Occipital Condyle | deg |
| Neck Link Rotation about T1 | deg |
| T1 Rotation | deg |

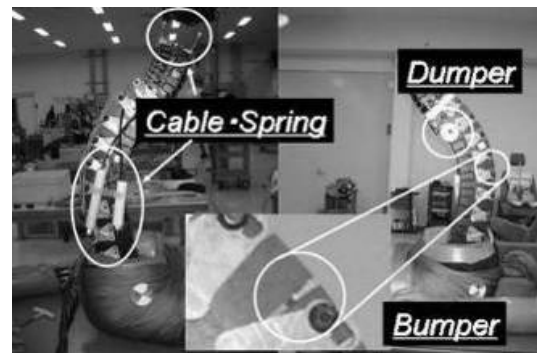


Fig.2 Adjustment Item of Calibration Test

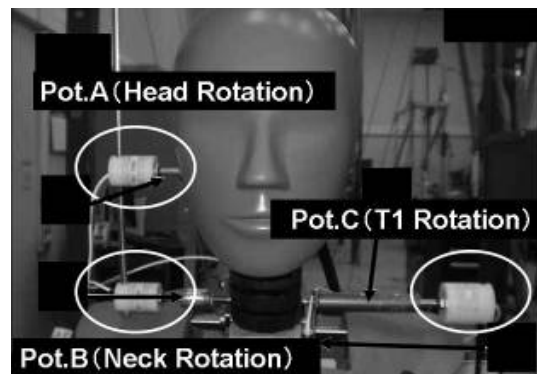


Fig.3 Rotation Angle of Calibration Test

3. Simulation Analysis of Calibration Test

In order to examine the variation in the dummy in a calibration test, it is necessary to ensure the reproducibility of a test. So, it is able to perform comparatively easily and its reproducibility examined using good simulation. The simulation used MADYMO7.2 for the solver while BioRID-II Facet Ver3.0 developed by TASS (TNO Automotive Safety Solutions) was used as the dummy model.

3.1 Simulation Model for Calibration Tests

A simulation model consisting of a dummy model and a mini sled model was produced in accordance with the existing method of calibration test of a BioRID-II dummy. Then parameter study was performed so that the corridor specified at the time of a calibration test might be satisfied. While in actual

calibration tests, impact is applied to the mini sled by using a probe, sled accelerations were provided as an input condition in the simulation. The results of the parameter study are showed in Fig.5, Fig.6 and Fig.7. Although Pot.C has failed from the corridor, in the present simulation model, Fig.7 is limited in the condition where each rotation angle becomes the closest to a corridor. So, the simulation was effected by this condition.

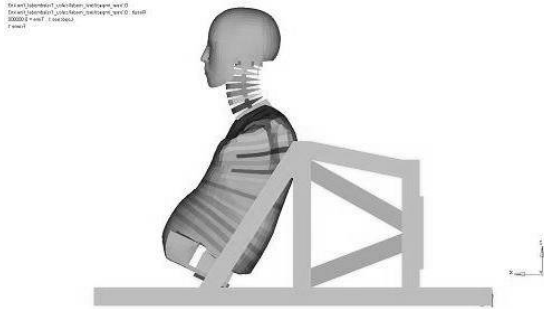


Fig.4 Simulation Model of Calibration Test

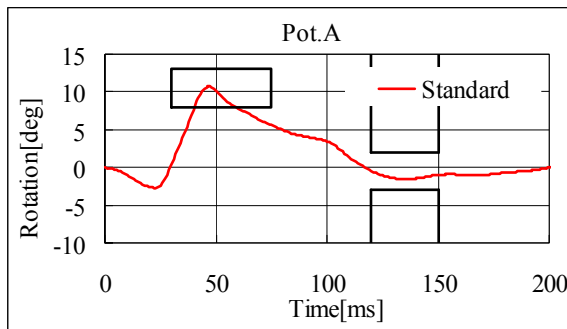


Fig.5 Pot.A (Standard Model)

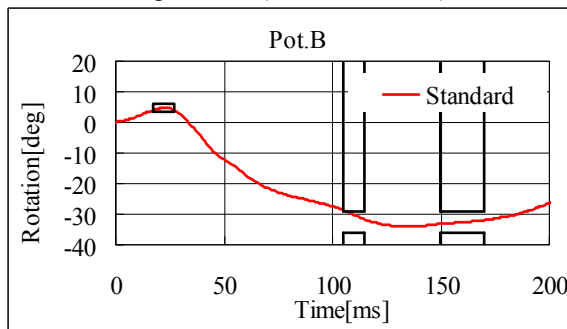


Fig.6 Pot.B (Standard Model)

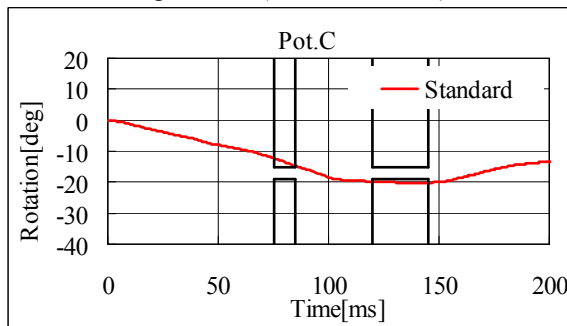


Fig.7 Pot.C (Standard Model)

3.2 Simulation Conditions

As calibration test conditions in the simulation, the input acceleration of the mini sled was used, shown in Fig.8. In addition to the item specified in the calibration test, the measurement items were made up of the head acceleration, neck load, and neck moment⁽⁸⁾.

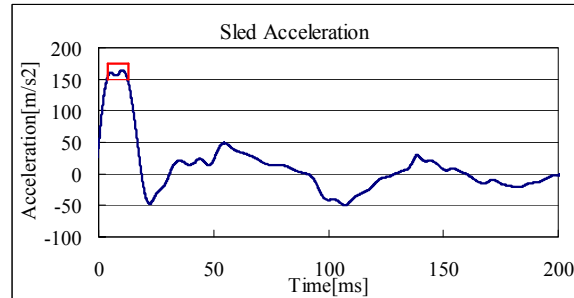


Fig.8 Sled Acceleration for Calibration Test

3.3 Simulation Parameters

This research has applied the existing method of calibration testing. And the factors of the variation in the dummy contained in a calibration test are varied. In those factors, the present study was focused on the corridor widths of Pot.A, Pot.B, and Pot.C. Even though the corridors passed and the calibration test was satisfactory, the injury values would vary if the passing values within each corridor differed. So, simulation models were produced for the cases of passing the upper, middle and lower portions of each corridor for Pot.A, Pot.B, and Pot.C. Note that among the plural number of corridors provided for Pot.A, Pot.B and Pot.C, only one corridor was selected. When a corridor in Pot.A was divided into upper, middle and lower portions, conditions were made so that all the other corridors in Pot.B and Pot.C would, as much as possible, is satisfied. The same method was also used when a setup for Pot.B and Pot.C was performed.

3.3.1 Corridors for Pot.A (Head Rotation Angle)

Pot.A of the simulation model represents the angle of head rotation against neck rotation and has two corridors. The present study was focused on the first corridor which corresponded with time of the first contact of the head to the head restraint. Pot.A was adjusted by modifying the characteristics of the simulation model's cervical spine joint covering C1-C2. Specifically, as torque characteristics against the angle were defined into the cervical spine joint, adjustment of the cervical spine joint was made by scaling its torque characteristics. The characteristics of the cervical spine joint corresponded with the characteristics of bumpers that were inserted between the cervical vertebrae of BioRID-II in the calibration test.

Table 2 shows the adjustment volumes of the cervical spine joint characteristics. Fig.9 shows the

results of the parameter study on Pot.A. Fig.10 and Fig.11 show changes in rotation angles in Pot.B and Pot.C as a result of adjustments in Pot.A.

Table.2 Volume of adjustment (cervical spine joint No.1 - No.2)

| | |
|--------|------|
| Upper | 0.7 |
| Middle | 0.3 |
| Lower | 0.15 |

unit : times

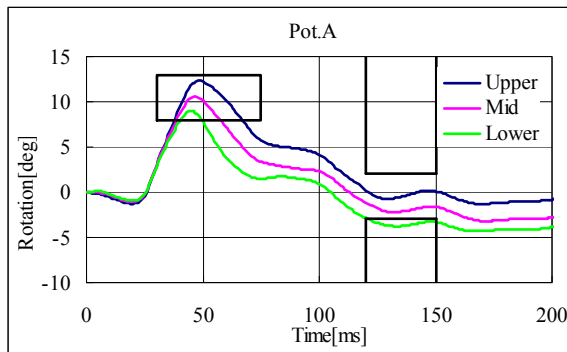


Fig.9 Pot.A

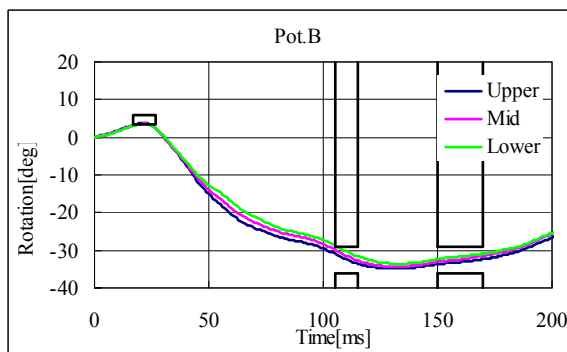


Fig.10 Pot.B

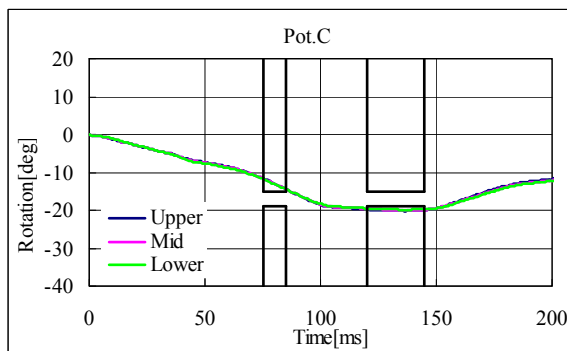


Fig.11 Pot.C

modifying the characteristics of the simulation model's cervical spine joint covering C1-C2. In addition, adjustment of the two thoracic spine joints covering C7-T1 and T1-T12, respectively, were performed by scaling of their torque characteristics against the angle. The characteristics of these joints corresponded with the characteristics of bumpers inserted between the cervical and thoracic vertebrae of BioRID-II in the calibration test.

Table 3 shows the adjustment volumes of cervical spine joint characteristics. Table 4 shows the adjustment volumes of the characteristics of the two thoracic spine joints. Fig.12 shows the results of the parameter study on Pot.B. Fig.13 and Fig.14 show changes in rotation angles at Pot.A and Pot.C as a result of Pot.B adjustments.

Table.3 Volume of adjustment (cervical spine joint No.1 - No.2)

| | |
|--------|-------|
| Upper | 0.005 |
| Middle | 0.1 |
| Lower | 0.25 |

unit : times

Table.4 Volume of adjustment (cervical spine joint No.7 - thorax spine joint No.1 and thorax spine joint No.1 - No.12)

| | |
|--------|----|
| Upper | 12 |
| Middle | 6 |
| Lower | 1 |

unit : times

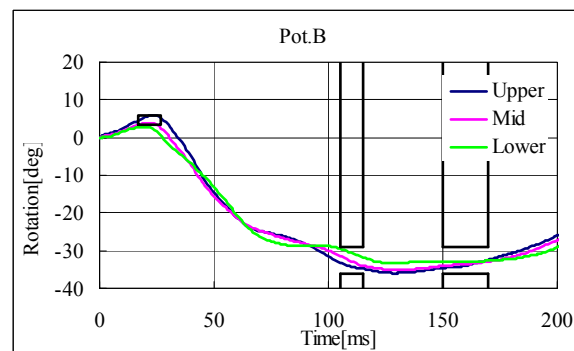


Fig.12 Pot.B

3.3.2 Corridors for Pot.B (Neck Rotation Angle)

Pot.B of the simulation model represents the angle of neck rotation against T1 rotation and has three corridors. The present study focused on the second corridor which among the three had the greatest width. As in Pot.A, Pot.B was likewise adjusted by

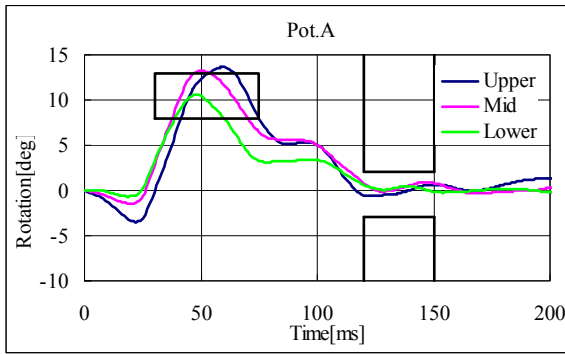


Fig. 13 Pot.A

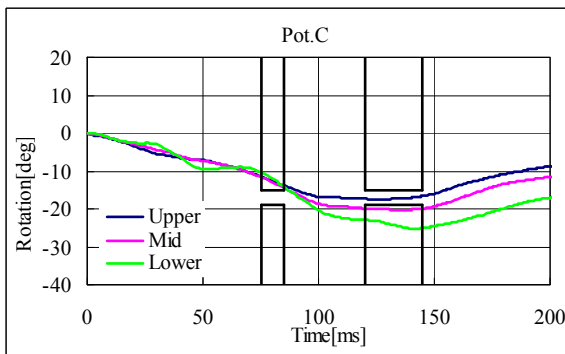


Fig. 14 Pot.C

3.3.3 Corridors for Pot.C (T1 Rotation Angle)

Pot.C of the simulation model represents the angle of T1 rotation against the mini sled and has two corridors. The present study focused on the second corridor with a greater width. As in Pot.A and PotB, Pot.C was also adjusted by modifying the characteristics of the simulation model's cervical spine joint covering, C1-C2. In addition as in Pot.B, adjustment of the two thoracic spine joints covering C7-T1 and T1-T12, respectively, were performed by changing their characteristics. The characteristics of these joints corresponded with the characteristics of bumpers inserted between the cervical and thoracic vertebrae of BioRID-II in the calibration test.

Table 5 shows the adjustment volumes of cervical spine joint characteristics. Similarly Table 6 shows the adjustment volumes of the characteristics of the thoracic spine joint covering C7-T1, while Table 7 shows those of the thoracic spine joint covering T1-T12. Fig.15 shows the results of the parameter study on Pot.C. Fig.16 and Fig.17 show changes in rotation angles at Pot.A and Pot.B as a result of Pot.C adjustments.

Table.5 Volume of adjustment (cervical spine joint No.1 - No.2)

| | |
|--------|-------|
| Upper | 0.025 |
| Middle | 0.08 |
| Lower | 0.1 |

unit : times

Table.6 Volume of adjustment (cervical spine joint No.7 - thorax spine joint No.1)

| | |
|--------|----|
| Upper | 12 |
| Middle | 6 |
| Lower | 6 |

unit : times

Table.7 Volume of adjustment (thorax spine joint No.1 - No.12)

| | |
|--------|----|
| Upper | 18 |
| Middle | 12 |
| Lower | 9 |

unit : times

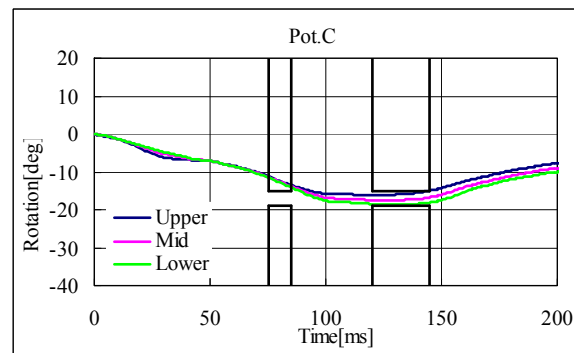


Fig. 15 Pot.C

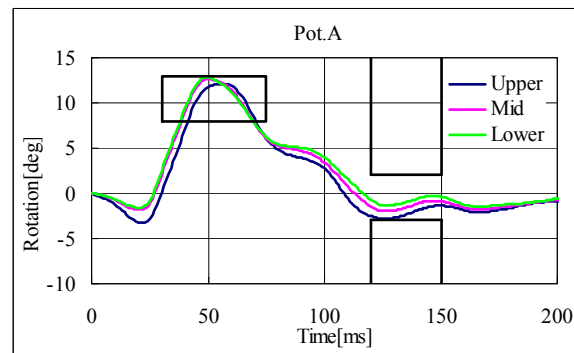


Fig. 16 Pot.A

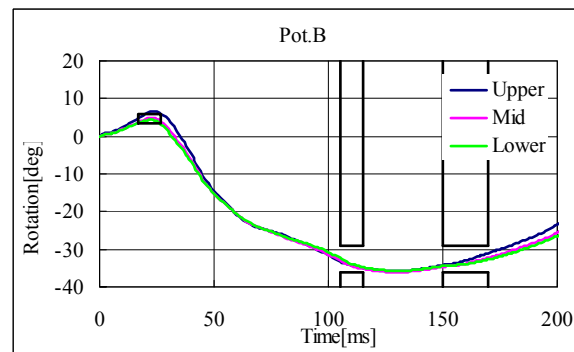


Fig. 17 Pot.B

3.4 Results of the Simulation

Simulation was conducted under various test conditions, and injury values were determined in relation to changes made in Pot.A, Pot.B and Pot.C. For each injury value, the coefficient of variation (C.V.) and the standard deviation were calculated in order to evaluate injury value variations.

3.4.1 Pot.A

Table 8 shows injury value results when the conditions for Pot.A were changed. UpperNeck-MY(Flx) was the only injury value with a C.V. that exceeded 10%. All the other injury value items recorded a C.V. of less than 10%.

Table.8 Injury value of Pot.A

| Result | NIC [m ² /s ²] | UpperNeck | | | |
|---------|--|-----------|-----------------|-----------------|-----------------|
| | | FX [N] | FZ [N] | MY-Flx. [Nm] | MY-Ext. [Nm] |
| Upper | 51.1 | 235.4 | 220.5 | 11.8 | -16.4 |
| Mid | 50.3 | 228.9 | 210.7 | 13.4 | -15.0 |
| Lower | 49.3 | 224.6 | 237.2 | 15.0 | -14.0 |
| Average | 50.2 | 229.6 | 222.8 | 13.4 | -15.1 |
| S.D. | 0.9 | 5.5 | 13.4 | 1.6 | 1.2 |
| C.V.[%] | 1.8 | 2.4 | 6.0 | 12.0 | 7.7 |
| Result | LowerNeck | | | | |
| | FX [N] | FZ [N] | MY-Flx. [Nm] | MY-Ext. [Nm] | |
| Upper | 280.7 | 230.9 | 2.0 | -35.2 | |
| Mid | 272.0 | 218.3 | 2.1 | -33.4 | |
| Lower | 263.2 | 242.0 | 1.9 | -32.5 | |
| Average | 272.0 | 230.4 | 2.0 | -33.7 | |
| S.D. | 8.8 | 11.9 | 0.1 | 1.4 | |
| C.V.[%] | 3.2 | 5.2 | 5.8 | 4.1 | |

3.4.2 Pot.B

Table 9 shows injury value results when the conditions for Pot.B were changed. The injury values with a C.V. that exceeded 10% were the UpperNeck-FX, UpperNeck-MY(Flx), LowerNeck-FX, LowerNeck-MY(Flx), and LowerNeck-MY(Ext). All the other injury value items recorded a C.V. of less than 10%.

Table.9 Injury value of Pot.B

| Result | NIC [m ² /s ²] | UpperNeck | | | |
|---------|--|-----------|-----------------|-----------------|-----------------|
| | | FX [N] | FZ [N] | MY-Flx. [Nm] | MY-Ext. [Nm] |
| Upper | 49.3 | 306.7 | 209.3 | 8.8 | -20.1 |
| Mid | 51.4 | 245.1 | 222.8 | 10.9 | -17.2 |
| Lower | 48.9 | 173.9 | 222.6 | 13.6 | -18.0 |
| Average | 49.8 | 241.9 | 218.2 | 11.1 | -18.5 |
| S.D. | 1.3 | 66.5 | 7.7 | 2.4 | 1.5 |
| C.V.[%] | 2.7 | 27.5 | 3.5 | 21.5 | 8.1 |
| Result | LowerNeck | | | | |
| | FX [N] | FZ [N] | MY-Flx. [Nm] | MY-Ext. [Nm] | |
| Upper | 318.5 | 234.3 | 1.8 | -41.2 | |
| Mid | 285.2 | 235.1 | 2.0 | -36.2 | |
| Lower | 247.9 | 226.6 | 1.6 | -23.0 | |
| Average | 283.9 | 232.0 | 1.8 | -33.4 | |
| S.D. | 35.3 | 4.7 | 0.2 | 9.4 | |
| C.V.[%] | 12.4 | 2.0 | 13.6 | 28.1 | |

3.4.3 Pot.C

Table 10 shows injury value results when the conditions for Pot.C were changed. The injury values with a C.V. that exceeded 10% were UpperNeck-FX and LowerNeck-MY(Flx). All the other injury value items recorded a C.V. of less than 10%.

Table.10 Injury value of Pot.C

| Result | NIC [m ² /s ²] | UpperNeck | | | |
|---------|--|-----------|-----------------|-----------------|-----------------|
| | | FX [N] | FZ [N] | MY-Flx. [Nm] | MY-Ext. [Nm] |
| Upper | 47.0 | 331.0 | 222.8 | 10.7 | -17.6 |
| Mid | 49.5 | 268.6 | 243.5 | 11.5 | -17.4 |
| Lower | 50.3 | 259.9 | 231.0 | 11.3 | -17.8 |
| Average | 48.9 | 286.5 | 232.4 | 11.2 | -17.6 |
| S.D. | 1.7 | 38.8 | 10.4 | 0.4 | 0.2 |
| C.V.[%] | 3.6 | 13.5 | 4.5 | 3.7 | 1.0 |
| Result | LowerNeck | | | | |
| | FX [N] | FZ [N] | MY-Flx. [Nm] | MY-Ext. [Nm] | |
| Upper | 340.4 | 249.9 | 2.3 | -44.0 | |
| Mid | 318.4 | 266.1 | 1.6 | -39.8 | |
| Lower | 308.9 | 246.5 | 1.6 | -38.3 | |
| Average | 322.5 | 254.2 | 1.9 | -40.7 | |
| S.D. | 16.2 | 10.4 | 0.4 | 2.9 | |
| C.V.[%] | 5.0 | 4.1 | 21.7 | 7.2 | |

3.5 Conclusions of simulation analysis of calibration test

To examine the injury value variations in the calibration test, the effect of the rotation angle corridors was analyzed. It was found that the rotation angle that had the most effect on injury value variations was Pot.B, On the other hand, the rotation angle that had the least effect on the variation was Pot.A.

4. Simulation Analysis of Sled Test

An examination was made to determine the effect of injury value variations in calibration test on the corresponding variation in the sled test.

4.1 Simulation Model for Rear Impact Sled Tests

A rear impact sled simulation model consisting of a dummy model and a seat model was produced. For the dummy model, the one produced for the preceding section (Section 3) was used. For the seat model, a simple model consisting of a head restraint, a seatback and a seat cushion was produced. For the compression characteristics of the seatback and head restraint, the results obtained in the static test were applied. The value of each characteristic was adjusted in the simulation of a rear impact sled test with an impact speed of $\Delta V16$ km/h. Fig.18 shows the simulation model, Fig.19 shows the mechanical characteristics of the seat model, and Fig.20 shows the derived values and validation results.

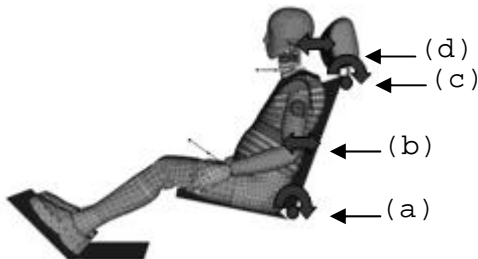


Fig.18 Simulation Model of Sled Test

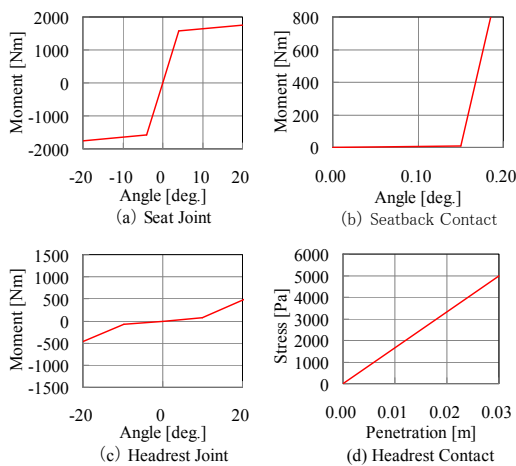


Fig.19 Property of seat and headrest

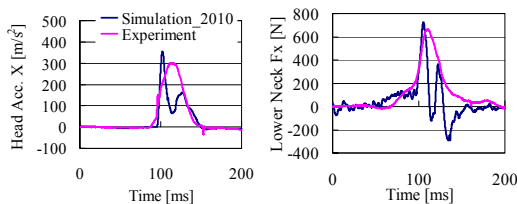


Fig.20 Validation of Simulation Model

4.2 Simulation Conditions

As a rear impact sled test simulation condition, a triangular pulse used in the EuroNCAP rear impact test and the medium waveform were employed (Fig.21). The test speed (speed change) was set at $\Delta V16$ km/h. Measured were head acceleration, T1 acceleration, neck load and neck moment. The setting values used for the seated dummy are as shown in Table 11.

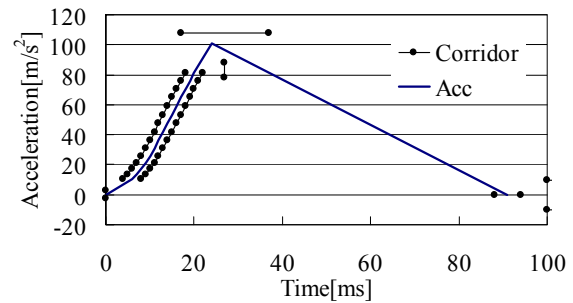


Fig.21 Sled Pulse

Table.11 Dummy Setting

| <i>Initial Position of Dummy</i> | | |
|----------------------------------|----|-----|
| Backset | 60 | mm |
| Head - HeadRestraint (Height) | 42 | mm |
| Head Angle | 0 | deg |
| Pelvis Angle | 22 | deg |
| SeatBack Angle | 20 | deg |

4.3 Simulation Parameters

As the parameters to be changed in the simulation, the Upper, Middle and Lower corridor portions for Pot.A, Pot.B and Pot.C were employed. The same conditions as those applied to the simulation of the calibration test were applied to the simulation of the rear impact sled test.

4.4 Results of the Simulation

Simulation was conducted under varied conditions, and injury values were determined in relation to changes recorded in Pot.A, Pot.B and Pot.C. For each injury value the coefficient of variation (C.V.) and the standard deviation were calculated to evaluate injury value variations.

4.4.1 Pot.A

Table 12 shows injury value results when the conditions for Pot.A were changed. UpperNeck-MY indicated the largest injury value variation, and its waveforms are shown in Fig.22. As shown in Table 12, UpperNeck-MY(Flx) and LowerNeck-MY (Flx) recorded a C.V. that exceed 10%. All the other injury value items recorded a C.V. of less than 10%.

Table.12 Injury value of Pot.A

| Result | NIC [m ² /s ²] | UpperNeck | | | |
|---------|--|-----------|-----------|-----------------|-----------------|
| | | FX [N] | FZ [N] | MY-Flx. [Nm] | MY-Ext. [Nm] |
| Upper | 24.0 | 152.3 | 1058.1 | 20.9 | -12.0 |
| Mid | 24.0 | 150.7 | 1050.8 | 26.6 | -12.7 |
| Lower | 23.4 | 149.4 | 1040.2 | 37.2 | -12.5 |
| Average | 23.8 | 150.8 | 1049.7 | 28.2 | -12.4 |
| S.D. | 0.3 | 1.4 | 9.0 | 8.2 | 0.4 |
| C.V.[%] | 1.3 | 1.0 | 0.9 | 29.2 | 3.0 |
| Result | NIC [m ² /s ²] | LowerNeck | | | |
| | | FX [N] | FZ [N] | MY-Flx. [Nm] | MY-Ext. [Nm] |
| Upper | 672.0 | 711.9 | 11.8 | -32.2 | |
| Mid | 678.4 | 704.3 | 10.2 | -32.4 | |
| Lower | 665.5 | 693.5 | 9.2 | -32.2 | |
| Average | 672.0 | 703.3 | 10.4 | -32.3 | |
| S.D. | 6.4 | 9.2 | 1.3 | 0.1 | |
| C.V.[%] | 1.0 | 1.3 | 12.6 | 0.3 | |

Table.13 Injury value of Pot.B

| Result | NIC [m ² /s ²] | UpperNeck | | | |
|---------|--|-----------|-----------|-----------------|-----------------|
| | | FX [N] | FZ [N] | MY-Flx. [Nm] | MY-Ext. [Nm] |
| Upper | 23.1 | 174.5 | 1035.1 | 20.0 | -7.1 |
| Mid | 24.3 | 155.1 | 1066.9 | 19.3 | -11.3 |
| Lower | 20.1 | 130.3 | 1071.4 | 32.7 | -9.3 |
| Average | 22.5 | 153.3 | 1057.8 | 24.0 | -9.2 |
| S.D. | 2.2 | 22.2 | 19.8 | 7.6 | 2.1 |
| C.V.[%] | 9.6 | 14.5 | 1.9 | 31.5 | 22.7 |
| Result | NIC [m ² /s ²] | LowerNeck | | | |
| | | FX [N] | FZ [N] | MY-Flx. [Nm] | MY-Ext. [Nm] |
| Upper | 724.2 | 675.6 | 13.4 | -34.9 | |
| Mid | 671.9 | 715.8 | 13.0 | -31.9 | |
| Lower | 625.1 | 684.3 | 9.3 | -27.5 | |
| Average | 673.7 | 691.9 | 11.9 | -31.4 | |
| S.D. | 49.6 | 21.1 | 2.3 | 3.7 | |
| C.V.[%] | 7.4 | 3.1 | 19.0 | 11.9 | |

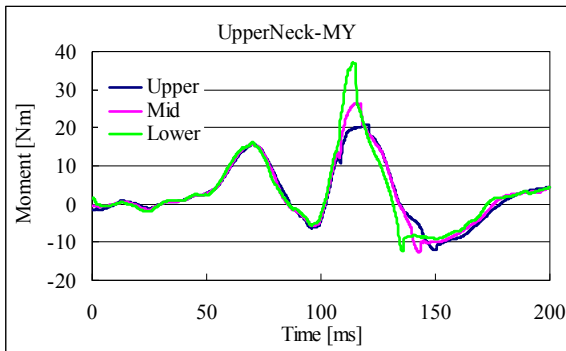


Fig.22 UpperNeck-MY

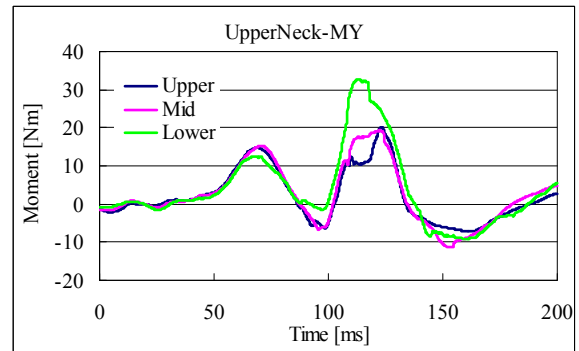


Fig.23 UpperNeck-MY

4.4.2 Pot.B

Table 13 shows injury value results when the conditions for Pot.B were changed. Fig.23 shows the waveforms of UpperNeck-MY which recorded the largest injury value variation. As shown in Table 13, the injury values with a C.V. that exceeded 10% were the UpperNeck-FX, UpperNeck-MY(Flx), UpperNeck-MY(Ext), LowerNeck-MY(Flx), and LowerNeck-MY(Ext). All the remaining injury value items recorded a C.V. of less than 10%.

4.4.3 Pot.C

Table 14 shows injury value results when the conditions for Pot.C were changed. Fig.24 shows the waveforms of UpperNeck-MY which recorded the largest injury value variation. As shown in Table 14, the injury values with a C.V. that exceeded 10% only the UpperNeck-MY(Ext). All the other injury value items recorded a C.V. less of than 10%.

Table.14 Injury value of Pot.C

| Result | NIC [m ² /s ²] | UpperNeck | | | |
|---------|--|-----------|-----------------|-----------------|-----------------|
| | | FX [N] | FZ [N] | MY-Flx. [Nm] | MY-Ext. [Nm] |
| Upper | 23.0 | 146.1 | 1040.4 | 16.2 | -8.0 |
| Mid | 23.4 | 167.6 | 1043.1 | 17.5 | -10.2 |
| Lower | 24.2 | 159.4 | 1060.1 | 18.3 | -11.3 |
| Average | 23.5 | 157.7 | 1047.9 | 17.3 | -9.8 |
| S.D. | 0.6 | 10.9 | 10.7 | 1.1 | 1.7 |
| C.V.[%] | 2.6 | 6.9 | 1.0 | 6.3 | 17.1 |
| Result | LowerNeck | | | | |
| | FX [N] | FZ [N] | MY-Flx. [Nm] | MY-Ext. [Nm] | |
| Upper | 721.2 | 638.7 | 14.4 | -35.0 | |
| Mid | 725.4 | 677.6 | 13.5 | -35.3 | |
| Lower | 685.0 | 710.3 | 13.6 | -32.8 | |
| Average | 710.5 | 675.5 | 13.8 | -34.4 | |
| S.D. | 22.2 | 35.8 | 0.5 | 1.4 | |
| C.V.[%] | 3.1 | 5.3 | 3.6 | 4.0 | |

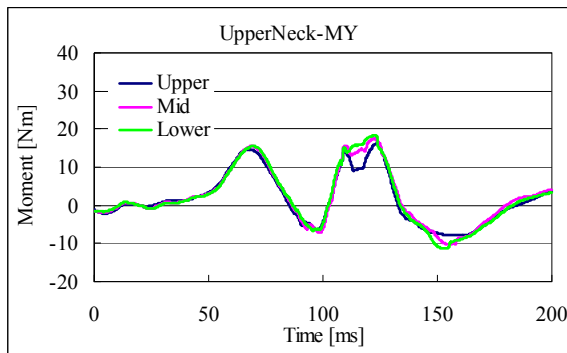


Fig.24 UpperNeck-MY

4.5 Conclusions of Simulation Analysis of Sled Test

Injury value variations in rear impact sled testing were examined. The same dummy sub-model as the one reported in Section 3 was used. The simulation results indicated that the rotation angle that had the most effect on injury value variations was Pot.B, while the rotation angle that had the least effect on the variation was Pot.C.

5. Comparison of Variations between Calibration Tests and Sled Tests

A comparison was made between the injury value variations observed in the calibration test and in the sled test.

5.1 Pot.A

Table 15 shows injury value results when the conditions for Pot.A were changed in both the calibration test and sled test. UpperNeck-MY(Flx) was the only injury value with a C.V. that exceeded 10% in both tests. LowerNeck-MY(Flx) indicated a C.V. of less than 10% in the calibration test but a C.V. that exceeded 10% in the sled test. All the other injury value items recorded a C.V. of less than 10%.

Fig.25 shows the time-history of UpperNeck-MY which registered the largest injury value variation in both the calibration test and the sled tests. The time-histories indicate differences in peak times and time-history shapes between the two tests. In addition, as shown in the time-history of the calibration test of Fig. 25, the minus-value is outputted at the time of Time=0. Since a dummy model has many joints in its backbone, it is difficult to set it up in posture wherein the loads to all the joints are removed completely, in early stages of calculation.

Table.15 Coefficient of variation of Pot.A

| Result | NIC [m ² /s ²] | UpperNeck | | | |
|-------------|--|-----------|-----------------|-----------------|-----------------|
| | | FX [N] | FZ [N] | MY-Flx. [Nm] | MY-Ext. [Nm] |
| Calibration | 1.8 | 2.4 | 6.0 | 12.0 | 7.7 |
| Sled | 1.3 | 1.0 | 0.9 | 29.2 | 3.0 |
| Result | LowerNeck | | | | |
| | FX [N] | FZ [N] | MY-Flx. [Nm] | MY-Ext. [Nm] | |
| Calibration | 3.2 | 5.2 | 5.8 | 4.1 | |
| Sled | 1.0 | 1.3 | 12.6 | 0.3 | |

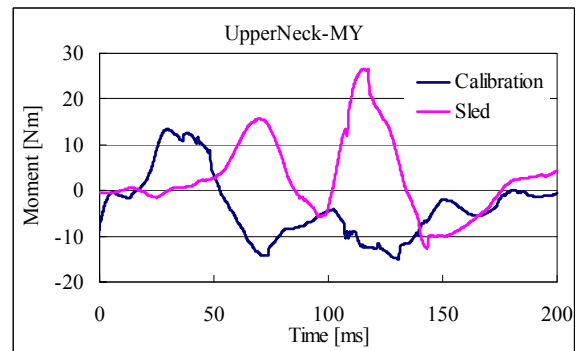


Fig.25 UpperNeck-MY

5.2 Pot.B

Table 16 shows injury value results when the conditions for Pot.B were changed in both the calibration test and the sled tests. UpperNeck-FX, UpperNeck-MY(Flx), LowerNeck-MY(Flx), and LowerNeck-MY(Ext) were the injury values with a C.V. that exceeded 10% in both the calibration test and the sled test. UpperNeck-MY(Ext) indicated a C.V. of less than 10% in the calibration test but had a C.V. that exceeded 10% in the sled test. On the other hand LowerNeck-FX recorded a C.V. that exceeded 10% in the calibration test but had a C.V. of less than 10% in the sled test. NIC, UpperNeck-FZ, and LowerNeck-FZ indicated a C.V. of less than 10% in both tests.

Fig.26 shows the time-history of the UpperNeck-MY which registered the largest injury value variation in both the calibration test and the sled test. The time-histories indicate differences in peak times and in time-history shapes between the two tests.

Table.16 Coefficient of Variation of Pot.B

| Result | NIC [m ² /s ²] | UpperNeck | | | |
|-------------|--|-----------|-----------|-----------------|-----------------|
| | | FX [N] | FZ [N] | MY-Flx. [Nm] | MY-Ext. [Nm] |
| Calibration | 2.7 | 27.5 | 3.5 | 21.5 | 8.1 |
| Sled | 9.6 | 14.5 | 1.9 | 31.5 | 22.7 |
| Result | NIC [m ² /s ²] | LowerNeck | | | |
| | | FX [N] | FZ [N] | MY-Flx. [Nm] | MY-Ext. [Nm] |
| Calibration | 12.4 | 2.0 | 13.6 | 28.1 | |
| Sled | 7.4 | 3.1 | 19.0 | 11.9 | |

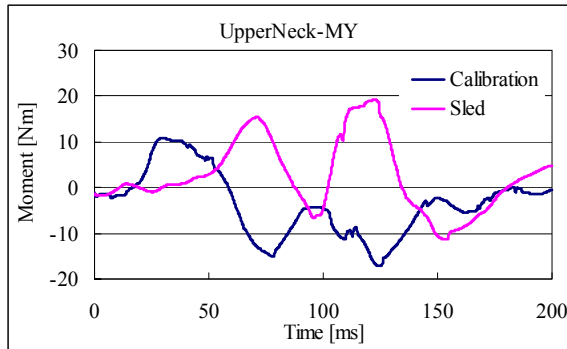


Fig.26 UpperNeck-MY

5.3 Pot.C

Table 17 shows injury value results when the conditions for Pot.C were changed. There were no injury value items with a C.V. that exceeded 10%. UpperNeck-MY(Ext) indicated a C.V. of less than 10% in the calibration test but had a C.V. that exceeded 10% in the sled test. On the other hand UpperNeck-FX and LowerNeck-MY(Flx) recorded a C.V. that exceeded 10% in the calibration test but had a C.V. of less than 10% in the sled test. All the other injury value items recorded a C.V. of less than 10%.

Fig.27 shows the time-history of UpperNeck-MY which registered the largest injury value variation in both the calibration test and the sled tests. The time-histories indicate differences in the peak times and the time-history shapes between the two tests.

Table.17 Coefficient of variation of Pot.C

| Result | NIC [m ² /s ²] | UpperNeck | | | |
|-------------|--|-----------|-----------|-----------------|-----------------|
| | | FX [N] | FZ [N] | MY-Flx. [Nm] | MY-Ext. [Nm] |
| Calibration | 3.6 | 13.5 | 4.5 | 3.7 | 1.0 |
| Sled | 2.6 | 6.9 | 1.0 | 6.3 | 17.1 |
| Result | NIC [m ² /s ²] | LowerNeck | | | |
| | | FX [N] | FZ [N] | MY-Flx. [Nm] | MY-Ext. [Nm] |
| Calibration | 5.0 | 4.1 | 21.7 | 7.2 | |
| Sled | 3.1 | 5.3 | 3.6 | 4.0 | |

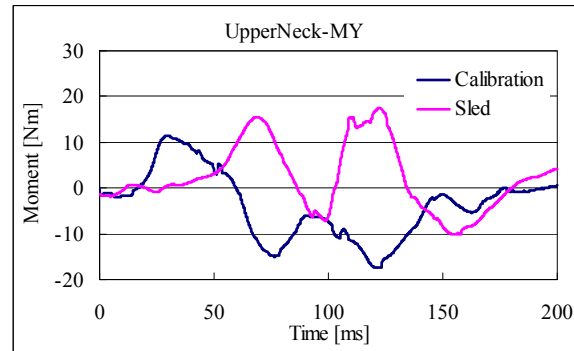


Fig.27 UpperNeck-MY

5.4 Discussions

The results of the present study indicated that injury values with a large C.V. in the calibration test also gave a large C.V. in the sled test. In addition, Pot.B was the rotation angle that gave the largest injury value variation in both the calibration test and the sled tests. On the other hand, Pot.A of the calibration test result, and Pot.C of the sled test result were the rotation angles that gave the least variation of injury values. It was found that the injury values that registered a C.V. of less than 10% at calibration test but registered a C.V. that exceeded 10% at the sled test were the LowerNeck-MY(Flx) of Pot.A, UpperNeck-MY(Ext) of Pot.B, and UpperNeck-MY(Ext) of Pot.C.

Initially, the reason why the variation of Pot.B became large was considered. Pot.B is the neck rotation angle, or the difference of head rotation angle and T1 rotation angle. Therefore, Pot.B is affected by the rotation angles of both Pot.A and Pot.C. In contrast, Pot.B influences the rotation angles of both Pot.A and Pot.C. So, from the result of the simulation, if it becomes possible to reduce the variation in Pot.B, it is thought that reducing the variation in Pot.A and Pot.C is also possible. Moreover, regarding Pot.B, cable adjustment and exchange of the bumper affects the actual dummy. So, when making those adjustments, caution is required. Next, the reason why the injury values that registered a C.V. of less than 10% at calibration test but registered a C.V. that exceeded 10% at sled test was considered. In the current calibration test without headrest, the dummy motion and behavior differed from the sled test. So, a difference was found in the peak value of the injury value and the timing which became a peak value was also different. This was considered as one reason. Consequently it may be possible to reduce injury value variations by reproducing in the calibration test the same dummy behavior observed in the sled test. In other words, one way of reducing injury value variations may be to conduct a calibration test with a headrest. However, the kind and structure of the seat are varied. So, the motion of sled test, the peak value of an injury value, etc. varies depending on the seats. Therefore,

headrest, seat and other factors need to be considered in order to develop a new calibration test method. On the other hand, in considering a calibration test with a head restraint, it will be necessary to note that the range of motion of the dummy's head will be restricted by the headrest. Specifically, extension behavior will be restricted while flexion behavior will not be affected as much. Therefore, the range of motion by the side of expansion is not read correctly. In a calibration test, since evaluation of the range of motion of the neck is also needed, the calibration test without headrest is likewise needed. However, the current calibration test without headrest does not require the measurement of load and moment for UpperNeck and LowerNeck. And in contrast, the sled test shows variations in load and moment for UpperNeck and LowerNeck. It is therefore necessary to examine the possible addition of these measurement items into the calibration test.

6. Conclusions

In the present study the calibration test and the sled test were analyzed by simulation, and factors affecting the variation of dummy injury values were examined for both tests.

The results indicated that if injury value variations are generated in the calibration test, similar variations will be generated in the sled test. Consequently it will be possible to reduce injury value variations in sled test by reducing such variations in calibration test. To do so, it is thought that one method is by carrying out a more exact calibration test by narrowing the corridor of Pot.A, Pot.B, and Pot.C (especially Pot.B) of calibration test.

Another method of solving the variation problem is to reproduce in the calibration test the dummy behavior that is similar to the dummy behavior observed in sled test. For example, a calibration test with a headrest may be introduced. However, since the introduction of a headrest may also bring forth new problems (such as measurement of neck load and reduce the variation) in the calibration test, it is necessary to conduct calibration test both with and without a headrest.

As a future topic, the current calibration test without headrest needs to be reviewed, as a new calibration test method with headrest is developed. It will be necessary to find out these correspondences to immediately reduce the variation of dummy injury values. Moreover, in the current calibration test, measurement of the injury value of each part of a dummy is not effected. By evaluating neck load and neck moment, etc. in calibration test, we believe that this would lead to the reduction of the variation in the dummy.

References

- (1)Ono.K et.al : Evaluation Criteria for the Reduction of Minor Neck Injuries during Rear-end Impacts Based on Human Volunteer Experiments and Accident Reconstruction Using Human FE Model Simulations, IRCOBI Conference, (2009)
- (2)Sato.F et.al : Evaluation Parameters and Criteria for the Reduction of Minor Neck Injuries during Rear-end Impacts -Human Volunteer Experiments and Accident Reconstruction using Human FE Model Simulations- (Research Paper), 41(2), JSAE, p233-240
- (3)Sawada.M et.al : Development of Neck Injury Evaluation Method in Rear Impact -Proposal for Adopting in Vehicle Assessment.- (Technical Paper), 41(2), p241-246
- (4) Kubota.M et.al : A Comparison between Human Volunteer and Rear Impact Dummies Response, JSAE Annual Congress (Spring), (2004)
- (5) D.JOHAN : BioRID-II final report, CHALMERS (1999)
- (6) K.Bortenschlager et.al : DETAILED ANALYSIS OF BIORID-II RESPONSE VARIATIONS IN HARDWARE AND SIMULATION, 21st ESV Proceedings (CD), (2009)
- (7) Denton ATD : BioRID Users Manual (2009)
- (8) T. Ikari, K. Kaito et al : Japan New Car Assessment Program For Minor Neck Injury Protection in Rear-End Collisions, 21th ESV conference, Paper No.09-0364(2009)

Comparison of WorldSID and Cadaver Responses in Low-Speed and High-Speed Nearside Impact

Jonathan D. Rupp, Carl S. Miller, Matthew P. Reed, Kathleen D. Klinich, and Lawrence W. Schneider
University of Michigan Transportation Research Institute
United States of America

Paper Number 11-0080

ABSTRACT

A series of lateral impact tests was performed in which the WorldSID midsize-male crash-test dummy was struck with a segmented padded impactor that separately loaded the thorax, abdomen, iliac wing, greater trochanter, and mid thigh. Tests were conducted using 8 m/s and 3 m/s initial impact velocities with velocity histories that mimic those produced in staged side-impact tests. A 5.1-cm abdomen offset was used to produce similar loading conditions as were used in a recently reported set of side-impact tests performed using seven male cadavers.

WorldSID thorax, abdomen, iliac crest, pelvis, and mid thigh forces, internal/external deflections, and pelvis accelerations were compared to ± 1 SD corridors developed from the 3-m/s and 8-m/s cadaver responses. Results of these comparisons indicate that the WorldSID abdomen produces impact forces that are higher than the associated cadaver response corridor and external deflections that are lower than the associated response corridor for both the 3 m/s and 8 m/s loading conditions, suggesting that the abdomen rib stiffness should be reduced. Greater-trochanter and iliac-wing forces in 3-m/s tests were within, or slightly above, response corridors while these same measurements were substantially above response corridors for the 8-m/s tests. Lateral accelerations of the pelvis in the 3-m/s tests were slightly above target response corridors while lateral pelvic accelerations in the 8-m/s tests were within target response corridors. The combination of these results suggest that the WorldSID pelvis is too stiff and has too much tightly coupled mass.

INTRODUCTION

The responses of the WorldSID midsize male crash-test dummy thorax, abdomen, and pelvis are based on tests in which whole cadavers were dropped onto rigid plates, decelerated into rigid and padded segmented impactors, and impacted using ballistic masses (ISO TR9790). Although these tests have provided seminal data on lateral impact response, they have several important limitations, including not providing usable data on abdomen force-deflection

characteristics and not independently measuring iliac crest and greater trochanteric responses during whole-body side-impact tests. Further, most previous whole-body side impact sled tests used a single-size load wall for different sized subjects and, as a result, produced response data for the thorax, abdomen, and pelvis that are confounded with responses of adjacent body regions. Lastly, the lowest impact velocity used in the side-impact sled tests used to develop WorldSID was 6.7 m/s, which is well above some door-to-crash-test-dummy initial impact velocities in FMVSS 214 tests. Further, as vehicle side structures improve and side-impact airbags are phased into the vehicle fleet, the velocities at which the intruding side structures load the dummy in FMVSS 214 and other side-impact tests is likely to decrease. For these reasons, there is a need to characterize human impact response for low-speed nearside impact conditions using non-rigid impact surfaces.

To address this need, a series of side-impact tests was performed with seven whole cadavers using a sled-to-sled side-impact test facility (Miller and Rupp 2011). A padded segmented “impact wall” with a 5.1-cm abdomen offset attached to one sled was used to separately load the thorax, abdomen, iliac wing, greater trochanter, and thigh of a subject seated on the other sled. Sizes and locations of the impactor segments used to load different parts of the body were scaled with subject anatomy so the same anatomic regions were loaded in tests of different sized cadavers. Cadavers were impacted on one side of the body with an initial loading velocity of 3 m/s and on the contralateral side with an initial loading velocity of 8 m/s. These impact velocities represent the lowest and mean ± 1 SD door velocities at the time of crash-dummy contact measured in a series of SNCAP moving-deformable-barrier tests of passenger cars performed between 1998 and 2005. CT scans of the cadavers were performed before and after the 3-m/s test to verify that rib fractures were not pre existing or produced by the low-speed test. Fifty-nine channel chestbands were used to measure deformation histories of the thorax and abdomen during impact loading. Responses from these tests were normalized to midsize-male anthropometry and used to generate ± 1 SD corridors using the methods described by Maltese et al. (2002).

This paper describes a series of lateral impact tests that were conducted to evaluate the response of the WorldSID midsize-male crash test dummy relative to 3-m/s and 8-m/s corridors reported by Miller and Rupp (2011).

METHODS

Similar to cadaver tests, the WorldSID (WSID) tests were performed using a custom-designed dual-sled impact facility consisting of a 725-kg impactor sled with a set of padded impactor surfaces that represent a generic door interior, and a second 360-kg occupant sled with the WISD positioned facing lateral to the direction of impactor loading. A rendering of this test facility is shown in Figure 1.

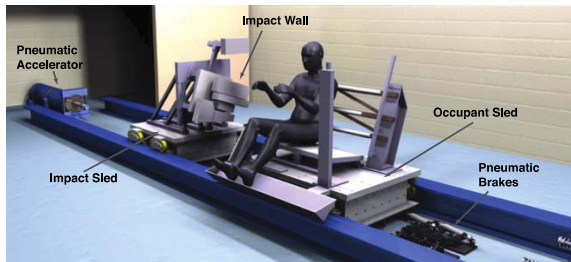


Figure 1. Rendering of the custom-designed dual-sled impact facility used for cadaver and WorldSID side-impact testing.

The process for conducting a test involved using a pneumatic accelerator to accelerate the impactor sled to a pre-impact velocity of 3 m/s, 8 m/s, or 10 m/s. The first two velocities are the same as those used by Miller and Rupp (2011) to develop cadaver response corridors. The 10-m/s test velocity was selected because an ongoing series of side-impact cadaver tests will provide additional data that can be used to develop response corridors at this impact velocity. After reaching the target pre-impact velocity, the impactor sled contacted energy absorbing material on the occupant sled. The timing of this impact was set so that it occurred at the same time that the impactor contacted the WorldSID in the 8-m/s and 10-m/s tests. In the 3-m/s tests, the impactor contacted the WorldSID before the impactor sled contacted the occupant sled. For the 10-m/s and 8-m/s tests, aluminum honeycomb was used as the energy absorbing material to produce the desired impactor velocity profiles determined from analysis of a series of 1999-2005 NCAP side-impact tests (Miller and Rupp 2011). Figure 2 compares the impactor sled velocity profiles for the 10-m/s, 8-m/s and 3-m/s tests to mean ± 1 SD corridors of door velocities reported by Rupp and Miller (2011), and shows the timing of impactor and occupant sled contact for the three

impact velocities. Note that t_{zero} in Figure 2 is the time of WorldSID contact.

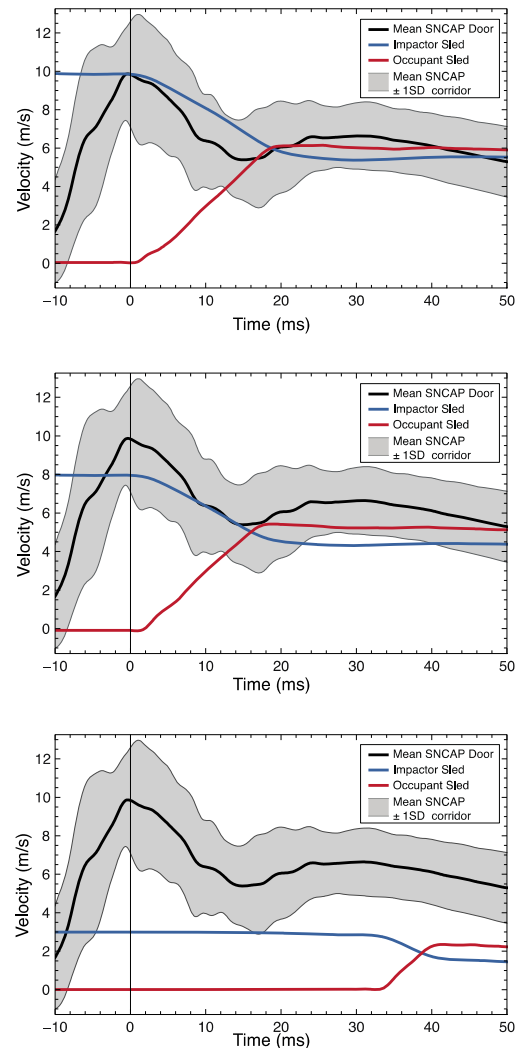


Figure 2. Comparison of impactor and occupant sled velocities to mean ± 1 SD SNCAP door velocity-time corridors for the 10-m/s (top), 8-m/s (middle), and 3-m/s (bottom) dual-sled tests.

The impact “wall” was segmented to allow independent measurement of loads applied to the thorax, abdomen, iliac wing, greater trochanter, and mid thigh. The positions and sizes of the load plates were set so that the plates contacted parts of the WorldSID corresponding to the body regions that were loaded in the cadaver tests. Forces applied to each of the body region were measured by load cells connected to 12.7-mm thick aluminum plates, and were inertially compensated using accelerometers attached to each loading plate. Each plate was

covered with 80-mm thick blocks of Microcell 1900 foam (72 kPa). The deflection of each block of foam was measured by a linear potentiometer that was mounted to the posterior surface of the load-cell plate with the end of the moving shaft connected to the anterior surface of the foam. This particular type of foam was selected because, as shown in Figure 3, when this foam was used in a series of pilot tests conducted using a SID Hybrid III in the 10 m/s impact condition, it resulted in pelvis and lower spine accelerations that were similar to those measured in the SNCAP tests from which the door velocity corridors were derived. In addition, cyclic compression testing where a block of the foam was repeatedly compressed to 20% of its pre-deformed height resulted in no change in force-deflection characteristics.

The WorldSID test matrix is shown in Table 1. Data and videos from all tests are available in the NHTSA biomechanics database, as are force-deflection characteristics of the foam padding used on the impactor surfaces. The abdomen, thorax, and pelvic responses of the WorldSID were calibrated before, in the middle of, and after the end of the test series. No body regions were found to be out of calibration in any of the calibration tests.

Table 1. WorldSID Test Matrix

| Impactor Velocity (m/s) | Chestband Location | Test IDs (NBAW10XX) |
|-------------------------|--------------------|---------------------|
| 3 | None | 07, 08, 25, 26 |
| 3 | Thorax | 30 |
| 3 | Abdomen | 15, 27 |
| 8 | None | 09, 10, 17, 20 |
| 8 | Thorax | 29 |
| 8 | Abd. | 16, 28 |
| 10 | Abdomen | 13, 14, 18, 19 |

All WorldSID tests used an impactor configuration in which the plate that loaded the abdomen was offset 5.1 cm towards the WorldSID from the other portions of the impactor, as shown in the illustration of Figure 4. A separate series of abdomen-plus-pelvis-offset tests was performed so that WorldSID responses can be compared to responses measured in an ongoing series of cadaver tests that uses an abdomen-plus-pelvis offset.

In a subset of ten tests, the external deflection of the thoracic and abdomen regions of the WorldSID were measured using a single 59-channel chestband. Separate tests were conducted to measure external abdomen versus the external thorax deflections due to

the limited number of available data-acquisition channels.

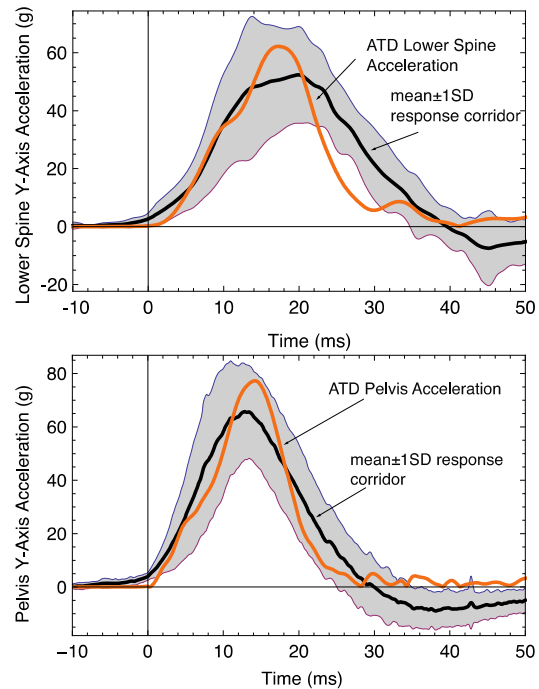


Figure 3. Comparison of WorldSID lower-spine (top) and pelvis (bottom) acceleration histories produced during a 10-m/s sled-to-sled impact to ± 1 SD response corridors developed from analysis of SNCAP data measured by a SID Hybrid III.

Images of the WorldSID configured for external thoracic and abdominal deflection measurements are shown in Figure 5. For tests where external thoracic deflection was measured, the chestband was wrapped around the exterior of the WorldSID at a level corresponding with the second and third thoracic ribs and aligned with the approximate center of the thoracic loading plate. The ends of the chestband were overlapped and secured with tape to prevent changes in the circumference of the chestband during the impact event. The portion of the chestband aligned with the ATD spine was attached to the spine box to provide a fixed reference point. The setup for the abdomen chestband experiments was similar to the thoracic chestband tests except that the chestband was positioned around the WorldSID abdomen ribs 1 and 2 and aligned with the center of the abdomen loading plate.

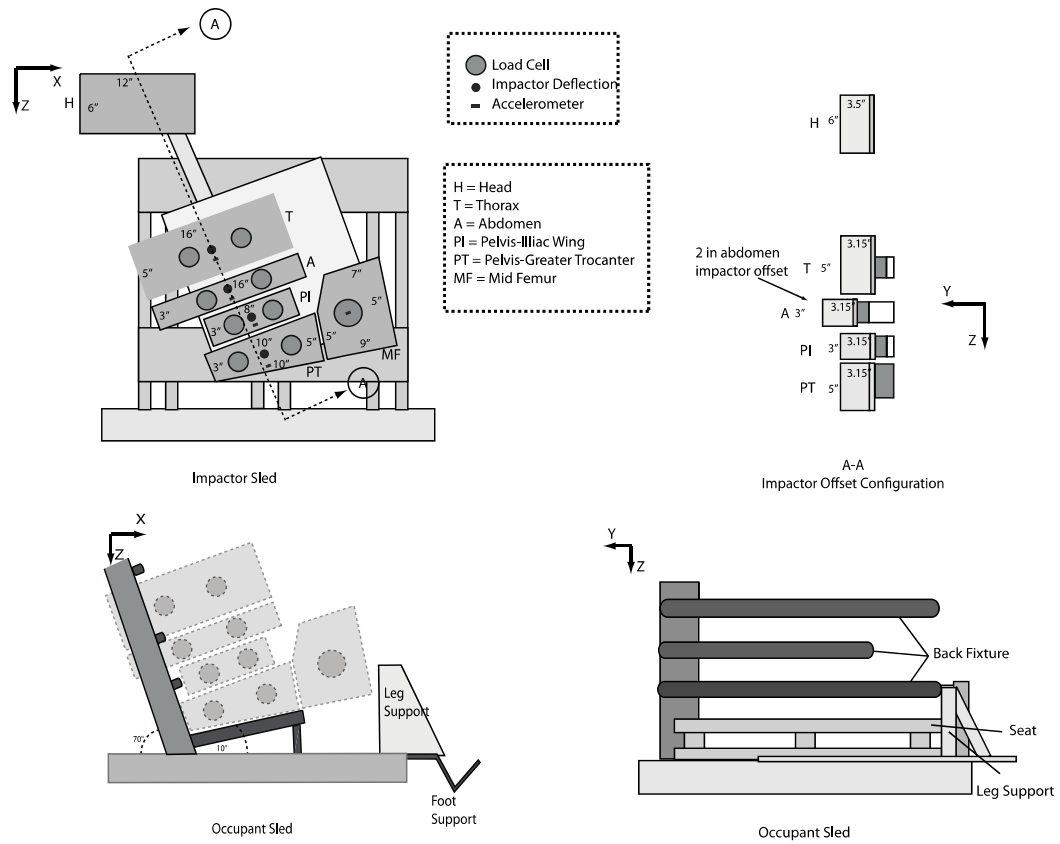


Figure 4. Illustration showing the configuration of the dual-sled door-shaped impactor on the impactor sled and the occupant sled.

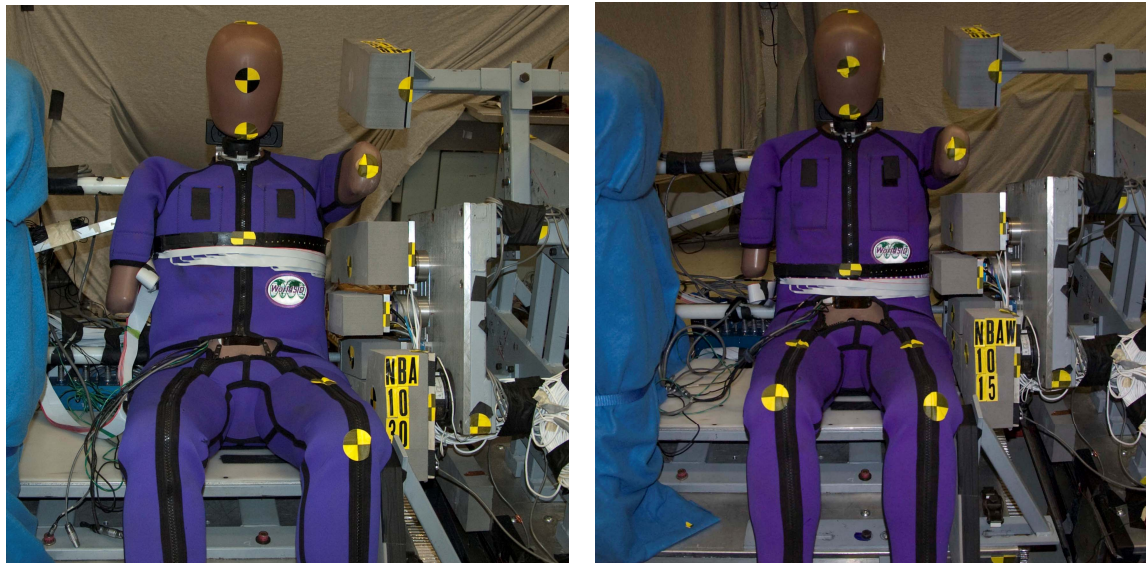


Figure 5. WorldSID configured for external thoracic (left) and abdominal (right) deflection measurements using the abdomen-offset impact condition and a single 59-channel chestband.

External deflections were calculated from chestband contours by using methods described by Pintar et al. (1997) and Maltese et al. (2002). These involve first defining a reference line connecting the point on the contour located at the spine and a point corresponding to the location of either the sternum or the anterior-most point on the abdomen. Next, vectors were defined that were perpendicular to these lines and passed through the lateral most points on the abdomen and thorax chestbands on the sides of the chestbands that interacted with the impactor. The change in the lengths of these vectors relative to their lengths at the time of impact were used to estimate half-thorax and half-abdomen deflection histories. Internal chest and abdomen deflections were calculated using measurements of rib motions made using IR-TRACCs.

RESULTS

Applied force histories at the five measured WorldSID regions (thorax, abdomen, iliac wing, greater trochanter, and mid thigh) as well as corresponding mean cadaver response and mean \pm 1 SD response corridors for the 3-m/s and 8-m/s tests are shown in Figure . Mean peak applied forces for 3-m/s and 8-m/s tests are listed in Tables 2 and 3, respectively.

Table 2. Mean WorldSID and Cadaver Peak Applied Forces from 3-m/s Tests

| Body Region | Applied Force | |
|--------------------|---------------|--------------|
| | WorldSID (kN) | Cadaver (kN) |
| Thorax | 1.2 | 1.3 |
| Abdomen | 1.9 | 1.5 |
| Iliac Wing | 0.74 | 0.73 |
| Greater Trochanter | 1.6 | 1.4 |
| Mid thigh | 2.1 | 1.5 |

Table 3. Mean WorldSID and Cadaver Peak Applied Forces from 8-m/s Tests

| Body Region | Applied Force | |
|--------------------|---------------|--------------|
| | WorldSID (kN) | Cadaver (kN) |
| Thorax | 2.5 | 2.9 |
| Abdomen | 3.2 | 2.8 |
| Iliac Wing | 1.6 | 1.3 |
| Greater Trochanter | 3.1 | 2.2 |
| Mid thigh | 4.1 | 2.4 |

For both the 3-m/s and 8-m/s tests, the magnitudes of peak force applied to the WorldSID and cadaver thoraces are similar. However, for the 8-m/s tests, the shape of the WorldSID thoracic response differs from that of the cadaver. Applied abdominal forces are slightly higher for the WorldSID than the cadaver during both the 3- and 8-m/s tests, with the percent difference being greater during the 3-m/s tests. WorldSID iliac wing and greater trochanter peak forces are similar to the cadaver peak forces for the 3-m/s tests with the WorldSID peak force leading the cadaver peak force slightly. These peak forces are higher for the WorldSID than the cadaver for the 8-m/s tests. Mid-thigh peak forces are higher for the WorldSID for both the 3-m/s and 8-m/s tests, with the difference being greater during the 8-m/s tests.

Table 4. Peak WorldSID and Cadaver Pelvis Y-Axis Accelerations

| Test Condition | Pelvis y-axis Accelerations | |
|----------------|-----------------------------|-------------|
| | WorldSID (g) | Cadaver (g) |
| 3 m/s | 18 | 14 |
| 8 m/s | 50 | 49 |

Pelvis y-axis accelerations for the WorldSID and cadaver are shown in Figure 7, and the mean peak values are listed in Table 4. WorldSID pelvis y-axis accelerations are slightly higher than the mean peak values for the cadaver for the 3-m/s tests, but are almost identical for the 8-m/s tests.

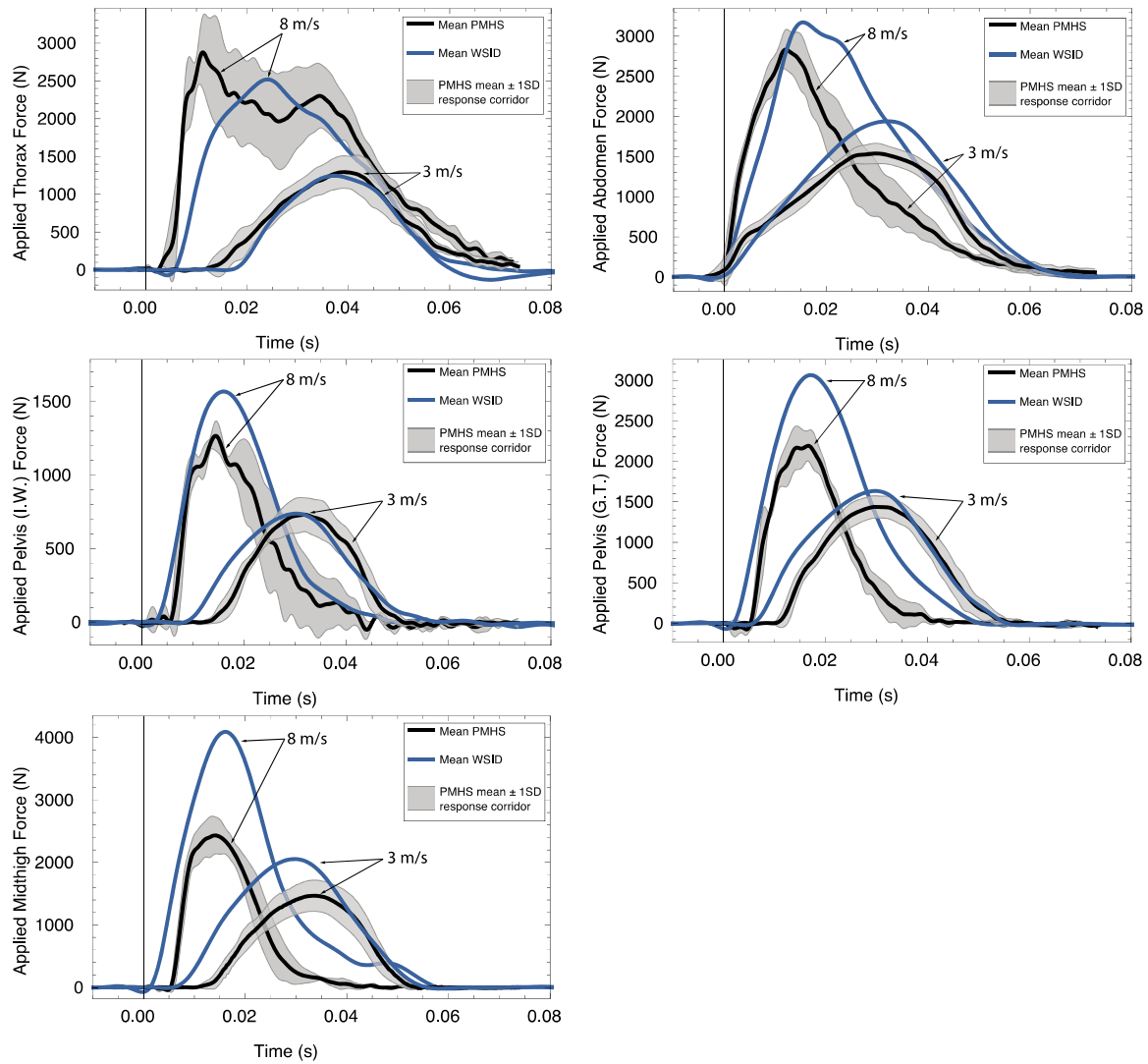


Figure 6. Applied force histories for the thoracic (top left), abdomen (top right), iliac wing (middle left), greater trochanter (middle right), and mid thigh (bottom left) for the 3- and 8-m/s tests.

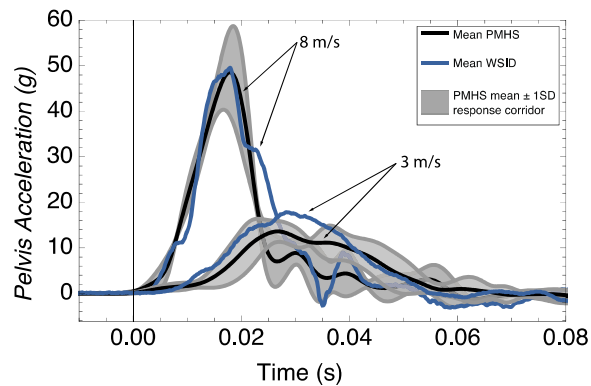


Figure 7. Comparison of WorldSID pelvis accelerations to mean ±1SD cadaver response corridors for 3-m/s and 8-m/s tests.

Figure 8 compares the WorldSID internal thoracic deflection measured by the IRTRACCs on the first and second thoracic ribs and chestband-measured WorldSID external thoracic deflection in the 3-m/s and 8-m/s tests to the associated cadaver corridors. Peak external thorax deflections for both the WorldSID and the cadaver are listed in Table 5. Chestband contours from the WorldSID thorax at the time of contact and at the time of peak deflection are shown in Figure 9 for both the 3-m/s and 8-m/s tests. Magnitudes of the external WorldSID deflections for both the 3-m/s and 8-m/s tests are less than the mean external deflection of the human cadaver for similar loading conditions.

Table 5. WorldSID and Cadaver Peak Internal and External Thoracic Deflections

| Test Condition | WorldSID | | Cadaver |
|----------------|---------------|---------------|---------------|
| | External (mm) | Internal (mm) | External (mm) |
| 3 m/s | 31 | 12, 10 | 47 |
| 8 m/s | 44 | 27, 23 | 54 |

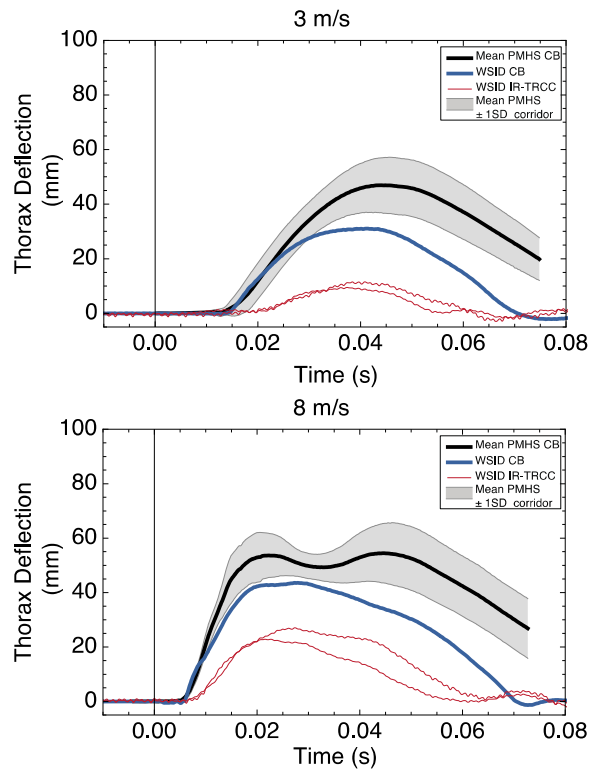


Figure 8. Comparison of mean cadaver and WorldSID thoracic deflection histories for the 3-m/s (top) and 8-m/s (bottom) tests.

Figure 10 compares WorldSID internal and external abdomen deflection histories measured in the 3-m/s and 8-m/s tests to the associated cadaver response corridors. External WorldSID deflections (blue line) and internal (red line) deflections of the first and second abdomen ribs are shown. Mean peak abdomen deflections for the WorldSID and cadaver tests are listed in Table 6. Peak values of the external WorldSID deflections for both the 3-m/s and 8-m/s tests are less than the mean peak external deflection of the human cadaver. The difference between peak external and internal WorldSID abdomen deflections is approximately 12 -13 mm, which is approximately equal to the thickness of the chest jacket.

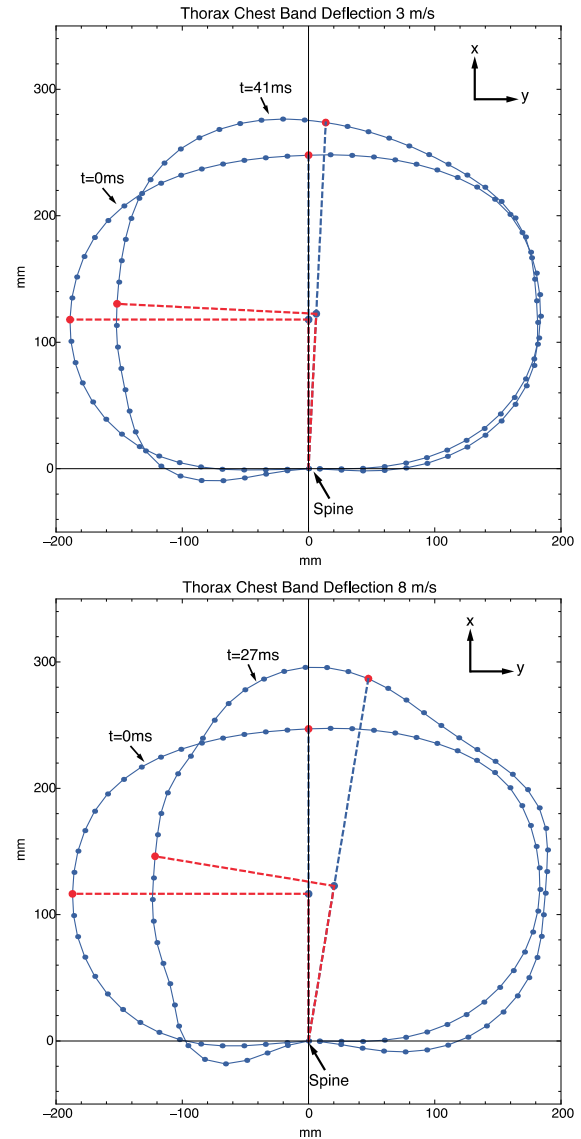


Figure 9. External WorldSID thorax chestband contours for the 3 m/s (top) and 8 m/s (bottom) at the time of abdomen contact and time of peak thorax deflection.

Table 6. WorldSID and Cadaver Peak Internal and External Abdomen Deflections

| Test Condition | WorldSID | | Cadaver |
|----------------|---------------|---------------|---------------|
| | External (mm) | Internal (mm) | External (mm) |
| 3 m/s | 29 | 18, 17 | 74 |
| 8 m/s | 48 | 36, 35 | 75 |

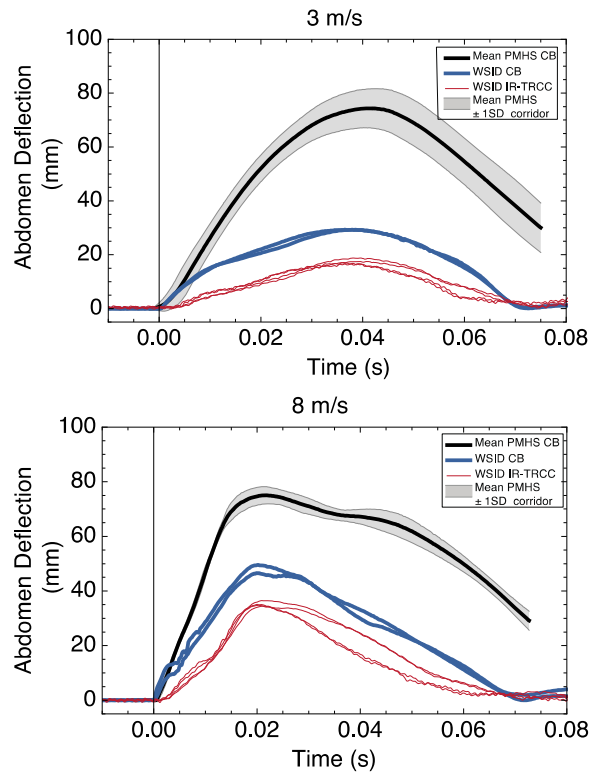


Figure 10. Comparison of internal and external abdomen deflection histories to cadaver abdomen deflection history corridor for the 3-m/s (top) and 8-m/s (bottom) tests.

Chestband contours of the external surface of the WorldSID abdomen at the time of loading and at the time of peak deflection are shown in Figure 11 for both the 3- and 8-m/s tests. External abdomen force-deflection responses from the WorldSID and cadaver tests at 3-m/s and 8-m/s are compared in Figure 12. WorldSID and cadaver external thoracic force-deflection responses from 3-m/s and 8-m/s tests are compared in Figure 13. In both cadaver and WorldSID force-deflection responses, there is force at zero deflection because abdomen and thorax impactor plates contacted parts of the abdomen and thorax before contacting the chestbands.

In general, the WorldSID abdomen is stiffer than the cadaver abdomen with the difference being greater for the 3-m/s tests than the 8-m/s tests. As indicated by Figure 6 and the force-deflection responses in Figure 10, this is primarily because the WorldSID abdomen does not deform as much as the cadaver abdomen under similar applied forces rather than the WorldSID abdomen producing higher impact forces than the cadaver abdomen.

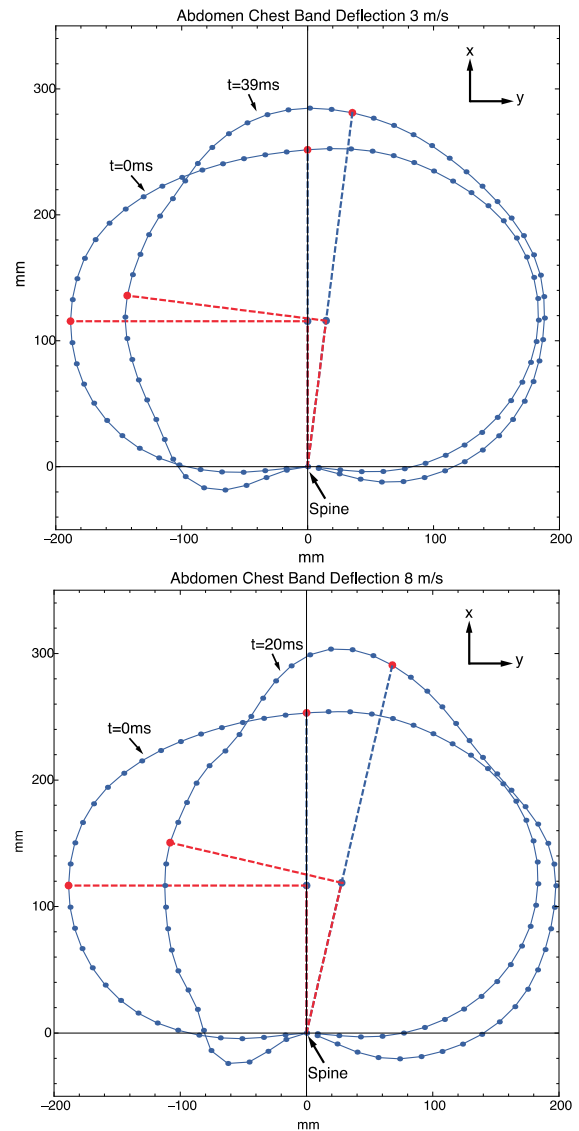


Figure 11. External WorldSID abdomen chestband contours for the 3-m/s (top) and 8-m/s (bottom) tests at the time of abdomen contact and at the time of peak abdomen deflection.

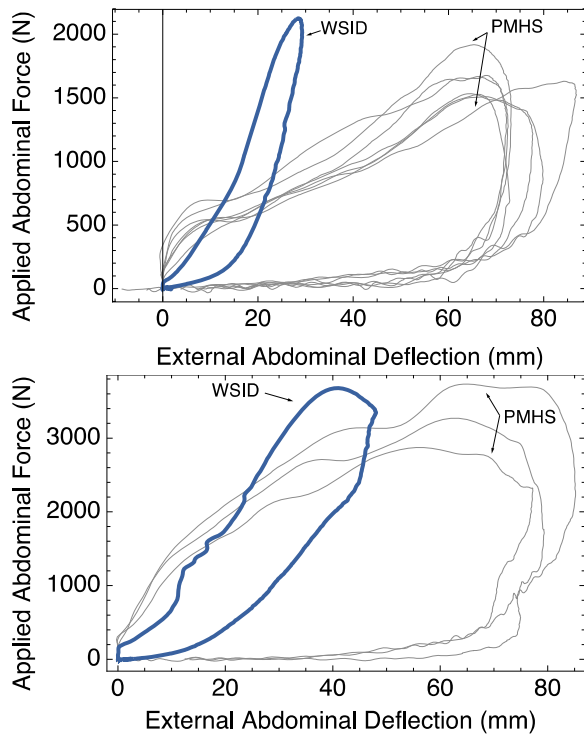


Figure 12. External abdominal force deflection curves for the 3 m/s (top) and 8 m/s (bottom) impact velocities.

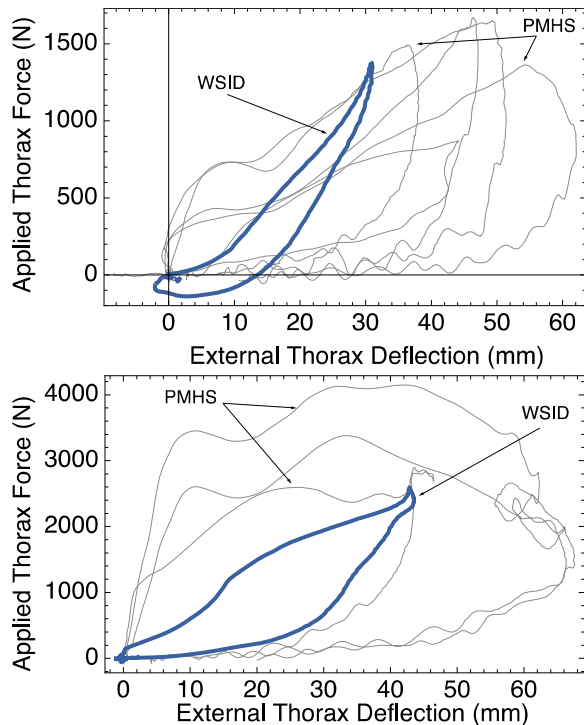


Figure 13. External thorax force deflection curves for the 3 m/s (top) and 8 m/s (bottom) condition.

DISCUSSION

In both the 3-m/s and 8-m/s tests, forces applied to the WorldSID abdomen were slightly greater than response corridors from cadavers, while peak deflection of the WorldSID abdomen was about half of the peak deflection of the cadaver abdomen. The combination of these observations indicates that the WorldSID abdomen lacks the rate sensitivity of the cadaver abdomen and therefore V*C measurements made with WorldSID may be questionable.

In the 3-m/s tests, WorldSID iliac wing and trochanteric peak forces were within, or slightly above, the cadaver response corridors, while in the 8-m/s tests, these WorldSID responses were both substantially above the cadaver response corridors. Coupled with the observation that WorldSID pelvis y-axis acceleration responses are above 3-m/s cadaver response corridors, but within the 8-m/s response corridors, this suggests that the WorldSID pelvis is too stiff and probably has too much tightly coupled mass.

The forces applied to the WorldSID thigh were higher than the forces applied to the cadaver thigh in both the 3-m/s and 8-m/s tests. This is partially because the WorldSID has more thigh flesh than most of the cadavers that were tested. As a result, the WorldSID thigh was loaded earlier in the impact than the cadaver thigh. However, the large differences between peak forces applied to the cadaver and WorldSID thighs also suggest that either the WorldSID thigh flesh is too stiff and/or the tight coupling between the femur and knee causes more mass coupling to the WorldSID thigh. This suggests the need for further research on the impact response of the thigh and leg with the lower extremities in a seated posture, particularly since ISO TR9790 doesn't provide impact response specifications for the thigh independently of the pelvis.

Peak forces applied to the WorldSID thorax in the 3-m/s and 8-m/s tests were generally within the cadaver response corridors, although the shape of the WorldSID applied thoracic force history produced in the 8-m/s test is different from the shape of the cadaver corridor. The peak external thoracic deflection of the WorldSID was also less than peak external thoracic deflections for the cadavers tested at 3 m/s and at the low end of the range of cadaver thoracic deflections produced in the 8-m/s tests. One potential explanation for this difference is that the WorldSID thoracic spine lacks the flexibility that is present in the cadaver thoracic spine and, as a result, WorldSID torso tends to tilt towards the impactor

rather than deforming around it like the cadaver torso.

The magnitude of the difference between the peak external and internal deflections of the WorldSID abdomen was approximately 12-13 mm, which is similar to the thickness of the chest jacket, suggesting that the measurements of WorldSID abdomen deflection are primarily due to compression of the chest jacket. In contrast, the difference between peak internal and external WorldSID thorax deflections was approximately 20 mm, which is larger than the thickness of the chest jacket. One reason for this difference may be the chest jacket slipping relative to the ribs, such that the chestband remains more aligned with the axis of motion of the plate that loads the thorax than do the ribs. Multipoint 3D chest deflection measurements have the potential to help resolve this issue.

Some part of the response differences between the WorldSID and cadavers is due to variations in load sharing among body regions that occur from differences in external body contours. Specifically, the cadaver abdomen tends to protrude laterally more than the WorldSID abdomen, the WorldSID thorax is less tapered than the cadaver thoraces, and the WorldSID thigh flesh is slightly thicker than the cadaver thigh flesh. The former and latter of these observations likely result from the ages and sizes of the cadavers used to develop the response corridors. These cadavers were slightly heavier than the WorldSID and, as a result, had slightly wider abdomens. Cadavers were also generally older, which tends to result in lower amounts (thickness) of thigh flesh.

CONCLUSIONS

The responses of the WorldSID midsize-male thorax, abdomen, iliac wing, greater trochanter, and mid thigh were measured in a series of nearside-occupant sled-to-sled impact tests. The WorldSID was loaded with a segmented padded impactor with a 5.1-cm abdomen offset at initial velocities of 3-m/s and 8-m/s. These responses were compared to mean \pm 1SD response corridors developed from cadaver tests conducted using similar loading conditions.

Comparisons between WorldSID and cadaver responses suggest that:

- the WorldSID abdomen is stiffer and less rate sensitive than the cadaver abdomen, and that

- the WorldSID pelvis is likely stiffer than the cadaver pelvis and has more tightly coupled mass.

ACKNOWLEDGMENTS

This research was funded by the National Highway Traffic Safety Administration under contract number DTNH22-10-H-00288. The authors are grateful to Rodney Rudd and Steve Ridella for their advice on all phases of this project.

REFERENCES

ISO/TC22/SC12/WG5, Technical Report 9790 – Road Vehicles – Anthropomorphic Side Impact Dummy – Lateral Impact Response Requirements to Assess the Biofidelity of the Dummy, 2000.

Maltese, M., Eppinger, R., Rhule, H., Donnelly, B., Pintar, F., & Yoganandan, N. (2002). Response corridors of human surrogates in lateral impacts Stapp Car Crash Journal 46:321-351.

Miller, C.S. and Rupp, J.D. (2011). PMHS impact response in low and high-speed nearside impacts. UMTRI Report 2011-10. University of Michigan Transportation Research Institute, Ann Arbor, MI.

Pintar, F. A., Yoganandan, N., Hines, M. H., Maltese, M. R., McFadden, J., Saul, R., Eppinger, R., et al. (1997). Chestband Analysis of Human Tolerance to Side Impact. Society of Automotive Engineers, Warrendale, PA.

REAL WORLD OLDER OCCUPANT CRASH DATA AND SENSITIVITY OF THOR-NT AND WORLDSID DUMMY THORACES

Heather Rhule

National Highway Traffic Safety Administration

Ann Mallory

Alena Hagedorn

Transportation Research Center Inc.

United States

Paper Number 11-0397

ABSTRACT

Thoracic injury to elderly occupants in motor vehicle crashes is a serious concern. If these injuries to elderly occupants are to be reduced, several things need to be considered: 1) How is crash severity (Delta V) related to serious thoracic injury of older occupants? 2) Are crash test dummies sensitive enough for use in estimating thoracic injury risk to older occupants? and 3) What are the injury measurements in advanced dummies related to injury risk for older occupants?

Analysis of National Automotive Sampling System Crashworthiness Data System (NASS CDS) cases was performed to study the relative risk of serious thoracic injury among younger and older males and females, examine the distribution of Delta V (velocity change) for older occupants with serious thoracic injury, and identify Delta V's with the largest percentage of older occupant serious thoracic injury cases in frontal and side impacts. Cases of occupants in motor vehicle crashes were drawn from NASS CDS for vehicle model years 1997-2008 for side impacts (all seat positions) and for vehicle model years 1994-2008 for frontal impacts (front seat only). Age groups utilized for data analysis included 20-39 and 65+ for side impacts and 20-39 and 60+ for frontal impacts.

To evaluate sensitivity of current midsize male crash test dummies, certification-type pendulum impacts to the thorax of the Thor-NT and the WorldSID dummies were conducted at impact velocities between 1.0 and 6.5 m/s.

Age-adjusted injury risk curves for the WorldSID midsize male were generated based on data by Petitjean et al. (2009). Injury risk curves for the Thor-NT dummy are not yet available.

Results of the current study show that occupant gender has a negligible effect on injury vulnerability in side impacts, whereas in frontal impacts, gender

appears to play a more important role than age. In recent model year vehicles, the distribution of Delta V for older occupants with serious thoracic injury was approximately 10 km/h lower than that for seriously injured younger occupants in side impacts, but they were similar among seriously injured older and younger occupants in frontal impacts. The rate of older female injury was 6.5 times higher than that for younger females in frontal impacts, warranting further research. In real-world side impacts, 70% of older occupants with serious thoracic injuries were in crashes with a Delta V of 26 +/- 10 km/h in the current data set. In real-world frontal impacts, 42% of older occupants with serious thoracic injuries were in crashes with a Delta V of 29 +/- 10 km/h in the current data set. The WorldSID and Thor-NT dummies demonstrate excellent sensitivity and could potentially be used for evaluating injury risk for elderly occupants in lower severity impact tests. Injury risk curves for the WorldSID dummy have been generated for 65 year old mid-sized male occupants, from which a risk level can be established for use in evaluating injury risk to older occupants in side impact.

INTRODUCTION

Thoracic injury to elderly occupants in motor vehicle crashes is a serious concern. Although older occupants travel fewer miles, are involved in fewer crashes (Cerelli, 1998), and are more likely to be belted than younger occupants (Kent et al., 2005; NHTSA, 2009), the relative rate of serious injury and/or fatality is higher for older occupants than younger occupants (Kent et al., 2005; Evans, 2001; Zhou et al., 1996, Welsh, et al., 2006). Kent et al. (2005) also found that of the injuries sustained by drivers in fatal frontal impacts, the majority of injuries were to the chest for older drivers and to the head for younger drivers. Similarly, Morris et al. (2003) found that the chest was more frequently seriously injured in frontal crashes than the head for older occupants. In addition, Augenstein et al. (2005) found that the chest is the most frequently injured

body region for older occupants in frontal and near-side crashes. If these serious thoracic injuries to elderly occupants are to be mitigated, several things need to be considered before developing a crash test for older occupants. First, how is crash severity (Delta V) related to serious thoracic injury of older occupants? Second, are crash test dummies appropriately sensitive to be used for estimating thoracic injury risk to older occupants? And third, are there injury risk curves available for estimating thoracic injury risk of older occupants based on crash test dummy deflections?

METHODS

Real World Older Occupant Crash Data

To identify the relative risk of serious thoracic injury among younger and older males and females and to examine the range of velocity change (Delta V) for seriously injured older occupants, real-world crash data was analyzed. A dataset from the National Automotive Sampling System Crashworthiness Data System (NASS CDS) was selected utilizing the following search criteria:

- NASS CDS crash years 1993-2008
- Front and side crashes
- Model years 1994-2008 for frontal crashes; 1997-2008 for side crashes
- Age groups: Frontal crashes – “younger” = 20-39 years old and “older” = 60+ years old; side crashes – “younger” = 20-39 and “older” = 65+
- Front seat occupants only for frontal crashes
- All seat positions included for side impact crashes (near and far side included)
- Primary event rollovers were excluded by rejecting any crash where the primary damage (variable TDD1) was overturn damage.
- No ejections
- Occupants with number of injuries coded as injured with severity unknown (INJNO=97) were excluded.
- For analyses using Delta V, cases with unknown Delta V were excluded.
- For analyses using occupant gender, cases with unknown gender were excluded.

Frontal impacts were those with direction of force (DOF1) from 11 o'clock to 1 o'clock, as well as those at 10 or 2 o'clock only if the general area of damage (variable GAD) was to the front of the vehicle. Side impacts were defined as all other cases with direction of force from 2 to 4 o'clock and 8 to 10 o'clock. The model years and age groups selected

for frontal and side impacts were chosen based on an analysis of the rates of serious thoracic injury. Serious thoracic injury cases were identified by AIS (Abbreviated Injury Scale) codes in NASS CDS, which were based on the Association for the Advancement of Automotive Medicine's AIS-90 from 1993 to 1999, and on AIS-90/98 Update from 2000 to 2008. Serious injuries are those with AIS score of 3 to 6. Analysis was performed with SAS statistical software, Version 9.2 (SAS Institute Inc, Cary, NC). Standard errors were calculated for the rate estimates using SAS's survey analysis procedures to account for the variance in the weighting of CDS cases and reflected the estimated error that occurs as a result of using probability sampled case data.

The following data analyses were performed on the weighted data from the selected datasets for front and side impacts:

- Rate of serious thoracic injury cases were estimated by age group and gender.
- The cumulative distribution of Delta V among all serious thoracic injury cases was estimated by age group and by gender.

In addition, in order to illustrate the frequency of crashes in the Delta V ranges where injuries are occurring most frequently, the cumulative Delta V distribution of all front and side crashes, whether injury occurred or not, was estimated by age group for NASS CDS crash years 2006-2008, without regard to vehicle model year. All other inclusion criteria were the same as that used for serious injury cases described previously. Crash years 2006-2008 were used in order to obtain more recent crash exposure data.

Sensitivity of Thor-NT and WorldSID Dummy Thoraces

In order to determine whether the Thor-NT and WorldSID dummy thoraces were sensitive, the dummies were each subjected to certification-type pendulum impacts at various energy levels. The WorldSID was tested without the arm and the Thor-NT was tested in the upper thorax region. Both dummies were tested using a 23.4 kg mass pendulum with 152.4 mm diameter face. Before sensitivity tests began, each dummy was subjected to its thorax certification test to establish acceptable performance. Each of these certification tests was conducted at the prescribed velocity range of 4.2-4.4 m/s. Once dummy performance was deemed acceptable per the certification responses, the dummies were tested at velocities above and below that of the certification

test, ranging from approximately 1 to 6 m/s. The tests followed the procedures prescribed in each dummy’s certification manual (GESAC, 2005; ISO, 2009), with the exception of the impact velocity.

Transducer data from the dummy tests were recorded according to the digital data sampling requirements of SAE J211-1 (SAE, 2003). Following acquisition, all transducer data were processed in software as follows:

- WorldSID IR-Tracc displacements – filtered at CFC 600
- Pendulum force, Thor-NT upper thorax left and right crux displacements, WorldSID spine lateral accelerations – filtered at CFC 180
- Thor-NT left and right crux displacements were processed using THORTEST software (GESAC, 2010) and averaged together to obtain total chest deflection, per the Thor Certification Manual (GESAC, 2005).

Injury Risk Curves

In order to determine how injury measurements in advanced dummies are related to injury risk for older occupants, age-adjusted injury risk curves for the appropriate dummy needed to be generated. Petitjean et al. (2009) presented thoracic injury risk curves (and the data used to generate them) scaled to a 45 year old for the WorldSID midsize male side impact dummy. As part of that analysis, a relationship among post mortem human subject (PMHS) injury, WorldSID thorax deflection and PMHS age was established and the linear regression coefficients were reported (Equation 1, Petitjean et al., 2009).

$$AIS_x = a * WSD_x + b * Age_x + c \quad (1).$$

where AIS_x = the injury severity for PMHS subject x
 Age_x = the age of PMHS subject x
 WSD_x = scaled WorldSID deflection corresponding to PMHS subject x
 $a = 0.066, b = 0.044, c = -4.077$.

In the current study the relationship and coefficients established by Petitjean et al. in Equation 1 were used to generate age-adjusted WorldSID deflections for a given level of risk for a 20 year old, a 65 year old and a 75 year old. For example, for two PMHS having the same injury severity (AIS), where one is 65 years old (left side of Equation 2) and the other is X years old (right side of Equation 2), then:

$$a * WSD_{65} + b * 65 + c = a * WSD_x + b * X + c \quad (2).$$

$$WSD_{65} = WSD_x + (b/a) * (X - 65)$$

$$WSD_{65} = WSD_x + (0.044/0.066) * (X - 65)$$

The age-adjusted scaled WorldSID deflection data for a 20-, 65- and 75-year old, paired with the corresponding PMHS injuries, were used in performing survival analysis with Weibull distribution to generate injury risk curves for the three ages. The age adjustment was performed prior to the survival analysis, rather than as a variable in a multivariate survival analysis, in order to follow the same method as in Petitjean et al. Appendix A shows the data utilized from Petitjean et al., the age-adjusted scaled WorldSID deflections, and the resulting scale and intercept values from the survival analysis which were used to generate the risk curves.

Injury risk curves for the Thor-NT dummy thorax response do not exist at the current time.

RESULTS

Real World Elderly Crash Data

Tables 1 and 2 show the number of raw and weighted serious thorax injury cases for side and front impacts, respectively, utilized from NASS CDS. In addition, for the analyses that used Delta V, the percentage of cases with known Delta V is indicated in Tables 1 and 2.

Rate of Serious Thoracic Injury Figure 1 shows the rate of serious thoracic injury for younger and older females and males in front and side crashes, where the rate of injury is the number of occupants with at least one serious thoracic injury in a given age/gender/crash mode bin divided by the number of occupants in the bin.

Table 1.
Number of raw and weighted occupants with at least one serious thorax injury (AIS 3+) for selected side crashes by age group and gender

| Impact Mode | Side | | | | | |
|---|-----------------|-----|------|-------------|-----|-----|
| | Younger (20-39) | | | Older (65+) | | |
| Age Group | | | | | | |
| Gender | M | F | B | M | F | B |
| n (Raw) | 142 | 109 | 251 | 65 | 67 | 132 |
| n (Weighted) 1000's | 8.7 | 5.5 | 14.2 | 4.9 | 4.3 | 9.2 |
| % of (Weighted) Occupants in Crashes with Known Delta V | 73 | 82 | 77 | 94 | 89 | 92 |

M = male; F = female; B = male & female

Table 2.
Number of raw and weighted occupants with at least one serious thorax injury (AIS 3+) for selected frontal crashes by age group and gender

| Impact Mode | Front | | | | | |
|---|-----------------|------|------|-------------|------|------|
| | Younger (20-39) | | | Older (60+) | | |
| Age Group | | | | | | |
| Gender | M | F | B | M | F | B |
| n (Raw) | 377 | 220 | 597 | 180 | 194 | 374 |
| n (Weighted) 1000's | 21.7 | 11.7 | 33.4 | 12.0 | 16.8 | 28.8 |
| % of (Weighted) Occupants in Crashes with Known Delta V | 55 | 62 | 58 | 54 | 67 | 62 |

M = male; F = female; B = male & female

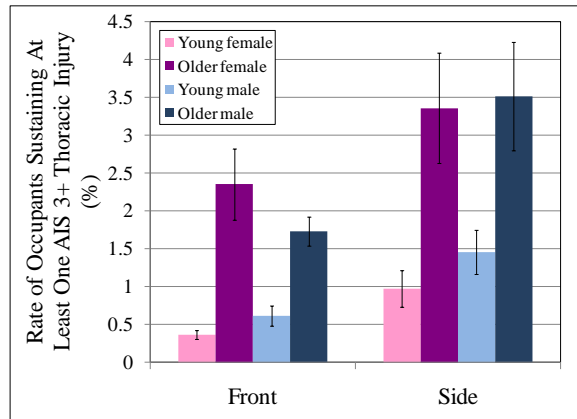


Figure 1. Rate of serious thorax injury for younger and older females and males in front and side impacts (with standard error).

The following observations can be made from Figure 1.

- The injury rate for side impact is higher than that for frontal impact for each occupant age/gender group.
- The injury rates for older occupants are significantly higher than those for younger occupants in both side and front impacts, regardless of occupant gender.
- In side impacts the injury rates for older men and women are approximately the same.
- The injury rate of older women is 6.5 times that of younger women in frontal impacts, whereas the older-to-younger ratios for all other occupant groups are in the vicinity of three (Table 3).

Table 3.
Relative injury rate between older and younger occupants

| Relative injury rate = older rate/younger rate | | |
|--|-------|------|
| | Front | Side |
| Female | 6.5 | 3.5 |
| Male | 2.8 | 2.4 |

Occupant Age, Delta V and Serious Thoracic Injury Figure 2 shows the cumulative distribution of Delta V in serious thorax injury cases for younger (red line) and older (blue line) occupants in side impacts (all seat positions). Fifty percent of older occupants with serious thoracic injury were in crashes with Delta V of 25 km/h or below. Fifty percent of younger occupants with serious thoracic injury were in crashes with Delta V of 35 km/h or below. The 25th and 75th percentile Delta V's for seriously injured older occupants were approximately 10 km/h lower than those of seriously injured younger occupants. The Delta V range for the lowest 25% of seriously injured older occupants was between 10-17 km/h, compared to 16-29 km/h for seriously injured younger occupants.

Figure 3 shows the cumulative distribution of Delta V in serious thorax injury cases for younger (red line) and older (blue line) occupants in the front seat only in frontal impacts. The median Delta V for older occupants with serious thorax injury in frontal impacts is 38 km/h, compared to 41 km/h for younger occupants with serious thorax injury. The 25th and 75th percentile Delta V's for seriously injured older occupants were approximately 2-4 km/h lower than those for seriously injured younger occupants.

Occupant Age and Gender, Delta V, and Serious Thoracic Injury Figure 4 shows the cumulative distribution of Delta V in serious thorax injury cases for younger and older males and females in side impacts (all seat positions). The median Delta V's for seriously injured younger and older males (dashed lines) are 36 and 24 km/h, respectively, compared to 34 and 25 km/h for seriously injured younger and older females (solid lines), respectively. The median Delta V's for male and female occupants (per age group) are not very different from the median Delta V's for younger and older from Figure 2. The same general trend from Figure 2 is evident among seriously injured older and younger males and females in side impact: the Delta V's for older males and females with serious thoracic injury are approximately 10 km/h lower than those for younger males and females with serious thoracic injury.

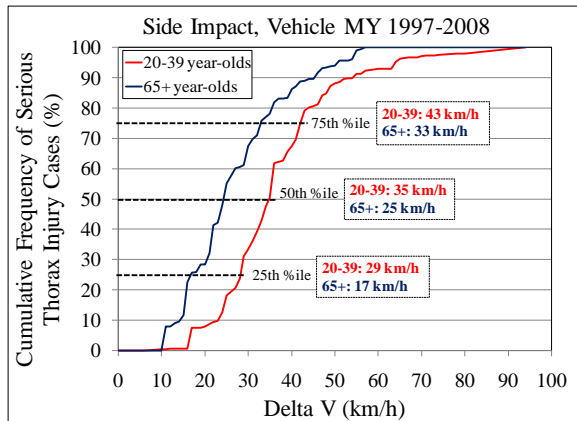


Figure 2. Cumulative Delta-V distributions for younger and older occupants with serious thoracic injuries in real world side impacts in vehicles with model years 1997-2008.

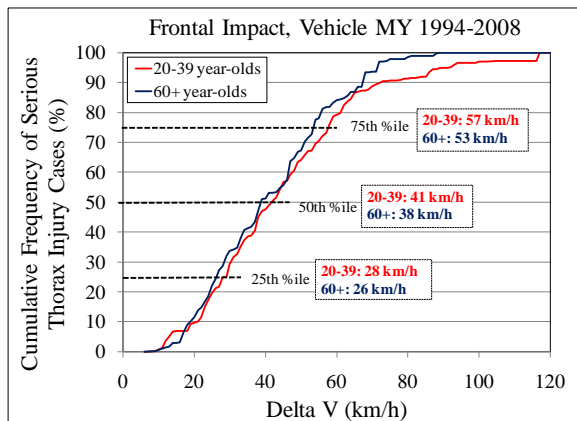


Figure 3. Cumulative Delta-V distributions for younger and older front seat occupants with serious thoracic injuries in real world frontal impacts of vehicles with model years 1994-2008.

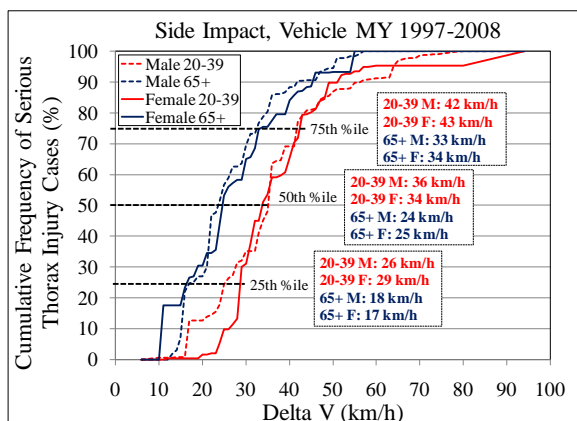


Figure 4. Cumulative Delta-V distributions for younger and older males and females with serious thoracic injury in real world side impacts in vehicles with model years 1997-2008.

Figure 5 shows the cumulative distribution of Delta V in serious thorax injury cases for younger and older males and females in the front seat in frontal impacts. Among seriously injured younger occupants (red curves) in frontal impacts, the median Delta V is 44 km/h for men and 37 km/h for women. The 25th and 75th percentile Delta V's for younger female occupants with serious thorax injury were approximately 9-13 km/h lower than those of younger male occupants with serious thorax injury.

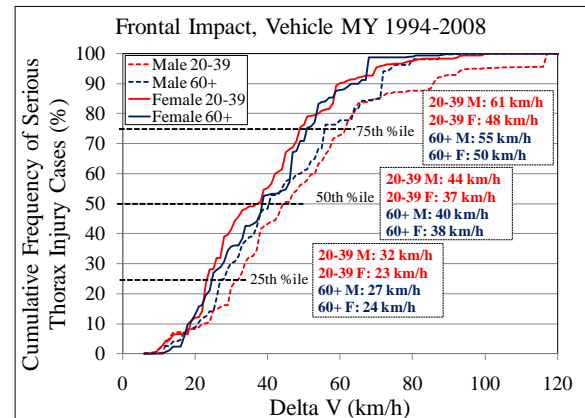


Figure 5. Cumulative Delta-V distributions for younger and older males and females with serious thoracic injury in real world frontal impacts in the front seat of vehicles with model years 1994-2008.

Among seriously injured older occupants (Figure 5, blue curves) in the front seat in frontal impacts, the median Delta V is 40 km/h for men and 38 km/h for women. The 25th and 75th percentile Delta V's for older female occupants with serious thorax injury were approximately 3-5 km/h lower than those of older male occupants with serious thorax injury.

Among seriously injured females, (Figure 5, solid curves) in frontal impacts, the median Delta V is 37 km/h for younger females and 38 km/h for older females. The 25th and 75th percentile Delta V's were approximately the same for seriously injured younger and older females.

Among seriously injured males, (Figure 5, dashed curves) in frontal impacts, the median Delta V is 44 km/h for younger males and 40 km/h for older males. The 25th and 75th percentile Delta V's were approximately 5 km/h higher for seriously injured younger males compared to seriously injured older males.

Sensitivity of Thor-NT and WorldSID Dummy Thoraces

Tables 4 and 5 show peak responses for the measurements obtained during thorax pendulum tests with the WorldSID and Thor-NT, respectively. Table 4 shows that, for a range of impact velocities between 0.99 and 5.98 m/s, the WorldSID maximum rib deflections ranged from 4.1 to 58.8 mm, the maximum spine accelerations ranged from 2.7 to 24.2 g, and the maximum pendulum force ranged from 851 to 4663 N. Table 5 shows that, for a range of impact velocities between 1.30 and 6.59 m/s, the Thor-NT maximum upper thorax deflections ranged from 14.7 to 69.8 mm and the pendulum force at maximum deflection ranged from 718 to 5326 N.

Figure 6 shows peak force vs. impact velocity responses with 2nd order polynomial curves fit to each dummy's data. Figure 7 shows peak deflection vs. impact velocity responses with linear curves fit to each WorldSID rib deflection and to the Thor-NT average crux x deflection. Figure 8 shows peak spine

lateral acceleration responses at T4 and T12 for the WorldSID with linear curves fit to the data.

Injury Risk Curves

The resulting equations from the survival analysis using age-adjusted WorldSID deflections and PMHS injuries are shown in Appendix A. Figure 9 shows risk curves for AIS 3+ thoracic injury for a 20 year old, a 45 year old, a 65 year old and a 75 year old mid-size male, as a function of maximum WorldSID thorax or abdomen rib deflections in side impacts. The injury risk curves show, for example, that a WorldSID impact that produces 50 mm maximum deflection predicts a 29% risk of injury for a mid-size 45 year-old male and an 89% risk of injury for a mid-size 75 year-old male. A 50% risk of AIS 3+ thorax injury is associated with the following thoracic deflections measured by the WorldSID 50th percentile midsize male side impact dummy:

- 74 mm for a 20 year old,
- 57 mm for a 45 year old,
- 44 mm for a 65 year old,
- 37 mm for a 75 year old.

Table 4.
WorldSID Thorax Sensitivity Test Results

| | Velocity (m/s) | Upper Rib Deflection (mm) | Middle Rib Deflection (mm) | Lower Rib Deflection (mm) | T12 Y Acceleration (g) | T4 Y Acceleration (g) | Max Pendulum Force (N) |
|-------|----------------|---------------------------|----------------------------|---------------------------|------------------------|-----------------------|------------------------|
| | Filters | CFC 600 | CFC 600 | CFC 600 | CFC 180 | CFC 180 | CFC 180 |
| Specs | 4.2-4.4 | 33-43 | 35-43 | 32-40 | 14-22 | 14-20 | 3200-3800 |
| Data | 4.31 | 33 | 37 | 33 | 15 | 14 | 3764 |
| | 4.31 | 33 | 38 | 34 | 14 | 14 | 3769 |
| | 0.99 | 4.1 | 6.2 | 6.3 | 2.7 | 2.8 | 851 |
| | 1.50 | 8.1 | 10.7 | 10.1 | 4.0 | 4.7 | 1335 |
| | 1.51 | 8.1 | 10.0 | 10.2 | 4.5 | 4.8 | 1363 |
| | 1.97 | 12.6 | 15.4 | 14.5 | 5.9 | 6.5 | 1771 |
| | 2.50 | 14.8 | 18.8 | 17.8 | 8.3 | 8.6 | 2367 |
| | 2.50 | 15.3 | 19.6 | 18.1 | 7.5 | 8.4 | 2348 |
| | 2.99 | 21.2 | 24.9 | 22.7 | 9.5 | 9.9 | 2721 |
| | 3.00 | 17.5 | 21.8 | 21.5 | 12.0 | 10.0 | 2895 |
| | 3.61 | 26.8 | 31.0 | 29.4 | 11.2 | 11.5 | 3228 |
| | 3.81 | 29.1 | 32.7 | 30.9 | 12.4 | 12.5 | 3391 |
| | 3.99 | 31.4 | 35.3 | 33.1 | 13.0 | 12.6 | 3520 |
| | 4.70 | 37.9 | 41.0 | 36 | 15.4 | 15.6 | 3997 |
| | 5.18 | 43.4 | 46.0 | 40.6 | 18.8 | 18.5 | 4264 |
| | 5.64 | 52.1 | 53.1 | 46.5 | 20.3 | 19.8 | 4465 |
| | 5.98 | 55.2 | 58.8 | 52.1 | 24.2 | 21.3 | 4663 |
| Min | 0.99 | 4.1 | 6.2 | 6.3 | 2.7 | 2.8 | 851 |
| Max | 5.98 | 55.2 | 58.8 | 52.1 | 24.2 | 21.3 | 4663 |

Bold text indicates maximum rib deflection

Shaded rows indicate certification specs and data.

Table 5.
Thor-NT Thorax Sensitivity Test Results

| | Velocity (m/s) | Max. Avg. Upper Thorax X Deflection (mm) | Force at Maximum Average Deflection (N) |
|-------|----------------|--|---|
| Specs | 4.2-4.4 | 49.0 – 59.0 | 2450 - 2950 |
| Data | 4.4 | 49.1 | 2765 |
| | 1.30 | 14.7 | 718 |
| | 1.82 | 20.5 | 1032 |
| | 1.95 | 21.9 | 1060 |
| | 2.27 | 25.1 | 1207 |
| | 2.50 | 28.1 | 1366 |
| | 2.85 | 32.7 | 1500 |
| | 3.32 | 37.8 | 1884 |
| | 3.81 | 42.0 | 2211 |
| | 4.13 | 46.7 | 2579 |
| | 5.00 | 54.7 | 3397 |
| | 5.49 | 58.8 | 3875 |
| | 5.92 | 62.6 | 4440 |
| | 6.59 | 69.8 | 5326 |
| Min | 1.3 | 14.7 | 718 |
| Max | 6.59 | 69.8 | 5326 |

Shaded rows indicate certification specs and data

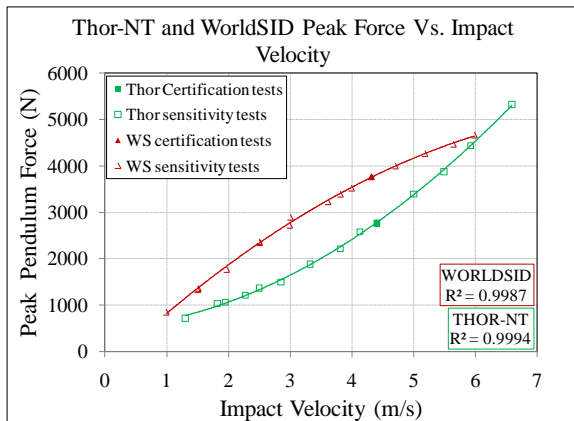


Figure 6. Peak pendulum force vs. impact velocity for Thor-NT and WorldSID thorax certification and sensitivity tests.

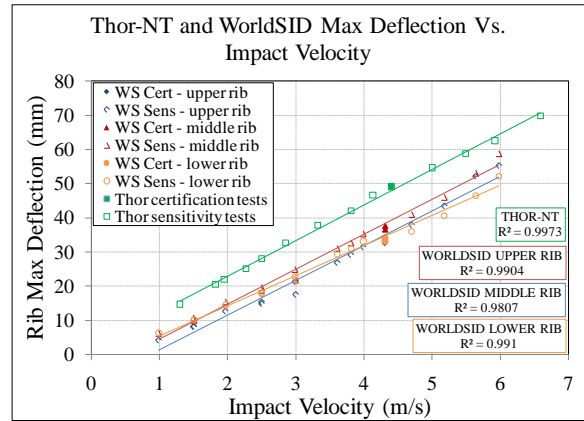


Figure 7. Peak thorax deflections vs. impact velocity for Thor-NT and WorldSID thorax certification and sensitivity tests.

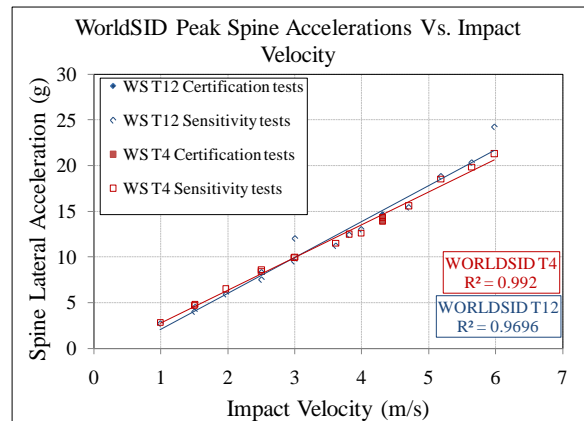


Figure 8. Peak spine lateral accelerations vs. impact velocity for WorldSID thorax certification and sensitivity tests.

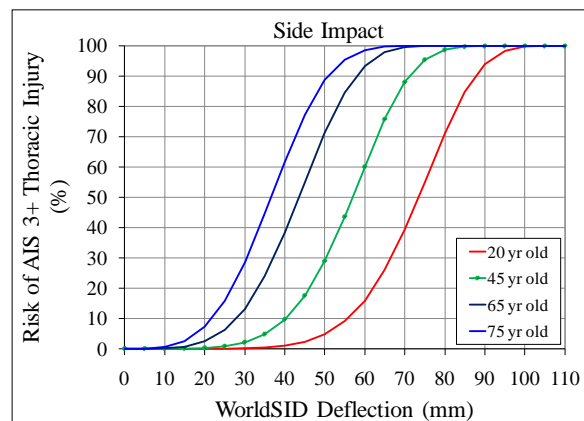


Figure 9. Risk of AIS 3+ thoracic injury for various ages of mid-sized male occupants as a function of maximum thorax or abdomen WorldSID deflection in side impact.

DISCUSSION

Real World Elderly Crash Data

Analysis of NASS CDS cases was performed to study the relative risk of serious thoracic injury among younger and older males and females, examine the Delta V for seriously injured older occupants and identify Delta V's with the largest percentage of older occupant serious thoracic injury cases in frontal and side impacts.

Rate of Serious Thoracic Injury The relatively increased injury rates for older occupants in the current study underscore the reported lower injury tolerance of older occupants relative to that of younger occupants (Evans, 2001; Zhou et al., 1996). In addition, the increased rates of serious thoracic injury in side impacts relative to front impacts in the current study supports that side impacts present a higher thorax injury risk for all age groups (NHTSA, 2009). However, in frontal impacts, the current study results showing that the rate of serious thoracic injury to older female occupants is 6.5 times greater than that to younger female occupants (Figure 1) is unexpected.

Accuracy of Delta V Funk et al. (2008) evaluated the magnitude of error in NASS-reported Delta V data. Delta V data for individual NASS cases were corrected for bias error, and distributions of Delta V data were corrected for scatter error. To illustrate the magnitude of the total error, Funk et al. calculated injury risk curves for frontal crashes as a function of age, gender, and belt use using the raw and corrected NASS Delta V data. The effect of the bias error and the effect of the scatter error in the NASS Delta V data counteracted each other. In spite of the considerable errors in the Delta V estimates in NASS, Funk et al. found that the risk curves calculated using uncorrected NASS data were generally accurate at low Delta Vs and somewhat conservative at higher Delta Vs. Therefore the Delta V distributions shown in the current study were analyzed without correction.

Effect of Vehicle Model Year On Serious Thoracic Injury In Frontal Crashes In frontal impact there is only a small difference in the distribution of Delta V's for older and younger seriously injured front seat occupants (Figure 3). In contrast, Kent et al. (2005) showed that for NASS CDS years 1992-2002 the distribution of Delta V for fatally injured older drivers (65+ years old) was in the range of 10 km/h lower than that of fatally injured younger (16-33 years old) drivers in frontal crashes;

however, early model vehicle years were not excluded. As a result, the Kent dataset is expected to describe a much earlier vehicle fleet than the current study which included only vehicle model years 1994 and newer (Figure 3). To illustrate the effect of limiting the current study to recent model year vehicles, Figure 10 shows the cumulative distribution of Delta V for older and younger occupants with serious thoracic injury in frontal impact in vehicles with model year between 1994-2008 (same as in Figure 3) and with model year previous to 1994.

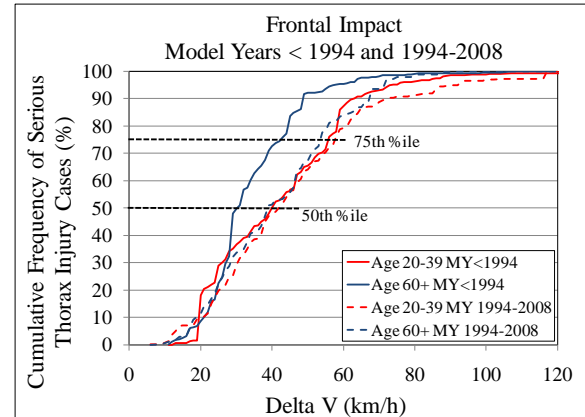


Figure 10. Cumulative Delta-V distributions for younger and older front seat occupants with serious thoracic injury in real world frontal impacts in vehicles with model years previous to 1994 and model years 1994-2008.

If model years prior to 1994 (solid lines, Figure 10) are compared to model years 1994-2008 (dashed lines, Figure 10) for front seat occupants in frontal crashes, a change is observed. For frontal crashes in older vehicles with Delta V > 29 km/h, a similar finding to that of Kent is illustrated in that the median Delta V for seriously injured older occupant crashes is approximately 10 km/h lower than that for younger occupants (Table 6). For the dataset that includes only vehicles from 1994 and more recent, it appears that this disparity between the Delta V's for younger and older seriously injured occupant crashes is greatly reduced. In addition, the median Delta V for serious thoracic injury crashes in frontal impacts is higher in the more recent model year vehicles than in the older model year vehicles (Table 6), especially for older occupants. This contrast suggests that vehicle design has had an effect on the frontal crash Delta V for occupants with serious thoracic injuries, in particular for those aged 60+.

The advent of frontal air bags and/or force-limiting belts may be partially responsible for the reduction in lower-speed injuries to the elderly in frontal crashes

(Morris et al., 2003). Due to the effect of more recent vehicle model year on older occupant serious thoracic injuries, further examination of the current frontal impact data set may include limiting the vehicle model years to even more recent, such as 2000+.

Table 6.
Delta V of 50th and 75th Percentiles of Cumulative Distribution of Front Seat Serious Thoracic Injury Cases in Frontal Crashes for Model Years 94-08 and Prior to 94

| Percentile | | Delta V (km/h) | | | |
|-------------|-------|------------------|-----|------------------|-----|
| | | 50 th | | 75 th | |
| Model Years | | 94-08 | <94 | 94-08 | <94 |
| Age | 60+ | 38 | 30 | 53 | 42 |
| Group | 20-39 | 41 | 39 | 57 | 55 |

Occupant Age and Gender, Delta V, and Serious Thoracic Injury When considering occupant gender in side impacts, the distributions of Delta V for older men and women with serious thoracic injuries are approximately the same; the same is true among younger men and women (Figure 4), indicating a negligible effect of occupant gender on an occupant’s vulnerability to injury in side impacts. However, the distributions of Delta V for side impact serious thoracic injury cases are lower for older males and females vs. younger males and females. These results may be indicative of the relative vulnerability of older occupants compared to younger occupants in side impacts.

In frontal impacts the effect of occupant gender appears to be more important than occupant age regarding the relative vulnerability of occupants (Figure 5). Among seriously injured female occupants in frontal impacts, the distributions of Delta V are approximately the same for younger and older ages. Among seriously injured male occupants, the distribution of Delta V for the older age group is slightly lower than that for the younger age group. The distribution of Delta V for seriously injured men is slightly higher than that for seriously injured women. These results may suggest that women are more vulnerable than men in frontal crashes, or perhaps the results may reflect the effect of occupant mass or occupant position/height relative to intruding structures. Additionally, restraint system components, such as force-limiting belts, may be tuned better to protect a larger occupant. These details concerning occupant size or mass, occupant position, contact surface and belt type/use deserve further examination, especially with regard to the elevated rate of serious thoracic injury to older females in frontal impacts as well as the lower Delta

V distribution for crashes with seriously injured younger and older women.

Range of Delta V’s For Older Occupants With Serious Thoracic Injury

The Delta V for the largest percentage of older occupants with serious thoracic injury was identified for front and for side impacts. A tolerance of +/- 10 km/h was utilized for selecting the range of Delta V that had the largest percentage of serious injury cases. In side impacts, because there is no significant difference in the Delta V distribution for seriously injured older male and female occupants, Delta V data for seriously injured older occupants in side impacts were not separated by occupant gender. In frontal impacts, because the difference was small between seriously injured older male and female occupants, Delta V data for seriously injured older occupants in frontal impacts were not separated by occupant gender. Figure 11 shows the cumulative frequency distributions of Delta V for all younger and older occupants who were in NASS CDS side crashes between 2006 and 2008, whether injury occurred or not (“exposed”, dashed lines). Figure 11 also shows cumulative Delta V distributions for seriously injured thorax cases for vehicle model years 1997-2008 (“injured”, solid lines, same as in Figure 2) by age in side impacts. The shaded region in Figure 11 highlights the range of Delta V for older occupants in which the largest percentage of serious injury cases occurred in side impact.

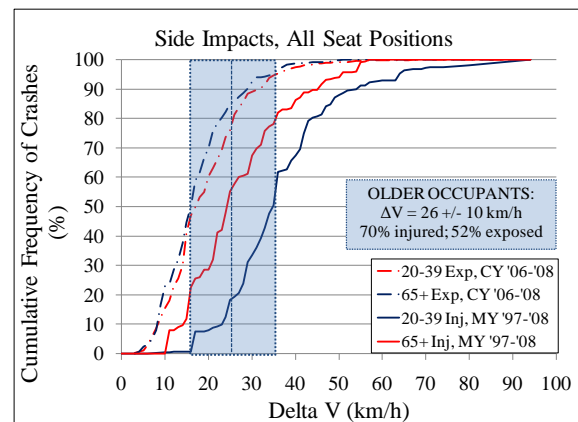


Figure 11. Cumulative distribution of Delta V for crashes with exposed (NASS CDS crash years 2006-2008) and seriously injured (NASS CDS model years 1997-2008) younger and older occupants in any seat position in side impact, shown with shaded area indicating the range of Delta V for which the largest percentage of older occupants with serious thoracic injury cases occurs.

Table 7 shows, for side and frontal impact, the range of Delta V with the largest percentage of older occupant serious thoracic injury cases, the percentage of older occupants seriously injured in that Delta V range and the percentage of older crash occupants exposed in that Delta V range.

Table 7.
Delta V +/- 10 km/h with Largest Percentage of Older Occupant Serious Thoracic Injury Cases in Side and Frontal Impact Crashes, Showing Percent Injured and Exposed in Given Delta V Range

| OLDER OCCUPANTS | Side Impact | Frontal Impact |
|-------------------------|-------------|----------------|
| ΔV Range (km/h) | 26 +/- 10 | 29 +/- 10 |
| % Injured | 70 | 42 |
| % Exposed | 52 | 31 |

In side crashes, 70% of older occupants with serious thoracic injury were in crashes with a Delta V of 26 +/- 10 km/h, which accounts for 52% of weighted NASS CDS older occupant side impact exposures (Figure 11, Table 7).

Figure 12 shows the cumulative frequency distribution of Delta V for all younger and older occupants who were in the front seat of NASS CDS frontal crashes between 2006-2008, whether injury occurred or not (“exposed”, dashed lines). Figure 12 also shows cumulative Delta V distributions for seriously injured thorax cases for vehicle model years 1994-2008 (“injured”, solid lines, same as in Figure 3) by age in frontal impacts (front seat only). The shaded region in Figure 12 highlights the range of Delta V in which the largest percentage of older occupant serious injury cases occurred in frontal impact.

In frontal crashes, 42% of seriously injured older occupants were in crashes with a Delta V of 29 +/- 10 km/h, which accounts for approximately 31% of weighted NASS CDS older occupant frontal impact exposures (Figure 12, Table 7).

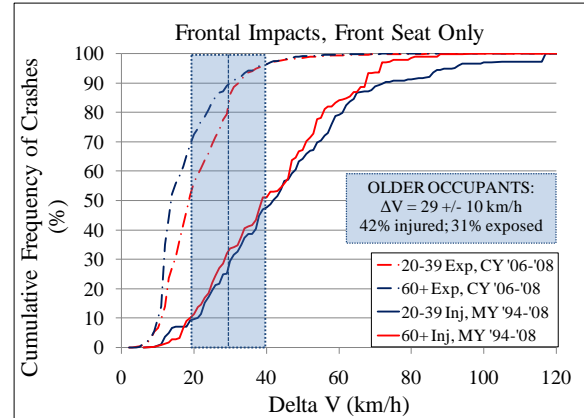


Figure 12. Cumulative distribution of Delta V for crashes with exposed (NASS CDS crash years 2006-2008) and seriously injured (NASS CDS model years 1994-2008) younger and older occupants in the front seat in frontal impact, shown with shaded area indicating the range of Delta V for which the largest percentage of older occupant serious thoracic injury cases occurs.

Summary The analysis of older occupant serious thoracic injury case data in NASS CDS showed the following observations:

- In both frontal and side impacts older occupants were more likely to sustain serious thoracic injuries vs. younger adults.
- Similar to younger occupants, older occupants were more likely to sustain serious thoracic injuries in side impacts vs. frontal impacts.
- The rate of older female injury was 6.5 times higher than that for younger females in frontal impacts, warranting further research.
- Occupant gender has a negligible effect on injury vulnerability in side impacts.
- In recent model year vehicles, the distributions of Delta V for older males and females with serious thoracic injury were approximately 10 km/h lower than those for seriously injured younger males and females in side impacts.
- In recent model year vehicles, Delta V's for seriously injured older occupants were similar to those of seriously injured younger occupants in frontal impacts. This finding is different from that of Kent (2005) who analyzed a dataset with older model year vehicles, indicating that model year plays a role in crash injury outcomes.
- In recent model year vehicles, the median Delta V for serious thoracic injury cases in

frontal impacts is higher than in older model year vehicles, especially for older occupants.

- In frontal impacts, the effect of occupant gender appears to be more important than occupant age regarding the relative vulnerability of occupants.
- In frontal impacts, Delta V's for females with serious thoracic injury were lower than those for seriously injured men.

Some of the most important observations from this NASS CDS study include:

1. Occupant size, seating position, contact surface and belt type deserve further examination, especially with regard to the elevated rate of serious thoracic injury to older females in frontal impacts as well as the lower Delta V for crashes with seriously injured younger and older women compared to seriously injured younger and older men.
2. In real-world side impacts, 70% of older occupants with serious thoracic injuries were in crashes with a Delta V of 26 +/- 10 km/h in the current data set.
3. In real-world frontal impacts, 42% of older occupants with serious thoracic injuries were in crashes with a Delta V of 29 +/- 10 km/h in the current data set.

NASS CDS Search Inclusion Criteria

Considerations In addition to limiting vehicle model year to 2000+ as previously mentioned, future NASS CDS data analysis may consider the effects of driver vs. front seat passenger and unbelted vs. belted vs. belted w/airbag deployment, as well as looking at occupant mass and height rather than gender for frontal impacts. Also, the effect of near side vs. far side seating position in side impacts could be investigated in order to gain further insight on crash and occupant characteristics that are associated with older occupant serious thoracic injury.

Sensitivity of Thor-NT and WorldSID Dummy Thoraces

In order to assess occupant injury risk in crash tests, the crash test dummy that predicts the injury level needs to be sensitive and biofidelic at the intended test severity level. If a low severity test were considered, the potential crash test dummies to be used need to be evaluated for sensitivity and biofidelity at this low severity level. There is a need for establishing human response in low severity impacts, especially among older occupants who sustain injury at a lower threshold, so that biofidelity

of the crash test dummies can be evaluated. The Thor-NT dummy exhibited thoracic deformation and kinematic responses similar to those observed in PMHS, with the exception of higher lap belt loads and pelvis accelerations, in 29 km/h Delta V sled tests (Forman et al., 2006). The WorldSID dummy achieved an overall biofidelity score of 8.0, indicating excellent biofidelity based on the ISO biofidelity ranking scheme, for tests outlined in ISO 9790 (ISO, 2009; ISO 1999).

The Thor-NT and WorldSID dummies demonstrate excellent sensitivity for the range of velocities experienced in the pendulum test condition. Since the dummies show linear relationships between deflection and impact velocity, these dummies could potentially be used for evaluating injury risk for older occupants. From the range of sensitivity tests performed the maximum WorldSID rib deflections of 4 and 59 mm are equivalent to 0% and 92% risk of AIS 3+ thoracic injury for a 65 year old midsized male, according to Figure 9, indicating that the dummy is sensitive enough to measure injury risk over a wide range of impact severities. Although risk curves have not been developed for the Thor-NT dummy to determine the corresponding range of risk levels, the wide range of deflection produced in sensitivity tests on the Thor-NT suggests that it also shows promise to predict risk over a wide range of impact severities.

Injury Risk Curves

For the WorldSID dummy, a 50% risk of AIS 3+ thoracic injury for a 65 year old occupant would be equivalent to 44 mm, 13 mm less than the current value for a 45 year old. However, in order to determine what level of risk would be appropriate for use in a crash test evaluation, it may be useful to examine the real-world rate of injury at the crash test speed. If IARV's in lower speed tests are set at less than 50%, the corresponding deflection limits could be determined from the risk-deflection relationship presented in this paper.

CONCLUSIONS

In real-world side impacts, 70% of older occupants with serious thoracic injuries were in crashes with a Delta V of 26 +/- 10 km/h in the current data set. In real-world frontal impacts, 42% of older occupants with serious thoracic injuries were in crashes with a Delta V of 29 +/- 10 km/h in the current data set. The WorldSID and Thor-NT dummies demonstrate excellent sensitivity and could potentially be used for evaluating injury risk for elderly occupants. Injury

risk curves for the WorldSID dummy have been generated for 65 year old mid-sized male occupants, from which an IARV can be established for use in evaluating injury risk to older occupants in side impact. Injury risk curves for the Thor-NT dummy are not yet available.

Additional research is warranted to determine why older females have such an increased rate of serious thoracic injury as well as a lower Delta V distribution compared to seriously injured men in frontal crashes. Variables that may be important in this effort include occupant mass and height, seating position, contact surface and belt use.

REFERENCES

Augenstein, J.; Digges, K.; Bahouth, G.; Dalmotas, D.; Perdeck, E.; Stratton, J. (2005) Investigation of the Performance of Safety Systems for Protection of the Elderly. Annual Proceedings /Association for the Advancement of Automotive Medicine, Vol. 49, pp. 361-370.

Austin, R.; Faigin, B. (2003) Effect of Vehicle and Crash Factors on Older Occupants. Journal of Safety Research, Vol. 34, pp. 441– 452.

Cerelli, E. (1998) Research Note: Crash Data and Rates for Age-Sex Groups of Drivers, 1996. National Highway Traffic Safety Administration, U.S. Department of Transportation, Washington, DC.

Evans, L. (2001) Age and Fatality Risk From Similar Severity Impacts. Journal of Traffic Medicine, Vol. 29, pp. 10-19.

Forman, J.; Lessley, D.; Shaw, C.G.; Evans, J.; Kent, R.; Rouhana, S.; Prasad, P. (2006) Thoracic Response of Belted PMHS, the Hybrid III, and the THOR-NT Mid-Sized Male Surrogates in Low Speed, Frontal Crashes. Stapp Car Crash Journal , Vol. 50, pp. 191-215.

Funk, J; Cormier, J; Gabler, H. (2008) Effect of Delta-V Errors in NASS on Frontal Crash Risk Calculations. 52nd Annual Proceedings /Association for the Advancement of Automotive Medicine.

General Engineering and Systems Analysis Company, Inc (2005) Thor Certification Manual, Revision 2005.2.

General Engineering and Systems Analysis Company, Inc. (2010) THORTEST Version 2.4-1, Boonsboro, MD.

Hampton, C. E.; Gabler, H.C. (2010) Evaluation of the accuracy of NASS/CDS delta-v estimates from the enhanced WinSmash algorithm. Annual Conference, Annals of Advances in Automotive Medicine Vol. 54.

Hampton, C.E.; Gabler, H.C. (2009) NASS/CDS Delta-V Estimates: The Influence of Enhancements to the WinSmash Crash Reconstruction Code. Annual Conference, Annals of Advances in Automotive Medicine, Vol. 53, pp. 91-102.

International Standards Organization (2009) Road Vehicles – Design and Performance Specifications for the WorldSID 50th Percentile Male Side Impact Dummy – Part 1: Terminology and Rationale (ISO WD 15830-1).

International Standards Organization (2009) Road Vehicles – Design and Performance Specifications for the WorldSID 50th Percentile Male Side Impact Dummy – Part 2: Mechanical Subsystems (ISO WD 15830-2).

International Standards Organization (1999) Technical Report 9790: Road Vehicles – Anthropomorphic Side Impact Dummy – Lateral Impact Response Requirements to Assess the Biofidelity of the Dummy.

Kent, R.; Henary, B; Matsuoka, F. (2005) On the Fatal Crash Experience of Older Drivers. Annual Proceedings / Association For The Advancement Of Automotive Medicine, Vol. 49, pp. 371-391.

Morris, A.; Welsh, R.; Hassan, A. (2003) Requirements for the Crash Protection of Older Vehicle Passengers. Annual Proceedings / Association For The Advancement Of Automotive Medicine, Vol. 47, pp. 165-180.

National Highway Traffic Safety Administration (2009) Evaluation of Thoracic Injuries Among Older Motor Vehicle Occupants. U.S. Department of Transportation, Washington, DC. (<http://www-nrd.nhtsa.dot.gov/Pubs/811101.pdf>)

National Highway Traffic Safety Administration (2009) Traffic Safety Facts: Older Population, 2008 Data. U.S. Department of Transportation, Washington, DC. (<http://www-nrd.nhtsa.dot.gov/Pubs/811161.pdf>)

Niehoff, P; Gabler, H.C. (2006) The Accuracy of WinSmash Delta-V Estimates: The Influence of

Vehicle Type, Stiffness, and Impact Mode. Annual Proceedings /Association for the Advancement of Automotive Medicine, Vol. 50, pp. 73-89.

Petitjean, A. (January 2011) Personal communication.

Petitjean, A. ; Trosseille, X.; Petit, P.; Irwin, A.; Hassan, J.; Praxl, N. (2009) Injury Risk Curves for the WorldSID 50th Male Dummy. Stapp Car Crash Journal 53: 1-34.

SAE. (2003) Surface Vehicle Recommended Practice, SAE J211-1, Rev. Dec. 2003. Society of Automotive Engineers, Warrendale, PA.

Welsh, R.; Morris, A.; Hassan, A.; Charlton, A. (2006) Crash Characteristics and Injury Outcomes For Older Passenger Car Occupants. Transportation Research Part F: Traffic Psychology and Behaviour, Vol. 9, Issue 5, pp. 322-334.

Zhou, Q.; Rouhana, S.; Melvin, J. (1996) Age Effects of Thoracic Injury Tolerance. No. 962421, Society of Automotive Engineers, Warrendale, PA.

APPENDIX A

| (Petitjean et al, 2009) | | | | Current Study | | | | |
|--|------------------------------|------------------------------|---|---|---|---|---|-------|
| Thorax test number | PMHS AIS (AIS _x) | PMHS Age (Age _x) | WorldSID scaled deflection (mm) (WSD _x) | WorldSID scaled deflection corrected to age 45 (mm) | WorldSID scaled deflection corrected to age 65 (mm) | WorldSID scaled deflection corrected to age 75 (mm) | WorldSID scaled deflection corrected to age 20 (mm) | |
| 76T062 | 3 | 69 | 41.7 | 57.6 | 44.3 | 37.7 | 74.2 | |
| 76T065 | 0 | 63 | 37.8 | 49.7 | 36.4 | 29.8 | 66.3 | |
| 77T071 | 0 | 60 | 35.5 | 45.5 | 32.2 | 25.6 | 62.1 | |
| 77T074 | 2 | 60 | 39.2 | 49.1 | 35.9 | 29.2 | 65.7 | |
| 0503LTH25R01 | 0 | 79 | 28.6 | 51.1 | 37.9 | 31.2 | 67.7 | |
| 0504LTH25L01 | 0 | 80 | 26.6 | 49.8 | 36.6 | 29.9 | 66.4 | |
| 0507LTH25R01 | 0 | 53 | 28.7 | 34.0 | 20.8 | 14.1 | 50.6 | |
| 0602LTH25R01 | 0 | 79 | 26.7 | 49.2 | 36.0 | 29.3 | 65.8 | |
| SC101 | 3 | 73 | 60.1 | 78.6 | 65.4 | 58.7 | 95.2 | |
| SC102 | 0 | 27 | 60.3 | 48.4 | 35.1 | 28.5 | 65.0 | |
| SC120 | 0 | 67 | 59.0 | 73.6 | 60.4 | 53.7 | 90.2 | |
| SC121 | 3 | 86 | 56.1 | 83.3 | 70.0 | 63.4 | 99.9 | |
| SC124 | 0 | 45 | 62.3 | 62.3 | 49.1 | 42.4 | 78.9 | |
| SC135 | 3 | 56 | 63.4 | 70.7 | 57.5 | 50.8 | 87.3 | |
| SC137 | 3 | 73 | 66.3 | 84.8 | 71.6 | 64.9 | 101.4 | |
| SAC102 | 3 | 51 | 69.0 | 73.0 | 59.8 | 53.1 | 89.6 | |
| SIC-07 | 4 | 66 | 59.7 | 73.6 | 60.3 | 53.7 | 90.2 | |
| SIC-05 | 4 | 67 | 63.7 | 78.3 | 65.0 | 58.4 | 94.8 | |
| SC125 | 3 | 68 | 68.1 | 83.3 | 70.1 | 63.4 | 99.9 | |
| SC129 | 3 | 51 | 65.4 | 69.4 | 56.1 | 49.5 | 86.0 | |
| SC144 | 3 | 76 | 55.5 | 76.0 | 62.8 | 56.1 | 92.6 | |
| SC139 | 3 | 56 | 58.4 | 65.7 | 52.4 | 45.8 | 82.2 | |
| SC110 | 3 | 78 | 52.4 | 74.3 | 61.1 | 54.4 | 90.9 | |
| SC111 | 4 | 84 | 48.8 | 74.6 | 61.4 | 54.7 | 91.2 | |
| SC115 | 3 | 72 | 43.3 | 61.2 | 47.9 | 41.3 | 77.8 | |
| SC136 | 3 | 54 | 45.1 | 51.1 | 37.9 | 31.2 | 67.7 | |
| SC138 | 3 | 58 | 47.8 | 56.4 | 43.1 | 36.5 | 73.0 | |
| SC119 | 3 | 75 | 32.3 | 52.2 | 38.9 | 32.3 | 68.8 | |
| SC107 | 3 | 50 | 64.6 | 67.9 | 54.7 | 48.0 | 84.5 | |
| SC133 | 4 | 73 | 71.3 | 89.9 | 76.6 | 70.0 | 106.5 | |
| SC116 | 3 | 67 | 65.0 | 79.6 | 66.4 | 59.7 | 96.2 | |
| SC134 | 3 | 58 | 68.3 | 76.9 | 63.6 | 57.0 | 93.5 | |
| 94LSI32P03= OSU323 | 3 | 59 | 72.3 | 81.6 | 68.3 | 61.7 | 98.1 | |
| 94LSI32P04= OSU321 | 3 | 75 | 66.6 | 86.5 | 73.2 | 66.6 | 103.0 | |
| 95LSI32P06= OSU320 | 5 | 82 | 71.6 | 96.1 | 82.9 | 76.2 | 112.7 | |
| LSI32P12=OSU581 | 3 | 80 | 71.6 | 94.8 | 81.6 | 74.9 | 111.4 | |
| LSI32P14 | 3 | 79 | 71.6 | 94.1 | 80.8 | 74.2 | 110.7 | |
| LSI32P15 | 4 | 68 | 76.1 | 91.3 | 78.0 | 71.4 | 107.9 | |
| LSI32P16 | 5 | 77 | 73.7 | 94.9 | 81.7 | 75.1 | 111.5 | |
| (Petitjean et al, 2009) | | | | After performing survival analysis with Weibull distribution on age-adjusted scaled WorldSID deflection data and PMHS AIS, the following results were obtained: | | | | |
| Linear Regression Coefficients | | | | | | | | |
| | | c(intercept) | b(Age) | a(WSD) | | | | |
| | | -4.077 | 0.044 | 0.066 | Scale = | 0.235 | 0.273 | 0.146 |
| | | | | | Intercept = | 3.86 | 3.7 | 4.35 |
| AIS _x = a*WSD _x + b*Age _x + c | | | | | | | | |
| For a given risk level: | | | | | | | | |
| a*WSD ₆₅ + b*65 + c = a*WSD _x + b*X + c | | | | | | | | |
| RISK OF INJURY = 1-EXP(-EXP(1/SCALE*LN(DEFLECTION VALUE)+(INTERCEPT/SCALE*-1)+(0/SCALE*-1))) | | | | | | | | |

MODIFICATIONS TO IMPROVE THE DURABILITY, USABILITY AND BIOFIDELITY OF THE THOR-NT DUMMY

Stephen A. Ridella

Daniel P. Parent

National Highway Traffic Safety Administration

United States of America

Paper Number 11-0312

ABSTRACT

A series of modifications were completed to improve the durability, usability and biofidelity of the THOR-NT (THOR) frontal crash dummy. There has been growing interest in the safety community to develop a frontal crash dummy that is more sensitive to new restraint systems and more kinematically biofidelic in crash conditions with lateral components, such as narrow-offset or small-overlap impacts. As the THOR had been developed with these goals in mind, it was determined that enhancements were needed to improve the response of the THOR dummy while taking advantage of newer biomechanical data to enhance the design. So called “mod kits” were designed to make changes to the head/neck, thorax, abdomen, and knee/femur/pelvis of the dummy. This paper describes the mod kits and the resulting improvements of the THOR dummy response. Specifically, head changes were focused on improving vibration response, while neck changes included improvements to assembly and disassembly as well as improved tension response. Thoracic changes included creating new clavicle load cells and improving the thoracic deflection instrumentation. Enhancements to the abdomen involved removing redundant upper abdomen instrumentation and improving the lower abdomen displacement instrumentation. The pelvis and pelvis skin were completely changed to improve geometry and fit as well as adding enhanced load cells to the anterior-superior iliac spines. Finally, the KTH (Knee-Thigh-Hip) complexes were completely rebuilt to accommodate more deflection and meet recently established biofidelic response corridors under vehicle impact conditions. This paper will describe the efforts that went into the creation of each of the mod kits completed for the THOR dummy. The rationale, process and results of the mod kits will be explained.

INTRODUCTION

The National Highway Traffic Safety Administration (NHTSA) has been researching advanced anthropometric test devices (ATDs) to succeed the Hybrid III ATD since the early 1980s (Haffner,

2001). The primary design objective of this research was to represent the response of automotive occupants in sophisticated restraint systems developed since the advent of the Hybrid III, such as force-limited three-point belts and air bags. This advanced ATD first took shape in the 50th Percentile Male Trauma Assessment Device (TAD-50M), which demonstrated realistic rib cage anthropometry. The TAD-50M evolved into the Test Device for Human Occupant Restraint (THOR), first as the THOR Alpha (Haffner, 2001) and later as the THOR-NT (Shams, 2005). This evolution coincides with continued advancements in the understanding of human impact response and injury biomechanics research. This paper presents recent modifications to the THOR-NT design intended to improve biofidelity, durability, and usability.

BACKGROUND

The THOR-NT ATD has been used in hundreds of vehicle, sled, and component tests in a wide array of conditions since its inception in 2005 (Shams, 2005; Forman, 2006; Martin, 2007; Yaguchi, 2009; Shaw, 2010). Throughout this process, feedback from the test facilities and researchers responsible for carrying out these tests has been collected and evaluated in coordination with the Society for Automotive Engineers (SAE) THOR Evaluation Task Group. Additionally, progress in biomechanics research since the release of the THOR-NT technical data package (TDP) has provided the opportunity for further enhancement of the design. The SAE THOR Evaluation Task Group developed short-term and long-term recommendations for improvements to the biofidelity, repeatability, reproducibility, durability, and usability of the THOR-NT ATD. These recommendations were developed based on the feedback provided by researchers in the automotive industry, academia, and the government, as well as ATD manufacturers and global users, through participation with the SAE THOR Evaluation Task Group. Over the past two years, NHTSA, with support from contractors, has implemented modifications intended to address the highest-priority short-term recommendations. Four projects were carried out, each addressing one key body region:

the head and neck, the thorax, the abdomen, and the knee-thigh-hip (KTH) complex. For each modification intended to enhance the design of the THOR-NT, details are provided to describe the necessity for the change, the implementation of the change, and the resulting improvement in biofidelity, durability, or usability.

METHODS

In collaboration with the SAE THOR Evaluation Task Group, NHTSA developed a list of achievable short-term enhancements to the biofidelity, repeatability, reproducibility, durability, and usability of the THOR-NT ATD. One such modification that was implemented based on requests from users and ATD manufacturers was to revise the drawings for all mod kit components to utilize metric units and fasteners. Additionally, the original design called for tilt sensors to be installed in the head, neck, thoracic spine, lumbar spine, and pelvis to assist in test setup and repeatability. In order to improve the reliability of the devices while harmonizing the THOR-NT ATD with other international ATDs such as the WorldSID (ISO, 2005), NHTSA required that the tilt sensor mounting locations be designed to accept both of the commonly-used sensors, the MSC 260D/GP-[L,M] (MSC Automotive GmbH) and the IES-1402e (Humanetics Innovative Solutions).

Head and Neck

After several minor modifications to the head design in the THOR-NT, the mass, center of gravity (CG) location, and moment of inertia (MOI) had drifted away from the original design targets. The CG, along with other commonly-measured anatomical features, had no physical manifestation on the skin of the head. Additionally, it was discovered during analysis of head drop tests that the seven-accelerometer array in the head would often experience resonance at frequencies below the high-pass filter frequency specified by SAE J211.1 (SAE, 2007) for processing of accelerometers. This ringing would produce noise that prevented accurate data reduction and obfuscated test results.

During comparative testing of the THOR-NT and the Hybrid III neck in axial extension, Dibb (2006) found that both ATD necks showed a significantly stiffer response than a Finite Element (FE) model of the human neck, which was validated based on post-mortem human surrogate (PMHS) testing corrected for musculature. It was demonstrated that the THOR-NT neck was almost ten times stiffer in axial tension than the simulated human response, while removing the center safety cable reduced the axial

tension stiffness to under three times the simulated human response (Figure 1). Thus, it was recommended that the center safety cable be removed from the THOR-NT design to increase biofidelity.

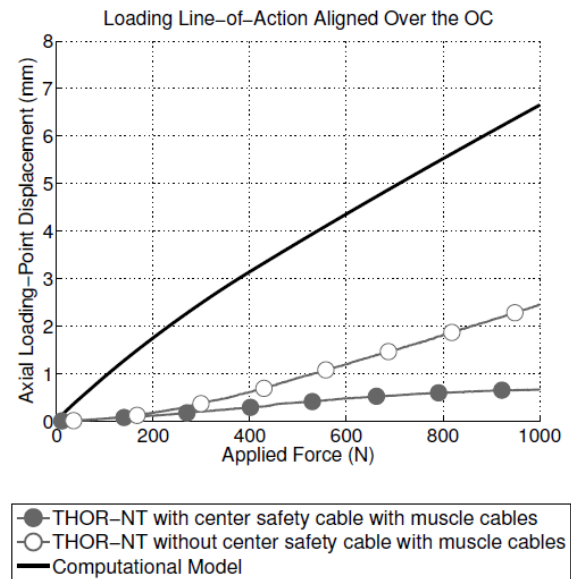


Figure 1. Axial tension of the THOR-NT both with and without the center safety cable, compared to a computer model representing PMHS response (From Dibb, 2006).

The head connects to the top of the neck at the occipital condyle (OC) joint assembly. The OC assembly consists of a bolt that spans attachments to the head and the upper neck load cell. This bolt, originally designed for the THOR Alpha ATD, interfaces with a nut, several washers, and a rotary potentiometer to provide biofidelic rotation while measuring such rotation of the OC joint. During both component and full-body testing of the THOR-NT, numerous issues have been reported with the OC assembly (Moorhouse, 2007). First, the fasteners were difficult to assemble correctly and adjust, and since they were specialty parts, they were difficult to repair or replace. For instance, a machined key washer was used to retain the position of the remaining washers during rotation of the head, but was difficult to replace if lost or damaged. Second, the potentiometer often reported non-physical measurements, potentially due to a lack of engagement of the OC bolt shaft and the potentiometer. The potentiometer itself introduced variability in the system, potentially due to wear of its plastic components during use, assembly, and disassembly. It was recommended that, since the cam and rubber stop system implemented in the THOR-NT design achieved the desired flexion-

extension response of the OC joint, the OC bolt could be simplified.

Thorax

In order to investigate the distribution of shoulder belt load during a restrained vehicle or sled test, the incorporation of load cells in the clavicle was recommended. Measurement of the load experienced by the clavicle in the anterior-posterior and vertical directions would allow a demonstration of the shoulder shielding effect that has been postulated based on PMHS test results (Shaw, 2005), as well as providing research functionality for the development of multi-point restraint systems.

In the THOR-NT design, the tri-axial accelerometer mount intended to measure the kinematics of the upper thoracic spine at the first thoracic vertebral body (T1) was attached to the lateral right aspect of the upper spine box roughly 75 millimeters inferior to the anatomical location of T1. To address this issue, it was recommended that the T1 accelerometer mount be redesigned to improve anatomical correlation.

The Compact Rotary Unit system (CRUX), installed at four locations within the thoracic cavity to measure three-dimensional rib deflection, was a frequent source of repeatability and usability complaints. Each CRUX unit consisted of three rotary potentiometers connected by two rods, the base mounted posterior to the lower spine and the arm attached anterior to the medial endpoint of the respective rib. Together, the CRUX units measured the bi-lateral three-dimensional deflection time-history of the 3rd and 6th ribs of the THOR-NT, which represent the anatomical 4th and 8th ribs. Processing of the CRUX measurements to convert the rotary potentiometer angles to three-dimensional displacements in the thorax coordinate system introduced both measurement and calculation error. Coupled with strict data acquisition system (DAS) requirements, the CRUX system compromised repeatability and reproducibility. Furthermore, the attachment of the upper rib instrumentation to the lower spine often overestimated anterior-posterior deflection, as rotation of the 3rd rib about its attachment to the upper spine would be measured as deflection relative to the lower spine. For these reasons, it was recommended that the thoracic instrumentation be redesigned.

As with the Hybrid III ATD, the original THOR-NT was required to achieve a specified thoracic force-deflection response in a sternal hub impact with a 23.4 kilogram impactor at a speed of 6.7 meters per second. However, it has since been demonstrated that sternal hub impacts at such velocities have

become rare with increases in restraint usage. In contrast to hub loading, shoulder belt loading presents a loading geometry distributed across the rib cage and loading rates in the range of 1 to 4 meters per second (Schneider, 1989). Thus, the 6.7 meter-per-second sternal impact was lowered in priority in favor of a more exposure-appropriate 4.3 meter-per-second sternal impact. The biofidelity targets for thoracic force-deflection response were determined from PMHS data (Neathery, 1974), corrected to remove the influence of muscle tensing for the 4.3 meter-per-second impact corridor (Kent, 2006).

Abdomen

The lower abdomen of the THOR-NT included two double-gimballed string potentiometers (DGSP) to measure three-dimensional deflection. The DGSP units performed a similar function to the CRUX units in the thorax, and experienced similar usability issues. Additionally, the high-tension string potentiometers required to measure high-velocity compression brought about permanent deformation of the foam lower abdomen insert. For these reasons, it was decided to replace the DGSP with a more robust instrumentation system that does not apply a static load to the abdomen.

A high-tension string potentiometer presented repeatability concerns for the upper abdomen as well, causing permanent set of the foam in the upper abdominal insert. The deflection measurement collected by the upper abdomen string potentiometer was somewhat redundant since the lower CRUX units provided a bi-lateral three-dimensional measurement of the anterior rib cage at the same inferior-superior level. Aside from use in the certification procedures, the upper abdomen string potentiometer was not often used, thus the removal of this redundant instrumentation was recommended.

The upper and lower abdomen inserts of the THOR-NT are necessarily individual units to allow for biofidelic pelvic rotation in frontal crash modes. To prevent penetration of vehicle and restraint components into the gap between the lower abdominal insert and the upper abdominal insert (also bounded by the bottom of the rib cage) metal stiffener strips were installed vertically into the jacket that serves as the thoracic flesh. Though this issue is more apparent in upright lumbar spine angles as opposed to the typical slouched or super-slouched automotive seating postures, direct impacts to this gap may not be biofidelic. Furthermore, the stiffeners may deform during routine testing, and thus require frequent inspection. As such, alternatives to the two-bag abdomen arrangement were investigated,

including options for both a fixed spine and an adjustable spine.

Knee-Thigh-Hip (KTH)

The original THOR-NT design featured a button load cell installed to the anterior surface of the anterior superior iliac spine (ASIS), which was intended to measure lap belt loads. Due to the limited size of the button load cell, the functionality of this feature was limited. To further improve the functionality of the THOR-NT in both standard and advanced restraint systems, the ASIS load cell design was revisited.

Several modifications to the pelvis flesh were investigated. First, removal of the upper femurs from the pelvis during disassembly would be facilitated by adding access holes to the pelvis flesh. Second, it had been demonstrated that the flesh, specifically below the proximal femurs, had a propensity to sag and permanently deform when rested on a rigid surface. It was recommended that this issue be addressed without changing the stiffness of the flesh or the outer contour. Finally, should a geometrical redesign result from the improved ASIS load cell, the pelvis flesh should be adapted accordingly.

Since the time of the original THOR-NT femur design, additional biomechanical data have been developed to quantify the axial compression response of the upper leg. While no biomechanical or certification requirements were specified for the THOR-NT knee slider alone, PMHS tests conducted to match the protocol defined for the Hybrid III knee slider certification procedure have indicated a new biofidelity target (Balasubramanian, 2004). Since the Hybrid III knee slider has a similar form and function to the THOR-NT knee slider, it was recommended that the Hybrid III knee slider certification procedure be adopted for the THOR-NT biomechanical requirements with the caveat that the performance targets be modified to meet the newly-developed biomechanical data (Figure 2).

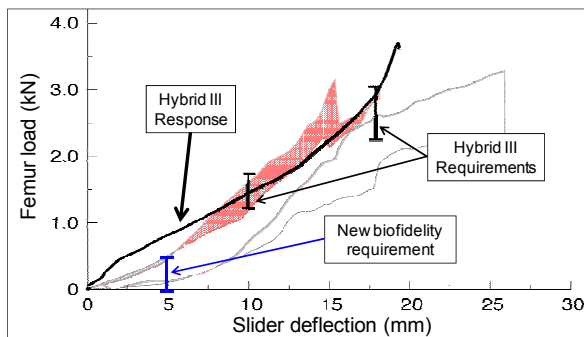


Figure 2. New response requirements for the THOR-NT knee slider during impact with a 12 kg pendulum at 2.75 m/s.

Similarly, new biomechanical corridors have been developed to describe the response of the femur when subjected to an axial impact at the intact knee while rigidly supported at the femoral head (Rupp, 2003). Whereas the existing THOR-NT certification procedures specify a response force corridor in a full-dummy seated knee impact, this additional biomechanical response requirement specifies a force-deflection corridor of the femur in isolation. Testing with the existing THOR-NT femur demonstrated an excessively stiff response compared to the PMHS corridor, as the femur puck did not allow sufficient stroke (Figure 3)

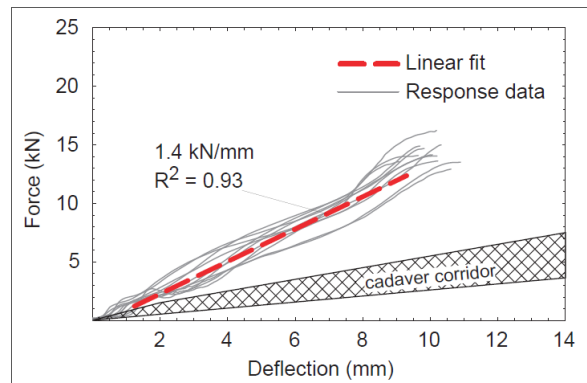


Figure 3. Force-deflection responses for loading of THOR knee/femur complex by a molded-knee interface at a 1.2-m/s platform velocity relative to the new cadaver response corridor (From Rupp, 2003).

Lower Extremity (LX)

In component, sled, and vehicle testing, the THOR-Lx lower extremity has demonstrated a need for improvement in durability and serviceability, specifically in the ankle region. Rostas and soft stops, deformable components in the ankle that represent the biomechanical characteristics of inversion/eversion (xversion) and plantarflexion/dorsiflexion (flexion), were often damaged during normal testing. In the xversion mode, the range of motion was narrower than existing biomechanical data (Rudd, 1999). Moreover, the potentiometers used to measure this motion were often subject to erroneous readings due to shaft slippage and were difficult to service and maintain. NHTSA, along with the SAE THOR Evaluation Task Group, recommended modifications intended to address these limitations.

The design of the original THOR-Lx included a molded rubber foot upon which a military-specified (MIL-spec) shoe was fitted during vehicle tests. Since the response of the leg is predicated on the impact properties of the MIL-spec shoe, which is not

controlled by NHTSA, a redesign of the foot and/or shoe was investigated.

RESULTS

The short-term recommendations made by NHTSA, in collaboration with the SAE THOR Task Force, for the improvement of the biofidelity, repeatability, reproducibility, durability, and usability of the THOR-NT ATD were implemented through four contracts carried out by three manufacturers: GESAC, Inc. (head and neck, abdomen), Denton ATD (KTH), and First Technology Safety Systems, Inc. (thorax), with additional technical and administrative support provided by the NHTSA Vehicle Research and Test Center (VRTC). One THOR-NT ATD (serial number 0007) has been adapted to include these modifications intended to enhance the performance (Figure 4).



Figure 4. THOR-NT with mod kit installed, without jacket

Head and Neck

The first modification to the head was to modify the head skin such that a uniform thickness was achieved throughout the scalp. This change allows for consistent head impact response independent of the precise location of the impact. In order to achieve a uniform head skin thickness while maintaining biofidelity of the head, the thickness of the skin at the forehead was chosen as the uniform thickness. Since the forehead was among the thinnest sections of the original THOR-NT head skin, the total mass of the head decreased as a result of this change (Table 1), as calculated using solid-modeling computer aided design (CAD) software. To rectify this change in

mass, the shape of the ballast, a steel block attached to the inside of the superior skull, was modified. The resulting mass and CG location was well within the tolerance. This CG location was marked on the head skin with a through hole, while dimples were created at the anatomical locations of the OC joint center, nasion, external auditory meatus, and infraorbital foramen.

Table 1. Inertial properties of the THOR-NT head

| | Units | Target | Tol. | Original Design | w/Modified Head Skin | Final Design |
|------|-------|--------|------|-----------------|----------------------|--------------|
| Mass | kg | 4.54 | 0.05 | 4.54 | 4.38 | 4.539 |
| CG X | mm | 8.80 | 2.5 | 9 | 9.3 | 8.87 |
| CG Y | mm | 0.00 | 2.5 | -1 | 0.05 | 0.02 |
| CG Z | mm | -58.0 | 2.5 | -58 | -56.9 | -57.99 |

Through frequency response testing carried out by impacting the skull in various states of assembly with a hammer and analyzing the accelerometer responses using a Fast Fourier Transform (FFT), it was determined that the ringing was not caused by the seven-accelerometer array mount itself, but by the ballast attached to the inside of the superior skull. The original ballast was attached posteriorly by two screws and not anchored anteriorly, resulting in a cantilevered design. In adjusting the mass of the ballast to achieve the proper mass for the head in total, the design was adjusted such that the ballast was attached at four locations instead of two to prevent low-frequency oscillations of the front of the ballast. Subsequent to this analysis, the seven accelerometers were replaced with three orthogonal angular rate sensors (ARS) attached to the same mount.

To investigate the need for the center safety cable in the original THOR-NT neck design, repeated neck extension certification tests were carried out without the cable installed. After roughly twenty tests, inspection of the neck showed areas of separation between the butyl rubber pucks and the aluminum plates at the point of bonding. While neither the removal of the cable nor the de-bonding of the rubber pucks resulted in a noticeable change in the measured extension moment, this durability concern warranted an investigation of alternative methods of safely improving neck biofidelity. One such solution to this problem retained the center safety cable, but employed a neoprene spacer in place of the original rigid nylon spacer at the attachment point to the lower neck load cell to provide compliance in axial tension. The resulting neck design did not show an appreciable difference in flexion, extension, and lateral bending response compared to either the original neck or the neck with no safety cable installed. While it was not possible to recreate the

testing performed by Dibb (2006), a simple axial tension test demonstrated that the neck with the neoprene spacer was nearly three times more compliant than the neck with the standard safety cable installed. This design compromise allows for safety while optimizing for neck response biofidelity.

To address the unnecessary complexity of the OC, several design changes were implemented. First, a single pin held in place laterally with a screw replaced the OC bolt and all of the associated specialty washers of the previous design. Second, a set screw was installed at the end of the OC pin at the attachment to the rotary potentiometer to ensure proper engagement. A new rotary potentiometer (ECO 50 ES, Vishay Intertechnology, Inc.) was selected to replace the original model, and the housing was modified to accept the new design. Note that this model was also selected to replace all of the rotary potentiometers in the THOR-NT, including those installed at the base of each IR-TRACC in the thorax, abdomen, and lower leg (for a grand total of 17 in each dummy). Finally, the custom fasteners were replaced with commonly-available fasteners that did not require subsequent machining where possible.

Thorax

The original THOR-NT clavicle design was modified to allow the incorporation of two-axis load cells at the attachment points to the sternum medially and to the shoulder assembly laterally (Figure 5). These load cells measure forces in the anterior-posterior and inferior-superior directions, or the X and Z axes of the SAE dummy coordinate system (SAE, 2007). The capacity of each clavicle was chosen to be 4 kN (2 kN at each end) based on both the available space constraints and the capacity of the Hybrid III clavicle load cell. Structural replacements were also designed for testing that does not require the measurement of clavicle loads.



Figure 5. Integration of load cells within the clavicle.

Several alternative locations for the T1 accelerometer were evaluated. Due to interference with the lower neck and the spine box, it was not possible to locate the accelerometers directly at the anatomical location

of T1. A compromise was reached by installing the accelerometers into the shoulder neck shroud support, an existing part that attaches to the top of the spine box and prevents contact between the articulated shoulder attachment to the spine box and the neck (Figure 6). While this location is still offset from the anatomical T1 location in the lateral direction, the proximity in the vertical direction was improved.

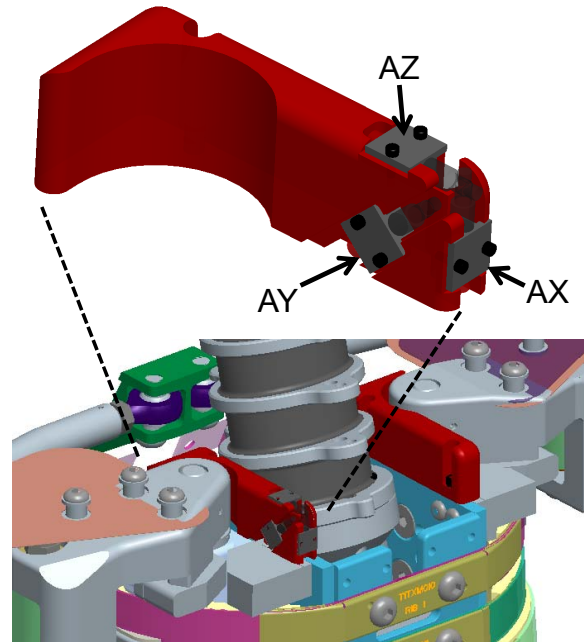


Figure 6. Installation of the T1 accelerometers in the shoulder neck shroud support.

To better evaluate the three-dimensional deformation of the rib cage, two changes were made to the existing THOR-NT design. First, the CRUX units were replaced with Infrared Telescoping Rod for Assessment of Chest Compression (IR-TRACC) linear potentiometers mounted in a double-gimballed configuration (Figure 7, Figure 8). The key benefit of the IR-TRACC units is their compact and linear nature, which allows for a greater range of rib cage deformations without interference of the instrumentation with the physical components in the thoracic cavity. Furthermore, the upper IR-TRACC units are mounted to the spine above the thoracic spine flex joint, the same rigid body to which the 3rd rib is mounted. This configuration presents a system that is less prone to measuring non-physical deflections, such as those resulting from rotation of the thoracic spine flex joint. These IR-TRACCs, on the other hand, present an elevated risk compared to the CRUX units due to the increased complexity and expense, and as such will be a key component in the evaluation of the repeatability, durability, and usability of the mod kit.

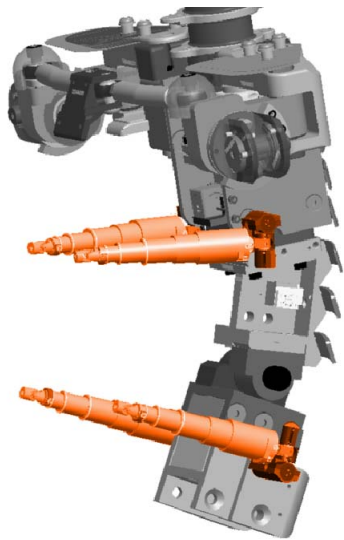


Figure 7. Installation of the IR-TRACC rib deflection measurement system.



Figure 8. Photograph of the lower left IR-TRACC assembly installed in the THOR-NT.

To improve the biofidelity of the THOR-NT in restrained impact conditions, the biomechanical response requirements, along with the certification procedures, have been modified to require agreement with response corridor in a sternal hub impact with a 23.4 kilogram pendulum traveling at 4.3 meters per second. While not required for certification, the high-speed (6.7 meters per second) thoracic impact test must be run to demonstrate that no physical interference occurs during this test. When manipulated to present deflection in the same coordinate system, the IR-TRACC demonstrates a similar response to that measured by the CRUX, though this response is not identical due to the inherent differences in the mounting locations of these instrumentation methods (Figure 9). Since the upper IR-TRACC measures rib deflection from a different measurement basis than the upper CRUX units, further investigation is necessary to refine the data processing techniques for biofidelity and certification testing.

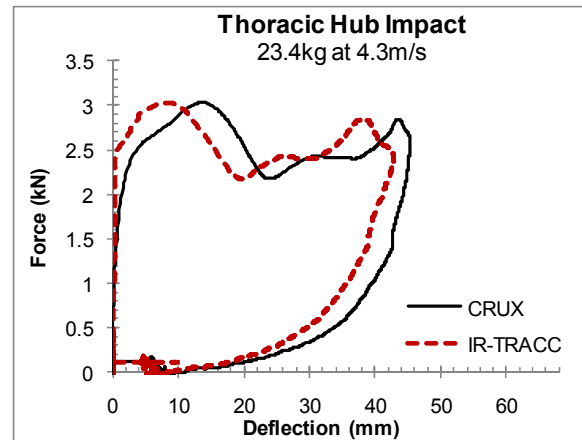


Figure 9. Response of the thorax to blunt impact with a pendulum, 23.4kg at 4.3m/s.

Abdomen

Two additional IR-TRACC three-dimensional displacement measurement devices were installed in the lower abdomen to replace the DGSP units in the original THOR-NT (Figure 10). Like the assemblies installed in the chest, two rotational potentiometers attach the base of the IR-TRACC to the measurement basis, in this case the lumbar spine. The IR-TRACC units installed in the lower abdomen have a measurement capacity of 90 millimeters, though investigation is underway to develop and install IR-TRACC units with a capacity of 120 millimeters. This additional capacity was required to capture the abdominal injury criterion of 40 percent compression proposed by the SAE THOR Evaluation Task Group, or roughly 100 millimeters for a 50th percentile male. Since the IR-TRACC units function on light emission and subsequent sensing as opposed to the original high-tension string potentiometer, there is no pre-load applied to the foam abdomen insert.

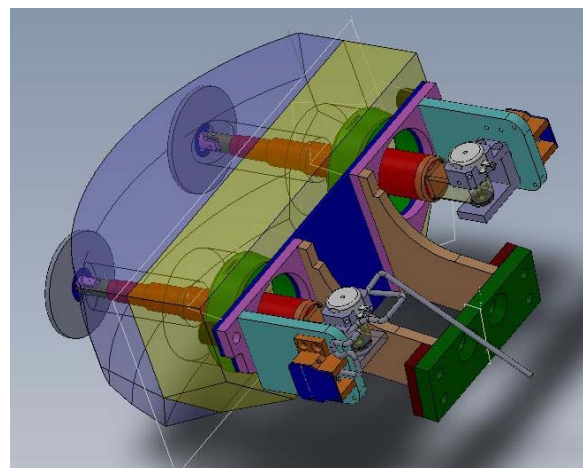


Figure 10. Bi-lateral three-dimensional displacement measurement devices (IR-TRACC, shown in red) installed in the lower abdomen insert.

In the upper abdomen, the string potentiometer was simply removed from the design. This design change required filling the holes in both the foam inside of the insert and the bracket that attached the insert to the spine. Despite a demonstration that the redesigned foam showed a similar force-deflection response in isolation (Figure 11), the resulting thoracic impact response with the new upper abdomen insert installed did not show sufficient deflection (Figure 12). A short-term solution to this problem was to re-install the original THOR-NT upper abdomen foam insert, while a longer-term solution is currently under investigation.

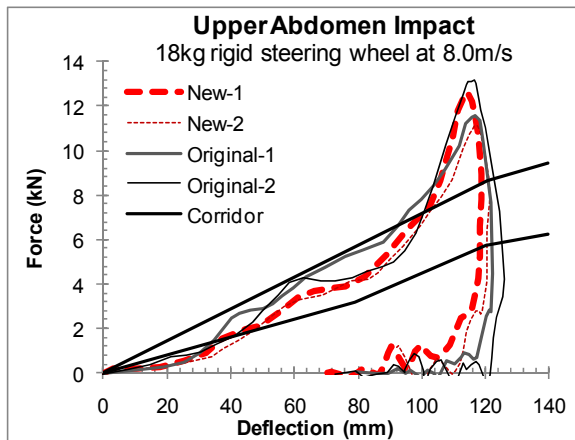


Figure 11. Comparison of the original (Dummy1, Dummy2) and modified (ua-05, ua-06) upper abdomen impact response.

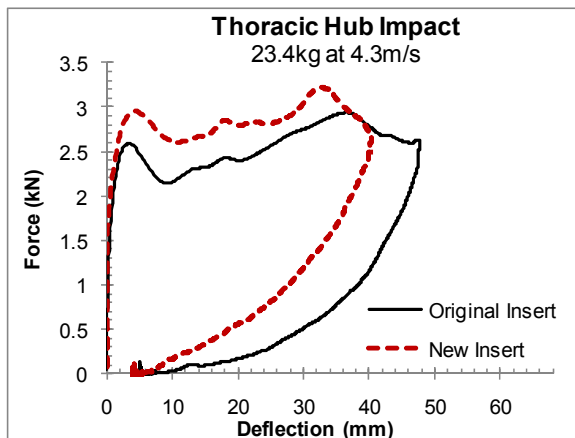


Figure 12. Comparison of the thoracic impact response with a 23.4 kg impactor at 4.3 m/s between the original and modified upper abdomen foam insert. Note that since the abdomen project was carried out before the thorax project, the responses shown here are from a different THOR with CRUX units than the responses shown in Figure 9.

An investigation of the feasibility of bridging the gap between the upper and lower abdomen inserts resulted in several design concepts. One proposed concept integrated both the upper and lower abdomen

inserts into a single pouch (Figure 13), with foam layers selected such that adjustment of the lumbar spine flexion angle by up to 30 degrees was possible without influencing impact response stiffness by more than 10 percent. Alternatively, the unified insert could be formed from expandable foam similar to that used in the pelvis or molded silicon with a rough urethane outer later, though there would be limitations to all of these methods due to both initial position adjustability (lumbar spine pitch change joint) and dynamic rotation (flexion during restraint loading) of the spine. Thus, for the short term enhancements of the THOR-NT, the two-part abdomen was retained.



Figure 13. Unified abdomen concept.

To evaluate the influence of the existing rib stiffeners installed in the jacket to bridge the gap between the upper and lower abdomen inserts, several impacts were carried out both with and without the stiffeners installed. When viewed with respect to the pendulum response, there was no substantial influence of the stiffeners on the upper abdomen response to steering wheel rim impact at 4.5, 6.0, or 8.0 meters per second. However, when viewed by the upper abdomen string potentiometer, the response without the stiffeners showed lower deflection. This finding suggests that without the stiffeners installed, the upper abdominal string potentiometer was not engaged by the impactor, resulting in this artifactual increase in stiffness. Since a pendulum-based certification procedure will be implemented in absence of the upper abdominal string potentiometer, this finding was determined to be no longer relevant.

Knee-Thigh-Hip (KTH)

Two improvements were made to the load-sensing capability of the ASIS load cells installed in the pelvis of the THOR-NT. First, the geometry was

improved by increasing the overall surface area over which load can be measured while retaining shape consistent with the anthropometry of the human ASIS (Figure 14). Second, a two-axis load cell was designed to record not only the longitudinal force on the ASIS (FX), but also the moment about the lateral axis (MY). The addition of the moment measurement allows interpretation of the fit of the lap belt across the pelvis, including the magnitude and timing of submarining. Structural replacements were also designed for use in testing that does not require the measurement of ASIS loads. Finally, the iliac wings of the pelvis were thickened to allow for a smooth interface with the ASIS load cells or the load cell simulators.

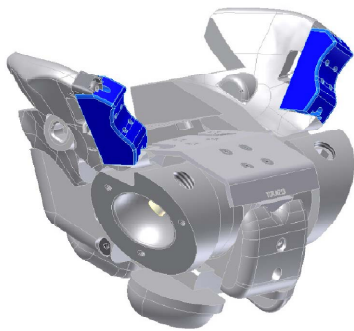


Figure 14. New ASIS load cells (in blue) incorporated into the pelvis bone.

To account for the additional mass of the load cells and the thicker iliac wings, material was removed from other bone areas. This material removal was carried out strategically to create engagement points that allowed for better fit of the pelvis flesh. Additionally, the area of the pelvis flesh near the iliac wing was adapted to create an overhang, which further prevented motion of the pelvis bone with respect to the flesh (Figure 15). To address the issue of permanent deformation of the thigh flesh under the proximal femurs, larger cutouts were created to allow an increased range of motion of the femur shaft (Figure 15). While primarily intended to prevent unnecessary loading of the flesh during storage and setup, these cutouts also allow for a decoupling of the femur with the pelvic flesh to increase biofidelity.

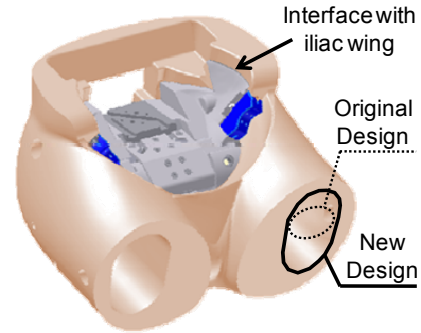


Figure 15. Modifications to the flesh around the pelvis to allow a) better engagement with the bone structure, and b) increased range of motion of the femur

To meet the newly-defined biomechanical response requirements for knee impact (Figure 2), modifications to the THOR-NT knee slider were necessary. Specifically, softening of the rubber shear section of the slider was necessary to achieve the lower force level at 5 millimeters of deflection, while a larger bump stop was necessary to achieve pass-through of the higher force level at 18 millimeters of deflection. The resulting response meets the first and third pass-through corridors, which represent the primary requirement, while the response exhibits a lower force than the second pass-through corridor, a secondary requirement (Figure 16).

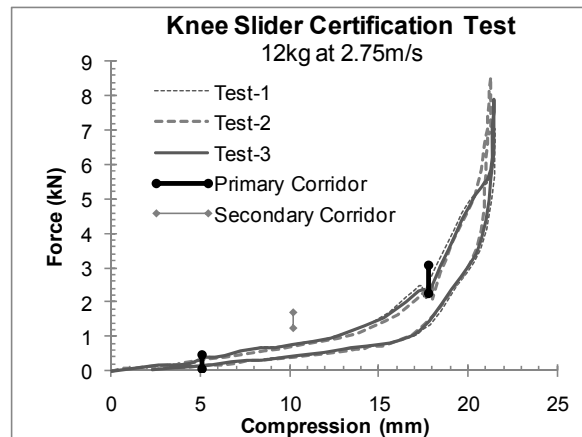


Figure 16. Response of the knee slider in impact with a 12 kg pendulum at 2.75 m/s.

For the assembled femur, it was not possible to achieve the newly-developed biomechanical response data with the original THOR-NT design. While there was a deformable element in the femur, its stiffness and maximum stroke were not sufficient to meet the proposed response corridor. Through an optimization study using the publically-available Finite Element (FE) model of the THOR-NT ATD, it was determined that a 57% increase in the length of the deformable element was necessary. The resulting femur impact response, aside from oscillations early

in the force-deflection characteristic, meets the corridor of the biomechanical requirements (Figure 17). The guide system that allows stroke of the deformable element was subsequently modified to incorporate a square shaft to reduce weight and manufacturing complexity (Figure 18). The key benefit of the femur redesign is the biofidelity of the femur in axial compression, which allows the dummy response to be evaluated directly against human injury tolerances in loading conditions such as knee bolster contact. Finally, the six-axis femur load cell currently used in the WorldSID 50th percentile ATD was installed fit the space constraints of the redesigned femur.

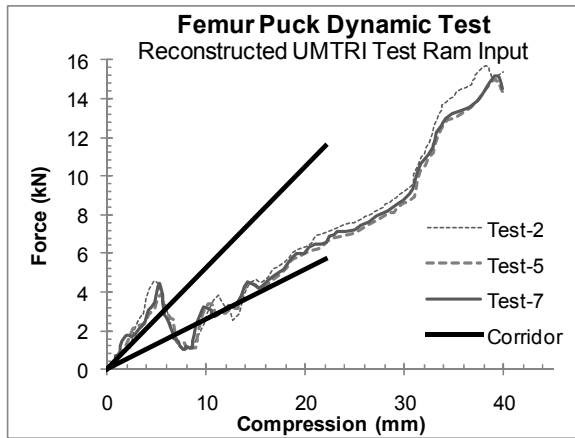


Figure 17. Force-deflection response of the assembled femur in a test condition developed to reproduce the UMTRI ram displacement-time history, compared to the biomechanical response corridor.

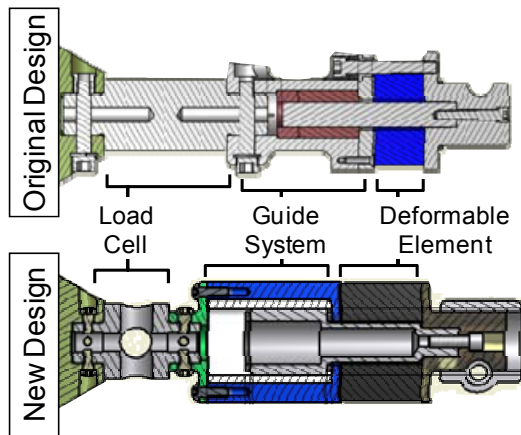


Figure 18. Comparison of the original (top) and modified (bottom) THOR-NT femur designs.

Lower Extremity (LX)

To improve the durability of the ankle joint, new materials were developed for the rostars, and a design

modification was implemented to improve the containment of the rostars in their housings. The soft stops defining the range of motion of the ankle were also improved through optimization of their size and shape (Figure 19), selection of better materials, and elimination of sharp corners that resulted in hard stops in the motion of the joint. Specifically, the xversion soft stops were modified to allow 40 to 45 degrees of motion. This increased range of motion has an additional durability benefit as a structural factor of safety in the event of extreme loading in a severe test condition. Rotational potentiometers of the same model as the OC joint potentiometer were selected for use in the ankle to provide improved accuracy, durability, and serviceability.

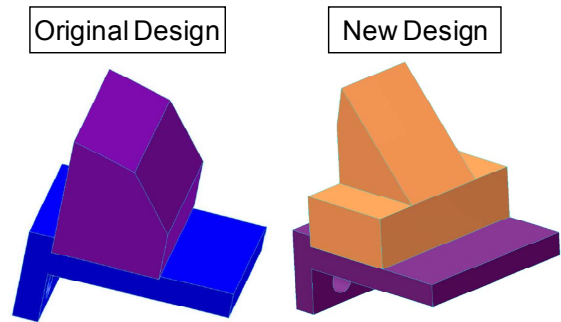


Figure 19. Comparison of the original (left) and modified (right) inversion soft stops in the THOR-Lx.

To improve the repeatability of the THOR-Lx response, a one-piece molded component was developed to represent the collective shoe and foot (Figure 20). This design, based on the molded shoe developed for the WorldSID family of dummies, effectively eliminates the uncertainty associated with the MIL-spec shoe.



Figure 20. One-piece molded shoe design with heel and toe inserts.

CONCURRENT AND FUTURE WORK

To date, one such THOR-NT mod kit ATD has been fabricated and is currently undergoing an assessment of biofidelity, repeatability, and reproducibility. Biofidelity and repeatability will be evaluated by comparing the ATD response to established biomechanical response corridors described in the THOR-NT Biomechanical Requirements manual (NHTSA, 2005a). As an additional biomechanical response evaluation, sled tests will be carried out in multiple conditions to compare the mod kit THOR-NT response to the original THOR-NT as well as the response of PMHS (Shaw, 2010). To evaluate lab-to-lab reproducibility, round-robin testing will be carried out in the same conditions at multiple test laboratories, including component, sled, and full-vehicle crash tests, ideally in the narrow-offset or small-overlap crash mode. Once more THOR-NT ATDs are upgraded with the mod kit, reproducibility between dummies will be evaluated by carrying out the same tests using multiple dummies. Throughout the biofidelity, repeatability, and reproducibility evaluation, the durability and usability of the mod kit THOR-NT, as well as its comparison to the Hybrid III 50th percentile male in like test conditions, will be documented.

Once an acceptable evaluation is achieved, the technical data package (TDP) describing the mod kit components will be finalized and published for public dissemination. This TDP will include updated versions of the Biomechanical Requirements (NHTSA, 2005a) and Certification Procedures (NHTSA, 2005b) manuals that include both newly-developed biomechanical response requirements, such as those for the knee slider and femur, as well as data processing for the improved instrumentation, such as the thoracic deflection measurement devices. The TDP will allow current owners of THOR-NT ATDs to upgrade their dummies to the current state. Coincidentally, the TDP describing the complete dummy will be updated such that full THOR-NT ATDs can be fabricated based on the latest design.

Additional work will be necessary to finalize criteria for the assessment of injury based on the measurements collected during testing. Preliminary injury criteria were discussed by the SAE THOR Evaluation Task Group; however, further research is necessary. For instance, the development of a chest injury criterion based on multi-point deflection will require the recreation of previously-conducted PMHS tests using the mod kit THOR-NT to provide the data necessary for a paired-sample study. Additionally, a seating procedure must be developed, as the existing procedures for the use of the Hybrid III 50th

percentile male ATD in federal regulation testing are not fully compatible with the different anthropometry of the THOR-NT pelvis and lower extremity. Development of the certification procedures, injury criteria, and seating procedure will be carried out by NHTSA in collaboration with the SAE THOR Evaluation Task Group.

CONCLUSIONS

Through the recommendations developed in collaboration with the SAE THOR Evaluation Task Force, NHTSA implemented a multitude of modifications intended to improve the biofidelity, repeatability, reproducibility, durability, and usability of the THOR-NT ATD. Following an evaluation of the mod kit dummy, an updated THOR-NT technical data package (TDP) will be published. A TDP describing only the mod kit components will also be published to allow owners of existing THOR-NT ATDs to upgrade their dummies to the design level of the final TDP.

ACKNOWLEDGEMENTS

The authors would like to express appreciation for the contributions of the SAE THOR Evaluation Task Group in the development of recommendations, as well as extensive contributions from Peter Martin, Ed Probst, Joe McFadden, and Dan Rhule in the development, implementation, maintenance, and documentation of the THOR-NT mod kit. Mike Beebe, Paul Depinet, Craig Morgan, Nagarajan Rangarajan, Tariq Shams, Sarath Kamalakkannan, Jerry Wang, and Eric Jacuzzi were instrumental to the execution of this project.

REFERENCES

- [1] Haffner, M., Rangarajan, N., Artis, M., Beach, D., Eppinger, R., Shams, T., "Foundations and Elements of the NHTSA THOR Alpha ATD Design," 17th ESV Conference, Paper No. 458, 2001.
- [2] Shams, T., Rangarajan, N., McDonald, J., Wang, Y., Platten, G., Spade, C., Pope, P., Haffner, M., "Development of THOR NT: Enhancement of THOR Alpha – the NHTSA Advanced Frontal Dummy," 19th ESV Conference, Paper No. 05-0455, 2005.
- [3] Forman, J., Lessley, D., Shaw, G., Evans, J., Kent, R., Rouhana, S., Prasad, P., "Thoracic Response of Belted PMHS, the Hybrid III, and the THOR-NT Mid-sized Male Surrogates in Low Speed, Frontal Crashes," Stapp Car Crash Journal, 50: 191-215, 2006.

- [4] Martin, P., Shook, L., "NHTSA's THOR-NT Database," 20th ESV Conference, Paper No. 07-0289, 2007.
- [5] Yaguchi, M., Ono, K., Masuda, M., Watamori, T., Seshita, T., Hibino, T., "Comparison of Dynamic Responses of the THOR-NT and Hybrid III in Offset Frontal Crash Test," 21st ESV Conference, Paper No. 09-0268, 2009.
- [6] Shaw, G., Parent, D., Purtsezov, S., Lessley, D., Crandall, J., Tornvall, F., "Torso Deformation in Frontal Sled Tests: Comparison Between THOR-NT, THOR-NT with the Chalmers SD-1 Shoulder, and PMHS," Proceedings of the International IRCOBI Conference, 2010.
- [7] International Standards Organization, "WorldSID Instrumentation," ISO TC22/SC12/WG5, WorldSID TG N397, 2005.
- [8] Society of Automotive Engineers, "Instrumentation for Impact Test – Part 1 – Electronic Instrumentation," SAE J211/1, July 2007.
- [9] Dibb, A., Nightingale, R., Chauncey, V., Fronheiser, L., Tran, L., Ottaviano, D., Myers B., "Comparative Structural Neck Responses of the THOR-NT, Hybrid III, and Human in Combined Tension-Bending and Pure Bending," Stapp Car Crash Journal, 50: 567-581, 2006.
- [10] Moorhouse, K., Probst, E., "A Repeatability Assessment of the THOR-NT ATD Response and an Evaluation of the Certification Procedures," National Highway Traffic Safety Administration, Docket No. NHTSA-2008-0102, May 2007.
- [11] Shaw, G., Lessley, D., Kent, R., Crandall, J., "Dummy Torso Response to Anterior Quasi-static Loading," 19th ESV Conference, Paper No. 05-0371, 2005.
- [12] Schneider, L., King, A., Beebe, M., "Design Requirements and Specifications: Thorax-Abdomen Development Task. Interim Report: Trauma Assessment Device Development Program," DOT HS 807 511, November 1989.
- [13] Neathery, R.F., "Analysis of Chest Impact Response Data and Scaled Performance Recommendations," Proceeding of the 18th Stapp Car Crash Conference, SAE Paper No. 741188, 1974.
- [14] Kent, RW, Bass, CR, Woods, WA, Salzar, RS, Lee, SH, Melvin, J., "The Role of Muscle Tensing on the Force-deflection Response of the Thorax and a Reassessment of Frontal Impact Thoracic Biofidelity Corridors," Journal of Automobile Engineering, Proceedings of the Institution of Mechanical Engineers, Vol. 220, No. 7, pp. 853-868, 2006.
- [15] Balasubramanian, S., Beillas, P., Belwadi, A., Hardy, W., Yang, K., and King, A., and Masuda, M., "Below Knee Impact Responses using Cadaveric Specimens," Stapp Car Crash Journal, 48: 71-88, 2004.
- [16] Rupp, J., Reed, M., Madura, N., Schneider, L., "Comparison of Knee/Femur Force-Deflection Response of the THOR, Hybrid III, and Human Cadaver to Dynamic Frontal Impact Knee Loading," 18th ESV Conference, Paper No. 160, 2003.
- [17] Rudd, R., Crandall, J., Butcher, J., "Biofidelity Evaluation of Dynamic and Static Response Characteristics of the THOR-Lx Dummy Lower Extremity," International IRCOBI Conference on the Biomechanics of Impact, Spain, 1999.
- [18] National Highway Traffic Safety Administration (a), "Biomechanical Response Requirements of the THOR NHTSA Advanced Frontal Dummy, Revision 2005.1," Report No: GESAC-05-03, U.S. Department of Transportation, Washington, DC, March 2005.
- [19] National Highway Traffic Safety Administration (b), "THOR Certification Manual, Revision 2005.2," Report No: GESAC-05-04, U.S. Department of Transportation, Washington, DC, March 2005.

THOR-NT: HIP INJURY POTENTIAL IN NARROW OFFSET AND OBLIQUE FRONTAL CRASHES

Peter G. Martin

Mark Scarboro

National Highway Traffic Safety Administration

U.S. Department of Transportation

Washington, D.C., USA

Paper No. 11-0234

ABSTRACT

Previous studies have shown that hip injuries are prevalent in frontal crashes, particularly those with an oblique, narrow overlap. This paper investigates whether the risk of sustaining such injuries can be evaluated in full-scale vehicle crash tests using the THOR-NT, a dummy that is uniquely equipped for such an evaluation. The THOR-NT is shown to measure acetabular loads that are consistent with pelvic injuries observed in real-world crash victims. Test results reveal that high acetabular loads occur in narrow offset and oblique crashes. Further analysis shows that acetabular loads are dependent upon the position of the thigh, the trajectory of the torso, and intrusion of the instrument panel. Results also show that right-to-left hip loads vary significantly. Abduction of the thigh is also correlated with hip loads. The study provides new insights into how injurious loads are transferred to the pelvis through the thigh via knee bolster contact in frontal offset conditions where oblique loading takes place.

INTRODUCTION

Although seat belt use rates have increased over recent years and vehicle crashworthiness has improved, occupants continue to sustain fatal injuries in frontal crashes. NHTSA sought to understand the crash circumstances leading to fatal injuries to belted occupants in contemporary passenger vehicles. In a detailed review of 122 real-world fatal crashes reported by Rudd et al. (2009), few if any of the 122 fatal crashes were full-frontal or offset-frontal impacts with good structural engagement, unless the crashes were of extreme severity or the occupants exceptionally vulnerable. The other major factors most prevalent in the fatal crashes were:

- Limited vertical structural engagement
- Elevated occupant age
- Semi-trailer underride

NHTSA concluded that corner impacts and oblique frontal crashes should be a priority area for future vehicle crashworthiness research.

Hip Injuries in the Narrow Offset Dataset. Prompted by the study of 122 fatalities, NHTSA began a new analysis of narrow offset and oblique collisions. To study the epidemiology of the problem, a dataset of more than 250 real-world crashes has been extracted from the National Automotive Sampling System-Crashworthiness Data System (NASS-CDS) and the Crash Injury Research and Engineering Network (CIREN). This dataset is referred to herein as the “Narrow Offset Dataset.” The inclusion criteria are described in Pintar et al. (2010) and Rudd et al. (2011) provides a full analysis of the dataset.

The dataset reveals that in narrow offset crashes, air bag coverage is not always sufficient to prevent occupant-to-vehicle contacts. In addition, narrow offset crashes are susceptible to intrusion of interior components contributing to lower extremity injuries and pelvic fractures. For reference, the various bone structures of the pelvis are shown in Figure 1. As compared to frontal crashes in general, pelvis injuries have been shown by Pintar et al. (2010) to be more prevalent in narrow offset crashes. Moreover, injuries to the outboard leg are much more frequent. When pelvic injuries in the narrow offset database are broken down further, acetabular injuries predominate as shown in Figure 2.

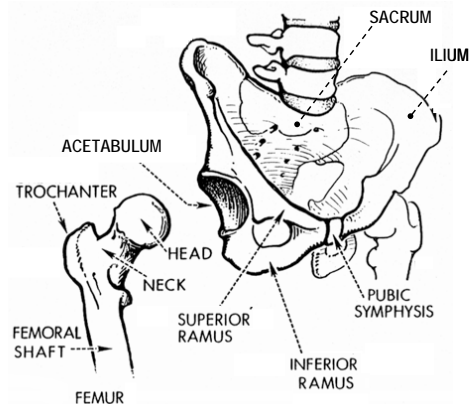


Figure 1. Structure of the Pelvis Bone

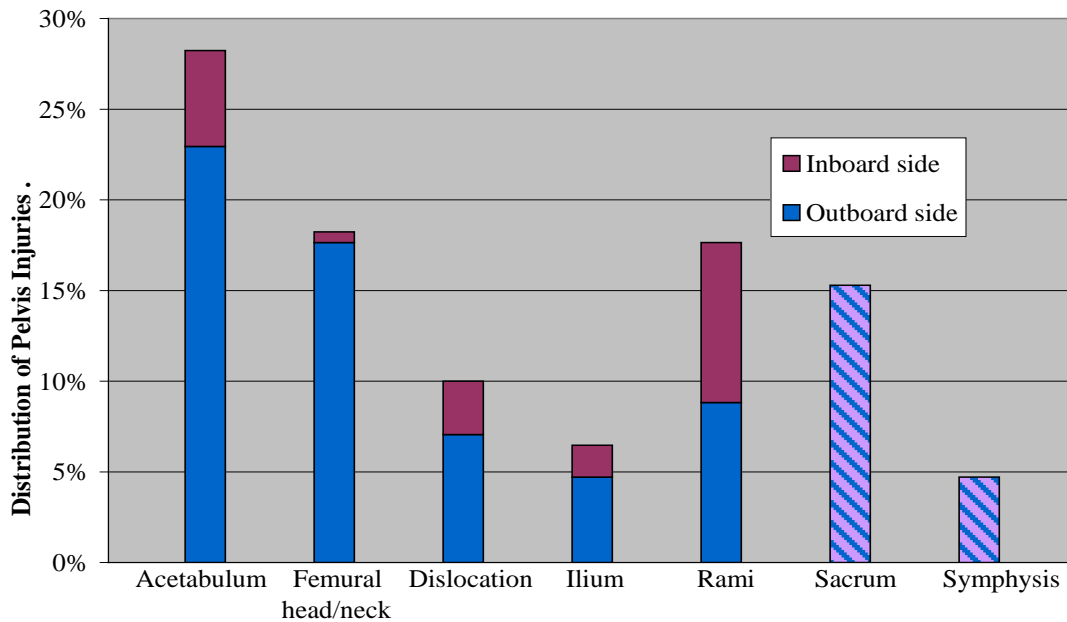


Figure 2. Incidence of AIS 2+ hip and pelvis fractures in the Narrow Offset Dataset. (One injury per pelvic bony structure per occupant. Each occupant sustained at least one AIS3+ pelvic injury).

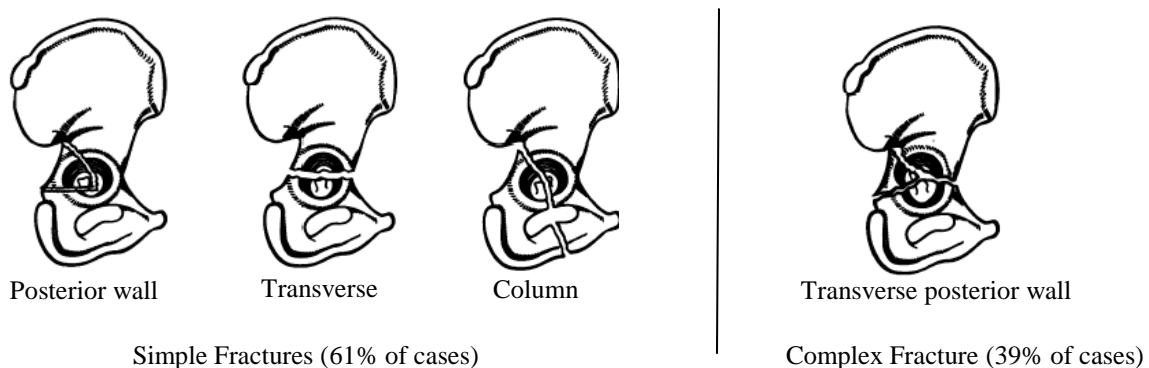


Figure 3. Examples of acetabular fracture patterns in the Narrow Offset Dataset.

The outboard aspect (left hip for drivers) is particularly susceptible to injury, as seen in Figure 2. When the cases within the dataset are examined for specifics on acetabular injuries, they can be grouped into three primary fracture patterns by wall, transverse, and column (Figure 3). These fracture patterns are described more fully by Saterbak et al. (1996). They are primarily used by clinicians to characterize fixation and therapeutic possibilities, and to assess outcome potential. A wall, column, or transverse fracture occurring in isolation is considered to be “simple” acetabular fracture. When simple fractures occur in combination, the resulting fracture pattern is considered to be a “complex” acetabular fracture.

The different fracture patterns highlight another area of concern. Although all acetabular fractures are rated alike on the Abbreviated Injury Scale (i.e., AIS

3 for open fractures and AIS 2 for all others in the 2005 version of AIS¹), they are very different in terms of post-operative complications.

In a meta-analysis of clinical data, Giannoudis et al. (2005) assessed acetabular fracture patterns using a functionality score (known as the Merle d’Aubigne score) based on mobility, pain, and walking ability. These included acetabular fractures from all sources, not just automotive trauma, and some fracture patterns – such as anterior wall fractures – were not observed in the Narrow Offset Dataset. But for the types of acetabular fractures that *were* observed, complex acetabular fractures were found to have a significantly higher percentage of fair/poor outcome

¹ In the Update 98 version of AIS 1990, comminuted and displaced acetabular fractures are also classified as AIS 3.

scores than simple fractures (about 30% vs. about 17%).

NHTSA's narrow offset/oblique crash test program. In conjunction with the findings of the real-world crash analyses, NHTSA has initiated a narrow offset/oblique crash test program to study the problems more fully. Two basic crash configurations are being evaluated: a small overlap configuration and an oblique impact configuration. These tests include vehicle-to-vehicle crashes, crashes involving a moving deformable barrier, and crashes into a pole with the intent to replicate vehicle crash characteristics, occupant kinematics and injury patterns seen in the real-world. Details of the crash tests are reported by Saunders et al. (2011).

In all, nineteen crash tests have been scheduled, including some with vehicles that are believed to have countermeasures that may be effective in narrow offset and oblique crashes. If tests results show potential for reducing the injury risk, NHTSA will perform a larger fleet study. This fleet study is likely to include vehicle-to-vehicle crashes of two vehicles with different size classifications and with different built-in structural countermeasure designs.

INJURY SOURCES AND THE THOR-NT

The THOR-NT 50th percentile male dummy is being used in NHTSA's oblique and narrow offset crash test program. The program is still underway (Saunders et al., 2011) and much of the data is yet to be reduced and analyzed. This paper focuses on just one of the many objectives of the test program: to provide insights into hip injuries that are prevalent in these types of crashes. The decision to use the THOR-NT was partly based on current knowledge of how hip injuries occur. It was felt that the dummy's enhanced biofidelity and instrumentation package made it the best choice to assess hip injuries. This is discussed in more detail later in this paper.

How hip injuries occur. In the years prior to the study of 122 crashes, NHTSA sought to understand why hip injuries had become more prevalent in all frontal crashes (not limited to oblique or narrow offset crashes). Beginning in 2000, this was the focus of NHTSA-sponsored research at the University of Michigan Transportation Research Center (UMTRI). Several studies focused on the knee-thigh-hip complex (referred to as "KTH") have been produced since then.

The UMTRI body of work on KTH produced an understanding that in a frontal crash, nearly all hip injuries arise from loads transferred axially through the femur to the hip. It was observed that newer cars have softer knee bolsters to reduce axial load thru the femur. The softer knee bolsters protect the knee and distal femur by lessening the contact force, but they increase the loading duration so that a higher percentage of the load is transmitted through the femur to the hip. And since the hip has a lower injury tolerance than the distal femur, pelvis fractures have become more commonplace.

In one of the more notable KTH studies, Rupp et al. (2008) explained how bolster contact produces force at the knee that is transferred all the way back to the hip. The percentage that is transferred depends upon:

- Mass recruitment (timing/impulse) – Hip loads increase with added "reaction mass" behind the hip. The recruitment of the reaction mass is impulse-dependent. Knee impacts having long impulses are needed to recruit a high reaction mass behind the hip.
- Bolster stiffness – This affects mass recruitment depending on ramping and rate.
- Symmetric loading of hip – Asymmetric loading can create a greater reaction mass behind one of the hips.
- Ab/adduction and flexion – If the femur attitude changes, the effective reaction mass behind the hip will change, too. For example, a greater reaction mass is associated with abduction because the femur is driven into the (massive) pelvis.

These findings are supported by cases within the Narrow Offset Dataset where pelvis fractures are present. In many such cases, abduction of the outboard leg of the driver of the vehicle was apparent. These cases are typified by an investigation highlighted in Dakin et al., (1999) where the driver sustained a transverse posterior wall fracture (complex fracture pattern) of the left acetabulum.

As a follow-on to this understanding of KTH injuries, NHTSA developed a hip injury criterion in full-frontal crash tests (Rupp et al., 2009) based on the axial load measured within the femur load cell of a crash test dummy. The criterion and its applicability to the THOR-NT are discussed later in this paper.

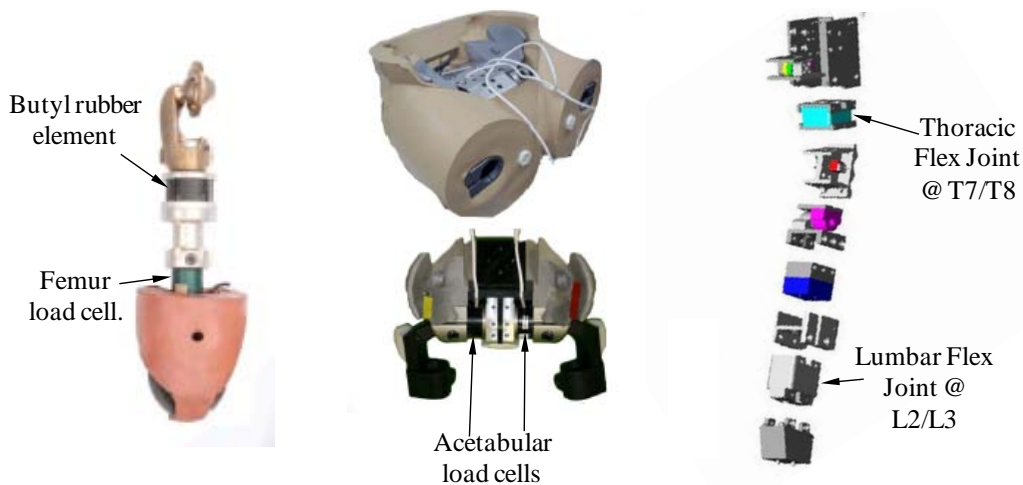


Figure 4. Unique features of the THOR-NT. Left: femur assembly; Center: pelvis within flesh (top) and removed (bottom) showing hip instrumentation; Right: exploded view of spine showing two butyl rubber flex joints in spine.

Use of THOR-NT in Narrow Offset Test Program A unique feature of the THOR-NT is that hip loads are measured directly at the acetabulum, which is where the majority of hip injuries occur in real-world frontal crashes. The THOR-NT pelvis itself provides a range of motion for the femur that is about the same as humans: 45 degrees in abduction, 30 degrees in flexion. Range of motion, as discussed later in this paper, is an important factor in assessing hip injuries under oblique loading.

These unique features are depicted in Figure 4, along with several others. As shown, the THOR-NT spine has two butyl joints for added spine flexibility over other ATDs and thus produces more realistic whole-body movement during a crash. The added flexibility in the torso results in greater right-to-left mass shift in an oblique crash, an important consideration when assessing injury potential in the acetabular region.



Figure 5. Range of motion of the THOR-NT. Maximum abduction is 45° from neutral position.

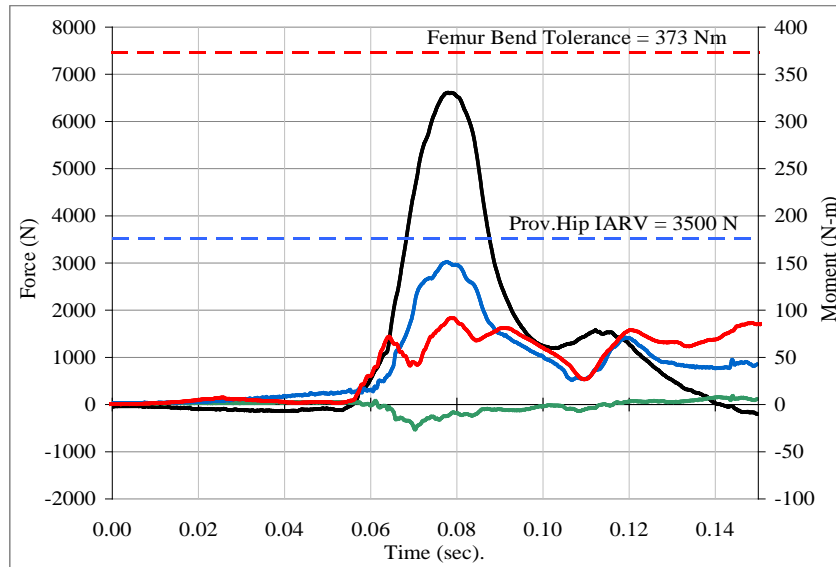
The buttocks of the THOR-NT promotes more human-like interaction with the vehicle seat. While other dummies have a pre-compressed buttocks flesh, the buttocks of the seated THOR-NT compresses under its weight and interacts with the cushion in a more realistic manner.

HIP INJURY REFERENCE VALUE FOR THOR-NT

NHTSA's work sponsored at UMTRI may be used to establish a provisional hip injury reference value applicable to the THOR-NT. The THOR-NT has a rubber element built into the femur as shown in Figure 4. Among other crash test dummies used in NHTSA's regulatory activities, this design feature is unique to the THOR-NT. It is meant to provide a more biofidelic response under knee loading. The femur assemblies of most other dummies do not have a rubber element and have been shown to be very stiff (Rupp et al., 2003).

Idealized sled tests. A series of THOR-NT tests were carried out to establish the rate of load transfer from the femur to the hip. The effects of pre-test posture on the rate of load transfer were observed by altering the amount of knee flexion and femur abduction. These 46 km/hr tests were conducted using an idealized knee bolster constructed from energy absorbing foam material with constant-stiffness properties.

The dummy was unbelted (a "catch" belt system was configured to catch the dummy late in the event to prevent total ejection) and was seated in a production seat. However, there was no instrument panel, air bag, steering wheel, or windscreen present. In other words, the only interaction between the dummy and the sled was through the knee bolster and the pelvis sliding along the seat. The full test matrix is given in the appendix.



Key:

- **Femur axial load, N.** Fz load as measured by a load cell in the distal portion of the femur (Fx and Fy loads were low in most tests). +Fz indicates femur compression (signal was inverted for display purposes.) A reference value of 10,000 N, represents a 25% probability of a femur fracture (Eppinger et al., 1999).
- **Acetabulum resultant force, N.** Resultant force measured by the load cell in the pelvis. The provisional injury reference value of 3500 N is indicated by a blue dashed line.
- **Femur bending moment, Nm** (use right axis). Resultant of the Mx and My components of moment as measured by the femur load cell. A femur bending tolerance of 373 Nm (reported in Martsen et al.) indicated by a red dashed line.
- **Acetabulum Fy-force, N.** The Fy component of the acetabulum force indicating a medial-lateral force at the acetabular cup (-Fy for right; +Fy for left).

Figure 6. THOR-NT left hip response in an idealized 46 km/hr frontal sled test. Maximum femur compression: 6605 N; maximum acetabular load: 2999N.

A typical result is shown in Figure 6 for the cases where the femur was placed in neutral positions of flexion (30°) and abduction (15°). In this test (test no. b9937) as in the others in the series, the resultant load in the acetabulum rises and falls with the femur axial load. A nominal transfer of force of 50% from the femur to the acetabulum is observed at the point of maximum femur compression. And since the femur remains unabducted throughout the event, it follows that loading of the acetabulum is mainly in the anterior-posterior direction so that lateral forces through the hip are very low and femur bending is modest. (This is seen in Figure 6 where acetabular Fy loads and resultant of the femur Mx and My moments are relatively low).

The result shown in Figure 6 is consistent among all other frontal tests in the test series. During pre-test positioning of the dummy, a modest increase in knee flexion (about 6 degrees) and abduction (apart by about 15 degrees) or adduction (together by about 5 degrees) did not effect the transfer rate appreciably. The effects of the pre-test positioning affected the resultant acetabular loads predictably: more

abduction gave greater lateral Fy contribution; more knee flexion resulted in greater Fz.

Oblique Tests. As an aside, two tests in this series were carried out in an asymmetric oblique mode in which the buck was angled 15°. For these tests, the transfer rate through the leading femur (right femur in this case) was elevated by about 3% and that through the left leg diminished by about 1%. This result mimics those observed previously in the human cadaver KTH complex as reported by Rupp et al. (2002): the oblique loading mode creates unequal reaction masses behind the right and left femurs. Since more mass is recruited by the forward-most side of the body, the reaction – or the percent of force transfer from femur to hip – is elevated. Higher moments and higher y-force contributions were also observed in the oblique mode. These observations are very relevant to the narrow offset/oblique test program and are discussed later.

Test reference information for all tests in this test series are provided in the appendix. The test data itself is available through NHTSA's on-line Biomechanics Database.

THOR-NT Hip Fracture Injury Reference Value. As reported in the UMTRI study by Rupp et al. (2009), the transfer of force from the knee to the hip in a human cadaver is about 55% for knee interactions with modern knee bolsters such as those represented by the idealized foam material described above. It was also shown that the force transferred from the knee to the femur load cell in the Hybrid III dummy is about 80% in such interactions. For the THOR-NT, the knee assembly is the same assembly as that of the Hybrid III. Since the femur load cell in both dummies is located just proximal to the knee assembly, we have assumed the knee-to-load cell transfer rate to be the same in the THOR-NT.

For the THOR-NT, the force transfer from the femur load cell to the hip is about 50% as shown in Figure 6. Thus, a scaling ratio of $(55\%) / (80\% * 50\%) \approx 1.3$ may be used to relate the human hip injury tolerance to THOR-NT load cell measurements. The 1.3 ratio is primarily an inertial compensation that accounts for the fact that the acetabular load cell is not located at the hip joint center. The 1.3 scaling ratio is used under the assumption that the THOR-NT produces the same force at the knee as a human. The validity of this assumption is discussed later in this paper.

Table 1 summarizes the THOR-NT provisional criteria for hip injuries. The value of 3500 N for hip injuries was derived from previous UMTRI studies and the 1.3 ratio described above. As reported in Rupp et al. (2010), a force at the acetabulum of 4560 N is shown to represent a 25% risk of a hip fracture for a 50th male human in a neutral posture. Using the 1.3 scaling rate, a provisional injury reference value of 3500 N represents the same 25% risk of a hip fracture as measured by the THOR-NT. This value is applied herein to assess injuries in the narrow offset and oblique crash test program.

Table 1. Provisional Hip and Femur Injury Reference Values for THOR-NT

| Value | Risk factor | Measurement | CFC | Reference |
|----------|----------------------------|---------------------------------------|-----|------------------------------|
| 3500 N | 25% risk of hip fracture | Resultant acetabular load, Fx, Fy, Fz | 600 | Rupp et al (2009) and herein |
| 10,000 N | 35% risk of femur fracture | Axial femur load, Fz | 600 | Eppinger et al. (1999) |
| 373 Nm | Femur bending tolerance | Resultant femur moment, Mx and My | 600 | Martsen et al. (1986) |

The femur bending tolerance was established by Martsen et al. (1986) for proximal femur shaft fractures. The 10 kN limit on axial femur compression is the reference value used in FMVSS No. 208 representing a 35% risk of a distal femur fracture (Eppinger et al., 1999).

CRASH TEST DATA: ACETABULAR LOADS

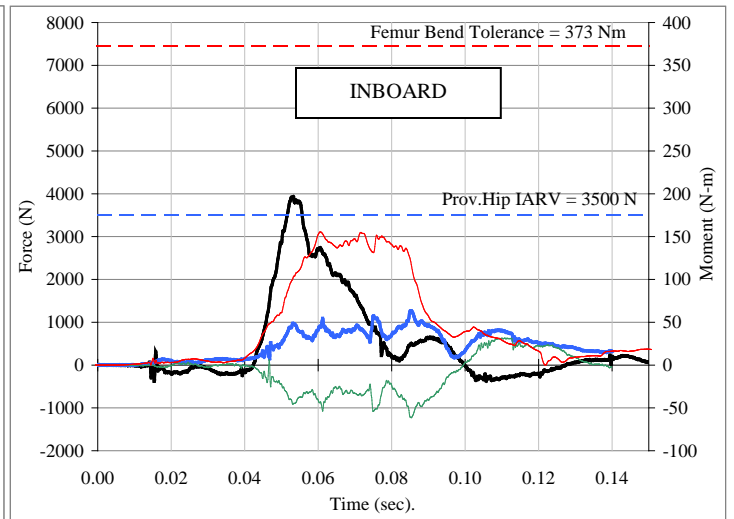
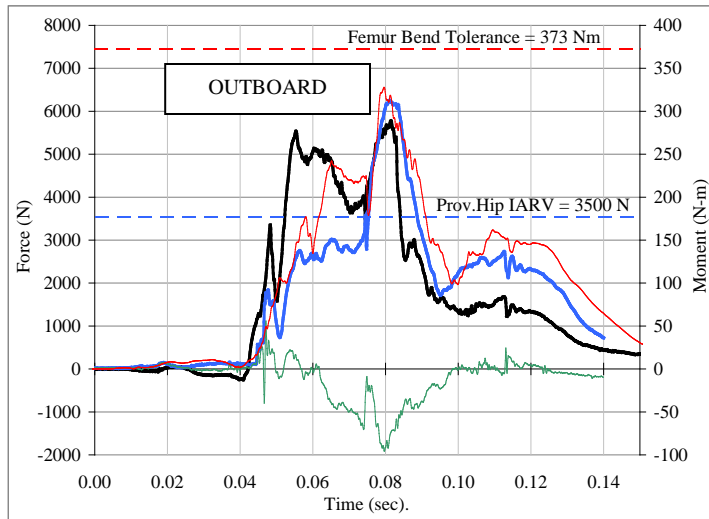
The advantages of using the THOR-NT in the narrow offset and oblique test program may be demonstrated by comparing femur and acetabular signals from three select tests as shown in Table 2. All three tests made use of the THOR-NT placed in the driver's position with the seat in the mid-track setting. Three-point seat belts were used in all three tests.

The oblique Taurus test was selected because it is representative of the oblique crash configuration in which high THOR-NT hip loads were experienced. The Yaris tests are included for comparative purposes. One test was run under the narrow offset crash configuration, and it also had high hip loads. The other was run using the crash configuration used by the Insurance Institute for Highway Safety (IIHS) to rate frontal crashworthiness. It had low hip loads as reported by Yaguchi et al. (2009). Both were run using similar versions of the Toyota Yaris – a 4-door sedan in the narrow offset test, a 5-door hatchback in the IIHS test. The two versions are considered sister vehicles in NHTSA's Five-Star Safety Rating program and received four stars for driver safety in a frontal impact under the pre-2011 rating criteria.

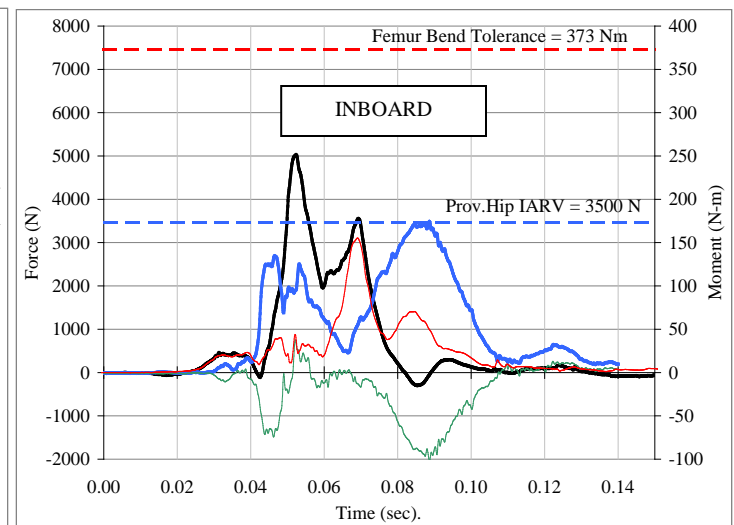
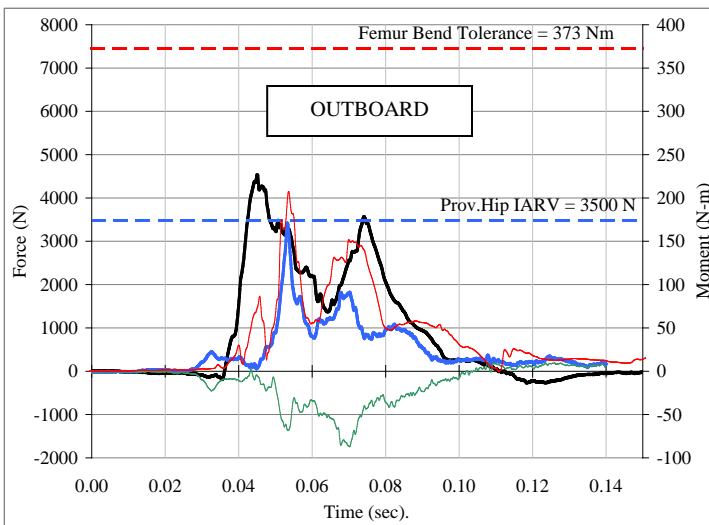
Sensor data related to femur and hip loads are given in Figure 7 and summarized in Table 3 to demonstrate how loading patterns in the hip vary depending upon the test configuration. Reference information for these tests is provided in the appendix. The test data itself is available through NHTSA's on-line Vehicle Crash Test Database.

Table 2. Select crash tests for study of THOR-NT hip response.

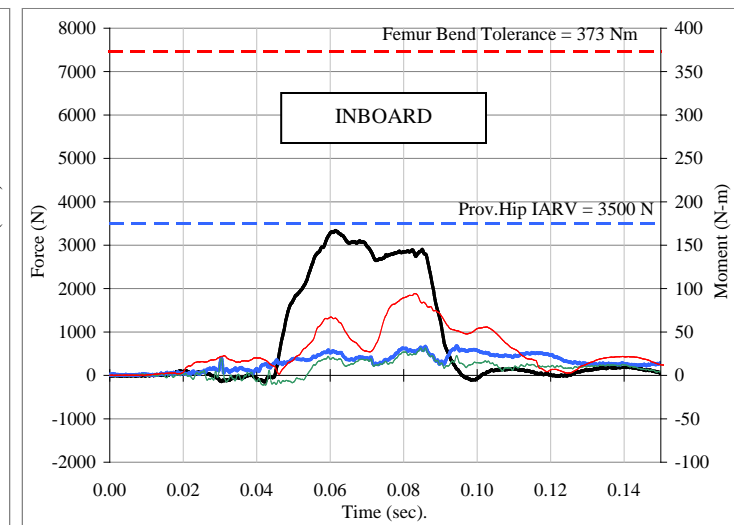
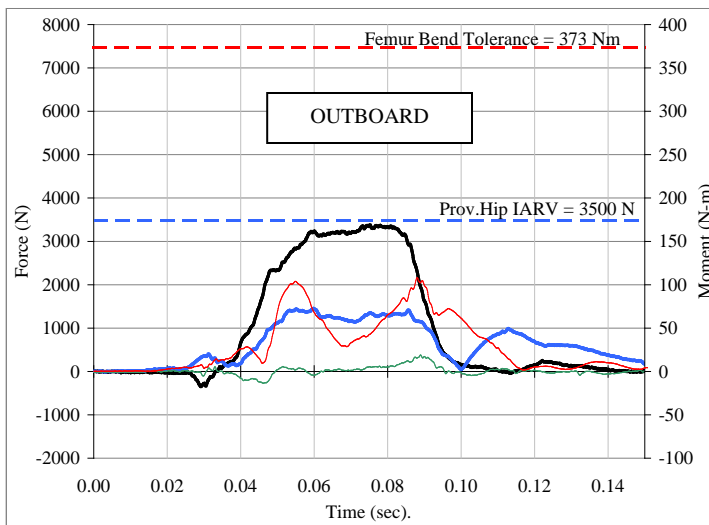
| Vehicle | Crash configuration | Delta-V (km/hr) | Angle | Overlap |
|------------------|----------------------------------|-----------------|-------|-------------------|
| '07 Ford Taurus | Oblique Vehicle to vehicle | 56 | 15° | 50% |
| '10 Toyota Yaris | Narrow offset Vehicle to vehicle | 56 | 7° | Align frame rails |
| '08 Toyota Yaris | IIHS Deformable barrier | 64 | 0° | 40% |



7a. Oblique Taurus test, v6830



7b. Narrow offset Yaris test, v7293



7c. IIHS Yaris test, b9894

Key (same definitions as previous key):
 — Femur axial load, N.
 — Acetabulum resultant force, N.
 — Femur bending moment, Nm (RH axis).
 — Acetabulum Fy-force, N.

Figure 7. THOR-NT femur and hip response in three crash tests.

Table 3. Peak measurements in test data. For medial-lateral loads, “out” equates to femur head pulled out of socket.

| Test | Aspect | Femur Compression Fz (N) | Femur Bending R(Mx,My) (Nm) | Acetabular Resultant R(Fx,Fy,Fz) (N) | Acetabular medial-lateral Fy (N) | Knee Bolster Intrusion (mm) | Lap Belt Load (N) |
|---------------------------|--------------|--------------------------|-----------------------------|--------------------------------------|----------------------------------|-----------------------------|-------------------|
| Idealized sled b9937 | Left | 6605 | 217 | 2999 | 543 (in) | --- | --- |
| | Right | 6236 | 149 | 3523 | 324 (in) | --- | |
| Oblique Taurus v6830 | Outboard (L) | 5773 | 327 | 6235 | 1939 (out) | 238 | 1651 |
| | Inboard (R) | 3993 | 155 | 1267 | 1226 (in) | 172 | |
| Narrow offset Yaris v7293 | Outboard (L) | 4537 | 207 | 3436 | 1719 (out) | 77 | 2044 |
| | Inboard (R) | 5031 | 155 | 3503 | 2015 (in) | 1 | |
| IIHS Yaris b9894 | Outboard (R) | 3378 | 108 | 1458 | 390 (out) | 24* | 3137 |
| | Inboard (L) | 3331 | 94 | 677 | 627 (in) | 16* | |
| <i>Injury Ref. Values</i> | | <i>10,000</i> | <i>373</i> | <i>3500</i> | <i>---</i> | <i>---</i> | <i>---</i> |

* Instrument panel intrusion. Knee bolster intrusion unavailable.

THOR-NT INSIGHTS ON HIP INJURIES

Loading Impulse. One of the more noteworthy trends seen in the data signals of Figure 7 is the differences in the load impulses to the outboard (left) leg in the oblique and narrow offset tests vs. the IIHS test.

In the IIHS Yaris test, femur and hip loading appear very controlled, indicative of an optimized, well-performing system. Right vs. left femur loads are about the same, and both reach a plateau that is safely below the injury reference value of 10kN. Femur bending and acetabular Fy-loads are also low, indicating minimal knee ab/adduction. As a result, outboard hip loads are also fairly low with a loading pattern very similar to that seen in the idealized sled test: the outboard hip load is essentially the same as the femur load scaled by 40%.

The hip loading patterns in the IIHS test are consistent with simple acetabular fractures seen in real-world crashes. Lacking the abduction, the femur head typically loads the isolated posterior wall of the acetabulum resulting in a simple fracture or dislocation. In other words, if a human (instead of the THOR-NT) was used in this test and suffered a

hip injury, it most likely would have been a simple acetabular fracture rather than a complex fracture.

In contrast to the IIHS-Yaris test, the narrow offset/oblique impulses exhibit much more unevenness. A double peak appears in the outboard acetabular loads. This loading pattern is repeated in several other tests in the series. Moreover, femur and acetabular loads are much higher in the narrow offset/oblique tests despite a lower crash Delta-V (56 km/hr vs. 64 km/hr in the IIHS test). The rate of the initial femur loading is also much higher in the narrow offset/oblique tests.

In all three tests, the risk of hip injury is directly related to the force impulses through the femur. Table 4 shows five critical factors which influence hip injuries that may be observed in the three crashes. These factors highlight the differences between narrow offset and oblique crashes versus collinear, 0° frontal crashes such as those represented by the IIHS barrier test and the idealized sled tests described earlier. The factors are discussed below in context with the biofidelity of THOR-NT and its ability to assess hip injuries.

Table 4. Factors influencing hip injuries in frontal crashes.

| FACTOR | HUMAN INJURIES | THOR-NT OBSERVATIONS | | | |
|--------------------------|---|-----------------------------|-------------------------------------|--|---|
| | <i>Indicative human injuries in Narrow Offset Dataset</i> | <i>Idealized sled tests</i> | <i>IIHS-type test</i> | <i>Narrow offset and oblique tests</i> | <i>Indicative THOR-NT dummy measurement</i> |
| Asymmetric hip loads | High incidence of outboard leg injuries vs. inboard leg. | Fully symmetric | Symmetry in distal femur load only. | Pronounced asymmetry. | High loads in outboard femur and hip; significant left-ward body trajectory seen in videos. |
| Femur ab/adduction | Abduction → complex hip fx. Adduction → simple hip fx. (Wide area of knee bolster contact seen in vehicle inspection report.) | None | None | Both ab- and adduction in many cases. | Significant acetabular Fy-loads; knee bolster paint transfer shows knee movement. |
| Femur bending loads | Femur shaft fracture. | Very low | Low | High in some cases. | High femur Mx and My loads usually accompanied by high lateral loads in acetabulum. |
| Medial-lateral hip loads | Medial: Complex acetabular fracture; Lateral: Hip dislocation. | Very low | Low | High in some cases. | High acetabular lateral (Fy) loads. |
| Belt-to-trochanter loads | Hip injury in absence of knee injury. | None (no belt) | Low | High in some cases. | High lap belt loads; high lateral acetabular loads in the absence of significant femur loads. |

Asymmetric loading. Force transferred to the hip from the knee is highly dependent upon the loading symmetry. In full-frontal crashes such as those represented by the idealized sled tests, knee loading is symmetric and both right and left hips experience about the same loads. Under such a condition, one may assume that the percentage of force applied to the knee that is transmitted to the hip is fixed. However, the farther a knee-loading condition deviates from applying similar forces to both knees, the less applicable the fixed assumption becomes. When knee loading is asymmetric, the amount of mass behind one of the hips is greater (usually the hip on the side in where knee force is higher). This will increase the percentage of force that is transmitted to the hip from the knee, which thereby increases the risk of hip injury.

As seen in the IIHS Yaris test, right and left femur loads are fairly alike, but the symmetry dissipates as loads are transferred to the hips. In the narrow offset/oblique tests neither the hip loads nor the femur loads show much symmetry. In particular, for the oblique Taurus test the outboard hip experiences

a load that exceeds that of the femur. It also exceeds the provisional hip injury criteria of 3500 N. Asymmetric loading is also evident in the narrow offset Yaris test.

In narrow offset/oblique crashes, significant outward body trajectory contributes to asymmetric loading. Even in the IIHS tests, a small left-to-right asymmetry appears to have affected mass coupling on different sides of the dummy. Shifting of mass also arises from the rotation of the pelvis induced by the crash configuration. The rotational inertia of the pelvis contributes to the mass imbalance, which increases the percentage of force applied to the knee that is transferred to the hip.

Femur abduction and adduction. Abduction is seen in many of the real-world cases of the Narrow Offset Dataset in which pelvis injuries occur. It is inferred by evidence of contact to the left portion of the driver's side lower instrument panel and knee bolster. Abduction is as evidenced by knee bolster damage seen in post test inspections. Fracture patterns of the hip are dependent on ab/adduction. Though the

dependence is not absolute, fractures generally occur as follows:

Abduction (knees apart) → complex hip fracture
(e.g., transverse-posterior wall fx)

Adduction (knees together) → simple hip fracture
(e.g., posterior wall fx)

Abduction raises the threshold for an acetabular injury because it forces the femur head into the socket, whereas adduction forces it out. In other words, wall fractures and dislocations have relatively low thresholds for injury because there is physically less bone to oppose the forces that cause them. Since abduction redirects these forces into the pelvis, overall hip injury risk is reduced. On the other hand, abduction increases the likelihood of a transverse-posterior wall (complex) hip fracture. And although a transverse-posterior wall fracture may have a higher force tolerance, the outcome for victims who sustain such an injury is much worse.

Real world data reveals that both types of fractures are occurring in narrow offset and oblique crashes. Thus, it is important that the knees of the dummy interact with the knee bolster in a human-like manner and it appears that the THOR-NT does so. In several of the narrow offset/oblique crash tests, the THOR-NT femurs were observed to undergo adduction (left leg) and abduction (right leg) as the pelvis moved leftward and the knees wedged against the bolster. Evidence of knee movement appears in test signals shown in Figure 7, where load signals are seen to rise initially, diminish, and then rise again. Evidence of abduction is also seen in post-test inspection of the knee bolster in the form of paint transfer.

The oblique Taurus and narrow offset Yaris data show hip loads that are consistent with both simple and complex fracture patterns. For the case of simple fractures, correspondingly high Fy acetabular loads appear in the inboard (adducted) hips. For the case of complex fractures, high Fy loads appear in the inboard (abducted) hip. All this is consistent with the injuries observed in the Narrow Offset Dataset.

Moreover, ab/adduction is usually associated with asymmetric loading. And if the adducted knee bears most of the load, then a higher knee-to-hip transfer of force will usually be experienced because a greater reaction mass opposing the axial femur load sits behind the hip. This will work to lower injury tolerance and further increase the probability of sustaining a hip injury in this loading condition.

Femur bending. Elevated acetabular forces are partly due to the fairly long impulse running axially thru the femur and partly due to a shift in mass to the left side of the body during the crash event. Moreover, femur bending is also elevated in the oblique Taurus and narrow offset Yaris tests. There appear to be multiple bending sources, not all of which stem from axial compression. Pocketing or entrapment of the knee in the presence of bolster intrusion and lateral pelvis excursion may contribute to pure bending of the femur in narrow offset and oblique crash modes.

In any event, the reaction to the bending moment at the hip probably contributes to the high acetabular load. This reaction gives rise to a significant acetabular Fy component acting to either pull the femur head out of the socket (dislocation: simple fracture) rather or drive it through the pelvis (complex fracture).

This observation is consistent with many injuries seen in the Narrow Offset Database. A high incidence of femur shaft fractures indicates significant femur bending. Moreover, the reaction at the hip associated with femur bending may have contributed to a high incidence of acetabular injuries.

Loading of trochanter by lap belt. In a typical 0° collinear crash test such as the IIHS test, lap belt loading is fairly low and the trochanter is essentially under no load. But in the narrow offset Yaris test and in other tests in the series, THOR-NT lateral hip loads are observed to be high even though femur loads are low both axially and in bending. This may be the result of other loading sources, such as lap belt loading of the trochanter. Crash test videos revealed a large inboard-to-outboard pelvis excursion which may have contributed to loading of the trochanter through the lap belt. On the other hand, hip loading via door intrusion does not appear to be a loading source in either the crash tests or real-world cases since the door panel buckles outward. These observations may help explain how some occupants in the Narrow Offset Dataset sustained a hip injury.

Hip flexion. Hip flexion occurs two ways: when the torso rotates forward and when the knee itself moves upward. Both of these instances are observed in videos of narrow offset and oblique tests. In other narrow offset crash tests, videos show that the left femur goes into flexion, sliding up so that the Fx and Fz loads in the acetabulum are diminished. Also, the Fx and Fz components of acetabular force are observed to swap as the femur goes into flexion. Flexion becomes most pronounced as the occupant space becomes compromised by intrusion. It occurs

during pelvis rotation as the torso of the dummy lurches to the outboard side of the air bag.

Hip flexion lowers the force threshold for an acetabular wall fracture or dislocation, and thus increases the risk of such an injury. Flexion acts to drive the femur in a direction inferior to the pelvis (+z direction) where there is physically less bone to oppose the forces. This is also consistent with the high incidence of hip dislocations seen in the Narrow Offset Dataset.

Utility of the THOR-NT. In the real-world Narrow Offset Dataset, left hip injuries outnumber right hip injuries by a margin of five to one. Thus, in order to accurately assess hip injury potential in narrow offset and oblique crash tests, it is important to use a dummy that is sensitive to asymmetric loading. The THOR-NT is well suited for this task. With its flexible spine, compliant femur, and soft buttocks flesh, it is able to move within the occupant compartment and interact with the seat and knee bolster in a life-like manner.

Furthermore, the THOR-NT's increased range of motion lessens the likelihood of binding of the hip joint which would result in unrealistic body kinematics and hip loading. (In comparison, the Hybrid III femur range of motion in abduction is only about +20°/-10° from the neutral position.)

INJURY ASSESSMENT: Narrow Offset/ Oblique vs. Frontal, 0° Colinear

KTH criteria background. In past work at UMTRI, the focus was placed on femur and hip loading in colinear (0°) frontal crashes. The KTH criterion developed by Rupp et al. (2009) is based on cadaver tests with femur loads that were primarily axial (Fz) with very little bending. Thus, it is only valid for loads borne by the hip axially thru the femur and is most suitable for use in 0° frontal crashes.

The KTH criterion was developed for use with the Hybrid III 50th male and 5th female dummies as demonstrated by Kirk and Kuppa (2009). As such, it predicts hip injuries without actually measuring force at the hip. Instead, the criterion is based on the axial force through the femur load cell in which the force impulse is used to indicate whether or not a sufficient amount of femur force is transferred to the hip. The criterion was developed for an ideal case of a force-limited knee bolster and symmetric knee loading with the femurs positioned in a neutral position (30° flexion, 15° abduction) similar to the position specified in a typical standardized frontal test.

The KTH injury criterion assumes that the percentage of force applied to the knee that is transmitted to the hip is fixed. But if the surface impacting the knee is rigid and loading durations are short, then the percentage of force transmitted from the knee to the hip is much smaller. Because the duration is short, there isn't enough relative motion of the femur to recruit the amount of mass behind the hip that is necessary to generate the reaction force at the hip. Thus, the actual force transfer is lower than the assumed (fixed percentage) force transfer. The KTH criterion tries to account for hard vs. soft knee impacts by adjusting the hip injury reference value downward as the length of the impulse at the femur load cell increases.

THOR-NT acetabular force criteria. Narrow offset and oblique crashes violate many of the assumptions under which Rupp et al.'s femur-based KTH criteria is applied. Femur loads alone do not account for important variables that influence hip injury potential, such as mass transfer, flexion, abduction, or other load sources (such as lap belts and door interaction). Furthermore, other established femur reference values (373 Nm for femur shaft fracture, and 10,000 N distal femur fracture) are not particularly useful in assessing hip injury potential.

In collinear, 0° frontal crashes like the IIHS Yaris test, femur moments have not generally been considered to be primary measurements for injury assessment because femur bending is caused by axial compression. Thus, femur fracture from bending is thought to be limited by injury criteria based on peak femur loads. This is not always observed to be the case in narrow offset tests, such as the narrow offset Yaris test (left leg). For this case, femur bending correlates to the acetabular load much more closely than to axial femur compression. Thus, an acetabular load-based criterion offers a measure of safeguarding against femur shaft fractures, which are also shown to be more abundant in real-world narrow offset and oblique impacts (Rudd et al, 2011).

Furthermore, lateral hip loads such as those associated with the reaction forces at the hip due to femur bending were not addressed in previous work at UMTRI. These loads were negligible in the UMTRI testing and modeling and they are shown to be negligible in the IIHS Yaris test. For the narrow offset and oblique tests, however, they are shown to be quite significant.

Thus, a provisional hip injury criterion for THOR-NT is necessary to assess hip injury potential in narrow

offset/oblique tests. Its basis is measurements from the three-axis load cell at the acetabulum which provides a direct measurement of the force at the hip. The acetabular load cells measure directly any non-symmetric loading, which has been observed to result in more force being transferred to the hip in oblique tests.

Applicability of criteria. We note that the criterion developed by Rupp et al. (2009) is very suitable to the hip loading seen in the idealized sled tests and the IIHS Yaris test. In these tests, the overall response of the knee, femur, and acetabular loading was very much like the loading patterns studied in the UMTRI cadaver tests from which the criterion itself is based. These tests indicate general adherence to the KTH criteria assumptions:

- Symmetry – equal femur loading right vs. left.
- Controlled knee bolster interaction.
- Acetabular force - 50% of axial femur load (outboard side).
- Very low lateral (Fy) force component into the acetabulum.
- No observable abduction or adduction.

As noted earlier, the Yaris performed well in the IIHS test under any injury measure, including the femur-based KTH impulse criterion. It is likely that the bolster design of the Yaris was optimized for the IIHS test using a Hybrid III dummy. The good performance using the THOR-NT provides added support that it would carry over to humans. Furthermore, a matching IIHS Yaris test run with a Hybrid III 50th male (reported by Yaguchi et al., 2007) reveals the THOR-NT and the Hybrid III to be essentially equivalent based on FMVSS No. 208 metrics (Femur Fz) and the Rupp et al. femur-based KTH criterion.

Thus, the well-performing Yaris knee bolster is reflected by low injury metrics as measured by either the THOR-NT or Hybrid III in an IIHS test. This applies to all relevant criteria, including Rupp et al.'s femur-based KTH impulse criterion and THOR-NT acetabular loads. We also observe that many of the unique features of the THOR-NT are not exercised to their full extent in the IIHS test configuration:

- Flex spine – not needed because all body movement is in the anterior-posterior direction.
- Femur range of motion – no abduction is observed, and little knee flexion.
- Compressive femur element – not as critical if injury criterion is based on femur load cell, which is located at proximal end of femur.

- General knee biofidelity – controlled interaction with knee bolster.

Most of the assumptions under which the Rupp et al. femur-based KTH impulse criterion applies held true in the IIHS Yaris test. However, nonconformities to the assumptions did exist to a limited extent. For example, acetabular loads were unequal despite near identical axial femur loads. And even in full frontal crashes with the THOR-NT, perfectly symmetric loading of the knees is rarely observed. Thus, when the THOR-NT is used in any frontal test, the use of an acetabular load criterion to assess hip injuries is advised.

CAVEATS

There are two caveats with applying the provisional hip criteria developed for the THOR-NT. We note that these caveats also apply to the femur-based KTH criterion developed by Rupp et al.:

Caveat 1, THOR-NT-to-human scaling ratio. As mentioned earlier, the 1.3 ratio compensates for the acetabular load cell not being located at the hip joint center. Moreover, the ratio is based on sled tests with symmetric loading and a neutral posture. We have assumed that it also applies to situations where there is hip flexion and femur ab/adduction. This assumption is buttressed by observations from the idealized sled tests where abduction and flexion do not influence the transfer rate appreciably. We have also assumed that the ratio applies to all forces, including lateral loads induced primarily by femur bending and trochanter loading.

For asymmetric loading, the ratio of knee-to-hip forces in the THOR-NT will vary due to mass effects. A reasonable assumption is that the ratio of forces in a human would vary similarly. Under this assumption, the scaling ratio of 1.3 applied herein would still be valid under asymmetric loading.

Caveat 2, knee-to-hip singular relationship. As discussed earlier, the knee-to-hip ratio of force is:

$$\begin{array}{l} \text{THOR-NT} = (0.80 * 0.50) = 40\% \\ \text{Human (cadaver)} = 55\% \end{array}$$

As shown in Figure 8, the injury tolerance scale of 55/40 \approx 1.3 applied herein is based on knee interaction with a force-limiting knee bolster.

For knee bolsters constructed with non-force limiting padding (or loading less than the limit), the peak force applied to the THOR-NT knee – and hence, the

force measured by the femur load cell – will always be greater than the peak force applied to the human knee. This is because the THOR-NT KTH complex has greater effective mass and stiffness than that of a human, and will therefore penetrate further into the knee bolster. In other words, there is no singular relationship between peak force at the THOR-NT femur load cell and peak human hip force that is valid over the full range of knee bolster force vs. deflection characteristics. So for many bolster loading cases, the criteria will over-predict injury.

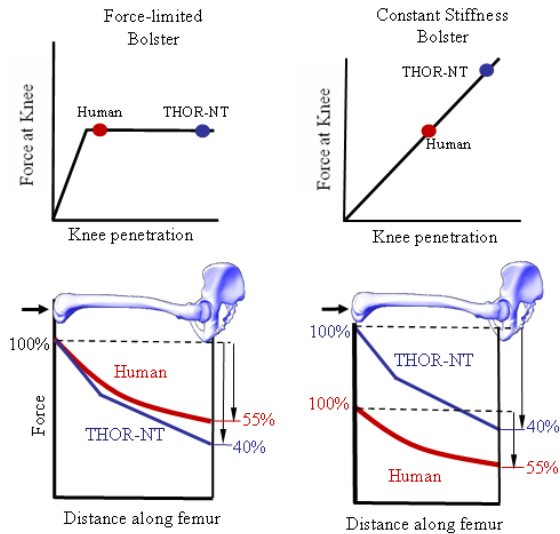


Figure 8. Effects of knee bolster characteristics on human vs. THOR-NT knee forces. Left: Force-limiting bolster: equivalent knee loads; Right: constant-stiffness bolster: higher knee loads in THOR-NT.

THOR-NT MOD KIT

The knee bolster limitation described in Caveat 2 has been relieved greatly by recent updates to the THOR-NT. Parent et al (2011) describes the latest hardware and instrumentation package to be installed in the dummy. These modification kits provide improved biofidelity in the knee-thigh-hip complex as well as other body regions. The modification kit provides additional femur compressive properties that results in knee loading equal to that of the cadaver for all types of bolsters, not just an ideal force-limiting bolster. Therefore, this modification overcomes the problem discussed earlier in Caveat 2. In other words, there does exist a singular relationship between the peak forces at the modified THOR-NT and cadaver hips that is valid over a wider range of knee bolster force vs. deflection characteristics.

In another feature of the modification kit, the pelvis flesh has been made so that it is less tightly coupled

to the femur bone. This makes it more like humans. It is important because the tight grip of the flesh to the femur in the current THOR-NT can influence the effective reaction mass behind the hip, and hence, the load to the hip – particularly when the dummy has rotational inertia as seen in the narrow offset and oblique tests.

OPPORTUNITIES FOR FINE TUNING INJURY CRITERION

The THOR-NT offers additional opportunities for an enhanced hip injury criterion. In a human, the area of the acetabular surface able to resist force applied through the femur and the volume of bone behind depends on hip posture. The observations from the Narrow Offset Dataset and from experimentation at UMTRI show that hip injury tolerance is dependent upon abduction. Hip injury tolerance is completely due to the manner in which posture changes how load is borne by the pelvic bone: knees together – hip more easily dislocated by an axial femur load (low tolerance); knees apart – femur vector is aimed more towards center of pelvis (higher tolerance).

A provisional THOR-NT hip injury criteria has been applied herein based on the resultant acetabular load (F_x , F_y , F_z). If there were a way to measure hip flexion/extension or ab/adduction in the THOR-NT it may be possible to come up with a hip injury criterion that was posture dependent rather than one that just uses a typical hip posture. One possibility would be to parse out the contributions of F_x , F_y , and F_z loads in the acetabular load cell. But using the relative F_x , F_y , F_z contributions of acetabular force to determine hip posture could be highly problematic given the likelihood of trochanter loading (either from the seatpan, the lap belt, or the door) and femur bending reactions which could induce considerable error into the calculated posture. Other instrumentation may be required.

Furthermore, our understanding of hip injury tolerances is based mostly on laboratory tests at UMTRI with very little lateral F_y loading into the acetabulum. We did not consider hip reaction to femur bending moments or trochanter belt loading as primary sources of hip loading. But high levels of lateral loads into the acetabulum were observed in the narrow offset/oblique tests. This is consistent with complex acetabular fractures observed in the Narrow Offset Dataset. Thus, further analysis of injury tolerances associated with complex acetabular fractures are needed in order to develop a criterion in which lateral loading is treated separately.

As for the THOR-NT dummy itself, there is currently no specification for the range of motion or joint torque requirements in ab/adduction, and it is unknown whether THOR-NT dummies are consistent from one to another in this regard. Given the importance of ab/adduction in determining hip injury potential, it may be important to specify joint torque requirements.

Also, there are no biofidelity specifications for the flesh that covers the trochanter. If belt loading is found to be a significant contributor to hip injuries, human flesh specifications would be needed so that the THOR-NT flesh properties could be adjusted as needed.

LIMITATIONS

- The study is limited to a sample of crash tests, each with unique features. There were no repeat tests. In addition, only the driver seating position was evaluated.
- We were not able to clearly observe or readily measure the amount of hip flexion and ab/adduction experienced by the THOR-NT during the crash events. Flexion and ab/adduction could only be approximated by observing video and post-test knee-to-bolster paint transfer.
- No attempt was made to determine the left to right variations in the reaction mass behind the hip with any precision. General inferences on mass recruitment were made based on the transfer of force from the femur to the hip and from dummy kinematics observed in crash videos.
- The THOR-NT modification kit has not been evaluated for its knee-to-hip transfer of force. In all likelihood, the kit will change the ratio of force transfer between the knee and the hip. Also, it has not been verified whether the THOR-NT modification kit produces the same knee force as humans for all bolster designs.
- The difference in knee-to-hip transfer rates between the THOR-NT and humans is partly due to the location of the acetabular load cell, which is not located precisely at the acetabulum. As shown in Figure 4, an aluminum socket adapter (0.3 kg) sits between the load cell and the femur head. As the pelvis (total mass: 11.7 kg) opposes femur loads during a dynamic event, the inertia of the socket opposes the inertia of the pelvis rather than adding to it. So, the force at the load cell will always be diminished by the mass of the socket. The pelvis modification kit does not change this configuration. Thus, even after the modification kit is in place, the

force recorded by the acetabular load cell will probably still need to be scaled up.

- In the IIHS Yaris test, the left acetabular Fx and Fz forces (those forces resisting the rearward, longitudinal movement of the femur) appear to be unreasonably low and may be the result of an error in the sensitivity factor or an instrumentation malfunction. The low forces are not consistent with other THOR-NT tests.
- In the idealized sled tests, the test conditions and dummy kinematics were highly symmetric, yet the left femur loads were about 5% greater than the right, and the right acetabular loads were about 15% greater than the left. This trend was consistent for all tests in the series. This result may indicate errors in the application of load cell sensitivity factors. Hence, the nominal force transfer factor of 50% used to establish the provisional injury criterion was based on an average of the left and right hip forces.

AVAILABILITY OF DATA

All reports and data, including time-history traces, videos, and still photos from the tests described herein may be downloaded by accessing NHTSA's online Biomechanics and Vehicle Crash Test Biomechanics Database at: <http://www.nhtsa.gov/Research/Databases+and+Software>. Reports include descriptions of the test set-ups and instrumentation. Data channels collected, but not reported herein, include over 100 signals per test.

SUMMARY

Full-scale vehicle tests were performed with the THOR-NT crash test dummy to gain insight into the root causes of injuries sustained by occupants involved in narrow offset and oblique crashes. The dummy was shown to measure hip loads that are consistent with pelvic injuries observed in real-world crash victims. Hip loads exceeded the expected injury threshold (3500 N) for an acetabular fracture. Moreover, hip loading patterns were shown to be very different in narrow offset and oblique crashes from those seen in co-linear 0° crashes such as an IIHS 40% offset crash test. Some of the key observations are listed below.

1. Hip loads are dependent upon the position of the thigh, the trajectory of the torso, and intrusion of the knee bolster.
2. As opposed to co-linear 0° tests, right-to-left femur and hip loads vary significantly in narrow offset and oblique tests.

3. In co-linear 0° crashes, hip loading extends from axial femur compression, whereas hip loading in narrow offset and oblique tests may emanate from other sources such as femur bending and trochanter loading.

4. Lateral hip loading – which is not seen in co-linear 0° tests – is manifested by the asymmetry and ab/adduction occurring in narrow offset and oblique tests. These loads are consistent with acetabular fractures observed in the real world.

5. Knee bolster interaction is much less controlled in narrow offset and oblique tests, and vehicle intrusion contributes to knee movement and high hip loads.

6. The THOR-NT – with its unique biofidelic features and instrumentation package – provides significant insight into hip injury causation. Such insights cannot be discerned from the signals of the femur load cell alone. An injury criterion based on THOR-NT's acetabular load cell measurements shows promise for assessing hip injuries in narrow offset and oblique crashes.

REFERENCES

Bean JD, Kahane CJ, Mynatt M, Rudd RW, Rush CJ, Wiacek C (2009), Fatalities in Frontal Crashes Despite Seat Belts and Air Bags, Review of All CDS Cases Model and Calendar Years 2000-2007 122 Fatalities, U.S Department of Transportation, Report No. DOT HS 811 102, September 2009.

Dakin GJ, Eberhardt AW, Alonso JE, Stannard JP, Mann KA (1999), Acetabular fracture patterns, associations with motor vehicle crash information, *Journal of Trauma*, V47(6), pp1063-82, Dec. 1999.

Eppinger RH, Sun E, Bandak F, Haffner M, Khaewpong N, Maltese M, Nguyen T, Takhounts EG, Tannous R, Zhang A, Saul R (1999), Development of Improved Injury Criteria for the Assessment of Advanced Automotive Restraint, Systems – II. NHTSA Report, U.S. Department of Transportation, Washington DC.

Giannoudis PV, Grotz MRW, Papakostidis C, Dinopoulos H (2005), Operative treatment of displaced fractures of the acetabulum, *Journal of Bone and Joint Surgery*, V87-B(1), pp2-9.

Kirk K and Kuppa S (2009), Application and evaluation of a novel KTH injury criterion for the Hybrid III dummy in frontal crash test environments. Paper No. 09-0196, Proceedings of the 21st International Technical Conference on the Enhanced Safety of Vehicles, Stuttgart, Germany, June, 2009.

Martens M, van Audekercke, R, de Meester P, and Mulier JC (1986), Mechanical behavior of femoral bones in bending load. *Journal of Biomechanics* 19(6): 443-454.

Parent D, Ridella SA (2011), Modifications to improve the durability, usability, and biofidelity of the THOR Dummy, Paper No. 11-0312, Proceedings

of the 21st International Technical Conference on the Enhanced Safety of Vehicles, Washington DC, June 2011.

Pintar FA, Yoganadan N, Halloway D, (2010), NASS analysis in support of NHTSA's frontal small overlap Program, Technical Report, DTNH22-09-X-00193, U.S. Dept. of Transportation, Washington DC..

Rudd R, Scarboro M, Saunders J (2011), Injury Analysis of Real-World Small Overlap and Oblique Frontal Crashes, Paper No. 11-0384, Proceedings of the 21st International Technical Conference on the Enhanced Safety of Vehicles, Washington DC, June 2011.

Rudd RW, Bean J, Cuentas C, Kahane CJ, Mynatt M, Wiacek C (2009), A study of the factors affecting fatalities of air bag and belt-restrained occupants in frontal crashes, Paper No. 09-0555, Proceedings of the 21st International Technical Conference on the Enhanced Safety of Vehicles, Stuttgart, Germany, June, 2009.

Rupp JD, Reed MP, Van Ee CA, Kuppa S., Wang SC, Goulet JA, and Schneider LW (2002), The tolerance of the human hip to dynamic knee loading. *Stapp Car Crash Journal* V46, 211-228.

Rupp JD, Reed MP, Jeffreys TJ, Schneider LW (2003), Effects of hip posture on the frontal impact tolerance of the human hip joint. *Stapp Car Crash Journal* V47, 21-33.

Rupp JD, Reed MP, Miller CS, Madural NH, Klinich KD, Schneider LW, Kuppa SM (2009), A development of new criteria for assessing the risk of knee-thigh-hip injury in frontal impacts using Hybrid III femur force measurements, Paper No. 09-0306, Proceedings of the 21st International Technical Conference on the Enhanced Safety of Vehicles, Stuttgart, Germany, June, 2009.

Rupp JD, Flannagan CA, Kuppa SM (2010), Development of an injury risk curve for the hip for use in frontal impact crash testing. Journal of Biomechanics 34(3):527-531.

Saterbak, AM, Marsh JL, Turbett T, Brandser E (1996), Acetabular fractures classification of Letournel and Judet – a systematic approach, Iowa Orthopaedic Journal, V15, pp 184-196.

Saunders J, Prasad A, Suway J (2011), Feasibility of using the moving deformable barrier in a small

overlap oblique test procedure, Paper No. 11-0343, Proceedings of the 21st International Technical Conference on the Enhanced Safety of Vehicles, Washington DC, June 2011.

Yaguchi M, Ono K, Masuda M, Watamori T, Seshita T, Hibino T (2009), Comparison of dynamic responses of the THOR-NT and Hybrid III in offset frontal crash test, Paper No. 09-2068, Proceedings of the 21st International Technical Conference on the Enhanced Safety of Vehicles, Stuttgart, Germany, June, 2009.

APPENDIX

Idealized sled tests

| Test No. | Knee position (ab/adduction) | Knee position (hip flexion) | Nominal Delta-V (km/hr) | Angle | Test No. | Knee position (ab/adduction) | Knee position (hip flexion) | Nominal Delta-V (km/hr) | Angle |
|----------|------------------------------|-----------------------------|-------------------------|-------|----------|------------------------------|-----------------------------|-------------------------|-------|
| b9937 | Neutral | Neutral | 46 | 0° | b9944 | Wide Apart | Neutral | 46 | 0° |
| b9938 | Neutral | Knees raised | 46 | 0° | b9945 | Together | Knees raised | 46 | 0° |
| b9939 | Wide Apart | Neutral | 46 | 0° | b9946 | Wide Apart | Knees raised | 46 | 0° |
| b9940 | Together | Knees raised | 46 | 0° | b9947 | Neutral | Neutral | 46 | 0° |
| b9941 | Neutral | Neutral | 46 | 0° | b9948 | Neutral | Neutral | 46 | 15° |
| b9942 | Wide Apart | Knees raised | 46 | 0° | b9949 | Neutral | Neutral | 46 | 15° |
| b9943 | Neutral | Knees raised | 46 | 0° | | | | | |

Full-scale vehicle crash tests

| Test No. | Vehicle | Test Type | Crash Configuration | Nominal Delta-V | Angle | Overlap |
|----------|-------------------|-------------------|---------------------|-----------------|-------|--------------------------------|
| b9894 | 2008 Toyota Yaris | IIHS - THOR-NT | DB | 64 km/hr | 0° | 40% |
| b9893 | 2008 Toyota Yaris | IIHS - Hybrid III | DB | 64 km/hr | 0° | 40% |
| v7293 | 2010 Toyota Yaris | Narrow offset | VTV | 56 km/hr | 7° | Coincident frame rails |
| v7292 | 2007 Ford Taurus | Narrow offset | VTV | 56 km/hr | 7° | Coincident frame rails |
| v7145 | 2010 Toyota Yaris | Narrow offset | Pole | 56 km/hr | 7° | --- |
| v7144 | 2007 Ford Taurus | Narrow offset | Pole | 56 km/hr | <7° | --- |
| v6873 | 2009 Honda Civic | Narrow offset | Pole | 56 km/hr | 7° | --- |
| v6872 | 2005 Honda Civic | Narrow offset | Pole | 56 km/hr | <7° | --- |
| v6855 | 2007 Ford Taurus | Narrow offset | MDB | 48 km/hr | 15° | 18% |
| tbd | 2007 Ford Taurus | Narrow offset | MDB | 56 km/hr | 7° | Align outer edge of frame rail |
| tbd | 2010 Toyota Yaris | Narrow offset | MDB | 56 km/hr | 7° | Align outer edge of frame rail |
| v6865 | 2007 Ford 500 | Oblique (HIII) | VTV | 56 km/hr | 15° | 50% |
| v6831 | 2007 Ford 500 | Oblique | VTV | 56 km/hr | 15° | 50% |
| v6830 | 2007 Ford Taurus | Oblique | VTV | 56 km/hr | 15° | 50% |
| tbd | 2010 Toyota Yaris | Oblique | VTV | 56 km/hr | 15° | 50% |
| v6937 | 2007 Ford 500 | Oblique | MDB | 56 km/hr | 15° | 50% |
| v6852 | 2007 Ford Taurus | Oblique | MDB | 56 km/hr | 15° | 50% |
| tbd | 2007 Ford Taurus | Oblique | MDB | 56 km/hr | 15° | 35% |
| tbd | 2007 Ford 500 | Oblique | MDB | 56 km/hr | 15° | 35% |
| tbd | 2010 Toyota Yaris | Oblique | MDB | 56 km/hr | 15° | 35% |
| tbd | 2010 Ford Fusion | Oblique | MDB | 56 km/hr | 15° | 35% |

ANALYSIS OF THORACIC LOADING, KINEMATICS, AND INJURIES IN SMALL OVERLAP IMPACTS: FIELD DATA AND FULL-SCALE VEHICLE TESTS WITH DUMMIES

Jason J Hallman
Narayan Yoganandan
Dale Halloway
James Rinaldi
Frank A Pintar
Medical College of Wisconsin
United States
Paper Number 11-0341

ABSTRACT

In the literature frontal crashes typically have been classified as full, large overlap, or small overlap impacts (SOI) in accordance with the degree of frontal area involvement. These classifications implicitly refer to the degree of longitudinal structure engagement during impact. While full and large overlap impacts have received considerable attention, SOI has undergone limited analyses through field and laboratory investigations. Limited structural engagements may expose occupants to increased intrusions and differing kinematics. The objective of this study was to summarize literature relevant to SOI, determine occupant injuries using CIREN data, and analyze occupant loading and motions using full-scale vehicle tests. CIREN results demonstrated lack of correlation between injury and typical crash severity parameters of ΔV , crush distance, and extent zone. Full-scale crash tests suggested that occupant kinematics in SOI may be unique among frontal impact configurations.

INTRODUCTION

Since the 1960's, traffic death rates have steadily declined in the United States. The National Highway Traffic Safety Administration (NHTSA) reported that traffic deaths per 100 million vehicle miles traveled fell from 5.5 to 1.13 between 1966 and in 2009 [1]. This decline may be attributed in part to advances in vehicle crashworthiness in frontal impacts, which remain the most common vehicle crash mode [1]. These advances were catalyzed in large part by consumer crash test programs such as those performed by the Insurance Institute for Highway Safety (IIHS) and the New Car Assessment Programs (NCAP) conducted by numerous governments. These tests evaluate occupant protection during impact into a fully-engaged flat rigid barrier (US-NCAP) or into a deformable barrier with 40% frontal width engagement (IIHS, EuroNCAP). Between 1979 and 2007, vehicles rated in frontal impact by

US-NCAP at four and five stars (max = five) increased from less than 30% of models tested to greater than 98% [2]. Between 1995 and 2009, tested vehicles achieving the highest IIHS frontal impact rating increased from less than half to 91% [3].

Vehicles performing well in NCAP and IIHS tests are typically designed with energy-absorbing structural members oriented longitudinally (Fig. 1) [4]. These longitudinal members lie bilateral to the powertrain (for front-engine configurations) and inside of the front wheel track and suspension components. During full and 40% frontal width engagements, at least one of these energy-absorbing components is loaded, dissipating crash energy and transferring it around the occupant compartment.

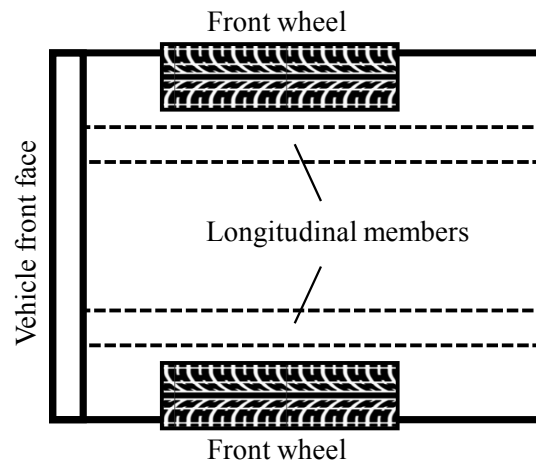


Figure 1. Vehicle overhead view demonstrating orientation of longitudinal structural members.

As a consequence of crashworthiness improvements in these crash scenarios, the small overlap impact (SOI) has emerged recently as the frontal crash mode of greatest risk to vehicle occupants. A recent report by NHTSA cited SOI as the most common scenario of preventable mortality amongst frontal impacts in

the National Automotive Sampling System / Crashworthiness Data System (NASS/CDS) during 2000-2007 [5]; these deaths occurred despite correct belt restraint usage and airbag deployment. Lack of structural engagement was cited as the primary factor leading to fatality in these crashes. Therefore, the objective of the present study was to distill current advances with regard to SOI through an examination of preexisting literature, recent CIREN injury data, and vehicle crashworthiness experiments.

LITERATURE

Using a collection of German crash data collected over a 20 year period, 502 crashes were found to result in injury [6]. Of these crashes, 62% corresponded to frontal impacts; 75% of these could be classified as partial overlap loadings, i.e., less than 50% frontal width engagement. Examination of this same dataset by another study revealed that 26% of frontal impacts were characterized by $\leq 30\%$ frontal width overlap [7]. Structural involvement characteristics were not reported, but a companion study described the structural modifications necessary to protect occupants when frontal width engagement was 40% or less [8]. The authors noted that these improvements, particularly occupant compartment stiffening, also may contribute to improved protection in more severe impacts, i.e., narrower overlap.

A sample of 1,872 frontal crashes in England between 1983 and 1990 was examined for vehicle damage and occupant injuries [9]. The authors defined SOI as an impact with less than 60% frontal width overlap (less than 45% when impacting rigid objects) and only one longitudinal member engaged. Comparing injuries to averages for all frontal crash modes, belted occupants in SOI crashes sustained higher incidences of head (66 vs. 58%), neck (24 vs. 22%), and thigh (53 vs. 43%) injuries. Occupants in SOI crashes sustained decreased incidence of torso injuries (66 vs. 69%). Yet, the authors' definition of SOI allowed for engagement of one structural member. This definition may more resemble the current IIHS test configuration.

Crash data from 52 fatal accidents in Great Britain were examined specifically for structural engagement [10, 11]. It was reported that in 25 cases (48%) only one longitudinal member was loaded. Yet, in 18 cases (36%) no major structures were fully engaged; in 4 of these cases one longitudinal member was considered to be partially loaded. A 40% frontal width overlap test with deformable barrier was recommended; this boundary condition was designed

to avoid engine block engagement, forcing energy transfer through the vehicle structural components.

Using a primarily Swedish dataset of crashes involving Volvo automobiles, frontal impacts were found to compose 36% of crashes [12]. SOI impacts, termed severe partial overlap collisions, were defined by less than 50% overlap, principal direction force (PDOF) = $0^\circ \pm 30^\circ$, and "extensive deformation." When SOI crashes were parsed from other crash types, e.g., frontal, side, rollover, etc., they composed 3% of all crashes but 14% of accidents with AIS 2+ injuries. Crash tests into a rigid barrier with 35% frontal width engagement were proposed to replicate case observations.

Many studies have utilized the Collision Deformation Classification (CDC) published by the Society of Automotive Engineers [13]. The CDC represents a standardized seven digit alphanumeric code describing the crash direction (PDOF), general area of involvement, horizontal and vertical regions of direct damage, type of damage distribution (e.g., wide impact area or sideswipe), and deformation extent into vehicle structure (Fig. 2). With regard to horizontal region of direct damage, the CDC documents the degree of frontal width involvement using three equal segments (Left, Center, and Right); documentation indicates segment(s) included, i.e., when direct damage is less than one-third, between one-third and two-thirds, or greater than two-thirds frontal width (Fig. 3). Further information is obtained from the type of damage distribution (Table 1) and the extent zone (Fig. 4). Information regarding vehicle structural engagement is not included explicitly in the CDC.

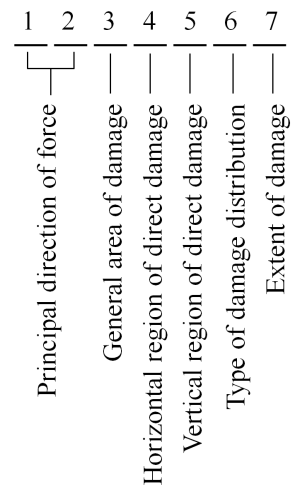


Figure 2. Collision Deformation Classification (CDC) system format.

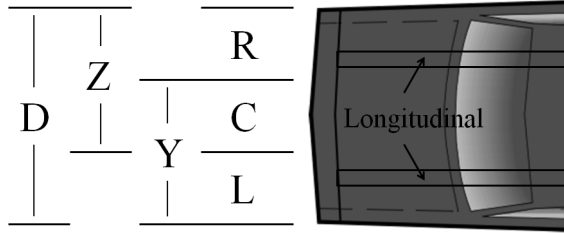


Figure 3. Relevant CDC codes with regard to horizontal region of direct front damage.

Table 1. Types of damage distribution in CDC.

| Type | Code | Engagement |
|---------------|------|----------------------|
| Sideswipe | S | Corner, ≤ 10 cm |
| Corner | E | Corner, 10 - 41 cm |
| Narrow Impact | N | < 41 cm |
| Wide impact | W | ≥ 41 cm |
| Overhanging | A | Inverted step |
| Conversion | K | >1 type |
| Unknown | 9 | - |

Using 1990-92 NASS data and CDC codes, 46% of frontal impacts were found to involve greater than 2/3 frontal area [14]. Of the remaining crashes, 20% involved less than 1/3 frontal area and 32% involved between one-third and two-thirds frontal area. To simulate a collinear two-vehicle impact with 50% frontal width overlap, vehicles were tested with a deformable barrier and frontal overlaps of 50% ($n = 3$), 40% ($n = 8$), and 30% ($n = 2$). While resulting structural engagement was not described; the authors noted that the CRASH3 algorithm, which estimated crash ΔV from vehicle crush, was inappropriate for the two vehicles tested with 30% overlap.

Following the introduction of vehicles which performed well in partial overlap deformable barrier impacts, field analyses reexamined the real-world performance of the new fleet. In place of the generalized CDC, a systematic analysis of structural components was proposed [15] and applied to a Swedish dataset of 53 fatal crashes involving 61 belted occupants [16]. In 20 of these crashes, no longitudinal members were loaded. Moreover, the most commonly reported load paths were the left side structure (e.g., door hinge), left wheel, and left shotgun beam. When these load paths were expressed as CDC codes, more than 45% of fatal crashes engaged less than one-third of the vehicle frontal width.

The relationship between injured body region and frontal crash type was examined using an Australian dataset containing 119 frontal impacts [17]. Frontal impact type was stratified according to the CDC;

narrow and wide overlap crashes were characterized by frontal width damage less than one-third or two-thirds, respectively. Narrow overlap composed 26% of frontal impacts; wide overlap composed 29%. Compared to fully distributed impacts, narrow and wide overlap crashes were more likely to result in MAIS 2+ injury to face, abdomen/pelvis, and lower extremities.

The relationship between injured body region and crash type was examined with US data contained in the NASS/CDS (2000-2006) and Crash Injury Research and Engineering Network (CIREN) database [18]. Only narrow overlap crashes were considered and were identified by CDC codes “FLEE” and “FREE” indicating involvement of the left or right one-third frontal width only. Damage type was also limited to corner impacts (Table 1). For CIREN cases, photographic documentation was reviewed to confirm no longitudinal member engagement. It was found that lower extremity injuries were most frequently reported, followed by head, chest, and pelvis injuries. Increased injury incidence was not consistently associated with increased occupant compartment intrusion, suggesting that occupant kinematics may play a unique role in SOI injury mechanisms.

A similar NASS/CDS study examined SOI crashes and injuries [3]. The authors highlighted the complexity in categorizing this crash mode using the CDC syntax. Therefore the CDC inclusion criteria were expanded to include impacts which may appear initially to be lateral impacts. Head, neck, thorax, and lower extremity injuries were most common, and a positive relationship we observed between occupant compartment intrusions and injury severity score (ISS).

The most sophisticated SOI definition to-date was recently published in the SAE Congress Proceedings [19]. This definition builds upon a previous refinement of the CDC [20] and utilizes CDC codes, damage measurements, and estimated structural geometry of the case vehicle to identify SOI frontal impacts which likely do not involve longitudinal member engagement. Both frontal and side impacts are considered by the algorithm, and structural geometry is estimated by published data for each vehicle weight- and body-class.

These previous studies demonstrated that continued work is necessary to reduce injury and mortality risk from frontal impacts. The subset of SOI may be most relevant to continued improvements, yet injury patterns and mechanisms have not been consistently

established. Further improvement to SOI crashworthiness therefore requires enhanced understanding of structural interactions and vehicle/occupant kinematic response to SOI loading.

METHODS

The present study examined occupant injury outcomes and biomechanical dummy responses in real-world and laboratory SOI impacts. Injury outcomes were obtained from real-world SOI crashes contained in the CIREN database of US crashes. Biomechanical dummy responses were measured during four full-scale small overlap crashworthiness tests.

Database Query

The CIREN database was queried manually for incidence of SOI. The CIREN database, formed in 1996, is a collaboration of clinicians and engineers at up to twelve Level 1 Trauma Centers in the US. Enrolled cases generally involve AIS 3+ (or multiple AIS 2) injuries occurring in late model vehicle crashes. SOI was identified by vehicle damage photography and CDC information. Vehicle data were examined for collision partner, extent zone, and crush distance. Occupant data was examined for seat position, gender, age, and ISS.

Vehicle Crash Tests

Four vehicle crash tests were conducted at the MCW Vehicle Crashworthiness Laboratory (Table 2). All vehicles were equipped with belt pretensioners and load limiters for the front seat occupants. For the third and fourth tests, vehicle make and model were identical but, in the latter test, the vehicle structure was advertised to promote greater structural engagement during diverse frontal impact configurations. SOI was simulated by positioning each vehicle on a moveable test platform incident upon a rigid pole fixture with 25 cm diameter (Fig. 4). In each test, the vehicle was positioned on the moveable test platform such that the left outside track width was aligned with the outboard margin of the pole fixture. Vehicle impact angle was adjusted such that the center of the occupant head in the driver position was aligned with the center of the pole fixture. Nominal impact velocity was 56 km/h.

For each test, a fiftieth percentile THOR anthropomorphic test dummy was belted in the driver’s seat position. The dummy was equipped with instrumented chest crux arms to measure anterior chest deflections in four quadrants (Fig. 5): upper left (UL), upper right (UR), lower left (LL),

and lower right (LR). The shoulder belt was positioned such that it overlaid the UR crux and passed superior to the LR crux. Deflections were examined in time domain and compared between test vehicles.

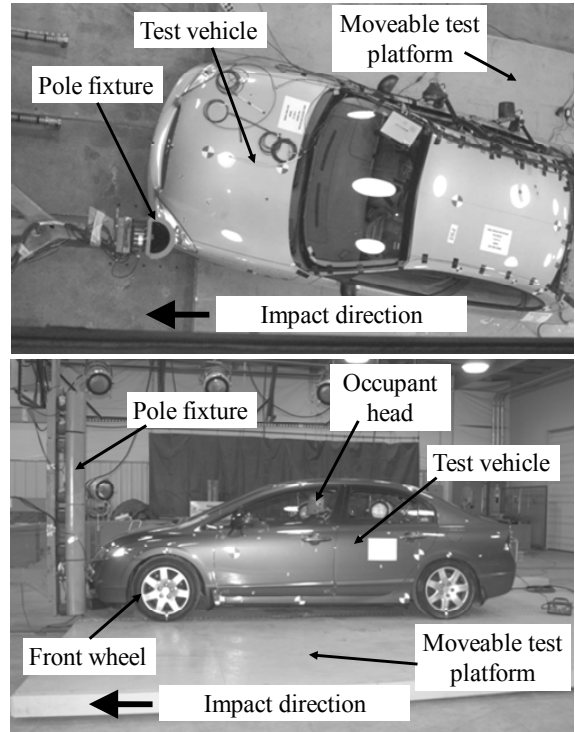


Figure 4. Setup for vehicle SOI test.

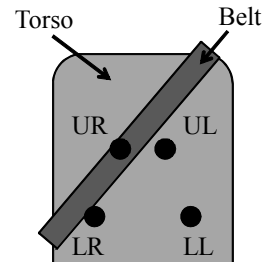


Figure 5. THOR crux locations with respect to belt pretest positioning, viewed from anterior.

Table 2. Description of test vehicles.

| Test | Model year | Class | Weight (kg) | Structure |
|------|------------|-------------|-------------|-----------|
| 1 | 2006 | Mid-sized | 1742.7 | Normal |
| 2 | 2010 | Sub-Compact | 1268.2 | Normal |
| 3 | 2005 | Compact | 1445.6 | Normal |
| 4 | 2010 | Compact | 1446.0 | Enhanced* |

* As advertised by manufacturer

RESULTS

Database Query

CIREN case query identified 82 crashes which could be categorized as SOI; a typical post-crash vehicle photograph is shown in Figure 6. In each crash, photographs and PDOF determination clearly demonstrated a front corner contact without longitudinal member engagement of the vehicle. These crashes were subcategorized by collision partner: vehicle-to-pole impacts (n = 34), matched-vehicle impacts (n = 25), and mismatched-vehicle impacts (n = 23). A mismatched vehicle pairing was defined as an impact in which the case vehicle weight was substantially less than that of the striking vehicle weight.

Among the 82 cases obtained, occupant and occupied vehicle characteristics are shown in Figure 7. Vehicle drivers represented the majority of case occupants. Additionally, males and younger ages represented a greater proportion of the dataset. The vast majority of vehicles were passenger cars.

Average ISS are shown in Figure 8 with respect to SOI subcategory. Mismatched vehicle impacts demonstrated the greatest average ISS, followed by vehicle-to-pole impacts. Matched vehicle impacts demonstrated the least average ISS but still exceeded 15, considered to be the threshold for severe (poly)trauma [21].

Intrusion was quantified both by crush distance into the vehicle and by deformation extent (Figs. 9 and 10). Extent zones between 2 and 5 represented “moderate” crush and extent zones 6 through 9 represented “severe” crush. Of 82 CIREN cases, 38 (46%) represented moderate crush; 32 (39%) represented severe crush. To identify the relationship between injury and indicators of crash severity, linear correlations were calculated between ISS and parameters of ΔV , crush distance, and extent zone. As demonstrated by Table 3, ISS was not correlated with these indicators of crash severity in SOI crashes.

Thorax injuries in CIREN cases also exhibited posterior rib fractures (Fig. 11). Because prior research has suggested anterior and right lateral fractures to result from restraints and/or steering wheel during structurally-engaged frontal impacts [22], these injuries suggested altered occupant kinematics during SOI. Therefore, attention was given specifically to the biomechanical response of the THOR thorax in the full-scale SOI crash tests.

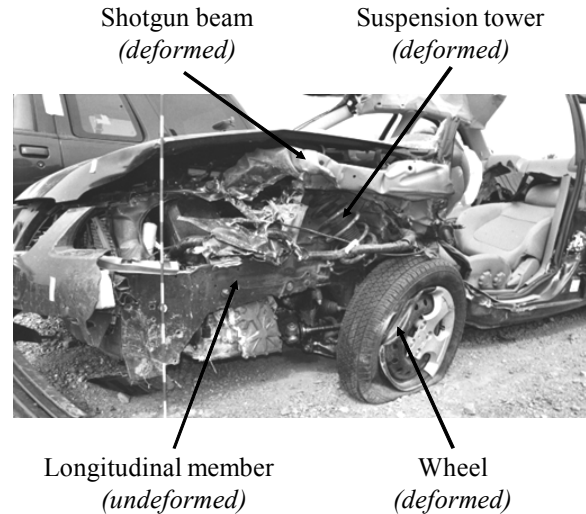


Figure 6. Typical CIREN case demonstrating SOI characteristics.

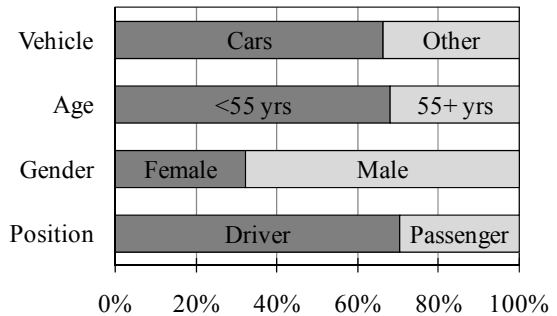


Figure 7. CIREN case distribution of occupant characteristics.

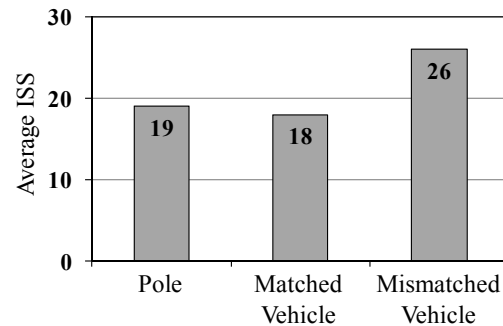


Figure 8. ISS with respect to SOI crash partner.

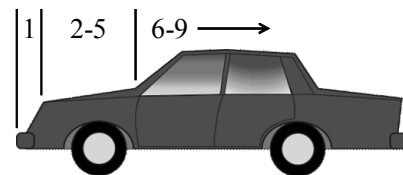


Figure 9. CDC extent zones relevant to SOI.

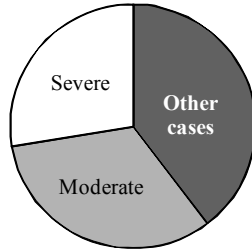


Figure 10. Distribution of SOI cases by extent zone category.

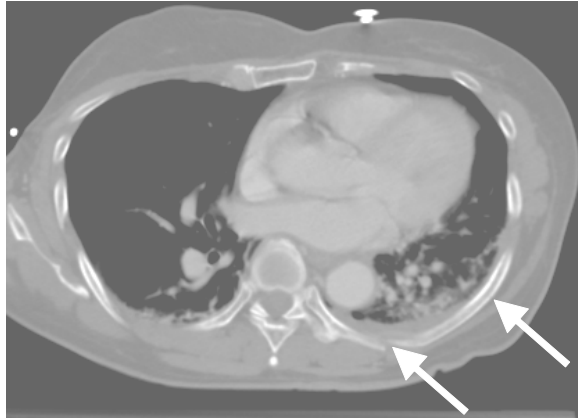


Figure 11. Exemplar posterior rib fracture pattern for SOI.

Table 3. Linear correlations with ISS.

| Parameter | R ² |
|----------------|----------------|
| ΔV | 0.0603 |
| Crush distance | 0.0988 |
| Extent zone | 0.0001 |

Vehicle Crash Tests

Final impact velocities of the four crash tests ranged from 56.0 km/h (Test 4) to 56.3 km/h (Test 3). Tests 1 and 2 both achieved 56.1 km/h. Resulting vehicle deformations were similar to case observations within the CIREN database (Fig. 12). Namely, lateral suspension and shotgun beam components were deformed, and the left front wheel was sheared away from the vehicle. The left longitudinal member remained undeformed as could be determined by visual inspection.

Deflections from the THOR dummy were examined in the time domain (Fig. 13). Time zero represented vehicle-pole contact. For all tests, resultant deflections were initially greatest at the LR crux. Later in impact progression the LR deflections were surpassed by UR; time at which this occurred ranged from approximately 75 ms (Test 4) to greater than

100 ms (Test 2). Examination of onboard videography suggested that deflections resulted both from belt loading due to vehicle deceleration and chest contact with the steering wheel and airbag. Chest contact was particularly prominent for Test 2, in which the dummy demonstrated substantially greater deflection response early in the impact progression. Particularly, both UL and LR cruxes deflected sharply at onset. Videographic documentation suggested the occupant of this subcompact vehicle may have contacted the steering wheel at this time. In all tests deflection responses appeared complex, with right side deflections generally exceeding left side deflections. Further, LL deflections were positive in three of four tests, indicating an exaggerated asymmetric chest loading.

Peak chest deflection values are contained in Table 5. In three of four tests, overall peak deflection was obtained from the UR crux. Comparing tests 1 and 2 (full-size vs. small car), an inverse relationship between vehicle mass and chest deflection was suggested. Recall that tests 3 and 4 represented similar vehicle make/model; the latter test represented a vehicle with structural design advertised to enhance structural engagement during a diverse set of frontal impact scenarios. Comparing THOR response between the occupants of these vehicles, structural modifications may have reduced chest deflections.

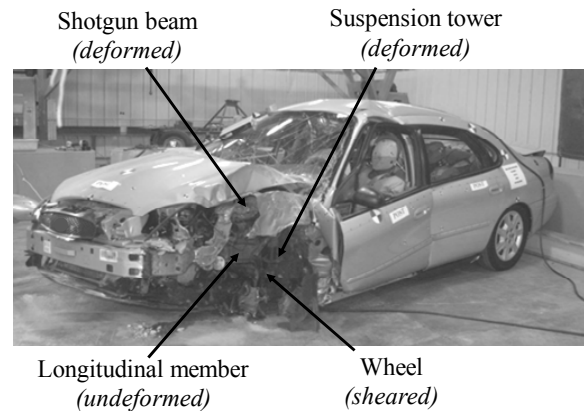


Figure 12. Exemplar deformation from SOI crash tests.

DISCUSSION

Distributed and wide overlap crashes (i.e., 40% frontal width) have received substantial attention with regard to research, testing, and resulting vehicle crashworthiness improvements. Consequently SOI crashes have emerged as a frontal impact mode posing great risk to properly restrained vehicle occupants.

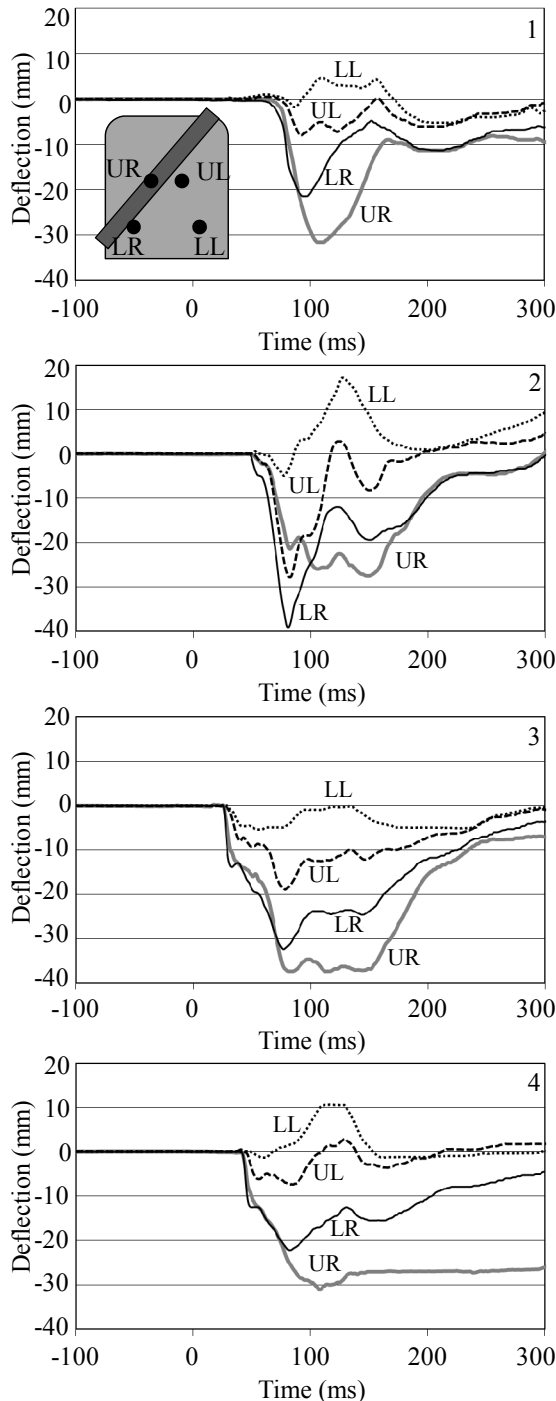


Figure 13. THOR chest deflections from four SOI vehicle tests.

Table 5. Peak THOR chest deflection results from four SOI tests (mm).

| Test | UL | UR | LL | LR |
|------|------|------|-----|------|
| 1 | 8.0 | 31.6 | 5.3 | 21.5 |
| 2 | 27.8 | 27.6 | 5.0 | 39.2 |
| 3 | 18.9 | 37.4 | 5.4 | 32.4 |
| 4 | 7.4 | 31.2 | 1.4 | 22.2 |

This study examined this crash mode through a review of published literature, injury observations in the CIREN database, and four full-scale SOI vehicle tests.

Although many studies have emphasized the role frontal engagement plays in frontal impact injury outcomes, consistent definitions of SOI have not been utilized. In prior studies, reduced overlap crashes have been considered “small” when estimated frontal width engagement was below specified thresholds; these thresholds were suggested anywhere from 60% [9] to less than 33% and less than 41 cm (16 inches) [18]. With continued examination of real world crash data, inclusion criteria were expanded to include impacts with CDC codes indicating side impact [3, 19]. Wide acceptance of a common SOI definition will enhance the utility of field data for statistical analyses of injury outcomes.

Existing CIREN data demonstrated a lack of correlation between injury severity and vehicle intrusion (deformation extent or crush distance) or ΔV . This may be explained in part by the inconsistencies between small overlap crash tests and ΔV algorithms [14]. Contributing to the SOI injury mechanism may be altered occupant kinematic response; this was suggested by posterior rib fractures in CIREN cases.

Altered occupant responses were observed in four vehicle crash tests. Specifically, peak deflections were observed to transition from UL to UR cruxes with opposite LL crux response polarity. This suggested that concentrated belt loading was shifting across the thorax with time, resulting in an exaggerated asymmetric response. This may also suggest that occupant kinematics are altered by SOI such that the occupant no longer receives maximum benefit from the restraint system.

In response to studies of vehicle crashworthiness compatibility [23, 24], automotive manufacturers have proposed modifications to enhance structural engagement and control crash load paths during impact. For example, the Honda Advanced Compatibility Engineering (ACE™) body structure includes structural components outside of the traditional longitudinal members [4]. Although not yet evaluated in SOI, structural modifications such as these were suggested by the present study to improve occupant safety in SOI.

CONCLUSIONS

Until recently, SOI crashes have received little attention compared to frontal impacts with distributed or wide overlap frontal engagement. Although the standard SOI definition, i.e., no longitudinal member engagement, is difficult to query from common crash databases, an operational SOI definition is developing. CIREN analysis found that injury severity may not be related to common indicators of crash severity, suggesting that altered occupant kinematics may contribute to SOI injury mechanisms. Four full-scale crash tests supported this hypothesis.

ACKNOWLEDGMENTS

This research was supported in part by the US Department of Transportation (DTNH22-07-H00173) and by the Department of Veterans Affairs Medical Research. Material presented in this manuscript represents the position of the authors and not necessarily that of the associated organizations.

REFERENCES

[1] NHTSA, 2010, "Traffic Safety Facts 2009," National Highway Traffic Safety Administration, DOT HS 811 402, Washington, DC.

[2] NHTSA, 2008, "Consumer Information; New Car Assessment Program," Federal Register, 73 pp. 40016-40050.

[3] Sherwood, C. P., Nolan, J. M., and Zubly, D. S., 2009, "Characteristics of small overlap crashes," 21st International ESV Conference, National Highway Traffic Safety Administration, Washington, DC.

[4] Saito, M., Gomi, T., Taguchi, Y., Yoshimoto, T., and Sugimoto, T., 2003, "Innovative body structure for the self-protection of a small car in a frontal vehicle-to-vehicle crash," 18th International ESV Conference, National Highway Traffic Safety Administration, Washington, DC.

[5] Bean, J.D., Kahane, C.J., Mynatt, M., Rudd, R.W., Rush, C.J., and Wiacek, C., 2009, "Fatalities in frontal crashes despite seat belts and air bags - review of all CDS cases - model and calendar years 2000-2007," National Highway Traffic Safety Administration, DOT HS 811 202, Washington, DC.

[6] Pletschen, B., Herrmann, R., Kallina, I., and Zeidler, F., 1990, "The significance of frontal offset collisions in real world accidents," Society of

Automotive Engineers, SAE 900411, Warrendale, PA.

[7] Scheunert, D., Justen, R., Herrmann, R., Zeidler, F., Decker, J., and Kallina, I., 1994, "What is a Realistic Frontal-Offset Test Procedure?" Accident; Analysis and Prevention, 26(3) pp. 347-360.

[8] Kaumann, K.H., Groesch, L., Holtze, H., and Schwede, W., 1990, "Frontal offset crash testing for approximately 15 years-Results, experiences and consequences," Society of Automotive Engineers, SAE Trans. 900413, Warrendale, PA.

[9] Hill, J. R., Frampton, R. J., and Mackay, M., 1993, "Appropriate frontal barrier tests for restrained occupants," 37th Annual AAAM Conference, Association for the Advancement of Automotive Medicine, Barrington, IL, pp. 287-302.

[10] Hobbs, C.A., 1995, "The rationale and development of the offset deformable frontal impact test procedure," Society of Automotive Engineers, SAE 950501, Warrendale, PA.

[11] Hobbs, C. A., 1991, "The need for improved structural integrity in frontal car impacts," 13th International ESV Conference, National Highway Traffic Safety Administration, Washington, DC, pp. 1073-1079.

[12] Planath, I., Norin, H., and Nilsson, S., 1993, "Severe frontal collisions with partial overlap - significance, test methods and car design," Society of Automotive Engineers, SAE 930636, Warrendale, PA.

[13] SAE, 1980, "Collision Deformation Classification," Society of Automotive Engineers, SAE J224, Warrendale, PA.

[14] O'Neill, B., Lund, A. K., Zubly, D. S., and Preuss, C. A., 1994, "Offset frontal impacts - a comparison of real-world crashes with laboratory tests," 14th International ESV Conference, National Highway Traffic Safety Administration, Washington, DC, pp. 649-670.

[15] Lindquist, M., Hall, A., and Björnstig, U., 2003, "Real World Car Crash Investigations — A New Approach," International Journal of Crashworthiness, 4 pp. 375-384.

- [16] Lindquist, M., Hall, A., and Björnstig, U., 2004, "Car Structural Characteristics of Fatal Frontal Crashes in Sweden," *International Journal of Crashworthiness*, 9(6) pp. 587-597.
- [17] Logan, D. B., Fitzharris, M. P., and Fildes, B. N., 2007, "Lower extremity risk and harm associated with narrow offset frontal impact crashes," 2007 International IRCOBI Conference, International Research Council on the Biomechanics of Injury, Zurich, Switzerland, pp. 115-126.
- [18] Pintar, F. A., Yoganandan, N., and Maiman, D. J., 2008, "Injury Mechanisms and Severity in Narrow Offset Frontal Impacts," *Annals of Advances in Automotive Medicine*. 52 pp. 185-189.
- [19] Halloway, D., Yoganandan, N., and Pintar, F.A., 2011, "An operational definition of small overlap impact for published NASS data," Society of Automotive Engineers, Warrendale, PA. In press.
- [20] Sullivan, K., Henry, S., and Laituri, T.R., 2008, "A frontal impact taxonomy for USA field data," Society of Automotive Engineers, SAE 2008-01-0526, Warrendale, PA.
- [21] Copes, W. S., Champion, H. R., Sacco, W. J., Lawnick, M. M., Keast, S. L., and Bain, L. W., 1988, "The Injury Severity Score Revisited," *The Journal of Trauma*, 28(1) pp. 69-77.
- [22] Yoganandan, N., Morgan, R. M., Eppinger, R. H., Pintar, F. A., Sances, A., Jr, and Williams, A., 1996, "Mechanisms of Thoracic Injury in Frontal Impact," *Journal of Biomechanical Engineering*, 118(4) pp. 595-597.
- [23] Shearlaw, A., and Thomas, P., 1996, "Study of vehicle dynamics and occupant response in side impact crash tests," 15th International ESV Conference, National Highway Traffic Safety Administration, Washington, DC.
- [24] Wykes, N. J., Edwards, M. J., and Hobbs, C. A., 1998, "Compatibility requirements for cars in frontal and side impact," 16th International ESV Conference, National Highway Traffic Safety Administration, Washington, DC, pp. 667-681.

EVALUATION OF THE THORACIC DEFLECTION MEASUREMENT SYSTEM 'RIBEYE' IN THE HYBRID III 50% IN FRONTAL SLED TESTS

Andre Eggers

Thorsten Adolph

Federal Highway Research Institute, BASt
Germany

Paper Number 11-0190

ABSTRACT

Thoracic injury is one of the predominant types of severe injuries in frontal accidents. The assessment of the injury risk to the thorax in the current frontal impact test procedures is based on the uni-axial chest deflection measured in the dummy Hybrid III. Several studies have shown that criteria based on the linear chest potentiometer are not sensitive enough to distinguish between different restraint systems, and cannot indicate asymmetric chest loading, which has been shown to correlate to increased injury risk. Furthermore, the measurement is sensitive to belt position on the dummy chest. The objective of this study was to evaluate the optical multipoint chest deflection measurement system 'RibEye' in frontal impact sled tests. Therefore the sensitivity of the RibEye system to different restraint system parameters was investigated. Furthermore, the issue of signal drop out at the 6th rib was investigated in this study. A series of sled tests were conducted with the RibEye system in the Hybrid III 50%. The sled environment consisted of a rigid seat and a standard production three-point seat belt system. Rib deflections were recorded with the RibEye system and additionally with the standard chest potentiometer. The tests were carried out at crash pulses of two different velocities (30 km/h and 64 km/h).

The tests were conducted with different belt routing to investigate the sensitivity of chest deflection measurements to belt position on the dummy chest. Furthermore, different restraint system parameters were investigated (force limiter level, with or without pretensioning) to evaluate if the RibEye measurements provide additional information to distinguish between restraint system configurations. The results showed that with the RibEye system it was possible to identify the effect of belt routing in more detail.

The chest deflections measured with the standard chest potentiometer as well as the maximum deflection measured by RibEye allowed the distinction to be made between different force limiter levels.

The RibEye system was also able to clearly show the asymmetric deflection of the rib cage due to belt loading. In some configurations, differences of more than 15 mm were observed between the left

and side areas of the chest. Furthermore, the abdomen insert was identified as source of the problem of signal drop out at the 6th rib. Possible solutions are discussed.

In conclusion, the RibEye system provided valuable additional information regarding the assessment of restraint systems. It has the potential to enable the evaluation of thoracic injury risk due to asymmetric loading.

Further investigations with the RibEye should be extended to tests in a vehicle environment, which include a vehicle seat and other restraint system components such as an airbag.

INTRODUCTION

Studies of accident data show that a high portion of severe and fatal injuries in motor vehicle accidents occur in frontal impacts even without intrusion in the passenger compartment. The mainly injured body part is the thorax (Carroll et al. 2010).

The assessment of the injury risk to the thorax in the current frontal impact test procedures is based on the uni-axial chest deflection measured in the dummy Hybrid III. Several studies have shown that criteria based on the linear chest potentiometer are not sensitive enough to distinguish between different restraint systems Petitjean et al. (2002), and cannot indicate asymmetric chest loading, which has been shown to correlate to increased injury risk (Shaw et al. 2009).

The RibEye system (Handman, 2007) allows multipoint measurements of chest deflection in the dummy Hybrid III 50%. With these additional deflection measurements it could be possible to obtain more detail of the location of highest deflection on the dummy chest and also capture the effect of asymmetric loading. If it would be possible to measure this asymmetrical deflection it could be a basis for improved chest injury risk criteria based on the Hybrid III.

The accuracy of the RibEye system was evaluated in quasi-static indenter tests and dynamic pendulum tests by Yogandan et al. (2009a, 2009b). The RibEye system installed in the dummy Hybrid III 5% female was evaluated by Tylko et al. (2007) in full scale crash tests. However, no systematic sled tests with the RibEye system have been reported so far.

Another multi-point chest deflection measurement system called THMPR (Thorax Multi-Point and high Rate measurement device) based on IR-Tracc installed in the Hybrid III was evaluated in sled tests by Petitjean (2002, 2003). It was found that with this type of multi-point deflection measurement it is possible to identify the point of highest deflection, which is not always the sternum. It was also reported that with this device it was possible to identify asymmetric chest deflection due to belt loading.

The objective of this study was a systematic evaluation of RibEye system installed in the Hybrid III 50% to investigate if it is also possible with this system to capture asymmetric loading, and achieve a higher sensitivity of possible criteria based on RibEye deflection measurement with respect to restraint system parameters.

METHODOLOGY

A series of 13 frontal impact sled tests were conducted with the dummy Hybrid III. The sled environment consisted of a rigid seat, a foot rest and a standard production three-point seat belt system.

Sled Test Setup And Restraint System

To be able to conduct a high number of tests in a repeatable test setup, a generic rigid seat and foot rest was used, which was available from sled tests completed under the European project FID (Frontal Impact Dummy). The same seat geometry was also used for tests at INRETS by Vezin and tests at BAST under the FID project, as reported in Vezin et al. (2002). The geometry of the seat, and the foot rest geometry is shown in Figure 1 and Figure 2.

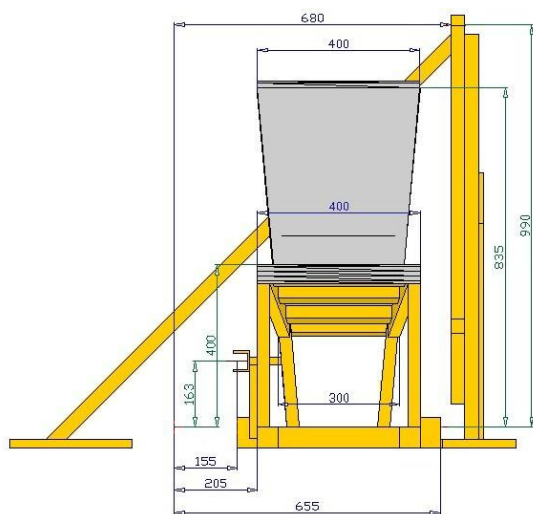


Figure 1. Front view of the seat geometry with dimensions.

For the test series a standard production three-point seat belt system was used, which consisted of a pretensioner and retractor. The belt geometry represents a midsize European vehicle. The belt attachment points were based on data collected from several European cars and published by Zellmer et al. (1998). The attachment points with respect to the dummy H-points are given in Table 1. The test setup is shown in Figure 3.

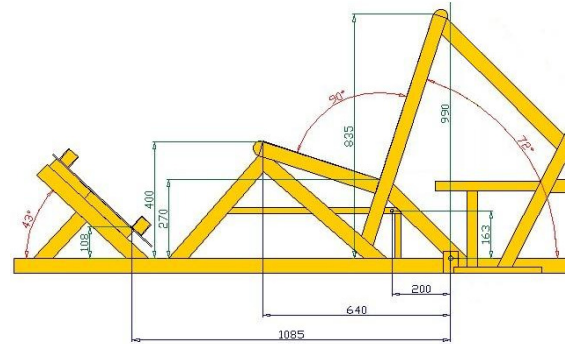


Figure 2. Lateral view of the seat and foot rest geometry with dimensions.

Table 1. Belt attachment points, which were used for all sled test in this test series

| Belt point w.r.t Dummy H-point | X (mm) | Y (mm) | Z (mm) |
|--------------------------------|--------|--------|--------|
| Retractor | -150 | -301 | -216 |
| Buckle | -191 | 233 | -194 |
| D-ring | -316 | -284 | 606 |
| Anchor | -316 | -284 | -462 |



Figure 3. The test setup consisted of a rigid seat, foot rest and a standard three-point belt system.

Instrumentation

The dummy was instrumented according to the standard requirements for the Euro NCAP frontal impact tests (Euro NCAP, 2009). Additionally, the rib deflection was measured at 12 points with the RibEye system. An overview of all measured

dummy data channels is given in Table 2. The dummy was equipped with a neck shield for all of the tests to avoid interaction between the belt and neck.

Additionally, the sled deceleration pulse and the belt forces at the shoulder and the lap belt force at the anchor were recorded. All data was filtered according to SAE J211 where applicable. The filter classes are also shown Table 2.

Table 2.
Instrumentation of the Hybrid III for the frontal sled tests according to standard Euro NCAP frontal impact instrumentation and additionally 2-axis, 12 point RibEye system

| Segment | Parameter | CFC |
|---------|---|------|
| Head | Acceleration ($a_{x,y,z}$) | 1000 |
| Neck | Upper forces ($F_{x,y,z}$) | 1000 |
| | Upper moments ($M_{x,y,z}$) | 600 |
| Chest | Deflection (δ_x) | 180 |
| | Acceleration ($a_{x,y,z}$) | 180 |
| | RibEye deflection ($\delta_{x,y}$) | 600 |
| Pelvis | Acceleration ($a_{x,y,z}$) | 1000 |
| Femur | Femoral left and right load (F_z) | 600 |
| Tibia | Tibia left and right upper loads ($F_{x,z}$) $M_{x,y,z}$) | 600 |
| | Tibia left and right upper loads ($F_{x,z}$) $M_{x,y,z}$) | 600 |
| Knee | Knee slider left and right (δ_x) | 180 |

RibEye Configuration

In addition to the standard Euro NCAP Hybrid III instrumentation shown in Table 2 (including the chest potentiometer), the dummy was equipped with the standard 2D RibEye system (Handman, 2007), which is able to measure the rib deflection in x and y directions at each of the six ribs located left and right of the sternum. A detailed description of the system is provided in earlier publications (Yoganadan, 2009a). The RibEye used in this study consists of 12 LEDs, which can be placed on arbitrary position along the ribs. In a study by Yoganandan et al. (2009b) the optimal LED position for this system was determined to be at 9 cm measured along the outer curvature of the rib (Figure 4). In this study, those LED positions were used for all tests.

Dummy Positioning

The Hybrid III dummy was positioned on the seat with the back against the back rest and the thighs on the seat. The feet were positioned flat on the foot rests. The H-point of the dummy was moved to the position as specified in Table 1. The distance between the knees was adjusted to 150 mm. The pelvis angle was set to $22.5^\circ \pm 2.5^\circ$ and the head angle between 0° and 2° .

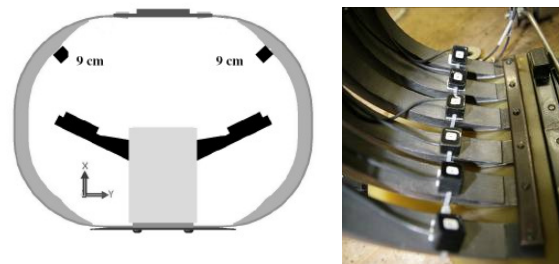


Figure 4. Attachment position of the LEDs at 9 cm measured from the centre of the sternum along the outer curvilinear path of the rib.

High Speed Film Cameras

Three digital high-speed fixed position cameras recording 1,000 frames per second were used to capture one lateral view, one top view and one frontal view.

Test Parameters

Within the test series several parameters including the impact severity and restraint system parameters were varied to investigate their influence on the deflection output measured by the RibEye and the standard chest potentiometer. The belt system, including retractor buckle and the belt itself were changed after each test.

Crash Pulse Two different crash pulses were applied; a 30 km/h pulse, required as per ECE regulation R44 (shown in Figure 5), and a 64 km/h Euro NCAP frontal ODB crash pulse of a midsize vehicle (shown in Figure 6).

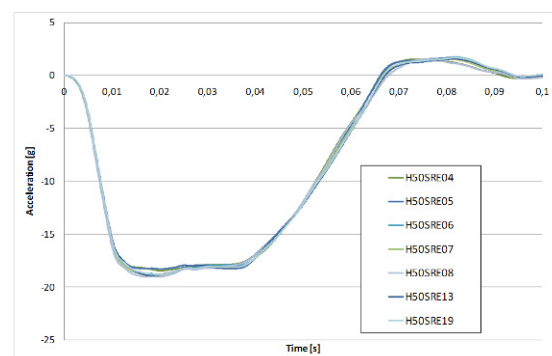


Figure 5. 30 km/h sled pulse (R44-03 regulation)

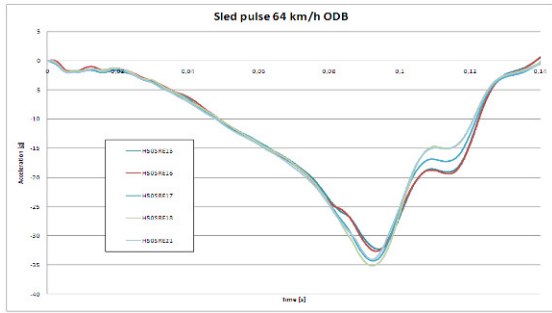


Figure 6. 64 km/h ODB Euro NCAP frontal sled pulse.

Pretensioner The belt retractor used in the tests was equipped with a pretensioner which was fired 17 ms after impact in some tests depending on the test configuration.

Load Limiter Two different load limiter levels were used. One load limiter had a torsion bar of 95 mm to get a high shoulder belt force. To achieve the desired belt force a residual lap of 640 mm was used on the spool for all tests with this load limiter. To achieve a lower shoulder belt force, a load limiter with a torsion bar of 42 mm diameter was used. For all tests with this load limiter, a residual lap of 475 mm was used to obtain the desired force at the shoulder belt.

Belt Routing On Dummy Chest The belt was positioned in two different ways. ‘Normal’ and ‘High’ positions were defined as follows. For the ‘Normal’ belt position the belt was routed in a way that it was just below the right of the two holes, which are part of the dummy chest flesh jacket (left photo in Figure 7). In the ‘High’ belt position the belt is touching the neck shield (right photo in Figure 7).



Figure 7. Normal belt position (left) and high belt position (right).

To investigate if the RibEye system is able to distinguish between different restraint systems and furthermore to evaluate the sensitivity to belt position a matrix of 10 configurations was defined

(Table 3.). Some tests configurations were repeated; resulting in a total number of 13 tests.

Table 3. Combination of test parameters

| Variations | Impact velocity [km/h] | Belt routing | Load limiter level | Belt pretensioner |
|------------|------------------------|--------------|--------------------|-------------------|
| 1 | 30 | Normal | Low | No |
| 2 | | | Low | Yes |
| 3 | | | High | No |
| 4 | | | High | Yes |
| 5 | | High | Low | Yes |
| 6 | | | High | No |
| 7 | 64 | Normal | Low | Yes |
| 8 | | | High | No |
| 9 | | High | Low | Yes |
| 10 | | | High | Yes |

Additional Tests To Investigate Signal Dropout At The 6th Rib

To investigate the signal drop out at the 6th rib which was frequently observed within this test series and was also reported by other researchers (Tylco et al. 2007) additional tests were performed. Four tests additional to the described test matrix were performed with a camera capturing the view inside the dummy chest. To achieve this, the head and neck of the dummy was removed, and an aluminum block was mounted to the neck support of the dummy. A high speed camera facing towards the chest interior was attached to the block (Figure 8).



Figure 8. A camera facing down into the inside of the chest of the dummy

The objective of this was to investigate possible interaction between the abdomen and LEDs attached to the 6th rib.

To ensure the chest flesh of the jacket would not obstruct the camera view during belt-induced

compression of the chest, part of the jacket was cut away in the required area. To have enough light available in the chest cavity of the dummy to enable high speed filming, three LED bands with a light intensity of 330 lumen each (Figure 9) were attached to the spine box of the dummy.

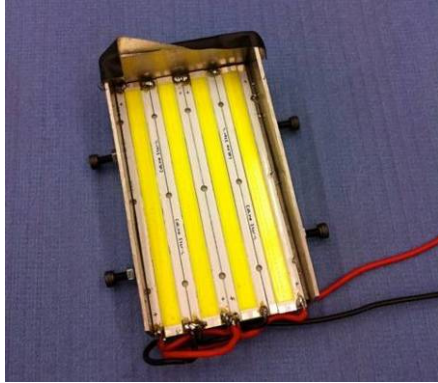


Figure 9. Four LEDs were attached to the spine box to illuminate the inside of the chest for high speed filming

In the tests with this additional camera it was not possible to record useful RibEye data during the tests. Due to the high illumination inside the chest, which was necessary for high speed filming, the optical sensors of the RibEye system were not able to record the light emitted by the RibEye LEDs.

In addition to these tests, one test was performed with the standard Hybrid III dummy equipped with RibEye, but without abdomen insert, to investigate if the signal drop out problem is eliminated in the case of the absence of the abdomen insert.

RESULTS

Table 4 shows a matrix of successful tests conducted within this test series, indicating the test parameters and corresponding test number.

Table 4. Configurations of the 13 tests to investigate the influence of tests parameters on output signals of the RibEye system

| Test No. | v [km/h] | Load limiter | Belt routing | Pretensioner |
|----------|----------|--------------|--------------|--------------|
| H50SRE04 | 30 | High | Normal | No |
| H50SRE05 | 30 | Low | Normal | No |
| H50SRE06 | 30 | Low | Normal | Yes |
| H50SRE07 | 30 | High | Normal | Yes |
| H50SRE08 | 30 | High | High | No |
| H50SRE13 | 30 | Low | High | Yes |
| H50SRE15 | 64 | Low | High | Yes |
| H50SRE16 | 64 | High | High | Yes |
| H50SRE17 | 64 | High | Normal | No |
| H50SRE18 | 64 | Low | High | Yes |
| H50SRE19 | 30 | Low | High | Yes |
| H50SRE20 | 30 | Low | High | Yes |
| H50SRE21 | 64 | Low | Normal | Yes |

Selected dummy sensor and belt force characteristic peak values from the 13 tests are shown in Table 5. For tests with high velocity and low load limiter level (15, 17, 21) the chest of the dummy contacted the femur during the forward movement of the chest. This happened after the belt-induced maximum chest deflection was reached. This ‘first deflection’ maximum due to belt loading is given in the table and is used for further analysis. A similar approach was used to determine the relevant peak values for the deflections measured by the RibEye system.

Table 5. Characteristic result values of the 13 sled tests

| Test No. | Peak Head Acceleration Resultant [g] | Peak Chest Deflection [mm] | Peak Upper diagonal Belt Force [kN] | Peak Pelvis Acceleration Resultant [g] |
|----------|--------------------------------------|----------------------------|-------------------------------------|--|
| H50SRE04 | 38.1 | 30.3 | 6.5 | 33.4 |
| H50SRE05 | 26.6 | 21.2 | 3.4 | 36.0 |
| H50SRE06 | 22.2 | 20.5 | 4.5 | 28.0 |
| H50SRE07 | 31.0 | 29.2 | 6.4 | 28.6 |
| H50SRE08 | 38.1 | 26.0 | 6.3 | 37.2 |
| H50SRE13 | 22.5 | 19.6 | 3.8 | 28.4 |
| H50SRE15 | 42.5 | 25.9 | 4.4 | 37.7 |
| H50SRE16 | 40.3 | 30.7 | 7.6 | 42.6 |
| H50SRE17 | 48.8 | 34.9 | 7.4 | 60.7 |
| H50SRE18 | 46.7 | 24.1 | 5.1 | 50.1 |
| H50SRE19 | 22.5 | 18.8 | 3.7 | 30.6 |
| H50SRE20 | 22.5 | 21.2 | 3.6 | 29.0 |
| H50SRE21 | 43.9 | 24.3 | 4.7 | 41.3 |

The highest chest deflection of 34.9 mm was observed in the configuration 64km/h, without pretensioner, high load limiter and normal belt position. The lowest chest deflection of 19.6 mm occurred in the configuration 30 km/h, with pretensioner fired, low load limiter level and high belt position.

In the following figures plots are shown of the RibEye outputs measured in the test H50SRE04 with an impact velocity of 30 km/h, high load limiter, normal belt routing and pretensioner not fired. The seat belt forces are also plotted for this test in Figure 10. The displacements of the ribs in x-direction and the left and right side are shown in Figure 11 and Figure 12.

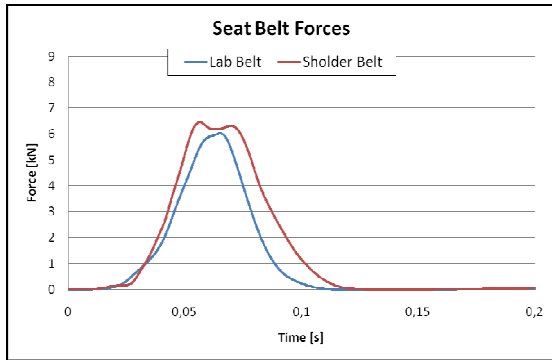


Figure 10. Seat belt forces in test H50SRE04

An effect can be observed in these figures which occurred in all tests reported here. The signal at the 6th rib is interrupted at both sides of the rib cage. At the right rib this occurs after the maximum deflection was already reached (Figure 11). At the left 6th rib the signal drops out at 55 ms and comes back at 200 ms. This problem can occur when the light path from the LED to one or both of the optical receivers is interrupted. The reason for this could be parts inside the dummy (such as the rod of the chest potentiometer), blocking the light path, or high deformations of the ribs, which cause the LED to move out of the range of sight of the optical sensors. The hypothesis also stated by other researchers who observed signal drop out at the 6th rib is interference with the abdomen insert, which moves up during the forward movement of the dummy and interacts with the LED or blocks the light path. This issue was investigated by additional tests within this study and is described later.

The highest rib deflections measured with the RibEye occurred at the right half of the rib cage at the 1st rib, 25.5 mm (Figure 11). This was observed in all tests reported in this test series. The reason could be that the shoulder takes most of the load at the retractor side, which shields the ribs. This leads to higher deflection at the buckle side.

The deflection measured at the 1st right rib is lower compared to the peak deflection measured with the chest potentiometer (30.3 mm). The peak deflection measured with the RibEye LED configuration used in this study was lower than the deflection measured by the chest potentiometer. Of course, this is dependent on the locations where the LEDs are attached to the ribs. The 9 cm position used in this study is quite far away from the center of the sternum. An LED position closer to the sternum (or even sternum-mounted LEDs), could result in deflections measured by RibEye which are higher than the peak deflections measured by the chest potentiometer.

Comparing the right and left x-deflection (Figure 11 and Figure 12) it can be noted that the deflections at the right side of the chest (the buckle side) are higher than the deflection at the retractor side. This was the case for all tests in this test series. The difference of left and right x-deflection was

calculated for all tests. For test H50SRE04 it is plotted in Figure 13. The peak difference calculated from this plot is quite high compared to the peak deflection itself, which is 11.0 mm for this test configuration. This shows that with the RibEye installed in the Hybrid III chest it is possible to capture asymmetric deflection due to belt loading.

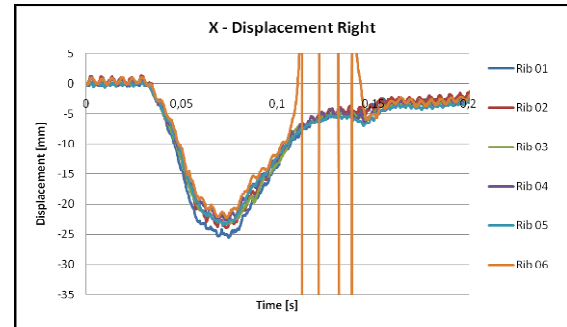


Figure 11. x-displacements of right ribs 1 to 6 in test H50SRE04

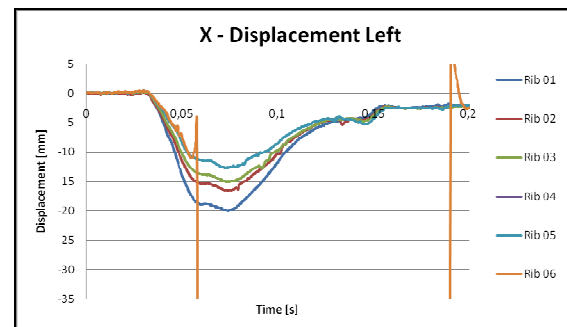


Figure 12. x-displacements of left ribs 1 to 6 in test H50SRE04

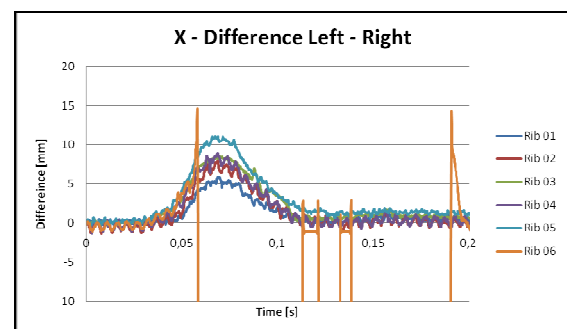


Figure 13. Deflection difference calculated between left and right for test H50SRE04

The y-displacements left and right for this test configuration are plotted in Figure 14 and Figure 15. The same signal drop out effect like for the x-deflection can be observed in these plots for the signals of the 6th rib. The peak y-displacements at the right ribs are notably high for this test configuration. The highest peak deflection of 12.5 mm was observed at the 1st right rib. The y-deflections at the right ribs were higher for all test configurations.

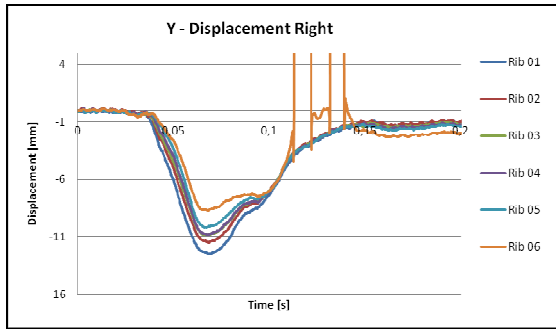


Figure 14. y-displacements of right ribs 1 to 6 in test H50SRE04

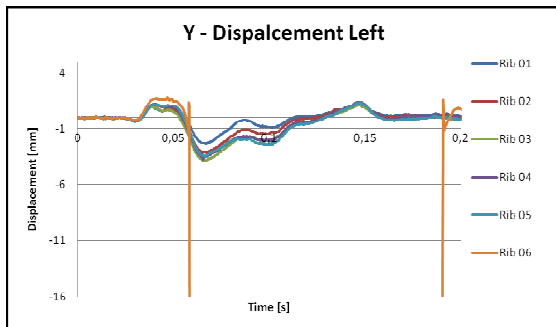


Figure 15. y-displacements of left ribs 1 to 6 in test H50SRE04

Plots of RibEye sensor data outputs from other test configurations are omitted from this paper, for brevity. However, all relevant signals were evaluated; characteristic peak values were calculated and are summarized in Table 6. The deflection measured by the chest potentiometer is also given in this table for comparison. The

maximum x-deflection measured by RibEye (which was always observed in at the 1st right rib), is also shown, along with the difference between peak deflection measured by the chest potentiometer and RibEye for each test, which was up to 7 mm in some tests.

The difference between deflection measured at the right and left side of the rib cage was calculated to understand the influence of test parameters on asymmetrical chest deflection. The values given in the table are not the difference of peak deflections at the left and right side. To obtain values for the right and left deflection, curves were subtracted for all rib levels respectively to obtain difference curves for each rib (see Figure 13 for example plot). Table 6 shows the peak value of the curve with the maximum difference between left and right. The next column in Table 6 indicates the rib level where the highest peak difference was observed, which was rib level 5 for most tests. Only in two cases the highest peak deflection occurred at rib level 3.

The maximum difference between left and right was 16.3 mm for the test configuration 64 km/h, high belt load limit, high belt position, with pretensioner fired. The lowest difference of 4.9 mm was observed in the test configuration 64 km/h, low load limiter level, normal belt routing, with pretensioner.

**Table 6
Rib deflection values measured and calculated based on RibEye output**

| Testno. | Peak Deflection from Chest Potentiometer | Maximum x-deflection (at Rib1Right) | Difference Rib1Right to Chest Potentiometer | Maximum Difference Left - Right | Rib Level of Maximum Left-Right Difference | Maximum y-deflection (at Rib1Right) |
|----------|--|-------------------------------------|---|---------------------------------|--|-------------------------------------|
| H50SRE04 | 30.3 | 25.5 | 4.9 | 11.0 | 5 | 12.5 |
| H50SRE05 | 21.2 | 17.9 | 3.3 | 7.1 | 5 | 9.5 |
| H50SRE06 | 20.5 | 16.3 | 4.2 | 5.1 | 5 | 8.7 |
| H50SRE07 | 29.2 | 24.9 | 4.3 | 10.4 | 5 | 10.8 |
| H50SRE08 | 26.0 | 25.1 | 0.9 | 14.8 | 5 | 7.7 |
| H50SRE13 | 19.6 | 17.4 | 2.2 | 6.9 | 5 | 6.7 |
| H50SRE15 | 25.9 | 23.9 | 2.0 | 9.5 | 3 | 6.9 |
| H50SRE16 | 30.7 | 29.0 | 1.7 | 16.3 | 5 | 7.4 |
| H50SRE17 | 34.9 | 27.9 | 7.0 | 12.6 | 5 | 15.2 |
| H50SRE18 | 24.1 | 21.8 | 2.3 | 8.5 | 5 | 7.9 |
| H50SRE19 | 18.8 | 17.4 | 1.4 | 6.6 | 5 | 6.5 |
| H50SRE20 | 21.2 | 19.2 | 2.0 | 7.7 | 3 | 6.0 |
| H50SRE21 | 24.3 | 20.0 | 4.4 | 4.9 | 5 | 9.9 |

Sensitivity Of Chest Deflection Values To Restraint Parameters

One main objective of the study was to investigate a correlation of test parameters (Table 4) and deflection values measured by chest pot and RibEye (Table 6). For the parameters; ‘load limiter level’ and ‘belt routing’ on the chest of the dummy, correlations to deflection parameters were found and are presented here.

Figure 16 shows the 13 tests performed with this test series, sorted from left to right in descending order by peak chest deflection measured by the chest potentiometer. The results show that the highest deflection occurs in the five tests with high load limiter level. In all tests with the lower load limiter level the deflection measured by the chest potentiometer is lower. This observation suggests that based on the tests conducted within this study, a criterion based on chest deflection measured by the chest potentiometer is able to show the positive effect of a load limiter.

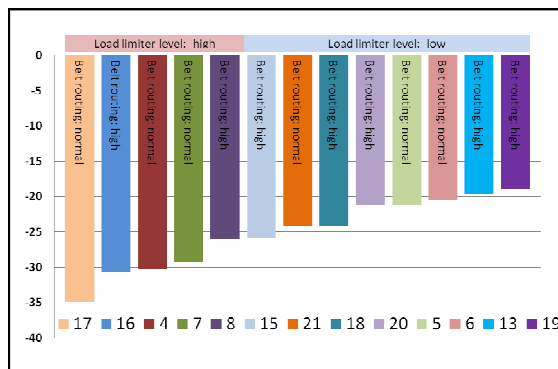


Figure 16. Peak chest deflections in mm measured by chest potentiometer

Figure 17 shows the peak x-deflection measured at the 1st right rib by RibEye sorted in descending order. The same effect as in Figure 16 is demonstrated. High deflection corresponds to test configurations with high load limiter level. Lower deflection values at the 1st right rib can be observed in tests with a lower load limiter level. This implies that peak deflection measured by RibEye in Hybrid III is also a parameter which can show the difference between different load limiter levels.

In both figures the belt routing is also indicated within the bars of the diagrams. Comparing this in Figure 16 and Figure 17 shows that the order of some adjacent bars (representing tests with high and low belt routing), is switched. For example, tests 16 and 17, tests 7 and 8, tests 21 and 18. This implies that both peak chest deflection measured by the chest potentiometer and RibEye are able to show the effect between different shoulder belt loads, but are both sensitive to belt position. The deflection measured by the chest potentiometer is higher for the normal belt position whereas the

maximum deflection value measured by RibEye is higher for the high belt position.

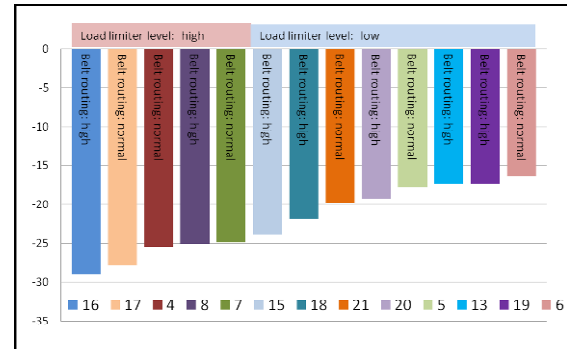


Figure 17. Peak x-deflection in mm measured by RibEye at 1st right rib

The effect of belt routing on the difference between peak deflection measured by the chest potentiometer and RibEye can be further understood by looking at Figure 18, which shows the tests sorted by this difference in descending order. It shows that the difference is higher for the 6 tests with normal belt routing. If the belt is moved to a higher position on the chest of the dummy, the deflection at the chest potentiometer decreases, whereas the deflection measured at the 1st right rib increase at the same time. This leads to a lower difference between the two measurements.

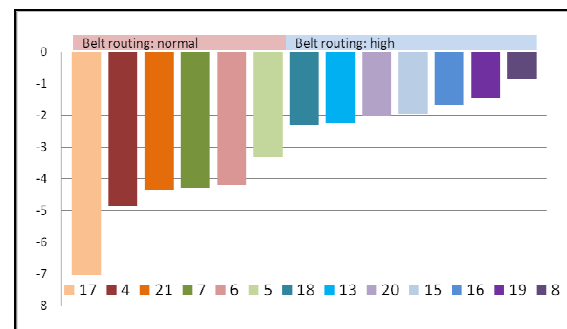


Figure 18. Difference in mm between peak chest deflection measured by chest potentiometer and RibEye

Figure 19 shows the peak difference of left at right deflection measured by RibEye, which occurred at rib level 5 for most test configurations. The graph shows that this parameter is higher in the five test configurations with high load limiter level. For the tests with low shoulder belt load this difference is lower. This result suggests that an assessment criterion based on the difference between right and left deflection would also be able to show the positive effect of a load limiter.

The last deflection parameter, which was considered in this sensitivity analysis, is the peak y-deflection, which was observed at the 1st right rib for all tests within this test series. The test configurations sorted in descending order by y-

deflection are presented in Figure 20. The graph shows that the peak y-deflection at the 1st right rib is sensitive to belt routing. The highest deflection values occur in tests with normal belt routing. Therefore, high belt routing appears to correlate with low y-deflection.

To illustrate the effect of parameters such as belt load level and belt routing not only on peak values on the first right rib, but also the distribution of deflection between the 1st and 6th, the resultant peak deflection values for all ribs on the left and right side of the rib cage are shown in Figure 21 and Figure 22 for selected test configurations.

In Figure 19 the peak deflection values are compared for different load limiters. Crash pulse (64 km/h), belt routing (high) and pretensioner (fired) are the same for both tests.

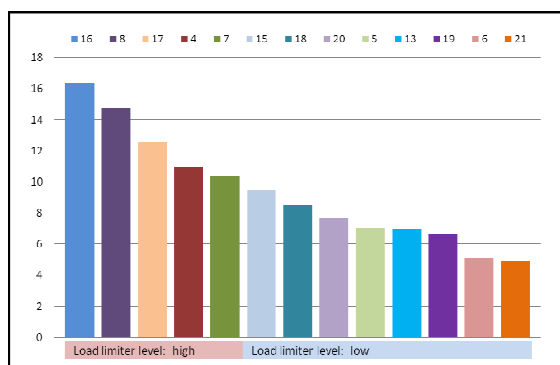


Figure 19. Maximum difference in mm between left rib deflection and right rib deflection

It is shown that a lower shoulder belt force results in a reduction of deflections measured by the chest potentiometer and the RibEye LEDs on the right part of the chest. For the left ribs only small reduction of deflection can be observed for the

upper ribs. The lower ribs sustain a very small increase in deflection for the lower belt load.

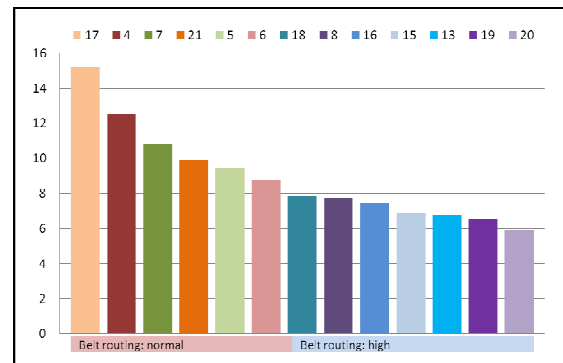


Figure 20. Maximum y-deflection in mm at 1st right rib

In Figure 22 the chest deflections are shown for two tests to compare the effect of belt routing. The other parameters 'sled pulse' (30 km/h), 'load limiter' (low) and 'pretensioner' (fired) were not changed between the two configurations. As previously explained, the figure shows that the deflection measured by the chest potentiometer is reduced for higher belt position on the chest of the dummy whereas the peak deflection measured by the RibEye 1st right rib increases.

It is shown that this is also true for the deflection at the right side of the chest down to the 4th rib. However, at the left side of the chest the deflection is decreased for a higher belt routing. This could be also due to the shielding effect of the shoulder as described before.

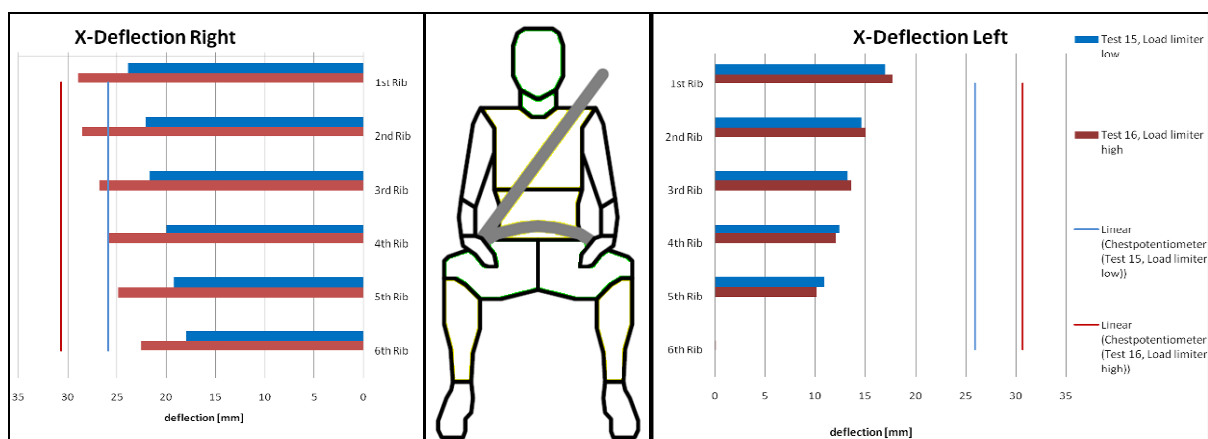


Figure 21. Peak chest deflection measured by chest potentiometer (straight line), peak deflections at ribs 1 to 6 left and right (bar graphs) compared for two tests with different load limiter.

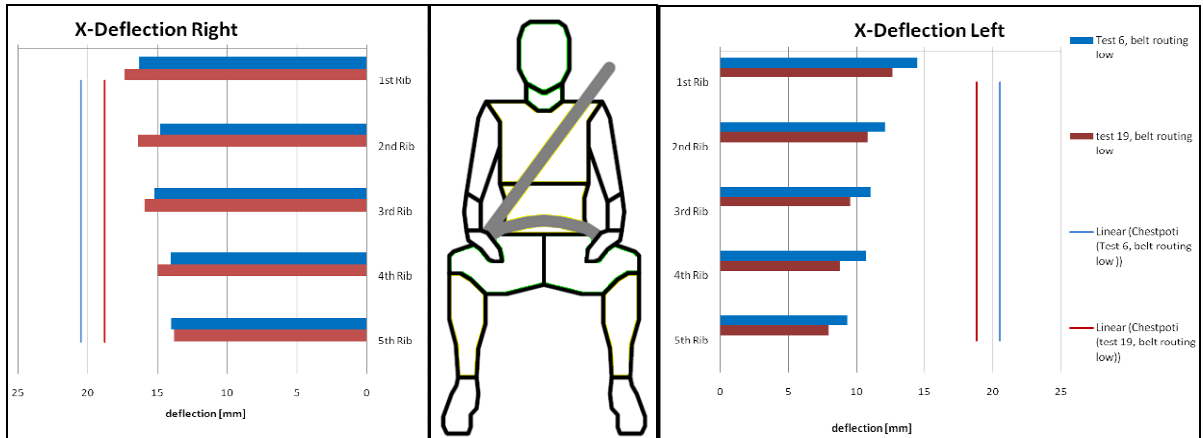


Figure 22. Peak chest deflection measured by chest potentiometer (straight line), peak deflection at ribs 1 to 6 left and right (bar graphs) compared for two tests with different belt routing.

Additional Tests To Investigate Interaction Between 6th Rib And Abdomen Insert

As observed within the test series reported here and also described by other researchers, signal dropout occurred at the LEDs attached to the 6th rib. The hypothesis stated by other researchers was that this effect could be a result of interaction between LEDs on the 6th rib and the abdomen insert. This was investigated by additional sled tests with a camera viewing inside the chest cavity of the

dummy. The 30 km/h sled pulse and a low belt load limiter were used in these tests. A diagram of one of the tests is shown in Figure 23. The left figure shows the dummy on the sled 46 ms after impact. The right figure shows an image captured by the high speed video inside the chest cavity. In this photo it is possible to see reflections of the red light emitted by the LED on the 6th left rib (highlighted by the green box). This explains the signal drop out which occurred in several tests on the 6th rib.

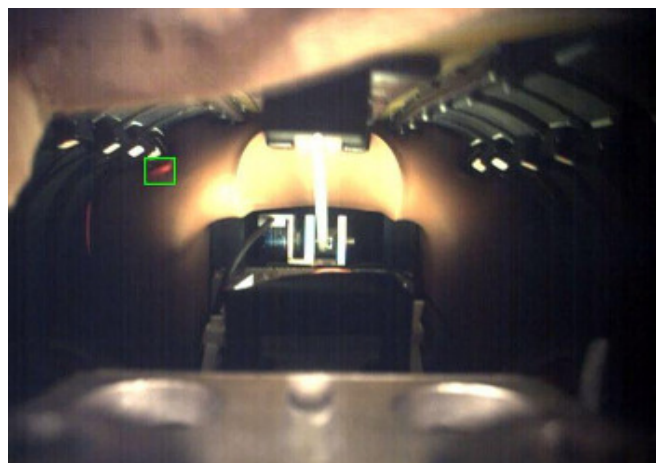


Figure 23. Dummy with camera mounted on neck viewing into the chest of Hybrid III at 46 ms during sled test (left photo). Screen shot of camera view inside dummy chest at 46 ms (right photo); reflection of RibEye LED-light (highlighted by green box) indicating abdomen insert blocking the light path.

To support this finding, one additional test was conducted without the abdomen insert. The configuration of the test was 64 km/h, low load limiter, high belt routing and the pretensioner was fired. In this test no signal dropout occurred, which is a further indication that the signal dropout observed in the other tests is caused by the abdomen insert.

Displacement signals measured by RibEye for this test are shown in Figure 24 and Figure 25.

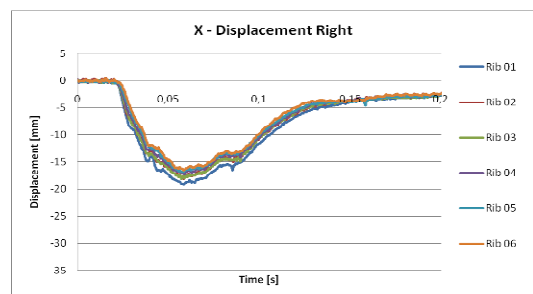


Figure 24. Deflections measured by RibEye at rib1 to rib6 right in test without abdomen insert

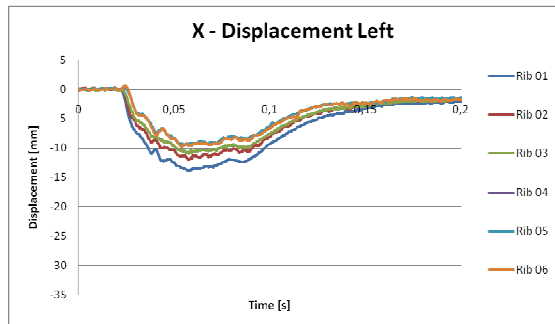


Figure 25. Deflections measured by RibEye at rib1 to rib6 left in test without abdomen insert

CONCLUSIONS AND RECOMMENDATIONS

This study aimed to systematically evaluate the possible benefit of additional deflection outputs measured by the RibEye installed in the dummy Hybrid III in a series of thirteen sled tests.

It was demonstrated that based on the peak chest deflection measured by the standard chest potentiometer as well as peak deflection measured by the RibEye on the 1st right rib, it was possible to distinguish between configurations with high and low belt load limiter level. Furthermore, it was shown that the peak deflection detected by the chest potentiometer is sensitive to the initial belt position on the chest of the dummy. The maximum peak deflection measured by RibEye, which always occurred at the 1st right rib is also sensitive to belt routing, but as the RibEye measures the deflection at multiple points, this effect can be better understood by reviewing the change of deflection due to different belt routing on both sides of the chest.

By considering the peak difference between left and right deflection it was also possible to distinguish between tests with high and low load limiters. The analysis of the peak difference between left and right chest deflection showed that the RibEye installed in the rib cage of Hybrid III is able to indicate asymmetric loading (as shown by Petitjean) even though the chest is very stiff compared to more biofidelic frontal impact dummies such as THOR. This implies that it would be worthwhile to investigate possible injury criteria, taking into account the right to left difference in chest deflection measurements of the Hybrid III.

A further objective of this study was to investigate the problem of signal drop out at the 6th rib. The dummy abdomen insert was identified as a source of interference. If the RibEye should be used in tests procedures to assess the effectiveness of restraint systems based on a criterion which takes into account measurements from the 6th rib, a solution to this issue is required.

One possibility could be to try different LED positions. For example, LEDs placed at a position 12 cm from the sternum center line would be out of

the interaction area with the abdomen insert. However, at this position they might be out of the regular range of sight of the RibEye system. Another possibility could be a modification of the abdomen. However, this would change the behavior of the entire dummy and should be avoided. A third possibility could be to change the design of the LED cases, which are presently relatively large, and thus offer a high area for interaction with the abdomen insert.

Limitation Of The Study And Further Research

This study was completed in a rigid lab seat environment with a belt system only. It should be extended to a sled environment, which more closely represents a vehicle, including a vehicle seat as well as state of the art restraint systems such as airbags, knee bolsters, or knee airbags.

Furthermore, it is recommended to investigate other LED configurations including LEDs closer to the sternum or sternum mounted LEDs. It would also be of interest to use other presently available RibEye systems which also allow for measurement of z-displacement of the ribs.

REFERENCES

Carroll, Jolyon; Adolph, Thorsten; Chauvel, Cyril. 2010. "Overview of serious thorax injuries in european frontal car crash accidents and implications for crash test dummy development." Proceeding of the IRCOBI conference 2010, Hannover.

EUROPEAN NEW CAR ASSESSMENT PROGRAMME (Euro NCAP). 2009. "FRONTAL IMPACT TESTING PROTOCOL, Version 5.0". www.euroncap.com

Handman, D.F.. Multipoint position measuring and recording system for anthropomorphic test devices. 2007. Boxboro systems. LLC. Newton. NA: USA.

Kent, R. Lessley, D.; Shaw, G.; Crandall, J. 2003. "The Utility of Hybrid III and THOR Chest Deflection for Discriminating Between Standard and Force-Limiting Belt Systems". Stapp Car Crash Journal, 47, pp. 267–297.

Petitjean, A.; Lebarbe, M.; Potier, P.; Trosseille, X.; Lassau, J.-P. 2002. "Laboratory Reconstructions of Real World Frontal Crash Configurations using the Hybrid III and THOR Dummies and PMHS". Stapp car crash journal, 46, pp. 27–54.

Petitjean, A.; Baudrit, P.; Trosseille, X. 2003. "Thoracic injury criterion for frontal crash

applicable to all restraint systems". " Stapp Car Crash Journal. 47. pp. 323–348.

Rouhana S. Elhagediab A. Chapp J. (1998) A High-speed Sensor for Measuring Chest Deflection in Crash Test Dummies. Proc. Sixteenth Enhanced Safety of Vehicles. pp. 2017–2045.

Tylko. S.; Charlebois. D.; Bussièeres. A. 2007."Comparison of Kinematic and Thoracic Response of the 5th Percentile Hybrid III in 40. 48 and 56 km/h Rigid Barrier Tests". Paper Number 07-0506. Technical Conference on the Enhanced Safety of Vehicles.

Veizin. P.; Bruyere-Garnier. K.; Bermond. F.; Verriest. J. P. 2002. "Comparison of Hybrid III. Thor-alpha and PMHS Response in Frontal Sled Tests. " Stapp car crash journal. 46. pp. 1–26.

Yoganandan. N.; Pintar. F. A. 2009a. "Evaluation of the Ribeye Deflection Measurement System". Paper number 09-0020. Technical Conference on the Enhanced Safety of Vehicles.

Yoganandan. N.; Pintar. F. A. 2009b. "Optimal Sensor Positioning to Track Rib Deflections from an Optical System in the Hybrid III Dummy". " Traffic Injury Prevention. 10. pp. 497–505.

Zellmer. H.; Brüggemann. K.; Lührs. S. 1998."Optimierte Rückhaltesysteme für Fondinsassen - Advanced Restraint Systems for Rear Seat Occupants". BAG & BELT '98. Cologne.

SCALING METHODS APPLIED TO THORACIC FORCE DISPLACEMENT CHARACTERISTICS DERIVED FROM CARDIOPULMONARY RESUSCITATION

Matthew R. Maltese

Kristy B. Arbogast

The Children's Hospital of Philadelphia
United States

Zhenwen Wang

Humanetics, Inc.
United States

Matthew Craig

The National Highway Traffic Safety Administration
United States
Paper Number 11-0313

ABSTRACT

Motor vehicle crashes are the leading cause of death for children and adults for every year of age from 3 to 36 years in the United States. Anthropomorphic Test Devices (ATDs) and computer models are key tools for evaluating the performance of motor vehicle safety systems, yet current data available for the validation of pediatric ATDs and computer models are derived from adult data through scaling or from sparse PMHS experiments. Recent measurement of large datasets of cardiopulmonary resuscitation (CPR) on children and adults provides valuable information for validating the aforementioned models. Thus, the objective of this work was to: a) evaluate the changes in the elastic force-displacement properties of the chest across the pediatric and young adult age range, and b) apply three published methods to estimate the composite modulus of the chest and scale the elastic force-displacement properties of the 8 to 10 year old to the 6 year old. In general, the data show a gradient of increasing stiffness (i.e. higher force at any given displacement) with age. CPR subjects in the 20 to 22 year old and 17 to 19 year old age ranges showed similar force-displacement behavior as did subjects in the 11 to 13 and 14 to 16 year old age ranges. The scaled elastic force-displacement curves for the 6 year old were quite similar for the femur and skull based modulus, but the CPR based curve was lower in stiffness. Elastic force-displacement properties for chests of subjects 8 to 22 years old are provided, along with similar data for 6 year old subject scaled from 8 to 10 year old subjects. These data are useful for validation of ATDs and computer models of the human pediatric chest.

INTRODUCTION

Motor vehicle crashes are the leading cause of death for children 5 to 14 years old in the United States (Xu et al. 2010). The Anthropomorphic Test Device (ATD) is a key tool for the evaluation and optimization of automotive restraint systems for occupant protection. The ATD thorax interacts with the restraints within the vehicle, and must do so in a biofidelic or human-like manner to ensure that restraint designs protect humans. More recently, computer models of the human chest have been developed and require data for validation of their force-displacement.

Post-mortem human subjects (PMHS) are the common surrogate used to represent live adults in biomechanical testing to validate ATD and computer model biofidelity. Owing to the paucity of pediatric PMHS, previous researchers have scaled adult impact data to estimate the response of the child subject (Irwin and Mertz 1997; Van Ratingen et al. 1997). More recently, pediatric PMHS have become available (Ouyang et al. 2006; Kent et al. 2009) but the number of subjects at a single age range is quite limited.

Recent measurement of large datasets of CPR events on children and adults provides valuable information for validating the aforementioned models. CPR, which involves the displacement of the sternum toward the spine to induce cardiac blood flow, provides a means to conduct mechanical "testing" of the human chest. Various electro-mechanical devices have been developed over the past three decades to improve the quality of CPR and to study the effect of CPR mechanics on clinical outcomes (Tsitlik et al. 1983; Gruben et al. 1990; Aase and Myklebust 2002). Recently, these devices have been extended to the pediatric and young adult population (Maltese et al. 2008; Sutton et al. 2009) and provide for the

measurement and recording of the forces applied to the sternum during CPR and the calculation of resulting deformation (sternal displacement) of the chest through integration of accelerometer data. These CPR studies directly assess thoracic stiffness using human subjects, and can provide valuable guidance for the design and performance certification of the human surrogates such as finite element computer models or physical ATDs.

Thus, the objective of this work was to: a) evaluate the changes in the elastic force-displacement properties of the chest across the pediatric and young adult age range, and b) apply three published methods to estimate the composite modulus of the chest and scale the elastic force-displacement properties of the 8 to 10 year old to the 6 year old.

METHODS

Thirty-nine CPR events from three data sources were used to develop the 6 year old elastic force-displacement characteristics. Four CPR events reported by Tsitlik et al (Tsitlik et al. 1983), 18 events reported by Maltese (Maltese et al. 2008), and 17 new events collected by the Children's Hospital of Philadelphia and analyzed using methods previously reported (Maltese et al. 2008) were gathered into a single dataset (Table A1). The research reported herein was approved by the Institutional Review Board of the Children's Hospital of Philadelphia.

Displacement (x) as used here is defined as the motion of the sternum in the anterior-posterior axis of the chest, with respect to the thoracic spine. Displacement is defined as positive when the sternum moves toward the spine. Force (F) as used here is the force applied to the sternum in the anterior-posterior direction. A positive force moves the sternum closer to the spine.

Each subject's chest was modeled with a spring and damper in parallel; both the stiffness and damping coefficients were linearly dependent upon displacement. Thus, the relationship between force and displacement for the spring (elastic) component of the model is,

$$F_e = xa_1 + x^2a_2 \quad (1)$$

where a_1 and a_2 are the stiffness coefficients of the chest as previously defined by Tsitlik (Tsitlik et al. 1983) and (Maltese et al. 2008). For each patient, F_e vs. x was plotted, stratified into the following age

groups: 8 to 10, 11 to 13, 14 to 16, 17 to 19, and 18 to 22 years, thus accomplishing our first objective of evaluating the elastic force-displacement properties of the chest across the pediatric and young adult age range. In each age group, mean and standard deviation corridors were drawn.

Scaling

Using model theory (Langhaar 1951; Eppinger et al. 1984), mechanical scale factors were developed for systems of varying size and modulus of elasticity, but similar shape and density. Given two systems (labeled 1 and 2 in the equations below) of differing size and elastic modulus, scale ratios (λ) can be written for modulus (E), density (ρ) and characteristic length (L),

$$\lambda_\rho = \frac{\rho_2}{\rho_1} \quad \lambda_E = \frac{E_2}{E_1} \quad \lambda_L = \frac{L_2}{L_1} \quad (2)$$

Assuming the chests have similar composite densities ($\lambda_\rho=1$), by dimensional analysis scaling relationships for displacement, force and stiffness can be written as,

$$\lambda_x = \lambda_L \quad \lambda_F = \lambda_L^2 \lambda_E \quad \lambda_K = \lambda_E \lambda_L \quad (3)$$

Where the subscripts 1 and 2 refer to system 1, the system being scaled from (the 8 to 10 year old in this case), and system 2, the system being scaled to (the 6 year old in this case).

Inspection of equation (3) reveals that λ_L and λ_E are both unknown. λ_L was determined from mean anterior posterior (AP) chest dimension data from a robust, population-representative study of pediatric anthropometry (Snyder et al. 1975). From the aforementioned study, the AP chest dimension was found to be 133 mm for the 6 year old. For the 8 to 10 year old, the AP chest dimension of the 9.5 year old was used, which was 148 mm.

The composite modulus of the chest (λ_E), was determined by three different methods. First, skull (parietal) bone modulus data of Thibault et al. (1999), Margulies and Thibault (2000), McPherson and Kriewall (1980) and Hubbard (1971) as reported by Ivarsson (2004) was used as a surrogate for the composite modulus of the chest. Using the exponential equation fit to the skull bone modulus data reported by Ivarsson, the modulus with respect to age equation is,

$$E_{skull} = 1.7373 + 7.2928(1 - e^{-0.17003age}) \quad (4)$$

From equation 4, we found the composite modulus of the 6 year old (6.65 GPa) and for the 8 to 10 year old (7.58 GPa). (9.5 years was used as the age variable for the 8 to 10 year old in Equation 4.) Thus,

$$\lambda_{E-skull} = \frac{6.4 \text{ GPa}}{7.58 \text{ GPa}} = 0.84 \quad (5)$$

Similar to the skull bone modulus method, the second method used the femur bone modulus as a surrogate for the composite modulus of the chest. The following equation based upon work by Curry and Butler (1975) as reported by Ivarsson (2004) was used,

$$E_{femur} = -0.0029316age^2 + 0.28851age + 8.3468 \quad (6)$$

Based upon equation 6, the composite modulus based upon femur data for the 6 year old was 9.97 GPa and for the 8 to 10 year old was 10.82 GPa (age = 9.5 years was used for the 8 to 10 year old).

$$\lambda_{E-femur} = \frac{9.97 \text{ GPa}}{10.82 \text{ GPa}} = 0.92 \quad (7)$$

The third method of determining λ_E was based upon extrapolation of CPR data in the 8 to 22 year old age range to the 6 year old. Briefly, the stiffness of the chest (k) in the 8 to 22 year old age range was determined by (Maltese et al. 2010) to be,

$$k = \frac{16.7(age) - 54}{L(0.15)} \quad (8)$$

where L_c is the anterior-posterior chest dimension for the subject. Writing the ratio of stiffness between systems 1 and 2,

$$\lambda_k = \frac{16.7(age_2) - 54}{16.7(age_1) - 54} \frac{L_1}{L_2} = \frac{16.7(age_2) - 54}{16.7(age_1) - 54} \left(\frac{1}{\lambda_L} \right) \quad (9)$$

and then incorporating the equation for λ_k in (3) above,

$$\lambda_E = \frac{16.7(age_2) - 54}{16.7(age_1) - 54} \left(\frac{1}{\lambda_L^2} \right) \quad (10)$$

From Equation 10, using the AP chest dimension of 133 mm for the 6 year old, and 148 for the 9.5 year old, the composite modulus scale factor for CPR is

$$\lambda_{E-CPR} = 0.55 \quad (11)$$

The three moduli of elasticity ($\lambda_{E-skull}$, $\lambda_{E-femur}$, and λ_{E-CPR}) were each applied in equation (3) above, yielding three force-displacement curves for the 6 year old.

RESULTS

Figures 1 through 5 show the force-displacement curves for the CPR subjects in the 8 to 10, 11 to 13, 14 to 16, 17 to 19, and 20 to 22 year old age ranges, along with the mean and standard deviations.

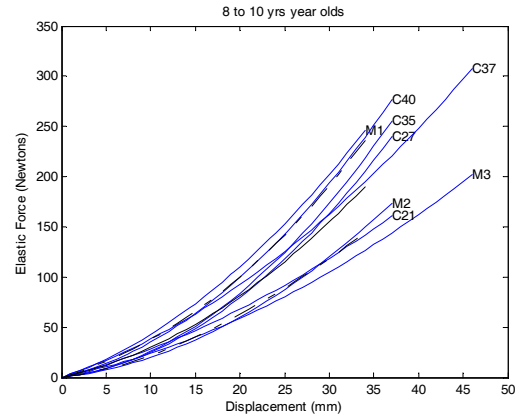


Figure 1 –Elastic force-displacement for the 8 to 10 year old subjects. Refer to Appendix Table A1 for data source for each curve. Dashed solid black line is the mean while the dashed black line is the standard deviation.

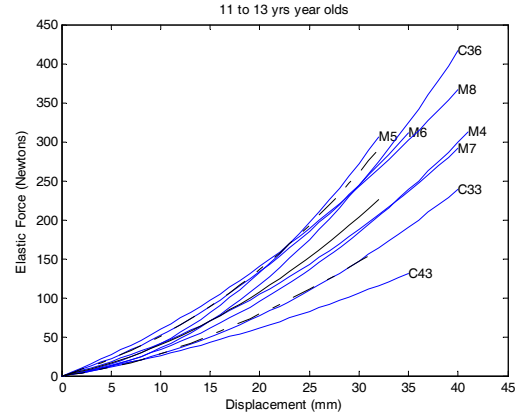


Figure 2 –Elastic force-displacement for the 11 to 13 year old subjects. Refer to Appendix Table A1 for data source for each curve. Dashed solid black line is the mean while the dashed black line is the standard deviation.

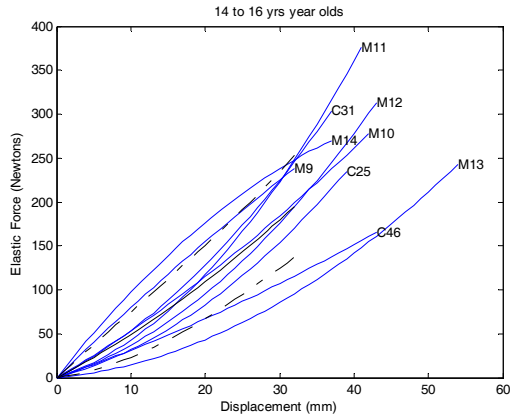


Figure 3 –Elastic force-displacement for the 14 to 16 year old subjects. Refer to Appendix Table A1 for data source for each curve. Dashed solid black line is the mean while the dashed black line is the standard deviation.

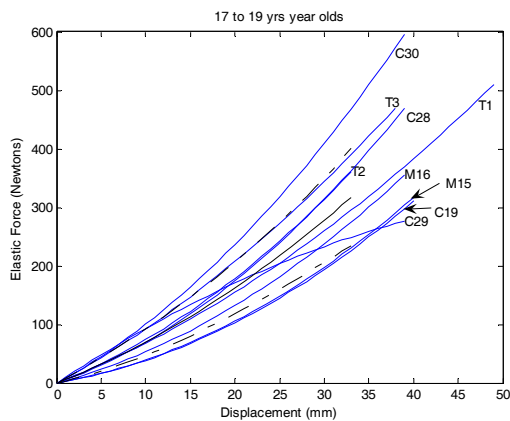


Figure 4 –Elastic force-displacement for the 17 to 19 year old subjects. Refer to Appendix Table A1 for data source for each curve. Dashed solid black line is the mean while the dashed black line is the standard deviation.

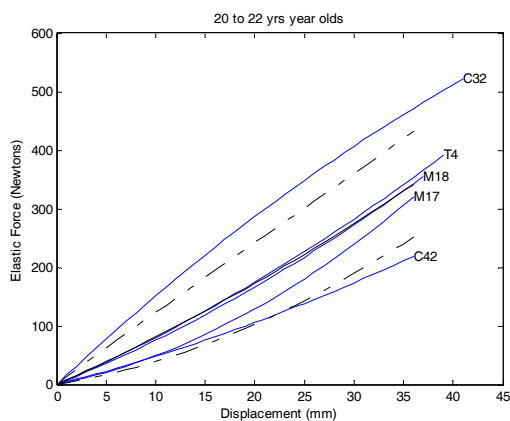


Figure 5 –Elastic force-displacement for the 20 to 22 year old subjects. Refer to Appendix Table A1 for data source for each curve. Dashed solid black line is the mean while the dashed black line is the standard deviation.

Figure 6 shows the mean elastic force for each of the age groups, as well as the scaled elastic force for the 6 year old using the three (femur, skull, and CPR) methods for finding the composite modulus of elasticity of the chest. In general, there is a gradient of increasing stiffness (i.e. higher force at any given displacement) with age. However, CPR subjects in the 20 to 22 years and 17 to 19 years age ranges showed similar force-displacement behavior as did subjects in the 11 to 13 and 14 to 16 year old age ranges.

Scaling of the 8 to 10 year old data to the estimate the 6 year old force-displacement based on femur and skull bone modulus produced similar curves with forces of 137 and 126 N at 30 mm displacement, respectively. However, scaling based on extrapolating the 8 – 22 year old CPR stiffness data produced significantly lower force of 81 N at 30 mm displacement. These differences are proportional to the differences in λ_E values in equations 5,7, and 11.

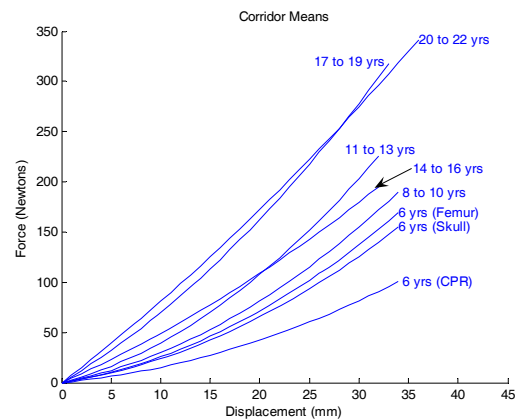


Figure 6 –Mean elastic force-displacement for the CPR subject age groups, and scaled data force-displacement for the 6 year old using the composite modulus of elasticity derived from skull, femur, and CPR.

Table 1 – Force (Newtons) at select displacements (mm) for Femur, Skull, and CPR-based Corridor means for the 6 year old (based upon curves in Figure 6).

| Cell value is Force (N) | | λ_E Data Source | | |
|-------------------------|----|-------------------------|-------|-----|
| | | Femur | Skull | CPR |
| Displacement (mm) | 10 | 26 | 24 | 15 |
| | 20 | 72 | 66 | 42 |
| | 30 | 137 | 126 | 81 |

DISCUSSION

This paper presents average elastic force-displacement curves for the human chest in the age

range of 8 to 22 years, based upon data collected during CPR. Understanding the force-displacement data of pediatric human subjects is an essential first step for validating ATD and computer models of the human body. This paper also employs model scaling laws to estimate the force-displacement of the chest for subjects close to, but outside, the age range of the CPR data collected which offers a potential improvement over current scaling methods that scale data from the elderly adult to the child.

The scaled estimates for force-deflection response of the 6 year old vary significantly depending on the method used. The force-deflection and stiffness estimates based on skull and femur modulus are roughly 50% higher than stiffness derived through extrapolating the CPR data. Until CPR stiffness data is available for ages overlapping and including the 6 year old, computer model validation could consider utilizing a force-deflection curve that falls roughly midway between the femur modulus and CPR data extrapolation based curves.

The data show a general increase in the force-displacement properties of the chest with age, though between the ages of 17 and 22 years old and 11 and 16 years old the force-displacement curves were quite similar. It is reasonable to assume that the mechanical properties of the chest of a 17 year old would be similar to that of a 22 year old, given that the chest has achieved adult size at that age. Conversely, the similarity observed in the force-displacement curves of the 11 to 16 year old age range cannot be explained by size similarity (since the chest is growing larger during this time period). Rather, inspection of the torso maturation process reveals dramatic material and morphological changes in this age range. Fusing between sternbrae begins at age 4 years and continues through age 20 years (Scheuer and Black 2000). The costal cartilage also calcifies with age, likely influencing its flexibility. The timing of these tissue changes during maturation may vary between subjects of the same age. Thus, age may not be the only explanatory variable for changes in thoracic stiffness during development, and another metric of skeletal maturity should be developed and employed.

The magnitude of chest deformation during CPR is in the range of relevance for motor vehicle crashes. At the time of data collection in this study, clinical resuscitation guidelines prescribed targets for CPR chest compressions: 38 to 51 mm of sternal displacement for the adult, or one-third to one-half the anterior-posterior (AP) chest depth for the child

(American Heart Association 2005). In terms of displacement, the CPR compression target for the 6 year old child is 47 to 72 mm, assuming an AP chest depth of 143 mm (Irwin and Mertz 1997). For comparison with the general chest displacements observed in impact experiments, chest displacements in hub impact testing with PMHS range from approximately 50 to 70 mm in adults (Lobdell et al. 1973) and from 31.5 to 73 mm overall deflection in children (Ouyang et al. 2006). Thus, chest compression magnitudes during CPR are similar to motor vehicle crash (MVC) events, however CPR rates of chest compression (0.25 m/s) (Maltese et al. 2008) are an order of magnitude lower than those observed in belt loading thoracic compression experiments with PMHS (1 to 2 m/s)(Kent et al. 2004). The low rate of compression during CPR is an advantage for determining thoracic stiffness, since the inertial forces are negligible and viscous forces are quantifiable (Bankman et al. 1990).

LIMITATIONS

It is important to note that CPR, unlike a car crash, loads the chest repeatedly (often hundreds of cycles). The consequences of this repeated loading are not fully understood. It is possible that the chest changes stiffness as the CPR chest compressions continue, though our current data do not show any consistent trend of increasing or decreasing stiffness.

The scaling laws used herein are subject to certain limitations as result of the assumptions made in their application. First, the composite modulus scale factor was applied solely in the anterior-posterior direction, which is the primary direction of chest compression during CPR and during frontal crashes. However, in doing so we assumed that the chest dimension scales equally in all directions ($\lambda_L = \lambda_x = \lambda_y = \lambda_z$) which most likely is not the case.

We presumed that skull and femur bone moduli were suitable surrogates for the composite modulus of the chest. Other researchers have used skull bone modulus as a material modulus for a component of the chest (i.e. rib) and then determined the composite stiffness scale factor based on a rib-hoop under compression using seated height as the length scale dimension (Irwin and Mertz 1997). Of note, aside from the choice of length scale dimension, our derived equation for chest stiffness (Equation 3) was the same as that which was derived by Irwin and Mertz.

The force-displacement data presented here are intended to be used to validate models subjected to *low-rate* loading. It is clear that the inertial and viscous properties of the human chest during high-rate loading will generate forces that are orders of magnitude higher than what we report herein. However, the value of our data is that we provide force-displacement data of subjects very close to the age range of interest (6 years), and data on such young subjects is limited in the literature (Ouyang et al. 2006; Kent et al. 2009).

Similarly, while the data presented herein are theoretically applicable to both physical ATDs and computer models, application of the data to the ATD is currently limited by the ability of the ATD to accurately represent both low- and high-rate loading conditions. Indeed, current ATDs are validated exclusively in the dynamic range similar to car crashes and, although validating the ATD to low-rate data presented here would expand the applicability of the ATD, such expansion may not be possible given the materials currently used to construct the ATD and the cost and durability requirements.

CONCLUSIONS

Herein we have provided low-rate thoracic force-displacement properties for subjects from 8 to 22 years old, and provided estimates for the 6 year old subject. The force-deflection or stiffness estimates for the 6 year old subject based on skull and femur modulus are roughly 50% higher than stiffness derived through extrapolating the CPR data. These data are useful for validation of computer models of the human pediatric chest.

ACKNOWLEDGEMENTS

Funding support was provided by the United States Department of Transportation, National Highway Traffic Safety Administration DTNH22-07-H-00085, and Laerdal Medical.

REFERENCES

Aase, S. O. and H. Myklebust (2002). "Compression Depth Estimation for CPR Quality Assessment Using DSP on Accelerometer Signals." IEEE Transactions on Biomedical Engineering **49**(3): 263-268.

American Heart Association. (2005). "2005 American Heart Association Guidelines for Cardiopulmonary Resuscitation and

Emergency Cardiovascular Care." Circulation **112**(24 Supplement).

Bankman, I. N., K. G. Gruben, H. R. Halperin, A. S. Popel, A. D. Guerci and J. E. Tsitlik (1990). "Identification of dynamic mechanical parameters of the human chest during manual cardiopulmonary resuscitation." IEEE Transactions on Biomedical Engineering **37**(2): 211-217.

Eppinger, R. H., J. H. Marcus and R. M. Morgan (1984). Development of dummy and injury index for NHTSA's thoracic side impact protection research program. SAE Government Industry Meeting and Exposition, Paper No. 840885. The Society of Automotive Engineers, Warrendale, PA.

Gruben, K. G., J. Romlein, H. R. Halperin and J. E. Tsitlik (1990). "System for mechanical measurements during cardiopulmonary resuscitation in humans." IEEE Transactions on Biomedical Engineering **37**(2): 204-210.

Irwin, A. and H. J. Mertz (1997). Biomechanical Basis for the CRABI and Hybrid III Child Dummies. 41st Stapp Car Crash Conference.

Ivarsson, B. J., J. R. Crandall, D. Longhitano and M. Okamoto (2004). Lateral Injury Criteria for the 6-year-old Pedestrian - Part I: Criteria for the Head, Neck, Thorax, Abdomen and Pelvis. SAE 2004 World Congress & Exhibition, Detroit, Society of Automotive Engineers.

Kent, R., D. Lessley and C. Sherwood (2004). "Thoracic response to dynamic, non-impact loading from a hub, distributed belt, diagonal belt, and double diagonal belts." Stapp Car Crash J **48**: 495-519.

Kent, R., R. Salzar, J. Kerrigan, D. Parent, D. Lessley, M. Sochor, J. F. Luck, A. Loyd, Y. Song, R. Nightingale, C. R. D. Bass and M. R. Maltese (2009). "Pediatric Thoracoabdominal Biomechanics." Stapp Car Crash J **53**.

Langhaar, H. L. (1951). Dimensional Analysis and Theory of Models. New York, Chapman & Hall.

Lobdell, T. E., C. K. Kroell, D. C. Schneider, W. E. Hering and A. M. Nahum (1973). Impact Response of the Human Thorax. Symposium on Human Impact Response. Warren, Michigan, Plenum Press.

Maltese, M., K. Arbogast, V. Nadkarni, R. Berg, S. Balasubramanian, T. Seacrist, R. Kent, D. Parent, M. Craig and S. Ridella (2010). "Incorporation of CPR Data into ATD Chest

Impact Response Requirements." Ann Adv Automot Med **54**: 79-88.

Maltese, M. R., T. Castner, D. Niles, A. Nishisaki, S. Balasubramanian, J. Nysaether, R. Sutton, V. Nadkarni and K. B. Arbogast (2008). "Methods for Determining Pediatric Thoracic Force-Deflection Characteristics from Cardiopulmonary Resuscitation." Stapp Car Crash J **52**: 83-106.

Ouyang, J., W. Zhao, Y. Xu, W. Chen and S. Zhong (2006). "Thoracic impact testing of pediatric cadaveric subjects." Journal of Trauma: 1492-1500, Dec.

Scheuer, L. and S. Black (2000). Developmental Juvenile Osteology. London, Academic Press Limited.

Snyder, R. G., M. L. Spencer, C. L. Owings and L. W. Schneider (1975). Physical Characteristics of Children as Related to Death and Injury for Consumer Product Safety Design, Consumer Product Safety Commission.

Sutton, R. M., D. Niles, J. Nysaether, B. S. Abella, K. B. Arbogast, A. Nishisaki, M. R. Maltese, A. Donoghue, R. Bishnoi, M. A. Helfaer, H. Myklebust and V. Nadkarni (2009). "Quantitative analysis of CPR quality during in-hospital resuscitation of older children and adolescents." Pediatrics **124**(2): 494-499.

Tsitlik, J. E., M. L. Weisfeldt, N. Chandra, M. B. Effron, H. R. Halperin and H. R. Levin (1983). "Elastic properties of the human chest during cardiopulmonary resuscitation." Critical Care Medicine **11**(9): 685-692.

Van Ratingen, M., D. Twisk, M. Schrooten and M. Beusenbergh (1997). "Biomechanically Based Design and Performance Targets for a 3-Year Old Child Crash Dummy for Frontal and Side Impact." 41st Stapp Car Crash Conference SAE Paper No. 973316.

Xu, J. K., KD, S. Murphy and B. Tejada-Vera (2010). National Vital Statistics Reports, Deaths: Final Data for 2007, Centers for Disease Control and Prevention. 58, No 19.

APPENDIX

Table A1 – CPR event data.

| Event | Age | sex | x_{max} | a_1 | a_2 |
|-------|-------|-----|-----------|-------|------------------|
| | years | | mm | N/m | N/m ² |
| M1 | 8 | F | 34 | 3062 | 122712 |
| C35 | 8 | F | 37 | 1018 | 158887 |

| | | | | | |
|-----|----|---|------|-------|--------|
| C40 | 8 | F | 37 | 2026 | 147394 |
| M2 | 9 | F | 37 | 1009 | 99622 |
| C21 | 9 | F | 37 | 2284 | 55657 |
| C27 | 9 | F | 37 | 1036 | 146994 |
| M3 | 10 | F | 46 | 1839 | 55344 |
| C37 | 10 | M | 46 | 3042 | 78972 |
| M4 | 12 | M | 41 | 2019 | 136757 |
| M5 | 12 | M | 32 | 1714 | 245459 |
| M6 | 12 | M | 35 | 3699 | 147971 |
| M7 | 13 | F | 40 | 3119 | 104030 |
| M8 | 13 | F | 40 | 4853 | 107487 |
| C33 | 13 | M | 40 | 1723 | 106291 |
| C36 | 13 | F | 40 | 1284 | 228117 |
| C43 | 13 | M | 35 | 2177 | 45029 |
| M9 | 14 | M | 32 | 8199 | -23276 |
| M10 | 14 | F | 42 | 4937 | 40001 |
| M11 | 14 | M | 41 | 2681 | 158551 |
| M12 | 15 | F | 43 | 2609 | 108554 |
| C31 | 15 | F | 37 | 4288 | 106059 |
| C46 | 15 | F | 43 | 2924 | 21665 |
| M13 | 16 | M | 54 | 786 | 68821 |
| M14 | 16 | F | 37 | 10608 | -89390 |
| C25 | 16 | F | 39 | 2184 | 98204 |
| M15 | 17 | F | 40 | 2612 | 132907 |
| T1 | 17 | F | 49.2 | 5920 | 91400 |
| C19 | 17 | F | 40 | 2537 | 130901 |
| T2 | 18 | M | 33.5 | 5900 | 152000 |
| C28 | 18 | M | 39 | 5248 | 174036 |
| C29 | 18 | M | 39 | 10037 | -75481 |
| C30 | 18 | M | 39 | 8205 | 181297 |
| M16 | 19 | F | 39 | 3997 | 131141 |
| T3 | 19 | M | 38.1 | 8150 | 111000 |
| C32 | 20 | M | 41 | 15878 | -77227 |
| C42 | 21 | M | 36 | 4317 | 48838 |
| M17 | 22 | F | 36 | 3412 | 151735 |
| M18 | 22 | M | 37 | 6821 | 75158 |
| T4 | 22 | M | 39.8 | 7350 | 68800 |

*Note: M indicates data from (Maltese et al. 2008), T indicates data from (Tsitlik et al. 1983), and C is new data collected at the Children’s Hospital of Philadelphia and analyzed using the methods of (Maltese et al. 2008).

MEASUREMENT OF AORTIC INJURIES IN LOWER SEVERITY NEAR-SIDE IMPACTS

Kennerly Digges

George Washington University; University of Miami, William Lehman Injury Research Center

Jeffrey Augenstein

University of Miami Miller School of Medicine; William Lehman Injury Research Center

Warren Hardy

Wayne State University, Virginia Tech

John Cavanaugh

Wayne State University

Jessica Steps Jermakian

George Washington University, IIHS

Cristina Echemendia

George Washington University, NHTSA

Chirag Shah

Wayne State University, Humanetics Innovative Solutions
USA

Paper Number 11-0265

ABSTRACT

NASS and Miami Trauma Center data were analyzed to determine the crash environments that produce aortic injuries in lower severity side impacts. Crash tests were analyzed to determine the injury producing acceleration and intrusion environments. Cadaver tests were conducted using high speed X-ray to examine aortic displacements in response to impacts. Biaxial tensile tests of aortic tissue were conducted to determine their dynamic response to loading. FEM and MADYMO models were run to determine the response of the vehicle structure, the human and the aorta when exposed to injury producing environments.

For the seriously or fatally injured population in the William Lehman Injury Research Center (WLIRC) database who were exposed to side impacts, 24% had aortic injuries. By contrast, the injury rate in NASS was about 5%. In WLIRC data, 60% of the aortic injuries occurred at crash severities below 30 mph delta-V. In NASS, 28% occurred at the lower crash severity.

Crash factors in lower severity near-side crashes that influence aortic injury risk include the extent of intrusion, the occupant age, and a D or Y vehicle damage pattern. The best predictor of aortic injury risk, based on currently available cadaver tests utilizes a combination of spinal z acceleration and chest viscous criterion. Based on this metric, the IIHS test condition produced a higher risk of aortic injury than the side NCAP or the side Y-NCAP tests.

Testing of aortic tissue found a general weakness in tension. The inner layer of aortic tissue was found weaker during tension tests of the tissue and initialized

tearing under yield tensile loading to the tissue. Rupture of the inner layer may not produce physiological changes immediately but sudden death can result should all three layers rupture. Death caused by delayed rupture of all layers occurred for 60% of the WLIRC patients with side impact induced aortic injuries who survived more than one hour. This result suggests that a large fraction of those with aortic injury produced in low severity side impacts could be treated successfully if diagnosed in time.

INTRODUCTION

This paper summarizes the results of ten years of research on aortic injury mechanisms directed by The George Washington University and the William Lehman Injury Research Center (WLIRC) and conducted with the collaboration of Wayne State University. The various funding sources are listed in the Acknowledgement Section. The project is referred to as the Cooperative Aortic Injury Research Project.

The project originated in 2001 and was based on observations at the University of Miami's Ryder Trauma Center. At this Level 1 Trauma Center, a high percentage of motor vehicle accident victims exposed to side collisions were found to have aortic injuries. In many cases, the aortic injuries were difficult to detect and the patients were not initially triaged to the Trauma Center, resulting in a high death rate. Those who were successfully treated generally suffered no subsequent impairment [Augenstein, 2003].

These results suggested two critical needs. First, better triage methods were required to permit early identification of the crash victims with incipient aortic injuries. Second, a better understanding of the injury

mechanisms was needed so that countermeasures could be designed and evaluated.

The first need was addressed by assessing the characteristics of crashes that produce aortic injuries. The results were intended to be used to raise the suspicion of aortic injury based on data from the vehicle sensors or observations at the crash scene.

The second need was addressed by comprehensive studies of existing cadaver test data, testing the properties of aortic tissue, modeling the vehicle, human and aorta, and conducting additional cadaver tests to study the motion of the aorta in response to impacts using high speed X-ray.

There exists a large amount of literature, dating back over a century that documents studies of Traumatic Rupture of the Aorta (TRA). Fundamental research during the 1980's by Mohan and Melvin [1982, 1983] and Viano [1983] provided a strong basis for the study of aortic trauma in motor vehicle crashes. Some of the most applicable studies are discussed in the paper by Hardy et.al. as part of the Cooperative Aortic Injury Research Project [Hardy, 2008]. Although much is understood about the nature of the injury, little is known about the mechanisms that produce this injury. This is because although there have been many studies examining the pathology of TRA, there have been few studies that have been successful in producing aortic rupture by blunt impact using the human cadaver or an animal as an injury model. Further, cadaver and animal studies have provided little information regarding the kinematics inside the chest and the deformation of the aorta during impact.

STUDIES OF AORTIC INJURIES IN REAL WORLD CRASHES

The NASS/CDS (National Automotive Sampling System/ Crashworthiness Data System) is a sample of tow-away crashes that occur on US roads each year. The sample is stratified by the severity of the crash. The sample rate for minor crashes is much lower than for severe crashes. In order to expand the stratified sample to the entire population it represents, an inflation factor is assigned to each case in the NASS/CDS sample. Each year approximately 6,000 cases are collected to represent about 6,000,000 occupants in tow-away crashes on the US highways. In this sample, specific injuries that occur in lower severity events are difficult to detect and to represent. For example, fifteen years ago, the severe injuries caused by airbags that deployed in low speed crashes were not observed in NASS. The phenomenon was, however, observed by the William Lehman Injury Research Center among patients transported to the

Ryder Trauma Center. This Trauma Center receives a near census of all the seriously injured crash victims in the surrounding area of South Florida. Since the Trauma Center population is based on the injury severity of the occupant rather than the crash severity of the vehicle, the WLIRC database of Ryder Trauma Center patients was able to capture all serious injuries regardless of the severity of the crash in which they occurred.

The Lehman Center database used in this study contains 168 cases of near-side crashes. In these crashes, 41 sustained aortic injury resulting in 35 fatalities. Of these cases, 21 were transported to the trauma center and 15 survived for more than an hour. Six of these cases were treated successfully with no long-term impairment. For the aortic injury cases, the injury rate was 0.24 and the fatality rate was 0.85. For the group with aortic injuries, 37% survived for over an hour and had the best chance of a full recovery [Augenstein, 2003].

Occupants who survive initially but have latent aortic injuries have a high fatality risk. However, if detected and treated promptly, the outcome is generally excellent with no long-term impairment. Latent aortic injuries are often difficult to detect at the scene or in the emergency room. Twenty-three percent of latent aortic injury cases in near-side vehicle-to-vehicle crashes in the WLIRC database did not meet traditional physiologic trauma criteria at the scene, although most were transported to the trauma center under the paramedic judgment of high suspicion of injury.

Some crashes are so severe that an occupant may have sustained aortic tear but also will have sustained other life threatening injuries. For this reason, the discussion to follow will divide the data into two groups: one group contains crashes of all severities and the second contains a subset of crashes with a crash severity (delta-V) of 13.4 m/s (48.3 km/h; 30 mph) and below. Crash victims in the lower severity group are likely to have fewer numbers of serious injuries in addition to the aortic injury. Consequently, their survival is more likely.

Eighty percent of the aortic injuries in near-side crashes occurred in vehicle-to-vehicle crashes and over 60% of these were at a delta-V less than 13.4 m/s. The population of WLIRC vehicle-to-vehicle near-side crashes at delta-V less than 13.4 m/s was analyzed by Steps [Steps 2003]. The database contained 98 cases, 21 of which had an aortic injury. The injury rate generally increased with occupant age and weight.

For vehicle-to-vehicle lower severity near-side crashes, the average age of the occupants with aortic tear was 49 years old. The youngest was 15 and the oldest 89. One-hundred percent of cases had more than six inches of intrusion into the occupant compartment. Sixty-eight percent of the vehicles exhibited Y or D damage patterns. The Y and D damage patterns are depicted in Figure 1.

Steps conducted a multiple regression analysis of a database that combined NASS and WLIRC and data from other trauma centers to assess factors that might best predict aortic injury in lower severity near-side crashes. The result is shown in Table 1. The DL variable in Table 1 refers to a vehicle damage pattern that involves the front 2/3 of the vehicle or the entire side of the vehicle. Figure 1 shows this damage pattern. The damage pattern is defined by the SAE's Collision Damage Classification (CDC) [SAE 1980]

Table 1.
Significant Individual Predictors of Aortic Tear in Crashes with Delta-V of 13.4 m/s (48.3 km/h) (30 mph) or Below (Steps, 2003)

| Variable | Odds Ratio | P value |
|-----------|------------|---------|
| Age | 1.03 | <0.01 |
| Delta-v | 1.105 | <0.01 |
| DL | 2.261 | 0.03 |
| Intrusion | 1.081 | <0.01 |

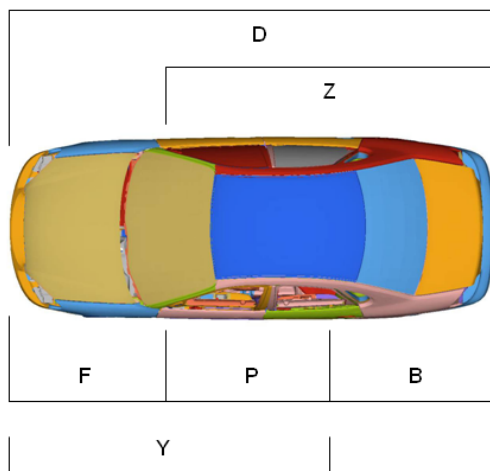


Figure 1. CDC Definition of Damage Location (SAE 1980) (DL, Includes Y and D Damage Patterns)

Age, delta-V and intrusion have been highlighted in the past as predictors of aortic tear. [Katyal, 1997; Horton, 2000]. However, Steps conducted the first analysis showing statistical significance of the vehicle's damage pattern. The high positive value of the DL coefficient suggests that the crash configuration may be an important factor that influences the risk of aortic injury.

Echemendia [2008] subsequently conducted a multivariate regression of NASS/CDS cases for the years 1993-2007. The condition for admission was a near-side crash with delta-V recorded. The database contained 783 cases that expanded to 59,112 using NASS weighting factors. There were 77 aortic injuries. The database was separated into two crash severity groups, as shown in Table 2. The highest speed for the low severity category was 13.4 m/sec (30 mph). The significant results of the multiple regression analysis of injuries at the lower speed are shown in Table 3.

Table 2 –
Baseline NASS Data for Studying Aortic Injuries in Near Side Impacts (Echemendia, 2008)

| Severity | Unweighted | | | Weighted | | |
|----------|------------|-----------------|-------|----------|-----------------|-------|
| | N | Aortic Injuries | Rate | N | Aortic Injuries | Rate |
| All | 783 | 77 | 0.098 | 59,112 | 2,913 | 0.049 |
| High | 385 | 59 | 0.153 | 26,602 | 2,108 | 0.079 |
| Low | 398 | 18 | 0.045 | 32,510 | 805 | 0.025 |

Table 3.
Results of Multivariate Regression Analysis of Factors that Influence Aortic Injury Risk in Lower Severity Near-side Impacts (Echemendia, 2008)

| Parameter | Unweighted | | Weighted | |
|---------------------------|------------|---------|------------|---------|
| | Odds Ratio | P-VALUE | Odds Ratio | P-VALUE |
| Age | 1.022 | <0.0001 | 1.018 | 0.0225 |
| Weight | 1.017 | 0.005 | 1.015 | 0.0018 |
| Intrusion | 1.494 | 0.0011 | 1.828 | 0.0041 |
| Damage Location | | 0.0379 | | <0.0001 |
| Damage Location Dvs.P | 2.336 | | 4.799 | |
| Damage Location Yvs.P | 0.949 | | 0.986 | |
| Damage Location YDvs.BZFP | 1.28 | | 2.037 | |

The analysis by Echemendia indicates that occupant weight is an additional factor that influences aortic injury risk in lower severity near-side crashes. The distributed damage pattern was found to induce a much higher risk than a pattern in which damage was confined to the occupant compartment. In addition, the distributed damage pattern (D) appears to be more influential than the front 2/3 damage pattern (Y). The combination of Y and D damage patterns was more influential than the combination of other damage patterns. This result confirmed the earlier findings of Steps, who used a different database. In the WLIRC database used by Stepps, the Y damage was much more frequent and influential than D damage.

STUDIES OF MATERIALS PROPERTIES OF THE AORTA

The aorta is a tubular structure and has two anatomical axes: the longitudinal (or axial) and the circumferential (or transverse) directions. The wall of the aorta has three layers, or tunics (Figure 2). The innermost layer is the tunica interna (the intima), which consists of a lining of endothelial cells supported by a layer of collagenous connective tissue containing a network of elastic fibers. The tunica media (the media) is the middle layer, which consists of elastic connective tissue, smooth muscle cells, and a fine network of binding collagen fibers. In the aorta, the media is the thickest layer. The outermost layer is the tunica externa (the adventitia), which is comparatively thin and consists of connective elastic and collagen fibers and bundles of smooth muscle tissue. It is in the circumferential direction that the overwhelming majority of aortic tears are observed clinically, and these tears typically involve the intima and the media (Cammack et al., 1959).

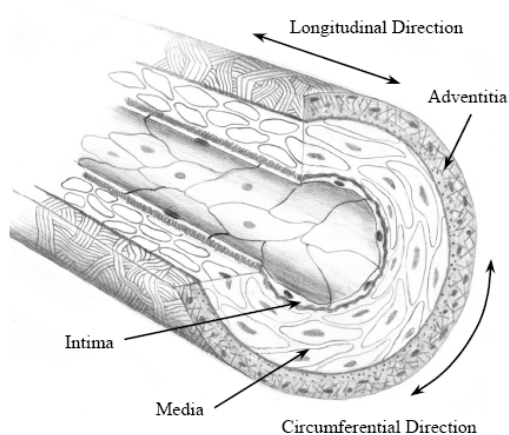


Figure 2. Wall Structure of the Aorta (Hardy, 2008)



Figure 3. Image of Aorta with Partial Rupture

Figure 3 shows a fluoroscopic image of an aorta that has a partial rupture of the two inner layers. The difference in elasticity and ultimate strength of the three layers can explain this failure mode.

Tensile tests of specimens from each of the three layers found that the unconstrained intima and media failed at a much lower circumferential strain levels than the adventitia [Holzapfel, 2005]. For the media, the failure strain level was about 50% and for the intima the level was only 10%. Computer modeling of a three layered section of the aorta indicated that the outer layers may apply a compression stress to the intima when in situ [Zhao, 2006]. It also predicted the earlier rupture for these two layers.

The consequence of this failure mode has a profound influence on the recognition and treatment of people with aortic injuries. The greater strain tolerance of the adventitia can sustain its integrity and prevent or minimize blood loss even after partial rupture of the inner layers. Consequently, there may be no physiological indicators of the injury. However, subsequent rupture of the adventitia long time periods after the injury has occurred can lead to sudden and unexpected death. As noted earlier, 37% of the patients with aortic injuries in the WLIRC study survived for more than one hour. The difficulty of recognizing this class of aortic injuries underscores the need for a better understanding of ways to predict and prevent them.

To further the understanding of TRA and provide materials properties for computer simulation, a unique dynamic bi-axial test device was developed at Wayne State [Mason, 2005]. Shah [2006] used this device to study the mechanical properties of tissue from various regions of the aorta. The tests were performed at a nominal speed of 1m/s and 5 m/s. Aorta tissue

properties and failure thresholds were obtained by conducting biaxial tissue tests on cruciate samples and longitudinal stretch tests on whole aortas. For the first time, aortic tissue was tested biaxially at an average strain rate of 85 s^{-1} which is commensurate with loading rates in the automotive crash environment. Three regions of the aorta: ascending, descending, and peri-isthmus were tested to investigate differences in the regional properties of the aorta. Structural response of the aorta was obtained by longitudinal stretch test at rate of 1 m/s.

The failure strain levels determined by Shah [2007] are presented in Table 4. Of primary interest is the longitudinal tensile failure threshold for the isthmus.

Table 4.
Aorta Tensile Failure Thresholds (Shah, 2007)

| Region | Ave. Maximum Principal Strain Rate (s-1) | Longitudinal Lagrange Failure Strain |
|------------|--|--------------------------------------|
| Ascending | 100.94 ± 31.34 | 0.277 ± 0.126 |
| Descending | 72.51 ± 49.24 | 0.244 ± 0.044 |
| Isthmus | 89.68 ± 58.18 | 0.217 ± 0.137 |
| Overall | 84.97 ± 48.07 | 0.244 ± 0.100 |

Shah's dissertation research [2007] concluded that the aorta fails with circumferential-direction tears and the intima layer fails before the media or adventitia layer. The aorta was characterized by a nonlinear stress-strain response. For the peri-isthmus and descending regions, the longitudinal failure stress increases as the strain rate increases. The aortic tissue is anisotropic with different material properties along longitudinal and circumferential directions. In the circumferential direction (Young's modulus 11.37 MPa) of the aortic tissue is stiffer than the longitudinal direction (Young's modulus 7.79 MPa). As a complete structure, the aorta fails within the peri-isthmus region and can transect completely at 92 N of axial tension or at an axial strain of 0.221. Intimal tears can accompany complete transections.

Shah's FE simulations demonstrated regions of relatively high stress and strain in the peri-isthmus region for near-side impact cases, which is indicative of those seen clinically. Shah concluded that the anterior sternum displacement may be important to TRA, as the aorta is pulled by the sternum away from the spine during side impacts.

Figure 4 shows the configuration of the aorta, its attachment to the spine and its connection to the heart. It is evident that chest compression that displaced the heart laterally could cause the aorta to stretch relative to the spine. Motion of the heart upward could also cause the aorta to stretch. Upward motion could be caused by positive displacement of the chest organs from chest compression or from vertical acceleration. Localized impacts to the chest of cadavers could be used to study the consequence of chest compression on aortic loading. However, the effects of vertical spinal acceleration cannot be easily measured by impact tests.



Figure 4. The Aorta Spine Attachment

STUDIES OF CADAVER SIDE IMPACT TESTS THAT PRODUCED AORTIC INJURIES

As noted earlier, aortic injuries have rarely been observed in cadaver tests that simulate motor vehicle crashes. Aortic injuries were observed in only 5 of 137 side impact cadaver tests in NHTSA's database [Steps 2003]. These five injuries occurred during a project funded by the U.S. Centers for Disease Control that involved a total of seventeen tests at Wayne State University conducted by Cavanaugh [1990, 1993]. In these tests, a side crash was simulated when the test sled impacted a barrier, allowing the instrumented cadaver positioned on a low-friction seat to impact an instrumented side wall at a predetermined velocity. One purpose of the tests was to evaluate variations in side padding stiffness and geometric configurations. A configuration of particular interest, called pelvic-offset, involved 152 mm (6 inch) offset of the metal wall at the height of the pelvic region. This offset in the wall caused the material surface to load and displace the lower body before the chest loading occurred.

For the 17 tests, 3 sled speeds were used: 6.7, 9.0, and 10.5 m/s. Three wall configurations were used - rigid flat wall, rigid wall with a 152 mm offset toward the pelvis, and a flat wall with padding of varying stiffness. Multiple load and acceleration measurements

were made on the wall and cadaver. Potential injury parameters were evaluated and their relative predictive abilities were examined.

Five of the seventeen tests resulted in AIS 4 or 5 TRA. Most were partial circumferential tears in the periisthmic region. All tears resulted from tests involving the rigid barrier or stiff padding. Tests involving softer padding did not result in TRA.

Cavanaugh performed a logistic regression analysis to determine if a relationship existed between TRA and independent variables in this study. Aortic injury was considered the dependent variable and was assigned a value of 0 or 1. Biomechanical responses including rib, spine and sternum accelerations, chest compression, viscous criterion and barrier forces as well as age were

analyzed as independent variables. ASA, VCmax and Cmax were evaluated as injury criteria. Cavanaugh et al. [1994] suggested that average spine acceleration (ASA) was a candidate predictor of chest injury. The other two predictors of chest injuries, VCmax (Lau and Viano, 1986) and Cmax (Kroell et al., 1974) are currently used as injury criteria measured by crash test dummies. The risk prediction accuracy of these three predictors and combinations with vertical spinal acceleration (T12Z) are shown in Table 5. The addition of spinal Z acceleration in conjunction with VCmax, Cmax or ASA provided the best prediction. Upper sternum displacement (UpsX in Table 5) and ASA also produced a good prediction. These results suggest that traction on the aortic arch through anterior displacement of the sternum or vertical displacement of the spine can increase the risk of aortic injury.

Table 5.
Logistic Regression Coefficients and Accuracy Measures for Aortic Injury Risk Prediction (Cavanaugh 2005)

| Variable or Combination | k1 | k2 | k3 | Chi-square | P value |
|-------------------------------|--------|--------|---------|------------|---------|
| ASA 10 at T12 | | | | 5.216 | 0.0224 |
| Cmax | | | | 2.329 | 0.127 |
| VCmax | | | | 3.959 | 0.0466 |
| $k1 * T12Z + k2 * ASA + k3$ | 0.0426 | 0.2123 | -12.03 | 8.985 | 0.0027 |
| $k1 * T12Z + k2 * Cmax + k3$ | 0.0236 | 0.3666 | -20.97 | 8.438 | 0.0037 |
| $k1 * T12Z + k2 * VCmax + k3$ | 0.0294 | 4.6622 | -10.452 | 9.76 | 0.0018 |
| $k1 * UpsX + k2 * ASA + k3$ | 0.0964 | 0.1889 | -16.168 | 8.405 | 0.0037 |

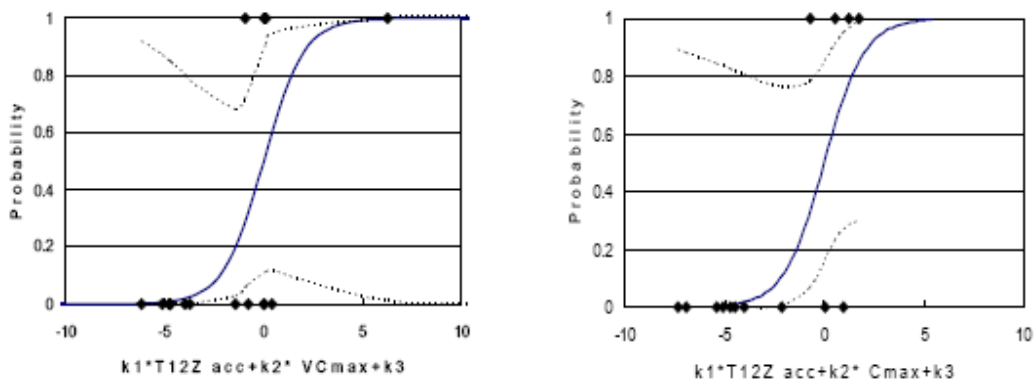


Figure 5. Logist Plot of Probability of AIS4 or Higher to the Aorta vs. Combination of T12Z acceleration and [VC]max (left) and Cmax (right) (Cavanaugh, 2005)

Plots of the probability of AIS 4+ aortic injuries based on T12 and VCmax or Cmax are shown in Figure 5. These plots are based on the population of 17 cadaver tests in the Cavanaugh et al study. The 95% confidence intervals for the probability curves of Figure 5 are fairly wide and the sample size is limited. Nevertheless, the results provide data that indicate that chest compression, vertical acceleration and sternum displacement are promising areas for further study regarding aortic injury mechanisms. Additional cadaver and simulation studies were carried to address these issues, as described in the following sections.

CADAVER TESTS DESIGNED TO STUDY AORTIC INJURIES

Under the Cooperative Aortic Injury Research Project, Wayne State University conducted 7 cadaver tests with markers on the aorta that could be observed during a chest impact by high speed x-ray [Hardy 2008]. The author observed that the position of the heart in cadavers subjected to crash tests was lower than it would be in a living human. The position of the heart may influence the risk of producing an aortic injury. To test this hypothesis, the cadavers in this test program were inverted to reverse the effects of gravity.

A specially designed cadaver fixture, first described by Hardy et al. [2006], and linear impactor were developed for this series of tests. The high-speed biplane x-ray system of the Motion Analysis Laboratory of Henry Ford Hospital was used to image the aorta during impact. This is the same system employed by Hardy et al. [2007] for the study of head impact kinematics. Visible light video cameras were used to observe the events overall and to estimate the motion of the cadaver spine.

Three side impact tests of cadavers conducted in the program. One purpose was to investigate the mechanism associated with anterior sternum motion as discussed by Cavanaugh et al. [2005] and Melvin et al. [1998] combined with lateral heart displacement. For the three side impacts (Test XR4, XR5, and XR6), the cadavers were inverted and pitched rearward. The cadavers were rotated 30-degrees from vertical for these tests. This configuration was used to investigate lateral chest compression and anterior sternum motion as a potential TRA mechanism. Test XR4 and XR5 involved side impacts with and without engaging the arm and shoulder. In tests XR4 and XR6 the arms were placed alongside the ribcage and were engaged by the impactor and backing support plate. In Test XR5, the upper extremities were allowed to dangle below the cadaver so that the ribs were engaged directly. The impactor was aimed at the approximate

location expected to be assumed by the humerus mid-diaphysis for a seated posture. The cadavers were impacted on the left side.

All three tests produced tears of aortic tissue that extended into the media. The tear in test XR4 also extended into the adventitia. All of the tears had a circumferential component, two of which were near the ligamentum arteriosum. The third was across the lesser curvature in an area involving substantial plaque.

Hardy results showed that the unique testing methods facilitated the generation of TRA in a cadaver. Circumferential tears through the intima, media, and adventitia were observed in the peri-isthmic region. High-speed biplane x-ray techniques were used to visualize the motion of the aorta and to measure longitudinal strain in the aorta. The results of this study provided a better understanding of the mechanisms associated with TRA. These results can be used for the validation of finite element models developed for the examination and prediction of TRA.

This Wayne State study found that clinically relevant TRA can be generated in the cadaver using the experimental techniques that were developed and employed. The tests showed that when atherosclerosis is present, TRA tends to occur within regions of plaque. When TRA occurs within a region of plaque, longitudinal tensile strain can be below established failure thresholds for the aorta.

The study described the motion of the aorta under side impact. The high speed X-rays showed that the isthmus of the aorta moves medially and anteriorly during impact to the left side. Dorsocranial and anteromedial motion of mediastinal contents result in axial tension in the aortic isthmus. Axial elongation (longitudinal stretch) of the aorta is central to the generation of TRA. Tethering of the descending thoracic aorta by the parietal pleura is a principal aspect of TRA. Consequently, the anterior sternum displacement may be important to TRA, as the aorta is pulled by the sternum away from the spine during side impacts.

CRASH TEST SIMULATIONS ADDRESSING AORTIC INJURY RISK

Steps [2003] used a finite element model of a Dodge Neon to evaluate the damage and intrusion observed in crash tests that produced Y and P damage patterns as defined in Figure 1. A FE model of the NHTSA barrier was used as the bullet vehicle. Two impact locations were simulated. The first duplicated the side NCAP test and produced P-damage. The second

impacted at the front wheels and produced Y-damage. The resulting door damage profile and intrusion were used as input data to a MADYMO simulation of the occupant response. Available side dummy models were used in the MADYMO simulations. The simulation results indicated that the MADYMO human facet model reported differences in injury risk in Y-damage crashes while the SID model did not. This result suggests that a more sophisticated dummy than the SID may be required to predict aortic injuries. A major feature of the MADYMO human facet model is a more human-like spine.

Alonso [2007] evaluated the kinematics of MADYMO dummies in far-side crashes. He found that the head excursion of the MADYMO human facet model closely matched that observed during a baseline cadaver test. Other MADYMO dummies including the BioSID, EuroSID and SID2s experienced less head excursion and did not react in a way similar to the cadaver in the baseline test. Alonso's research tends to confirm the observation by Steps that a more flexible spine is desirable to improve injury predictions that require head excursion or Z acceleration.

Shah [2005] reconstructed a crash from the WLIRC database that involved an aortic injury. He used a finite element model of a Ford Taurus and a whole-body human FE model [Shah 2001, 2004] developed by Wayne State University. The whole-body human FE model was not able to simulate rib fractures and

rupture of other tissues. Shah concluded that significant limitations need to be addressed before reconstruction of actual crashes can be used to reliably investigate aortic injury mechanisms.

Echemendia applied computer modeling to evaluate the test conditions most likely to produce aortic injury [Echemendia, 2008]. The finite element models of the vehicle and moving deformable barriers used in this study were developed and validated by the National Crash Analysis Center at The George Washington University. The vehicle model was of a 2001 Taurus. The NHTSA and IIHS barrier models were used as bullet vehicles. The research focused on the evaluation of how the crash environment produced by different test conditions would influence the risk of aortic injury.

The models were used to reproduce three different crash environments, as shown in Figure 6. The first environment, designated NCAP, was a crash test using the NHTSA barrier at an impact speed of 61.95 k/hr (38.5 mph) and impacting the occupant compartment in the same impact location and barrier orientation as the NCAP test. The second environment, designated Y-NCAP, was the same barrier and speed configuration as the first, but changing the impact location to the front wheels in order to produce Y damage. The third configuration, designated IIHS, used the IIHS barrier and test configuration – 50 k/hr and impact at the occupant compartment.

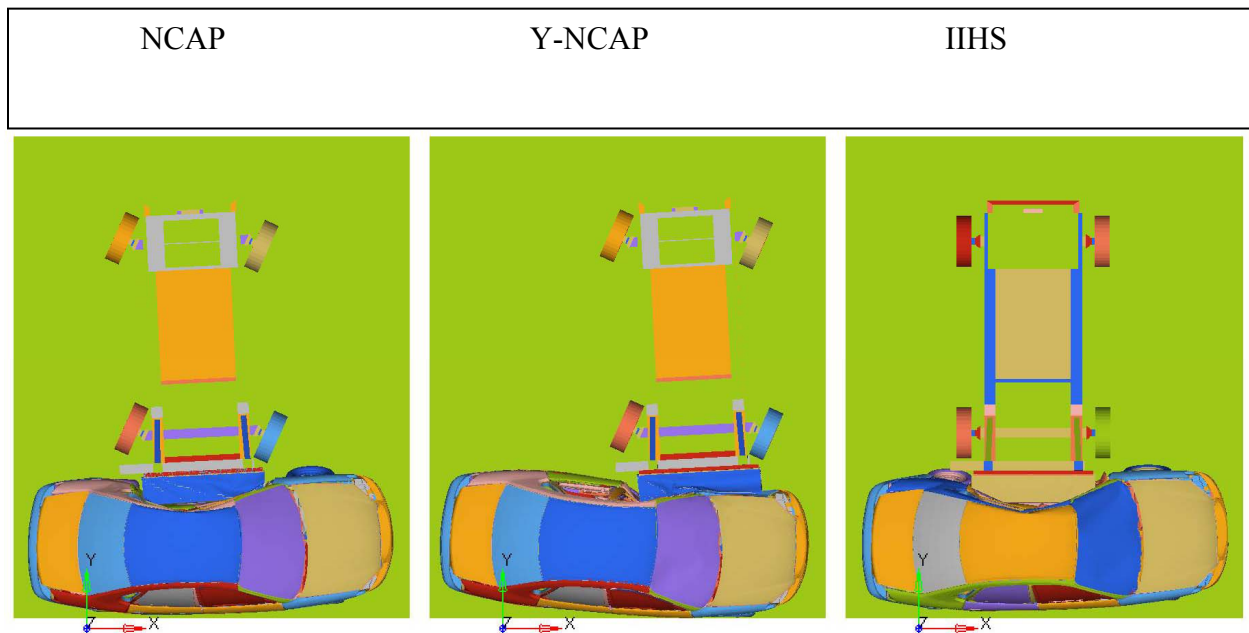


Figure 6. Top View of FE Simulations Side NCAP, Y-Damage NCAP and IIHS Tests

Figure 6 depicts the difference in damage patterns produced by the three test conditions. The NCAP test produced the maximum intrusion at the rear door. The Y damage test impacted the stiff front suspension inducing maximum intrusion at the center of the front door. The IIHS test produced uniform occupant compartment damage and the largest amount of door intrusion at the center of the front door.

The vehicle simulations produced the vehicle accelerations and the door intrusion profiles and velocities that were applied to an occupant model to evaluate injury response. The occupant model used was the MADYMO human facet model. This model replicates the response of the human spine more closely than the dummies currently used in side crash tests.

The human facet dummy was subjected to the three crash environments and the injury risks were calculated by applying aortic injury predictors suggested by Cavanaugh, Table 5. Cavanaugh risk functions that used T12Z in combination with VCmax and Cmax were calculated based on the maximum values produced by either rib 4 or rib 8. In both cases, the order of increasing severity was: NCAP, Y-NCAP, and IIHS. The increasing risk values for T12Z-VCmax were: 11%, 75% and 98%. The increasing values for T12Z-Cmax were: 35%, 48% and 100%. These results indicate that the IIHS barrier test produced the highest risk of aortic injury.

In order to gain insight into the role of the T12z as related to aortic injury risk, Echemendia incorporated a simple spring-mass model into the MADYMO human facet model. The mass of the heart was constrained to displace in the z-direction and was resisted by a spring with aortic properties as determined by a Wayne State University dissertation that was part of this project [Shah 2007].

Figure 7 shows the stress-strain response for the peristhismus region that was developed by Echemendia to represent a typical aortic response. Failure was assumed at a strain of 0.175.

Using Figure 7 as the basis for a spring model that represented the aorta, the percentage of the failure elongation for the three test conditions was: NCAP - 21%; Y-NCAP - 62% and IIHS - 76%.

In addition, Echemendia used the human facet model with the simple heart/aorta model to simulate the Cavanaugh cadaver tests with and without pelvic offset. The percentages for the aorta elongation results were - no pelvic offset: 9%; pelvic offset: 111%. The

T12-VCmax predictor of injury risk gave the following results - no pelvic offset: 14%; pelvic offset: 76%.

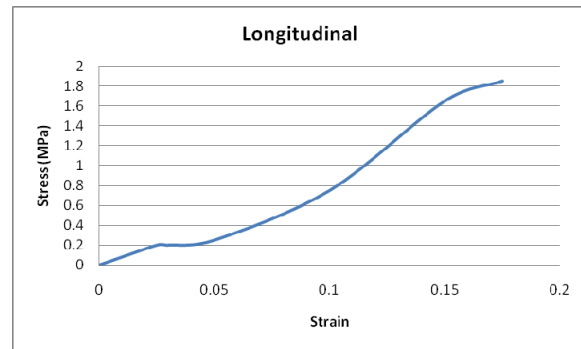


Figure 7. Longitudinal Stress-Strain Response for the Peri-Sithmus Region of the Aorta Adapted by Echemendia from Shah, 2007

DISCUSSION

The motivation for this study came from observations of patients in the William Lehman Injury Center (WLIRC) database who had been seriously or fatally injured in motor vehicle crashes. The WLIRC database is a near census of seriously or fatally injured occupants in South Florida who were involved in side crashes or in frontal crashes when protected by seat belts and/or air bags. Aortic injuries were frequently observed in both frontal and side crashes. However, those patients with aortic injury who were injured in frontal crashes generally had other injuries of equal or greater severity. In side crash population, the aortic injury was generally the most severe injury and the cause of death.

For the seriously or fatally injured population in the WLIRC database that was exposed to side impact, 24% had aortic injuries. By contrast, the aortic injury rate in NASS was about 5%. In WLIRC data, 60% of the aortic injuries occur at crash severities below 30 mph. In NASS, 28% occur at the lower crash severity.

There are several possible reasons to explain this difference in aortic injury rate. The first reason involves the difficulty in clinically recognizing many of the potentially fatal aortic injuries. Rupture of the inner two layers of the aorta may be undetected in some patients (when the adventitia remains intact) or may produce sudden death in others. A second reason may be that the NASS sample of fatalities with complete autopsies may be insufficient to accurately determine the frequency of aortic injuries. By contrast, medical personnel from WLIRC were present at the autopsies of fatally injured crash victims that were transported directly to the facilities of the

medical examiner without entering the Trauma Center. Autopsies were performed on 100% of the fatalities and the results were entered into the WLIRC database.

Crash factors in lower severity near-side crashes that influence TRA risk include extent of intrusion, occupant age and vehicle damage pattern. NASS data suggest that occupant weight is also a factor. With regard to damage pattern, two different patterns appear influential. Both NASS and WLIRC data indicate that the combination of D and Y patterns are most influential. However, NASS indicates that the D pattern has more influence while WLIRC shows that the Y pattern is more influential.

TRA was not produced in the cadaver tests that formed the basis of the side impact injury measures used on side impact dummies. Based on a limited number of cadaver tests with aortic injury, Cavanaugh found that ASA or VCmax in combination with T12Z are the best candidates for aortic injury risk measures. Hardy's tests of inverted cadavers impacted in the side found that the heart and aortic arch move anteriorly with the sternum to which they are tethered. When the impact is through the arms, the ribcage and shoulder (via connection to the clavicle) can force the sternum away from the spine to a greater extent than when the impact is administered directly to the chest. Motion and subsequent stretching of the aortic arch relative to the spine was reported to be the cause of TRA in Hardy's tests. The results of Melvin et al. [1998] and Cavanaugh et al. [2005] reinforce the importance of anterior motion of the sternum, and the importance of limiting chest compression and clavicle motion. Hardy's observations in conjunction with Cavanaugh's finding that T12Z is an influencing factor suggests that anterior motion of the sternum as well as a vertical motion component might be important to TRA.

The research of Hardy [2008] highlights the reasons that TRA has been largely absent in previous cadaver tests. The historical lack of success in generating TRA in whole-body cadaver testing is most likely related to the position and orientation of the heart and aorta in the cadaver. In the seated cadaver, the heart is typically more caudal and dorsal, and tends to pitch rearward as compared to the human [Gardner et al., 1960]. Therefore, the typical seated posture used for cadaver tests would place the heart and aorta in a configuration unlikely to generate the level of longitudinal tension in the aortic isthmus that is required for TRA to occur during impact. Further, loading modes designed to maximize longitudinal strain in the peri-isthmic region have not been investigated in all cases. Finally, appropriate perfusion techniques, which have not

always been employed as a rule, can aid in the ability to generate TRA in the laboratory.

The research of Shah [2005, 2006 and 2007] provides materials data and models to assist in modeling aortic injury. Hardy's tests [2008] provide strain and motion data for the peri-isthmic region during impact. These data can be used for model development and validation.

Using criteria suggested by Cavanaugh, the computer simulations by Echemendia [2008] indicate that the IHS side impact test produces a higher risk of aortic injury compared to the NCAP and Y-NCAP tests. The simulations further suggest that the pelvic offset configuration increased the aortic risk for the crash environments used by Cavanaugh.

CONCLUSIONS

Studies of the William Injury Research Center database of vehicle occupants with serious or fatal injuries from near-side crashes found that about half died at the scene. The other half was transported to a medical center. Of those transported to the medical centers, 60% survived for over one hour, but more than half of this group died. Survivors who were discharged suffered no long term impairment. Normal physiological indicators frequently give no indication of potentially fatal aortic injuries when rupture is limited to the inner layers, but when recognized and treated the outcome is good.

Aortic injuries represented 24% of the serious or fatal injuries in near side impacts in the WLIRC data compared to 5% in NASS. The death rate for WLIRC cases with aortic injury was 85%. About 60% of the WLIRC aortic injuries were in crashes with a delta-V less severe than 13.3 m/s (30 mph) compared to 28% in NASS.

Studies of aortic tissue subjected to dynamic bi-axial loading produced the following results:

- The aorta fails with circumferential-direction tears,
- The intima layer fails before the media or adventitia layer of the aorta,
- Material properties of aortic tissue subjected to dynamic bi-axial loading are now available.

Studies of cadavers subjected to lateral impacts provided the following results:

- The isthmus of the aorta moves medially and anteriorly during impact to the left side,

- Dorsocranial and anteromedial motion of mediastinal contents result in axial tension in the aortic isthmus,
- Axial elongation (longitudinal stretch) of the aorta is central to the generation of TRA,
- Tethering of the descending thoracic aorta by the parietal pleura is a principal aspect of TRA,
- The anterior sternum displacement may be important to TRA, as the aorta is pulled by the sternum away from the spine during side impacts.

Crash factors in lower severity near-side crashes that influence TRA risk include:

- Extent of intrusion,
- Occupant age,
- D or Y vehicle damage pattern as defined in Figure 1.

Studies of the Cavanaugh cadaver tests and modeling of crash and dummy tests produced the following results:

- The best predictor of aortic injury risk, based on Cavanaugh's tests was a combination of spinal Z acceleration and chest viscous criteria,
- Based on the spinal Z acceleration and chest viscous criterion, the IIHS test condition produced a higher risk of aortic injury than the side NCAP or the side Y-NCAP tests.

ACKNOWLEDGEMENT

The initial studies of aortic injuries at the WLIRC were sponsored by the Takata Corporation under the direction of Mr. K. Higuchi. The WLIRC database was developed with the support of the National Highway Traffic Administration. The subsequent funding for this research has been provided [in part] by private parties, who have selected Dr. Kennerly Digges [and FHWA/NHTSA National Crash Analysis Center at The George Washington University] to be an independent solicitor of and funder for research in motor vehicle safety, and to be one of the peer reviewers for the research projects and reports. Neither of the private parties have determined the allocation of funds or had any influence on the content of this report.

REFERENCES

Alonso, B., Digges, K., and Morgan, R. (2007) Far-side vehicle simulations with MADYMO. SAE 2007-01-0378, April 2007.

Augenstein, J, Digges, K., Steps, J., Higuchi, K., and Ato., T. (2003) Crash attributes that influence aortic injuries in near-side crashes. Paper 232, Proceedings of the ESV Conference, May, 2003.

Cammack, K., Rapport, R.L., Paul, J., and Baird, W.C. (1959) Deceleration injuries of the thoracic aorta. *AMA Archives of Surgery*, 79(2):244-251.

Cavanaugh, J.M., Koh, S.W., Kaledhonkar, S.L., and Hardy, W.N. (2005) An analysis of traumatic rupture of the aorta in side impact sled tests. SAE Technical Paper No. 2005-01-0304. Society of Automotive Engineers, Warrendale, PA.

Cavanaugh, J.M., Zhu, Y., Huang Y., and King, A.I. (1993) Injury Response of the thorax in side impact cadaveric tests. Proc. 37th Stapp Car Crash Conference, pp. 199-222.

Cavanaugh, J.M., Walilko, T.J., Malhotra, A., Zhu, Y., and King, A.I. (1990) Biomechanical response and injury tolerance of the thorax in twelve sled side impacts. *Stapp Car Crash Journal*, 34:28-38.

Echemendia, C., (2008) Inertia effects of the heart as a factor in aortic injuries in near-side impacts, Master's Thesis, The George Washington University, December, 2008.

Gardner, E., Gray, D.J., and O'Rahilly, R. (1960) *Anatomy*. W.B. Saunders Co., Philadelphia, PA.

Hardy, WN; Shah, CS; Mason, MJ; Kopacz, JM; Yang, KH; King, AI; Van Ee, CA; Bishop, JL; Banglmaier, RF; Bey, MJ; Morgan, RM; Digges, KH (2008) Mechanisms of Traumatic Rupture of the Aorta and Associated Peri-isthmus Motion and Deformation. *Stapp Car Crash Journal*, 52:233-265.

Hardy, W.N., Mason, M.J., Foster, C.D., Shah, C.S., Kopacz, J.M., Yang, K.H., King, A.I., Bishop, J., Bey, M., Anderst, W., and Tashman, S. (2007) A study of the response of the human cadaver head to impact. *Stapp Car Crash Journal*, 51:17-80.

Hardy, W.N., Shah, C.S., Kopacz, J.M., Yang, K.H., Van Ee, C.A., Morgan, R., and Digges, K. (2006) Study of potential mechanisms of traumatic rupture of the aorta using in situ experiments. *Stapp Car Crash Journal*, 50:247-265.

Hardy, W.N., Schneider, L.W., and Rouhana, S.W. (2001) Abdominal impact response to rigid-bar, seatbelt, and airbag loading. *Stapp Car Crash Journal*, 45:1-31.

- Holzapfel, A, Sommer G, Gasser TC, and Regitnig R. (2005) Determination of the layer-specific mechanical properties of human coronary arteries with non-atherosclerotic intimal thickening, and related constitutive modeling. *American J. Physiology Heart Circulation Physiology* 2005; 289: H2048-2058.
- Horton, T, Cohn, S., Heid, M., Augenstein, J., Bowen, J., McKenney, M., Duncan. R. (2000) Identification of trauma patients at risk of thoracic aortic tear by mechanism of injury. *Journal of Trauma-Injury Infection & Critical Care* 48(6): 1008-13; June, 2000.
- Katyal, D., McLellan, B.A., Brenneman, F.D., Boulanger, B.R., Sharkey, P.W., and Waddell, J.P. (1997) Lateral impact motor vehicle collisions: Significant cause of blunt traumatic rupture of the thoracic aorta. *The Journal of Trauma*, 42(5):769-772.
- Kroell, C., Schneider D., and Nahum, A. (1974) Impact tolerance and response of the human thorax II. Proc. 18th Stapp Car Crash Conference, pp. 383-457. Society of Automotive Engineers, Warrendale, PA.
- Lau, I.V., and Viano, D.C. (1986) The viscous criterion - basis and applications of an injury severity index for soft tissues. Proc. 30th Stapp Car Crash Conference, pp. 123-142. Society of Automotive Engineers, Warrendale, PA.
- Mason, M.J., Shah, C.S., Maddali, M., Yang, K.H., Hardy, W.N., Van Ee, C.A., Digges, K. (2005) A new device for high-speed biaxial tissue testing: application to traumatic rupture of the aorta. Transactions of the Society of Automotive Engineers, Paper No. 2005-01-0741.
- Melvin, J.W., Baron, K.J., Little, W.C., and Gideon, T.W. (1998) Biomechanical analysis of Indy race car crashes. Proc. 42nd Stapp Car Crash Conference, pp. 247-266. Society of Automotive Engineers, Warrendale, PA.
- Mohan, D. and Melvin, J. (1982) Failure properties of passive human aortic tissue. I-uniaxial tension tests. *Journal of Biomechanics*, 15(11):887-902.
- Mohan, D. and Melvin, J. (1983) Failure properties of passive human aortic tissue. II-Biaxial Tension Tests. *Journal of Biomechanics*, 16(1):31-44.
- SAE J 224 (1980) Collision deformation classification, Society of Automotive Engineers, Inc., Warrendale, Pennsylvania, USA, 1980.
- Shah, C.S. (2007) Investigation of traumatic rupture of the aorta (TRA) by obtaining aorta material and failure properties and simulating real-world aortic injury crashes using the whole-body finite element (FE) human model. PhD Dissertation, Mechanical Engineering, Wayne State University, Detroit, Michigan.
- Shah, C.S., Hardy, W.N., Mason, M.J., Yang, K.H., Van Ee, C.A., Morgan, R., and Digges, K. (2006) Dynamic biaxial tissue properties of the human cadaver aorta. *Stapp Car Crash Journal*, 50:217-245.
- Shah, C.S., Hardy, W.N., Yang, K.H., Van Ee, C.A., Morgan, R.M., and Digges, K.H. (2007) Investigation of traumatic rupture of the aorta (TRA) by simulating real-world accidents. 2007 Conference of the International Research Council on Biomechanics of Injury, pp. 349-359.
- Shah, C.S., Lee, J.B., Hardy, W.N., and King, K.H. (2004) A partially validated finite element whole-body human model for organ level injury prediction. Proc. 2004 ASME International Mechanical Engineering Congress and Exposition, IMECE2004-61844. American Society of Mechanical Engineers, New York, NY.
- Shah, C.S., Maddali, M., Mungikar, S.A., Beillas, P., Hardy, W.N., Yang, K.H., Bedewi, P.G., Digges, K., and Augenstein, J. (2005) Analysis of a real-world crash using finite element modeling to examine traumatic rupture of the aorta. SAE Technical Paper No. 2005-01-1293. Society of Automotive Engineers, Warrendale, PA.
- Shah, C.S., Yang, K.H., Hardy, W.N., Wang, K.H., and King, A.I. (2001) Development of a computer model to predict aortic rupture due to impact loading. *Stapp Car Crash Journal*, 45:161-182.
- Steps, J.A., (2003), Crash characteristics indicative of aortic injury in near side vehicle-to- vehicle crashes. Doctoral Dissertation, The George Washington University, April, 2003.
- Viano, D.C. (1983) Biomechanics of non-penetrating aortic trauma: A review. Proc. 27th Stapp Car Crash Conference, pp. 109-114. Society of Automotive Engineers, Warrendale, PA.
- Zhao A. Pericevic IO, Digges KH., Kan C., Moatamedi M., Augenstein J., (2006) FE modeling of the orthotropic and three-layer human thoracic aorta. The 2006 ASME Pressure Vessels and Piping/ICPVT-11 Conference, Vancouver, British Columbia, Canada, July 23-27, 2006

CHARACTERIZATION OF THE PEDIATRIC CHEST AND ABDOMEN USING THREE POST-MORTEM HUMAN SUBJECTS

Richard Kent, Francisco J. Lopez-Valdes, John Lamp, Sabrina Lau, Daniel Parent, Jason Kerrigan, David Lessley, Robert Salzar

Center for Applied Biomechanics, University of Virginia

United States

Paper Number 11-0394

ABSTRACT

This paper reports a series of experiments on 6, 7, and 15 year-old pediatric post-mortem human subjects (PMHS) undertaken to guide the scaling of existing adult thoracic response data for application to the child and to assess the validity of a juvenile porcine abdominal model. The pediatric PMHS exhibited abdominal response similar to the swine, including the degree of rate sensitivity. The thoraces of the PMHS were as stiff as, or slightly more stiff than, published adult corridors. An assessment of age-related changes in thoracic stiffness supports our earlier suggestion (2009) that the effective stiffness of the chest increases through the fourth decade of life and then decreases, resulting in stiffness values similar for children and elderly adults.

INTRODUCTION

Motor vehicle crashes are the leading cause of death and injury for children in the United States and head injuries are of principal concern for children involved in crashes. Regardless of the age group or crash direction, injuries to the brain and skull are the most common serious injuries sustained by children in crashes (Arbogast et al. 2002, 2004 and 2005, Durbin et al. 2003, Orzechowski et al. 2003) and are responsible for one-third of all pediatric injury deaths (Adekoya et al. 2002, Thompson et al. 2003). The abdomen is the second most commonly injured body region in young children using vehicle seat belts, and can be associated with significant health care costs and extended hospitalization (Bergqvist et al. 1985, Tso et al. 1993, Trosseille et al. 1997, Durbin et al. 2001).

The trajectory and attitude of the head during an impact are dictated by, among other factors, the interaction of the restraint system with the trunk.

Any thoracic model must represent this interaction in a biofidelic manner to ensure that restraint designs protect humans as intended. Despite the importance of this interaction and of abdominal loading as an injury mechanism in children, benchmarking data for pediatric models of the trunk are lacking.

The biomechanics of the pediatric abdomen have recently been described in detail using a juvenile swine model (Kent et al. 2006, 2008). The model was benchmarked against quasistatic human volunteer experiments and against the distribution of injuries sustained by children in the field, but was not benchmarked against pediatric force-deformation behavior in the high-rate, high-deformation loading environment relevant to crash conditions. Ouyang et al. (2006) reported thoracic blunt hub impact tests of nine PMHS aged 2 – 12 years, but the use of these experiments to elucidate thoracic response to belt loading is uncertain (see Kent et al. 2004). In 2009, Kent et al. reported a series of dynamic thoracoabdominal belt loading experiments using a 7-year-old PMHS, but acknowledged that the analysis was limited by use of a single subject.

Hence, there is currently a need for pediatric thoracoabdominal mechanics data in contemporary loading situations (non-impact harness loading). The objective of this study is to expand the dataset reported by Kent et al. 2009 with the inclusion of two additional pediatric PMHS. This paper reports a composite dataset of all three pediatric PMHS.

MATERIALS AND METHODS

Specimens

Three pediatric PMHS (Table 1) were obtained and tested in accordance with the ethical guidelines established by the Human Usage Review Panel of the

National Highway Traffic Safety Administration, and with the approval of the Office of the Vice President for Research and an independent Oversight Committee at the University of Virginia, and Institutional Review Boards at Duke University and The Children’s Hospital of Philadelphia.

Table 1.
Specimen Descriptions

| Specimen ID | DukeF (470F) | 484F | 485M | |
|--|--------------|------|------|-----|
| Gender | F | F | M | |
| Age at Death (years) | 7 | 6 | 15 | |
| Whole-body mass (kg) | 26.8 | 24.0 | 50.0 | |
| Torso breadth (mm) | 4th Rib | 273 | 217 | 271 |
| | 8th Rib | 270 | 202 | 240 |
| | Umbilicus | 278 | 217 | 239 |
| Torso depth (mm) | 4th Rib | 155 | 142 | 131 |
| | 8th Rib | 172 | 140 | 142 |
| | Umbilicus | 161 | 122 | 106 |
| Torso circumference (mm) | 4th Rib | 695 | 602 | 718 |
| | 8th Rib | 698 | 593 | 646 |
| | Umbilicus | 701 | 590 | 595 |
| Anatomical Lengths (along axis of body) (mm) | | | | |
| Stature | 1194 | 1280 | 1700 | |
| Sternal notch to xiphoid | 114 | 130 | 172 | |
| Xiphoid to umbilicus | 131 | 159 | 203 | |
| Vertex to pubic symphysis (seated height) | 625 | 640 | 840 | |

See Kent et al. (2009) for a detailed description of the 7 year-old female subject. The cause of death of the 6 year-old female was germ cell malignancy, but no acute gonadal tumors were found either in pre-test CT scans or during a post-test thoracoabdominal necropsy. Prior to the time of death the subject was on a ventilator and pre-test CT scans revealed an L5 vertebra plana, several cystic lung lesions, which is consistent with ventilator pneumonia, as well as visceral gas, evidence of postmortem necrosis. The subject was approximately 95th percentile in stature for a 6 year-old female, and between the 75th and 90th percentile for mass (Ogden et al. 2002). The cause of death of the 15 year-old male was malignant thalamic glioblastoma. A review of CT scans revealed mild dextroscoliosis of the thoracic spine, moderate bilateral pneumothoraces, and scattered gas, evidence of post mortem necrosis. The 15-year-old subject was approximately 50th percentile in stature and 25th percentile in mass, and was severely emaciated. The level of emaciation was deemed

sufficient to render that subject’s abdominal response meaningless (the anterior aspect of the lumbar spine was less than 5 mm posterior of the anterior abdominal wall). Upon receipt, the PMHS were stored in a freezer (-15°C) until they were removed and thawed at room temperature for at least 36 hours prior to testing. Computed tomography (CT) scans verified the absence of preexisting fractures or other bone pathology in all specimens, with the exception of sagittal asymmetry due to moderate scoliosis in the 7 year-old female.

Test Hardware and Methods

A hydraulic master-slave cylinder arrangement connecting a high-speed material testing machine to a table-top test rig was employed in this test series. The test rig is similar to that used previously by Kent et al. (2004) to allow for diagonal and distributed belt loading with defined anchor points. The test rig consisted of a frame made of steel tubing that supported slave cylinders (Figure 1, see additional images in Kent et al. 2009). In diagonal belt tests of the thorax, the cylinders drove a carriage, guided by linear bearings, up and down. The carriage was connected to the 5-cm-wide diagonal belt via steel cables that passed over pulleys. In the abdominal and distributed loading tests, the belt was attached directly to the slave cylinder pistons via steel cables that passed through channels cut in the center of the specimen-supporting hardware.

For the abdominal tests, a 5-cm-wide belt (similar to that used in Kent et al. 2006, 2008) was used. For the distributed belt tests, a 16.8-cm-wide belt was used on the 6 and 7 year-olds and a 20.3-cm-wide belt was used on the 15 year-old (the same distributed belt used on the adults reported by Kent et al. 2004). The distributed belt geometry was determined by scaling the belt geometry from the adult testing (Kent et al. 2004) using an average of scale factors relating the adult thoracic anthropometry to that of the pediatric PMHS. Polyethylene fiber-reinforced composite (Spectra®, E = 97 GPa) material was used for all belts rather than actual seatbelt webbing (which would stretch nominally 2%-4% in these tests) to isolate the thoracic response from a combined effect that includes belt stretch. The top of the test rig consisted of an aluminum plate attached to a load cell used to measure posterior reaction forces and moments. Plywood sheets were used to adjust the specimen’s height on the table to achieve realistic belt angles off of the shoulder and pelvis.

The diagonal belt passed over the left shoulder and crossed the anterior thorax approximately 30° from

the mid-sagittal plane. The centerline of the belt crossed the left clavicle approximately 60 mm from the sagittal plane, and exited the body at approximately the 10th rib laterally. For the distributed belt loading, the belt was centered over the xiphoid. Lower abdominal loading was conducted with the belt centered on the umbilicus (for the 7 year-old) and with the belt centered 29 mm

superior of the umbilicus (for the 6 year-old). Upper abdominal loading on the 7 year-old was performed with the belt centered 7 cm superior to the umbilicus (6.1 cm inferior to the xiphoid process). The upper abdominal loading location on the 6-year old was with the belt centered 7.6 cm superior of the umbilicus (6.4 cm inferior to xiphoid process).

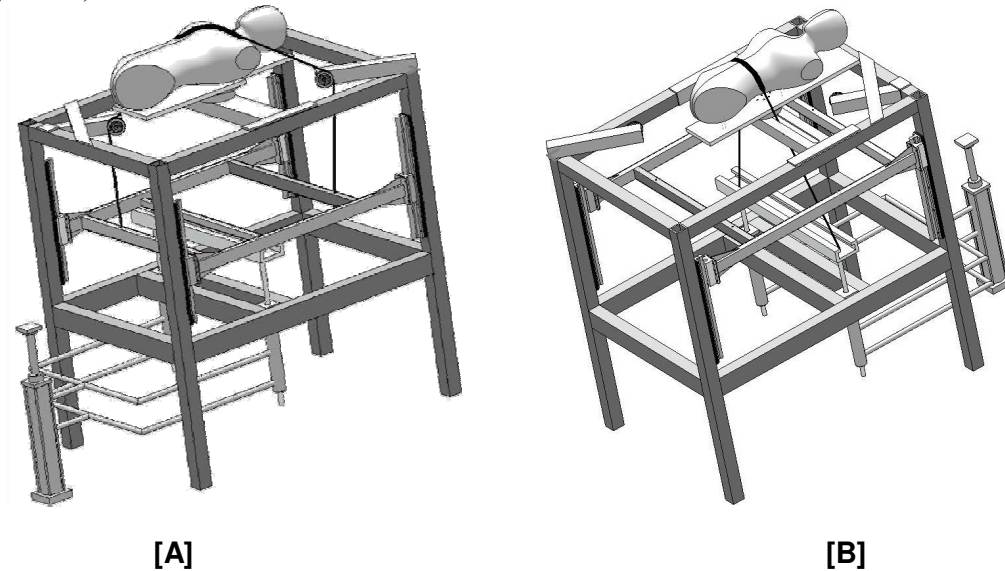


Figure 1. Table top test rig schematic in diagonal belt configuration ([A]) and abdominal configuration ([B]).

The table-top was instrumented with a six-axis load cell under the posterior support plate and tension load cells attached to the cable-belt system. Load cell data were sampled at 10 kHz with a DEWE-2600 (Dewetron Inc., Wakefield, RI) data acquisition system and hardware (anti-aliasing) filtered. The data were later processed with a low-pass 100 Hz 8-pole Butterworth filter. Kinematic data were sampled at 1000 Hz using an eight-camera Vicon MX™ three-dimensional (3D) motion capture system that tracked the motion of retroreflective spherical targets through a calibrated 3D space. The input displacement to the subject for each test condition was measured using targets secured to the belt. For all belt tests, displacement was measured using a single target secured at the intersection of the belt center line and the mid-sagittal plane. Displacements for all tests were calculated with respect to a spine-based SAE occupant coordinate system, in which the positive Z-axis was directed inferiorly along the spine and the positive X-axis was directed perpendicularly to the spine and toward the sternum, lying in the midsagittal plane. The X-axis displacement defined “chest displacement” for thoracic characterization and “penetration” for abdominal characterization. For ease of interpretation, all of the results present the absolute value of the magnitude of the chest

displacement, the abdominal penetration, and the posterior reaction force (i.e., positive sign), though the direction of the displacement was toward the spine.

After thawing the specimen, a tracheal tube was inserted to facilitate lung inflation. Prior to each test, a syringe was used to inflate the lungs with 300 mL of air via the tube, and then remove the same amount of air. A series of five inflation cycles was performed before a final inflation was performed. The air was free to flow in and out of the tube during the tests.

A series of 24 displacement-controlled tests was performed to measure the thorax/abdomen response under the four loading conditions (Table 2). A minimum of 10 minutes separated tests. Before each test, a nominal pretension load of 8 N was applied to each end of the belt. After all testing, the skin and superficial tissue of the torso were removed to assist in the process of identifying injuries. After palpating the rib cage for fractures, the specimens were CT scanned at high resolution (0.59 mm in-plane and 0.63 mm slice thickness), and a radiologist read the scans to assist in identification of any rib fractures or other trauma.

RESULTS

In general, consideration of two additional PMHS did not change the broad conclusions drawn by Kent et al. (2009) following the tests on the 7 year-old. The 6 year-old exhibited both thoracic and abdominal response similar to the 7 year-old, while the 15 year-old exhibited slightly stiffer thoracic response.

Abdominal Loading

Quasistatic and dynamic tests on the lower abdomen and dynamic tests on the upper abdomen were successfully performed on both female subjects. The responses were remarkably similar for the two subjects. Both subjects exhibited stiffer behavior in the dynamic test, and in the lower abdomen compared to the upper (Figure 2). The lower abdomen generated approximately 4-5 kN at 35 mm

of dynamic penetration, while the upper generated only approximately 2.5 kN. The lower abdomen generated approximately 1 kN at 28 mm of quasistatic penetration.

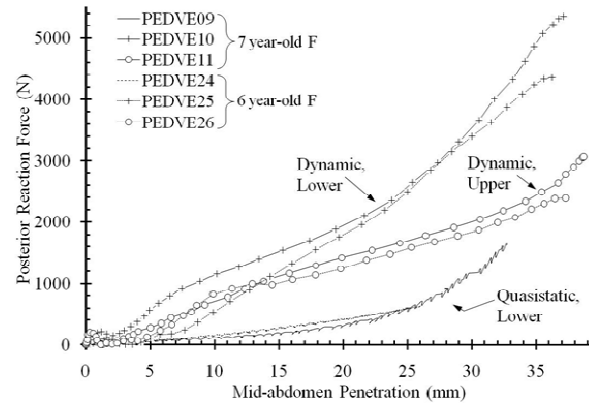


Figure 2. Biomechanical response to transverse belt loading on the abdomen (7 year-old and 6-year-old females).

Table 2. Test Matrix

| DAQ Index | Subject | Region | Loading Type | Description | Peak Input Displacement | Peak Posterior Reaction Force |
|-----------|---------|------------|------------------|----------------------|-------------------------|-------------------------------|
| PEDVE09 | DukeF | L. Abdomen | Transverse belt | Quasistatic | 32.6 mm | 1,608 N |
| PEDVE10 | DukeF | L. Abdomen | Transverse belt | Dynamic ¹ | 37.1 mm | 5,352 N |
| PEDVE11 | DukeF | U. Abdomen | Transverse belt | Dynamic | 38.6 mm | 3,051 N |
| PEDVE12 | DukeF | Chest | Distributed belt | 1-Hz | 27.5 mm | 2,826 N |
| PEDVE13 | DukeF | Chest | Distributed belt | Dynamic | 31.0 mm | 6,620 N |
| PEDVE14 | DukeF | Chest | Distributed belt | 0.5 Hz, 4 Hz | 25.8 mm | 3,417 N |
| PEDVE15 | DukeF | Chest | Diagonal belt | 1-Hz | 33.0 mm | 1,240 N |
| PEDVE16 | DukeF | Chest | Diagonal belt | Dynamic | 34.9 mm | 3,513 N |
| PEDVE17 | DukeF | Chest | Diagonal belt | 0.5 Hz, 4 Hz | 32.0 mm | 1,248 N |
| PEDVE18 | DukeF | Chest | Diagonal belt | Dynamic | 37.1 mm | 4,378 N |
| PEDVE19 | DukeF | Chest | Diagonal belt | Dynamic | 52.0 mm | 5,941 N |
| PEDVE24 | 484F | L. Abdomen | Transverse belt | Quasistatic | 25.7 mm | 607 N |
| PEDVE25 | 484F | L. Abdomen | Transverse belt | Dynamic ¹ | 36.2 mm | 4,363 N |
| PEDVE26 | 484F | U. Abdomen | Transverse belt | Dynamic | 37.3 mm | 2,389 N |
| PEDVE29 | 484F | Chest | Distributed belt | Dynamic | 34.3 mm | 4,224 N |
| PEDVE30 | 484F | Chest | Distributed belt | Dynamic | 39.2 mm | 6,968 N |
| PEDVE31 | 484F | Chest | Diagonal belt | 1-Hz | 30.6 mm | 934 N |
| PEDVE32 | 484F | Chest | Diagonal belt | Dynamic | 41.9 mm | 2,943 N |
| PEDVE33 | 484F | Chest | Diagonal belt | Dynamic | 42.0 mm | 3,155 N |
| PEDVE34 | 484F | Chest | Diagonal belt | Dynamic | 54.6 mm | 5,195 N |
| PEDVE40 | 485M | Chest | Distributed belt | 1-Hz | 21.7 mm | 1,574 N |
| PEDVE41 | 485M | Chest | Distributed belt | Dynamic | 27.3 mm | 4,533 N |
| PEDVE42 | 485M | Chest | Diagonal belt | 1-Hz | 23.1 mm | 1,359 N |
| PEDVE43 | 485M | Chest | Diagonal belt | Dynamic | 32.5 mm | 3,977 N |

See Kent et al. (2009) for detailed discussion of rate. All abdomen tests fall in “Rate Bin 1” from Kent et al. (2006).

Thoracic loading from a diagonal belt

Quasistatic and dynamic (approximately 1.5 m/s input belt displacement rate) tests with diagonal belt loading were successfully performed on all three

subjects. As with the abdominal loading, the two younger females exhibited remarkably similar response. The 15 year-old male was slightly stiffer at both rates (Figure 3).

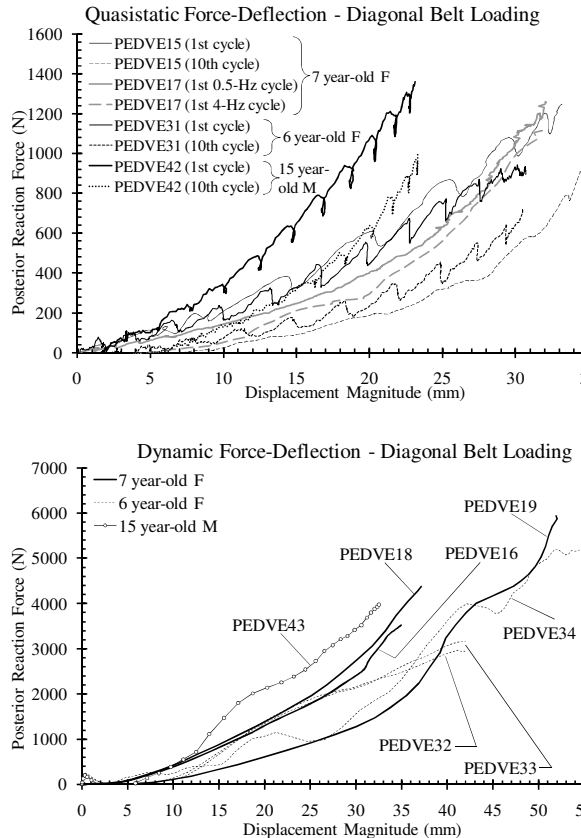


Figure 3. Biomechanical response to diagonal belt loading on the thorax (7 year-old and 6-year-old females, 15 year-old male) at quasistatic (top) and dynamic (bottom) rates.

Thoracic loading from a distributed belt

Quasistatic tests with distributed loading were successfully performed on the 7 year-old female and on the 15 year-old male. Dynamic (approximately 1.5 m/s input displacement rate) tests with distributed loading were successfully performed on all three subjects. The 7 year-old and the 15 year-old exhibited similar quasistatic behavior, while the 7 year-old had the stiffest dynamic response (Figure 4).

Trauma generated

Two rib fractures were identified during the post-test autopsy of the 6 year-old: one fracture on each of the 2nd and 3rd ribs on the left aspect. Since the diagonal belt passed over the left shoulder, these fractures are both in the region of concentrated diagonal belt loading. The 7 year-old sustained a total of 13 rib fractures. On the left side, ribs 2-6 were fractured approximately 1 cm from the costochondral junction. On the right side ribs 4-7 were fractured

approximately 1 cm from the costochondral junction, and ribs 3-6 sustained lateral fractures. Comparison with CT scans taken before any testing was performed confirms that the fractures were generated during the test series. The pattern suggests that the fractures were generated with diagonal belt loading and comparison of the responses measured in tests PEDVE16, PEDVE18, and PEDVE19 suggests that the structural stability of the rib cage was not compromised prior to the performance of test PEDVE18, but was afterwards. No rib fractures were observed on the 15 year-old subject. None of the subjects sustained any gross abdominal injury.

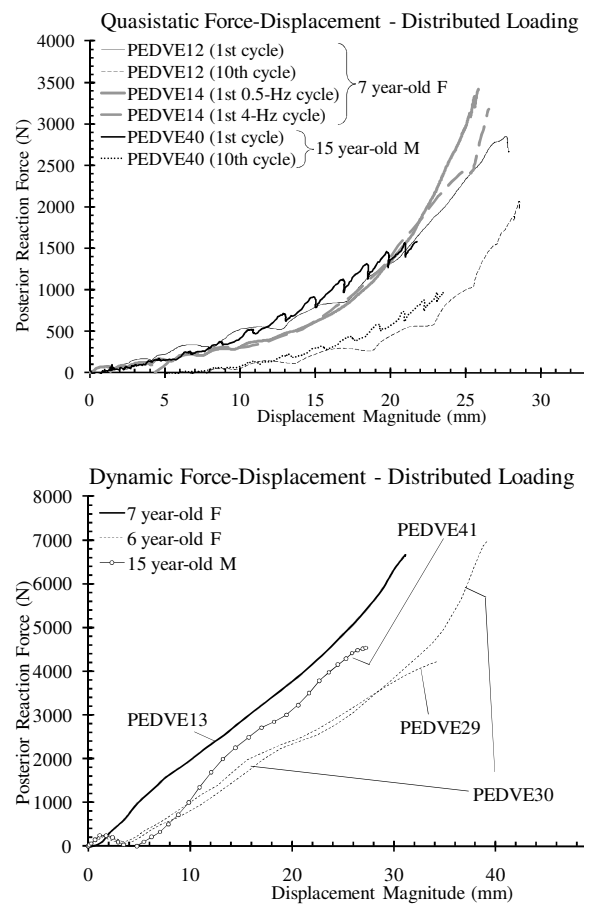
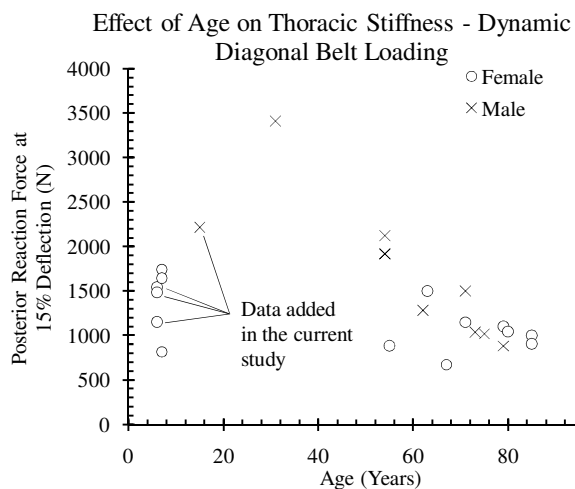


Figure 4. Biomechanical response to distributed loading on the thorax (7 year-old and 6-year-old females, 15 year-old male) at quasistatic (top) and dynamic (bottom) rates.

DISCUSSION AND CONCLUSIONS

The key contribution of this study is the expansion of the analysis originally published by Kent et al. (2009) with the addition of two pediatric subjects. Now,

based on a total of 3 pediatric PMHS tested utilizing an experimental protocol and scaled test apparatus used to characterize 15 adults PMHS (Kent et al. 2004, Salzar et al. 2009), the two main conclusions drawn in that earlier study can be re-stated with more confidence. First, the abdominal response of the juvenile swine seems to be a reasonable benchmark for the Hybrid III 6 year-old abdominal insert. The 6 year-old subject exhibited abdominal response remarkably similar to the 7 year-old, which represented the swine corridors reasonably well (cf. Kent et al. 2009). Second, the relationship between thoracic stiffness and age does not appear to be monotonic over the entire lifespan, and existing scaling algorithms do not adequately describe the relationship. The two new subjects reported here follow the general trend reported in the 2009 study, with pediatric and elderly PMHS having similar thoracic stiffness under dynamic diagonal belt loading with a greater stiffness associated with the late adolescent and young adult years (Figure 5). Additional data are needed in the age range between 15 and 50 years.



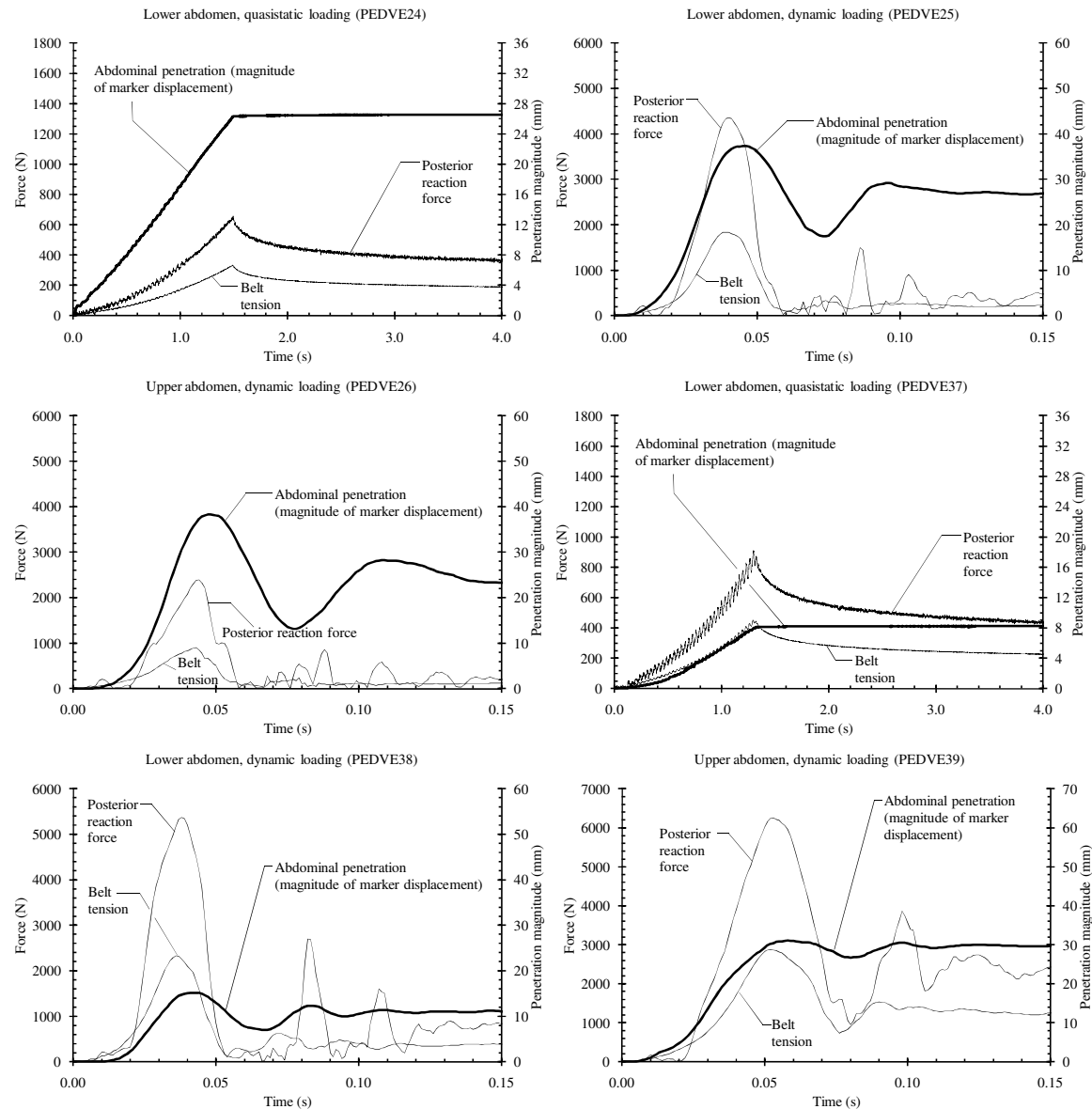
Bolton, J. (2009) Viscoelastic response of the thorax under dynamic belt loading. *Traffic Injury Prevention* 10:1-8.

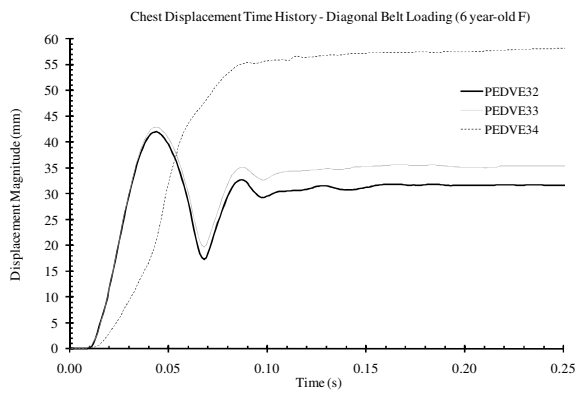
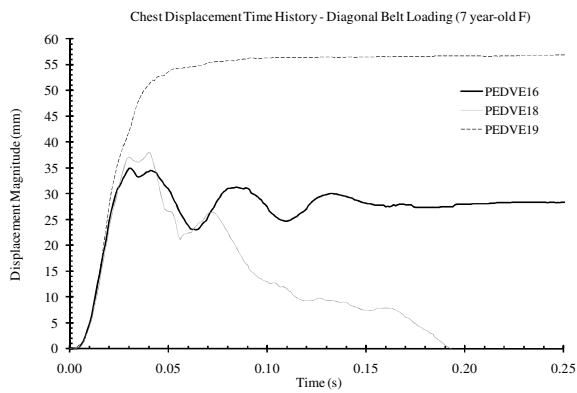
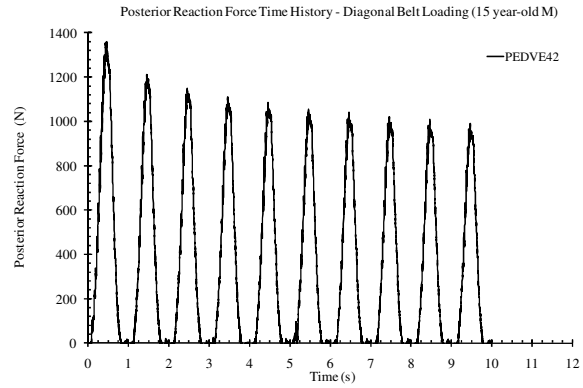
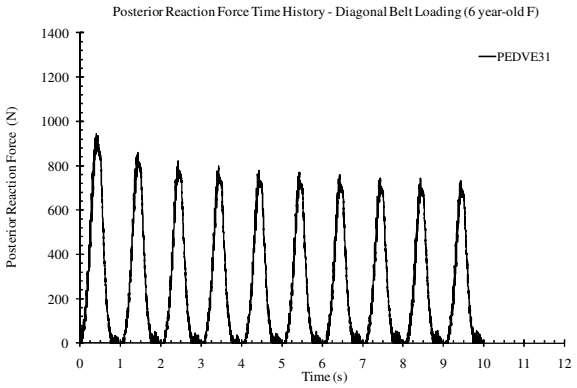
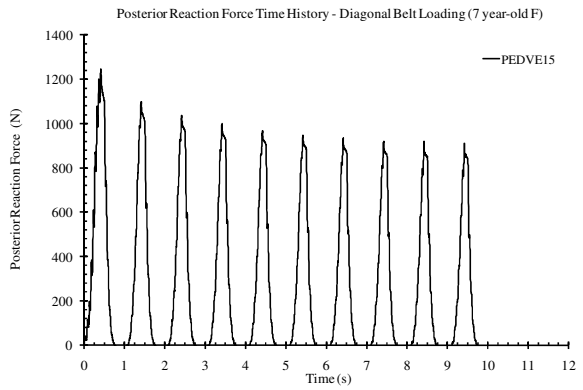
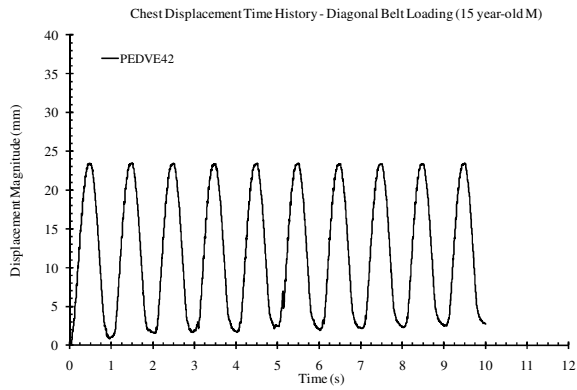
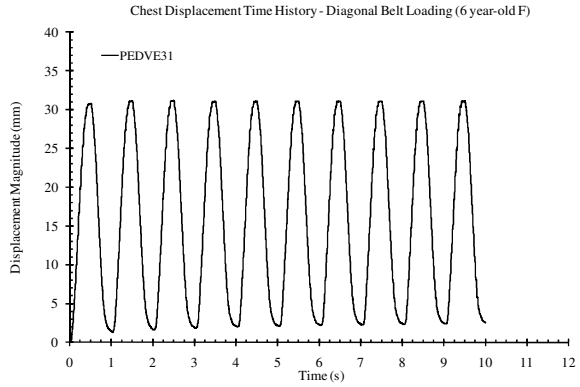
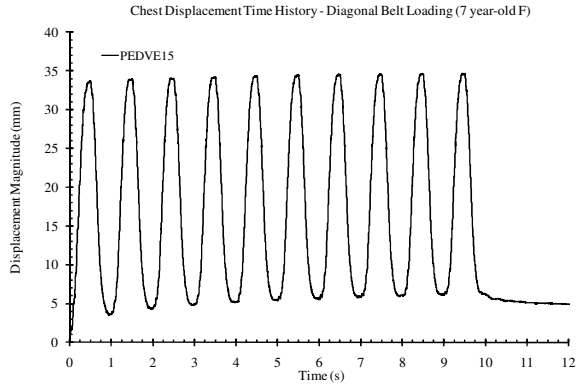
Thompson, E., Perkowski, P., Willarreal, D., Block, E., Brown, M., Wright, L., Akin, S. (2003) Morbidity and mortality of children following motor vehicle crashes. *Archives of Surgery* 138(2):142-145.

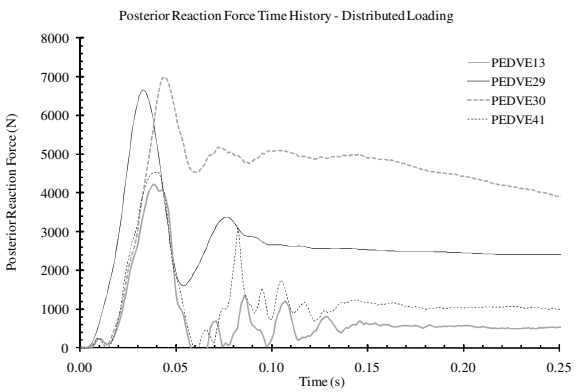
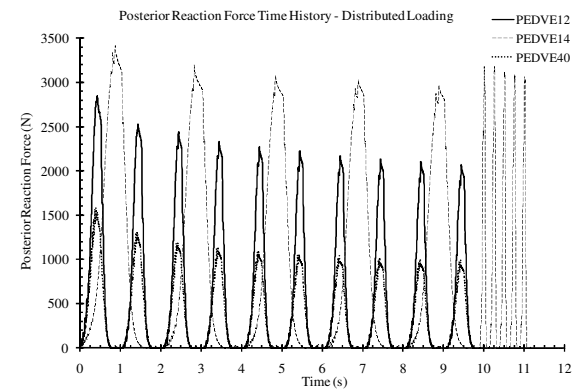
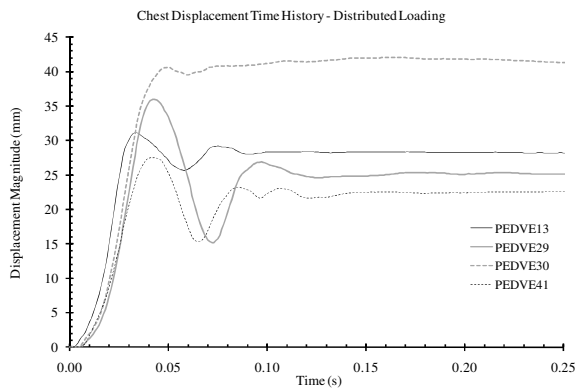
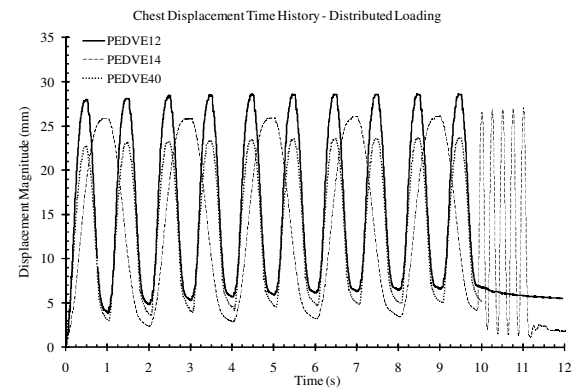
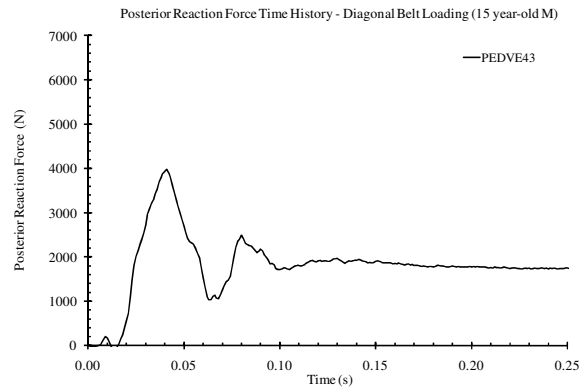
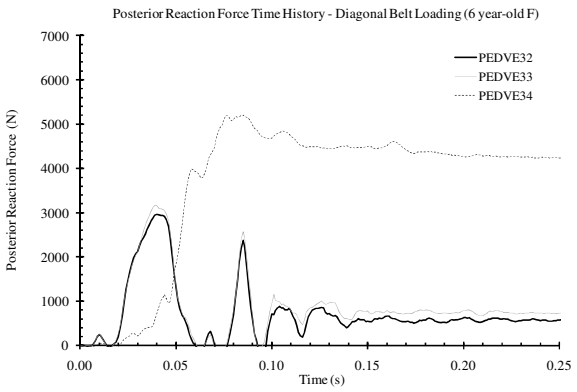
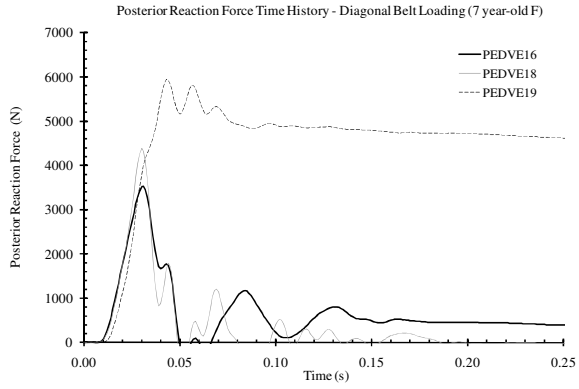
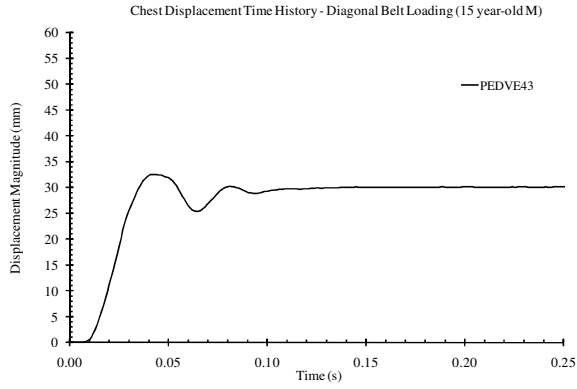
Tso, E, B Beaver and JA Halter (1993). Abdominal injuries in restraint pediatric passengers. *J Pediatric Surgery* 28(7): 915-919.

Trosseille, X., Chamouard, F., Tarriere, C. (1997) Abdominal injury risk to children and its prevention. *Proc. IRCOBI, Hannover, Germany*.

APPENDIX – RAW DATA PLOTS







CONTRIBUTION TO THE IMPROVEMENT OF CRASH TEST DUMMIES IN ORDER TO DECREASE ABDOMINAL INJURIES IN ROAD ACCIDENTS

Gaëtan Hanen

François Bermond

Université de Lyon, F-69622, Lyon, France
Ifsttar, LBMC, UMR_T9406, F-69675, Bron
Université Lyon 1, Villeurbanne
France

Sabine Compigne

Toyota Motor Europe NV/SA
Belgium

Mitsutoshi Masuda

Toyota Motor Corporation
Japan
Paper Number 11-0218

ABSTRACT

This paper describes the first steps carried out in a joint effort of Ifsttar and Toyota to contribute to the development of a new abdomen for THOR dummy.

Firstly, a review of accident data showed that abdominal injuries observed in frontal crashes were mainly caused by the steering wheel and the seat belt. However, abdomen injury rate was higher for side impacts, showing the importance of being able to predict such injuries for different impact angles. The steering wheel was mainly associated with injuries in the upper abdomen (liver and spleen injuries) whereas the seat belt was mainly associated with injuries to the lower abdomen (intestines). The former ones were well correlated with rib fractures and it was concluded that thoracic injury prediction could also give an indication of upper abdomen injury risk.

Secondly, existing abdomen designs were studied to rate technical solutions and orient future design. Notably, several technical solutions including external or internal pressure, force and deflection measurements were considered for the evaluation of abdominal injuries in the last past years.

Finally, all the conclusions were gathered in a design brief.

Before modifying the THOR abdomen, the biofidelity of different existing THOR abdomens was evaluated through impactor and static seat belt tests. None of these abdomens were able to fully meet the biofidelity corridors. These results represent the starting point for future modifications of the THOR abdomen response.

INTRODUCTION

The abdomen accounts for a smaller proportion of all vehicle crash-related injuries than head, thorax and extremities. However, the proportion of abdomen injuries increases significantly when considering serious to severe injuries. Elhagediab et al. (1998) showed that abdominal injuries represent 8% of all injuries of AIS \geq 3, 16.5% of all injuries AIS \geq 4, and 20.5% of all injuries of AIS \geq 5. The risk of abdominal injuries varies also with seating position and was demonstrated to be higher for rear occupants compared to front ones. Martin et al. (2010) found in frontal collisions a relative risk of AIS2+ abdominal injuries of 1.90 and 1.53 for rear occupants compared to drivers and front passengers respectively.

Therefore, to help study and improve abdominal protection, a joint project was set up by Ifsttar and Toyota to work on the development of a modified abdomen for the THOR-NT dummy. The first part of the project aimed at defining the ideal requirements for the abdomen by considering real world data and most recent knowledge on abdomen injury criteria. Biofidelity of existing dummy abdomens was also evaluated to identify required future improvements.

ACCIDENT DATA

Several analyses of abdominal injuries were performed from accident field data. The ones referred in this paper are listed in the Table 1.

Table 1.
Accident data study on abdominal injuries

| Reference | Dataset | Selection criteria |
|--------------------------|--|---|
| Elhagediab et al. (1998) | NASS CDS 1988-1994 | Frontal impacts Front occupants |
| Lamielle et al. (2006) | LAB Since 1970 | Frontal impacts All occupants |
| Klinich et al. (2008) | NASS CDS CIREN 1998-2004 | Frontal & Side impacts Front occupants |
| Martin et al. (2010) | Rhône Road Trauma Registry 1996-2006 | Frontal impacts All occupants |
| Klinich et al. (2010) | NASS CDS CIREN 1998-2008 | Frontal & Side impacts Front occupants |

Influence of seat position

Martin et al. (2010) highlighted the specificities of rear occupants regarding abdomen injuries. Using Rhône road trauma registry, which covers all road casualties which occurred in the “Département du Rhône (France)” (1.6M inhabitants), the study showed that among car belted occupants sustaining at least one serious injury (N=1219), 16% of the 74 rear passengers had abdomen injuries, which is more frequent than for drivers (7%) and for front passengers (10%) (Figure 1).

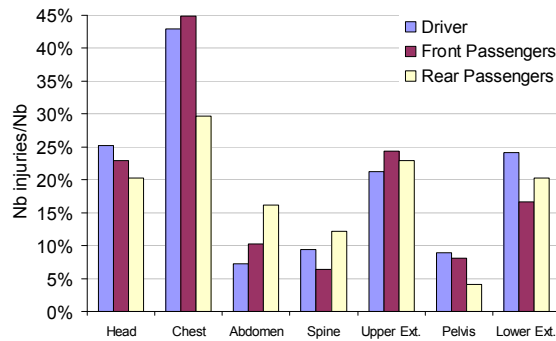


Figure 1. Car occupants with AIS 3+ injury (N=1219)(Martin et al., 2010).

Influence of impact direction and severity

Frontal impacts generally account for the highest numbers of AIS \geq 2 (AIS2+) and AIS \geq 3 (AIS3+) abdominal injuries. From NASS-CDS analysis, Klinich et al. (2010) estimated yearly 9000 front-row occupants with AIS2+ abdominal injuries due to front collisions whereas around 6000 were due to side collisions. However, the proportion of occupants with AIS2+ abdominal injuries increases substantially for near side crashes with a change in velocity (delta-V) greater than 32km/h (up to 40%), while for front

impacts, 27% of occupants sustain an AIS2+ abdominal injury for delta-V between 41 and 50km/h (Klinich et al., 2008, Figure 2).

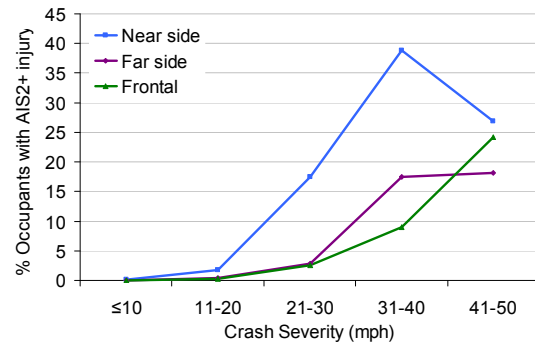


Figure 2. Risk of AIS2+ abdomen injury by delta-V and impact direction (Klinich et al., 2008).

Injury sources and types

Steering wheel was reported as the first injury source of AIS3+ abdominal injuries and represents 68% of this type of injuries. It was followed by seatbelt system (17%), interior parts (14%) and airbag (0.13%) (Elhagediab et al., 1998). More recently, Klinich et al. (2008, 2010) confirmed that airbag deployment in frontal impacts did not significantly affect the risk of abdominal injuries and was even slightly lower for belted occupants.

By looking at the injured abdominal organs with respect to car contact areas, steering wheel contacts result mainly in liver injuries (34% of all injured abdominal organs), followed by spleen injuries (14%), artery injuries (9%) and digestive organs injuries (6.5%). The seat belt was most often associated with injuries to the digestive system (almost 10%) (Figure 3).

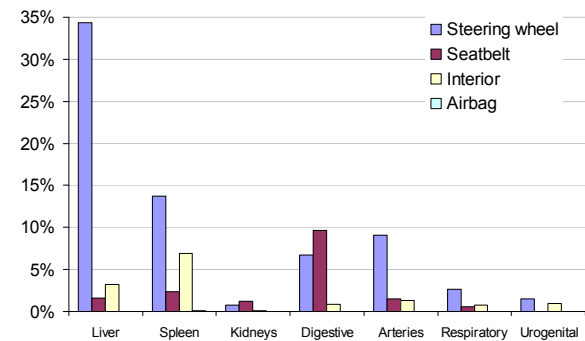


Figure 3. Contact object association with injured organs (N=38972) (Elhagediab et al., 1998).

Lamielle et al. (2006) divided abdominal organs into “solid” (e.g. liver, spleen, kidneys) and “hollow” (e.g. duodenum, jejunum, colon) categories and described different trends for each. It is important to note that

solid organs are partly protected by the rib cage and are part of what is called “upper abdomen”. Hollow organs are mainly between the rib cage and the pelvis bones in the forward plane and are part of what is called “lower abdomen”.

Table 2.

Hollow and solid organ injury frequency for belted and unbelted front occupants as a function of dashboard intrusion (Lamielle et al., 2006).

| Belted | ≤24cm | 25-45cm | >45cm |
|----------|-----------|----------|----------|
| Hollow | 138 (68%) | 17 (34%) | 6 (23%) |
| Solid | 66 (32%) | 33 (66%) | 20 (77%) |
| Unbelted | ≤24cm | 25-45cm | >45cm |
| Hollow | 17 (22%) | 9 (25%) | 8 (22%) |
| Solid | 61 (78%) | 27 (75%) | 29 (78%) |

Lamielle et al. (2006) noted that unbelted front occupants sustained solid organ injuries more often whereas belted ones suffer more from hollow organ injuries. Lamielle et al. (2006) also reported that in the case of lower intrusion (≤25cm), belted occupants suffered more from hollow organ injuries whereas unbelted ones suffer more from solid organ injuries. At higher intrusion, belted and unbelted occupants both sustain more solid organ injuries than hollow organ injuries (Table 2.).

Abdominal injuries and rib fractures

A significant link between the occurrence of abdominal injuries and rib fractures was observed by Klinich et al. (2008, 2010). The odds of sustaining a liver, spleen or kidney injury are respectively 9, 13 and 8 times higher with AIS 2+ rib fractures than without.

However, risk of sustaining abdominal organ injuries does not increase with occupant age whereas risk of rib fracture does. Klinich et al. (2010) hypothesised that “fractured ribs are not directly causing these types of abdominal injury... Rather, loading conditions likely to result in rib fracture are also likely to result in injury to these abdominal organs.” This analysis suggests that in crashes, abdominal organs are often loaded together with the rib cage and it is therefore unlikely to find abdominal injuries without rib fractures. However, rib fractures without abdominal injuries might be more frequent, especially for elderly, who are more subjected to sustain rib fractures even in low severity crashes.

Conclusions from the accident studies

Frontal impact accounts for the highest number of abdominal injuries due to the fact that frontal crashes

are the most frequent type of collision (Klinich et al., 2010).

Considering rear occupants, their risk to sustain an abdominal injury is higher than for front occupants. It is therefore important to assess such risk with a valid tool.

Accident field data revealed main issues regarding abdominal injuries and should be considered in ATD design:

- Even if a higher number of abdominal injuries are seen for frontal crashes, the risk of having abdominal injuries is higher in side impacts,
- Steering wheel contact for drivers and seat belt for front and rear passengers are coded as the main sources of abdominal injuries in frontal crashes. Airbag deployment was not found to increase injury risk,
- Solid organ injury occurrence correlates with steering wheel contact and to a lesser extent with seat belt and interior part contact, whereas hollow organ injuries are mostly linked with seat belt contact,
- Solid organ injuries are predominant, compared to hollow organ ones, for high intrusion whereas hollow organ ones are predominant, compared to solid organ ones, at low intrusion for belted occupants,
- Injury risk of organs such as liver, spleen and kidneys correlates with the risk of AIS2+ rib fractures. In a first approach, it seems suitable to assess upper abdomen injury risk together with thorax. In THOR-NT, the two multi-point 3D displacement measurement systems (CRUX) located on right and left sides of lower ribs seem suitable to assess such risk.

From these conclusions, it was decided to focus in our study on THOR-NT “lower” abdomen response and instrumentation.

EXISTING DUMMY ABDOMEN DESIGNS

Current frontal impact regulation does not consider the risk of abdominal injuries for car occupants, either children or adults. Side impact regulation includes an injury criterion for the Eurosid-2 dummy based on the maximum force applied to the abdomen block.

More recently, the need for abdomen injury estimation for children seated in a child restraint system (CRS) has been highlighted and several projects have been running for the ten last years on those topics (CREST, CHILD, CASPER in Europe, NASVA in Japan (Ono et al., 2005)). In European projects CREST, CHILD and CASPER, abdominal

sensors have been developed. A first one, designed by Ifsttar for Q-dummy series, is called Abdominal Pressure Twin Sensors (APTS) and consists of two bladders embedded in the abdomen foam. The APTS are filled with a gel-like material and equipped at one end with a pressure sensor (Johannsen et al., 2005) (Figure 4). The pressure measured by the APTS is expected to correlate well with the lap belt tension. The main advantages of these sensors were that they only require two channels and should be able to measure loads coming from different directions.

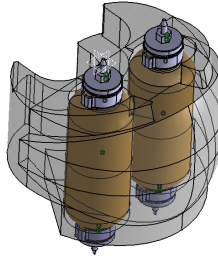


Figure 4. CAE model of Q3 abdomen equipped with Ifsttar-LBMC APTSs.

A second one was developed by Technical University of Berlin (Johannsen et al., 2005) and used Tekscan Flexiforce® sensors in an array of 20 sensors as depicted in Figure 5. The force map gave an overview of the load distribution but the total surface force was used as injury predictor as localised force could not be linked directly with Post Mortem Human Subjects (PMHS) measurements. However, the robustness of the sensor was judged to be not sufficient by Johannsen et al. (2007).

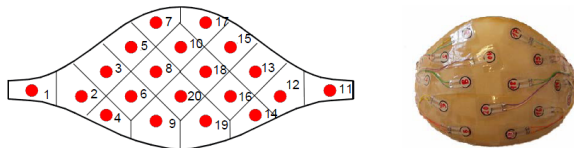


Figure 5. TUB child abdominal sensor (Johannsen et al., 2005).

A similar sensor concept was developed by the National Agency for Automotive Safety and Victims' Aid (NASVA) to be used in the Japanese CRS assessment program (Figure 6). The sensor used is an electric pressure sensor (Tekscan) which was applied to the dummy abdomen surface (Ono et al., 2005). One of the findings of the study is that measurement of abdominal compression discriminates various types of CRS.



Figure 6. Tekscan pressure map installed on the HIII 3 years old (Ono et al., 2005).

As for adult dummies, UMTRI and FTSS developed a special abdomen to simulate a 30-week pregnant woman dummy (Figure 7) and to assess possible damage to the mother's abdomen in crashes (Rupp et al., 2001). The MAMA-2B abdomen was instrumented with an anterior pressure sensor. A power-law relationship was defined to estimate the risk of adverse fetal outcome versus the anterior pressure.

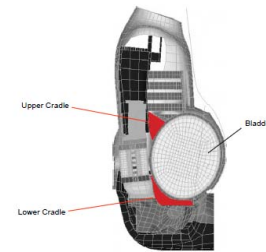


Figure 7. Side view of FEM of HIII pregnant dummy. The abdomen is represented by a urethane bladder attached by an upper and lower cradle (Rupp et al., 2001).

For the adult car occupants involved in a frontal collision, the submarining effect was identified thirty years ago (Leung et al., 1982) as the main cause of abdominal injuries. Its detection using load sensors placed on the pelvis iliac crests and the relationship between iliac crest loads and abdomen injuries were first looked at. The main drawbacks of this method were the loss of the load measurement once the lap belt slipped above the transducers and the inability to evaluate injury risk to the abdomen caused by sources other than the lap belt (shoulder belt, armrest, steering wheel...).

Similarly, JNCAP has introduced since 2009 on Hybrid III 5th percentile an "ON-OFF" rating based on the location of the lap belt during the crash: on the pelvis bones or not (Ikari et al., 2009).



Figure 8. Front view of liquid silicone rubber abdomen insert (Rouhana et al., 2001).

New abdomen design was considered for the Hybrid III 50th percentile, called Re-usable Rate Sensitive Abdomen (Rouhana et al., 2001). It consists of a bladder made from liquid silicone rubber filled with silicone gel (Figure 8) allowing the record of 3D deflection at 6 different locations on the abdomen surface through six anodes and a cathode. Recent improvements have been undertaken regarding the instrumentation (Elhagediab et al, 2010).

Finally, it exists two versions of the THOR dummy abdomen and its instrumentation, for NT and FT versions; they are presented later in this paper. In addition, a prototype has been developed by GESAC and Toyota Motor Corporation, also presented in this paper.

Other developments using THOR-NT abdomen were found for railway applications (Parent et al., 2005).

DESIGN RECOMMENDATIONS

From previous literature review, main requirements for a new THOR abdomen were listed as below:

- Match UMTRI 50th percentile anthropometry
- Reproducibility, repeatability
- Remain in position
- No major modification to the dummy design
- No effect on dummy posture, global kinematics

Abdomen response:

- Biofidelity according to impactor and seat belt tests (Cavanaugh, Hardy, Foster's PMHS corridors) as these two kinds of loading were predominant from the accident field data

Abdomen instrumentation:

- Continuous measurement
- Omni-directional
- Linear sensitivity
- Detect all loads applied to the abdomen
- Discriminate submarining
- Low sensitivity to deceleration and torso flexion
- No time lagging
- Simple calibration and use
- Reliability and robustness
- Abdomen biofidelity stable along time (e.g. for fluid filled concepts)

This partly meets the recommendations from EEVC WG12 in 2006, which notably included as well the fact that if 3D abdominal measure was desirable, the current instrumentation was not adapted due to frequent damage reported after tests. EEVC also recommended to unify upper and lower abdomens. This modification was as well foreseen for the long-term by SAE THOR Committee.

EVALUATION OF BIOFIDELITY OF DIFFERENT THOR ABDOMENS

Impactor and static seat belt tests were conducted on three different abdominal inserts compatible with current THOR-NT dummy:

- the standard instrumented THOR-NT abdomen
- a uninstrumented version of the THOR-FT abdomen inserted in THOR-NT's abdominal Cordura bag
- a uninstrumented prototype developed by GESAC

Material and Method

Impactor tests



Figure 9. Rigid-bar impact test set-up

Impactor tests reproduced those initially developed by Cavanaugh et al. (1986) where 12 PMHS were impacted at various velocities (4.87 to 13.01m/s) with a rigid-bar weighting 32 or 64kg. This kind of testing was also reproduced by Hardy et al. (2001) on 11 PMHS (free or fixed back) and Rouhana et al. (2001) to evaluate a prototype abdominal insert for Hybrid III dummy. This test procedure is now used as the certification test for the lower abdomen of THOR dummy. Yaguchi et al. (2007) evaluated THOR abdomen biofidelity under this kind of loading. Moorhouse et al. (2007) evaluated this procedure for the certification of the THOR dummy.

In the test conducted at Ifsttar, a 32 kg guided impactor equipped with a rigid bar (300mm long, 25mm diameter) impacting face was used. The rigid bar contacted the dummy at the level of L3 (Figure 9). The spine of the free-back dummy was adjusted in a slouched position. The dummy was wearing its jacket with straight legs on a Teflon sheet and its hands upon the head. It was loosely retained to avoid any

fall following impact. Impactor was equipped a uniaxial 100g accelerometer and a light gate for direct measurement of velocity at impact. The pelvis of the THOR was equipped with 3 uniaxial accelerometers to measure its backward displacement during test. All sensors recorded data at 10kHz. Three high speed cameras (1000fps) recorded the test. Two impact velocities, $3.0 \pm 0.1 \text{ m/s}$ and $6.1 \pm 0.1 \text{ m/s}$ were tested. Targets were placed on the ATD lower spine or pelvis block (target 2 on Figure 9), the rigid-bar impactor (target 1 on Figure 9) and on dummy pelvis foam.

Seatbelt loading tests

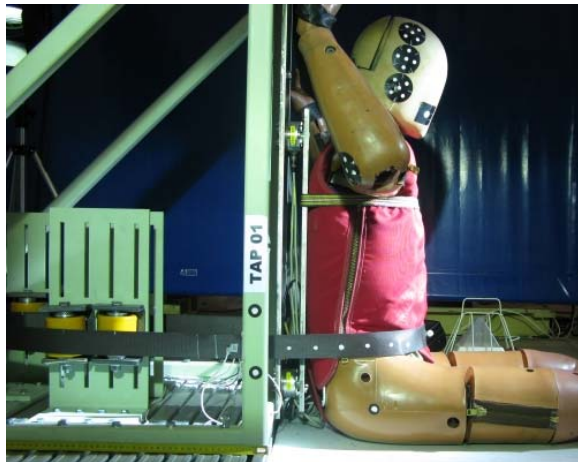


Figure 10. Side view of the pretensioner test set-up

Several studies in the last decade focused on abdominal seatbelt loading. In PMHS tests, the belt was wrapped around the abdomen and pulled backwards in a symmetrical way. Most of time, these loads tried to maximize seatbelt/abdomen interaction. Hardy et al (2001) used a ram to pull the belt placed on PMHS abdomens. A peak velocity of 3m/s and a sine curve shape were applied. 26 to 37% abdominal compression was recorded. Rouhana et al. (2001) used the same device to evaluate its silicone abdomen prototype for Hybrid III dummy. Trosseille et al. (2002) applied abdominal seatbelt loading on PMHS through one or two pretensioners. Velocity peaks of 8 to 12 m/s and compression between 25 to 32% were recorded. Steffan et al. (2002) loaded PMHS abdomen at 6m/s with a pretensioner system linked to a seatbelt cinching mechanism. Peak load between 2.9 and 7.1kN and pull-in distances from 104 to 200mm were observed. Foster et al. (2006a) performed PMHS abdomen seatbelt loadings through the help of single or dual systems of pretensioners. Velocity peaks of 4 to 13m/s and compression between 25 and 55% were recorded. Lamielle et al.

(2008) used either a ram or pretensioners and obtained velocity peaks from 4 to 5m/s (compression from 28 to 40%) and 5 to 6 m/s (compression 27 to 31%) respectively.

Seatbelt loading tests conducted in this study reproduced conditions from Foster et al. (2006a). Same pretensioners as in Foster's study were used, ensuring the reproducibility of input for the tests and allowing later comparison of the results. For this test, a specific structure was manufactured and attached to a working plan. The THOR dummy wore only its jacket and was seated on a Teflon sheet with its back resting on the structure. Legs were straight and arms were attached above elbows. Straps maintained the dummy against the backseat (Figure 10). The seat belt was wrapped around the lower abdomen at mid-abdomen height, attached on itself and guided in the back of the dummy to the retractor/pretensioner by a series of pulleys. The seatbelt was equipped on each side with a 16kN force cell and a 500g accelerometer. The seatback of the dummy was equipped with 4 250daN load cells. A laser (900mm range, 100 μm resolution) measured the backward displacement of the seatbelt and a light-gate returned a live (rough) estimation of the seatbelt retraction velocity. All sensors recorded at 20kHz. Three high-speed cameras (1000 and 2000fps) recorded the test.

Two kinds of pretensioner were used, corresponding to Foster's "B" and "C" systems. Targets were positioned on the ATD, every 50mm on seatbelt and on fixed reference points for the video motion analysis. An additional spherical target on the most prominent point of the umbilic was used for the measurement of the penetration.

THOR-NT abdomen

The THOR-NT lower abdomen is attached to the lumbar spine of the THOR dummy. It is composed of two foam layers enclosed in a Cordura nylon bag. Two DGSPs (Double Gimbal String Potentiometer) go through both foam layers from back of the insert to front cover of the bag. These devices record variation of angle in two dimensions as well as compression through two telescopic columns to derive deflection in 3D on the two points of DGSP attachments. Deflection of the abdomen is the mean of the two DGSPs records. Its total weight is 2.62kg.

Modified THOR-FT abdomen

The THOR-FT is an alternative version of THOR-NT. Based on former THOR- α , this dummy was developed in the frame of FID project. Its abdominal insert consists in a single foam block with a vinyl skin layer equipped with 2 IR-TRACCs (InfraRed

Telescoping Rod for Assessment of Chest Compression) measuring deflection and angle variation through an optical measurement. Similarly to DGSP, 3D motion of the IR-TRACC attachment points is derived. A uninstrumented, modified version of the abdomen was manufactured on demand by FTSS for the needs of this study, without sensors nor associated holes.

A specific setup was designed to attach the modified abdomen in its usual position. The virgin foam block was inserted in THOR-NT's Cordura bag (Part #T1LAF100) and fixed to the lumbar spine by using THOR-NT's spinal mounting elements and a simplified version of Internal Mounting Welded Assembly (Part #T1LAW081) in the back of the Cordura bag. The total mass was 2.30kg. The effect of the bag fabric layer in addition to the insert was considered as non-significant under dynamic loadings on the biomechanical response of the abdomen.

GESAC prototype abdomen

The GESAC abdominal insert is a 3.62kg prototype developed at the end of the 2000s by GESAC in partnership with Toyota Motor Corporation. It consists of a urethane core (shore hardness 35A) enclosed in a 20mm-thick skinned urethane shell in which three Cerobase™ weights are also moulded. GESAC abdomen is attached to the lumbar spine by using the same attach points as the THOR-NT insert. The abdomen is designed to include a pair of curvature sensors in its outer shell enabling the reconstruction of its deformation under impact and calculation of the abdominal compression. However, no instrumentation was available for these tests.

Post-Treatment

In rigid-bar loading tests, time “zero” corresponded to the first contact between impactor and abdomen. Penetration was obtained through video analysis by subtracting the backward movement of ATD's pelvis to impactor deflection. Force was obtained by the product of the deceleration of the impactor and the mass of the impactor - 32kg. All sensors data were filtered using CFC180. Data were then compared to biofidelity corridors or targets defined by Hardy et al. (2001) for each considered velocity, 3.0 and 6.1m/s.

For pretensioner tests, time “zero” corresponded to the firing of the retractor/pretensioner mechanism. Video analysis data were CFC1000 filtered and penetration was obtained through target tracking by

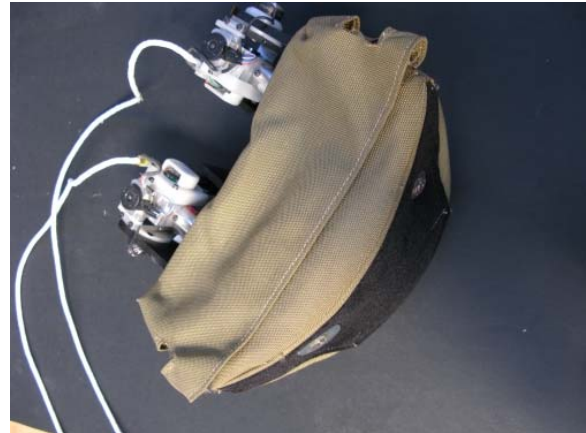


Figure 11. Top view of the THOR-NT lower abdomen insert prior to assembly on the dummy



Figure 12. Modified THOR-FT abdominal insert prior to assembly on the dummy



Figure 13. General view of the GESAC abdominal insert prior to assembly on the dummy

subtracting the backward movement of ATD's pelvis (even if limited) from the seatbelt displacement at the umbilic, followed by a CFC1000 filtering. All sensors data were filtered using CFC600. Data obtained with Foster's "B" system were compared to the biofidelity corridor developed by Foster for this particular configuration. Data obtained with Foster's "C" system were compared to PMHS scaled responses obtained by Foster. No scaling was performed in this study as Foster chose Eppinger's method (Eppinger, 1976) for scaling with a reference mass of 78.2kg, which is very similar to THOR-NT mass.

RESULTS

Rigid-bar impacts

Test matrix for impactor tests is presented in Table 3. Figure 14 presents the response of the three inserts at 3.0m/s overlaid with the biofidelity trend curve defined by Hardy et al. (2001). THOR-NT abdomen exhibits an exponential shape, close to biofidelity trend curve up to 40mm penetration. It then diverges until final penetration of 100mm for a 3kN force. THOR-FT follows a very similar loading path for a final force of 2.5kN but an equivalent penetration. GESAC abdomen presents a mostly linear slope of approximately 60kN/m (six times the slope defined in Hardy's study).

Figure 15 presents the response of the three inserts at 6.1m/s compared with the biofidelity corridor defined by Hardy et al. (2001). Corridors available in Rouhana et al. (2001) and Cavanaugh et al. (1986) are very similar. THOR-NT and THOR-FT inserts remain within corridor for approximately 80mm. A peak appears for THOR-FT around 80mm penetration, followed by a gap at 100mm. This phenomenon was observed on both tests performed at this velocity on this abdomen. Video analysis associates it with a contact between the rigid-bar impactor and the skin above pelvis iliac crests. The GESAC abdomen presented a much stiffer response, with an average slope of 100kN/m - approximately three times higher than the upper boundary of the considered biofidelity corridor.

The loading parts of THOR-NT and FT abdomen force-penetration curve are comparable. Response of THOR-FT abdomen could be improved by avoiding the contact between pelvis skin and the rigid bar (no peak at 80mm penetration), but the effect of removing the IR-TRACCs cannot be seen from our tests. The GESAC insert is stiffer than the upper limit of biofidelity corridors (Figure 14 and Figure 15).

Table 3.
Test matrix for rigid-bar impact tests on dummy abdomen

| Test | THOR NT | GESAC | THOR FT | Velocity (m/s) |
|------|---------|-------|---------|----------------|
| 01 | X | | | 3.03 |
| 03 | X | | | 2.75 |
| 04 | X | | | 6.16 |
| 05 | X | | | 6.15 |
| 06 | X | | | 3.02 |
| 09 | | X | | 3.00 |
| 10 | | X | | 3.01 |
| 11 | | X | | 6.10 |
| 12 | | X | | 6.12 |
| 13 | | X | | 6.11 |
| 14 | | X | | 3.02 |
| 16 | | | X | 3.04 |
| 17 | | | X | 3.01 |
| 18 | | | X | 6.20 |
| 19 | | | X | 6.16 |

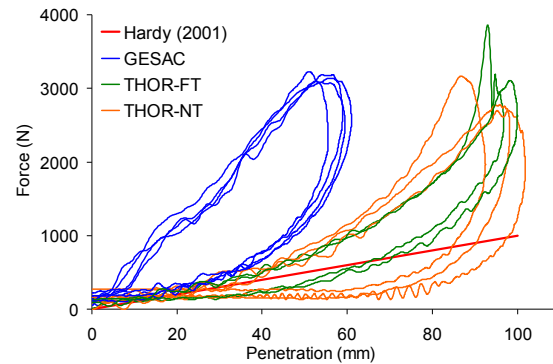


Figure 14. Force-penetration curves of the three inserts at 3.0m/s compared to Hardy et al. (2001)

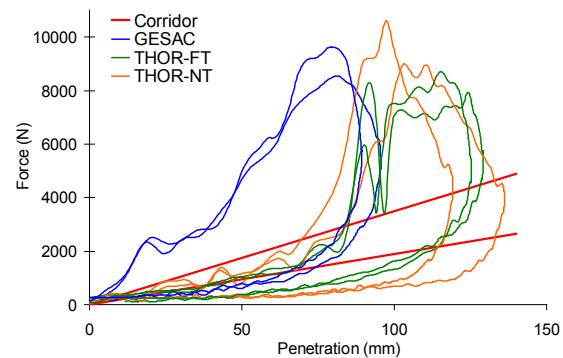


Figure 15. Force-penetration curves of the three inserts at 6.1m/s compared to biofidelity corridors by Hardy et al. (2001)

Seatbelt loading tests

Test matrix for seatbelt loading tests is presented in Table 4.

Figure 16 presents the results obtained with the three inserts using C-system ('lower velocity') pretensioner. Both PMHS curves, extracted from Foster's study, present a significant initial peak which is not visible in the tests performed on THOR. Both NT and FT inserts show a similar initial slope followed by a plateau below 1kN and a mean maximal penetration of 30mm. Tests on GESAC abdomen displayed a very different response, with a quasi-linear behaviour and a reduced penetration.

Figure 17 presents the results obtained with the three inserts using B-system ('higher velocity') pretensioner compared to associated biofidelity corridor defined in Foster's study. Both NT and FT abdomens display once again a similar response including an initial rise up to approximately 1kN followed by a linear and constant increase. However, the instrumented NT abdomen reached a slightly higher penetration than the uninstrumented FT insert with 110mm against 95mm. Response of both inserts mostly remains out of the corridor. GESAC abdomen presents an initial higher slope, and reaches a maximal penetration of 50mm and a maximal load of 5kN. If the initial expected peak is still missing, its response is mostly within corridor boundaries.

DISCUSSION

The present study underscores the limited biofidelity of THOR abdominal response.

For rigid-bar impacts, the manikin response was the most biofidelic under the 6.1m/s loading, which was used as a design guideline for both THOR-NT and THOR-FT inserts. However, their observed limited biofidelity performances above 80mm compression, were also reported during the development of THOR-FT (FID, 2003) and by Yaguchi et al. (2007) for THOR-NT. The same author remarked as well that the abdomen of this ATD was softer than the standard Hybrid III abdominal insert (Yaguchi et al., 2008). Tested under the same conditions, Rouhana's HIII silicone abdomen, exhibited a more human-like response (Rouhana et al., 2001).

No ATD were evaluated to our knowledge under 3m/s, 32kg rigid-bar impacts. The limited amount of PMHS data for this configuration tested by Hardy et al. (2001) should lead to a careful analysis of associated ATD biofidelity results.

Table 4.
Test matrix for seatbelt loading tests on dummy abdomen

| Nr | THOR NT | GESAC | THOR FT | Foster's system | Retraction Velocity (m/s) |
|----|---------|-------|---------|-----------------|---------------------------|
| 02 | X | | | B | 12.3 |
| 03 | X | | | B | 14.5 |
| 04 | X | | | C | 5.0 |
| 05 | X | | | C | 5.0 |
| 06 | | X | | C | 4.75 |
| 07 | | X | | C | 4.0 |
| 08 | | X | | B | 8.0 |
| 09 | | X | | B | 7.2 |
| 10 | | | X | C | 5.7 |
| 11 | | | X | C | 5.1 |
| 12 | | | X | B | 8.7 |
| 13 | | | X | B | 9.0 |

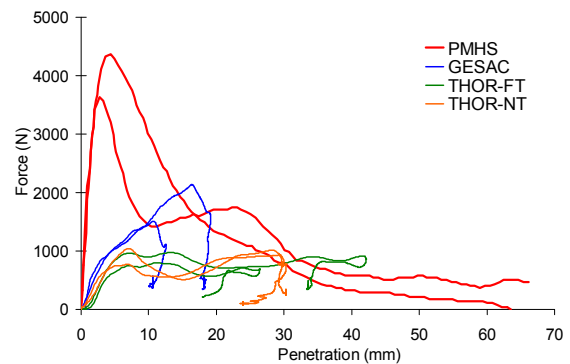


Figure 16. Force-penetration curves of the three inserts with C-system compared to PMHS curves (Foster, 2006b)

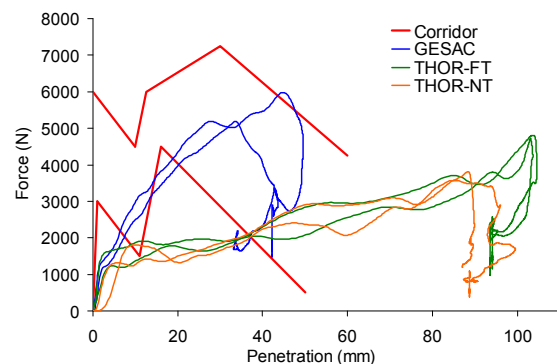


Figure 17. Force-penetration curves of the three inserts with B-system compared to PMHS corridor (Foster et al., 2006a)

It is difficult to compare results of existing studies involving 6.1m/s rigid-bar impacts. This paper focuses on biofidelity using the penetration calculated from external measurement; and two of the three evaluated inserts were not instrumented. Onda et al. (2006) compared the response of internal measurement (DGSP or IR-TRACCs) of NT and FT inserts to the certification requirements. Moorhouse et al. (2007) demonstrated that external and internal measurements were significantly different and could cause a 20 to 30mm difference in terms of penetration. Hence, any comparison between studies focusing on certification procedure and biofidelity requirements should be done with caution as first ones consider dummy internal measurements and the second ones consider external measurements. Figure 20 presents certification and biofidelity corridors. Similar responses of NT and FT concepts were observed in this study, confirming results by Onda et al. (2006). The same design targets of both inserts is a reasonable explanation for this observation.

Submitted to pretensioner seatbelt loading, both THOR-NT and THOR-FT behaviour differ greatly from biofidelity corridors. The tested GESAC prototype response was observed to be not biofidelic at low speed (Figure 18), but proved to have a more human-like response under high-velocity seatbelt loading, despite its absence of initial force peak (Figure 19). However, in absence of other published work on this abdomen, these conclusions are only based on the present study.

Responses under B-system and C-system seatbelt loading conditions for THOR- α and Rouhana's silicone abdomen (Foster, 2006b) were compared to the results of the present study in Figure 18 and Figure 19. THOR-NT and uninstrumented THOR-FT abdomens do not match biofidelity targets. They both present a good repeatability (Figure 17) but are particularly soft at low penetrations. They notably differ in response from THOR- α despite the fact that THOR-NT has a similar abdominal conception. No satisfactory explanation was found for this difference. In the meanwhile, THOR- α response is quite close to GESAC prototype under high-speed loadings and is very different at low speed.

Another aspect to be mentioned is the lack of human-like initial peak in the force response of abdomens submitted to seatbelt loading, with the exception of Rouhana's Hybrid III silicone concept. The post-treatment of the data in this study showed the high influence of force and penetration time alignment on the shape of the curve and its initial peak: a special care has to be given when creating such curves.

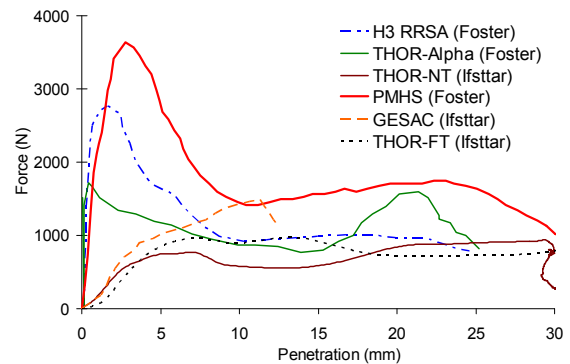


Figure 18. Compared response of various ATDs under Foster's C-system seatbelt loading (Foster, 2006b)

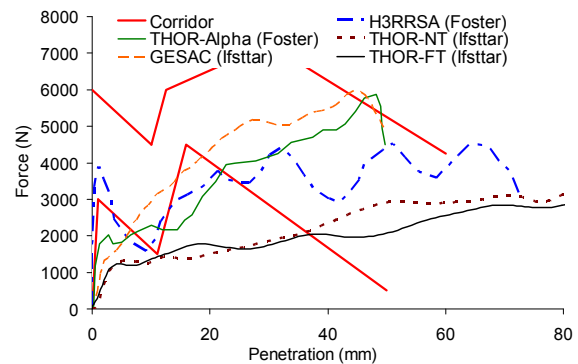


Figure 19. Compared response of various ATDs under Foster's B-system seatbelt loading (Foster et al., 2006a)

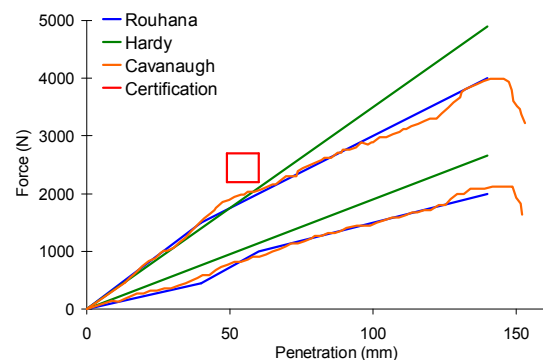


Figure 20. Certification requirements of THOR-NT's lower abdomen and biofidelity corridors available in literature for 6.1m/s, 32kg, rigid-bar impact on the abdomen

Currently, no currently existing THOR abdominal insert provides a human-like load-penetration response under both rigid bar and seat belt loadings.

CONCLUSION

The review of accident studies showed the need to further develop dummies to better evaluate the risk of sustaining abdominal injuries, especially for rear seat occupants.

The regulatory frontal impact dummy HIII does not have this capacity. During the last decade, THOR dummy was developed with instrumented lower and upper abdomens but with no associated tolerance limit. In addition, its response was mainly tuned under 6.1m/s rigid-bar impacts.

Human abdomen response was characterised by different authors under rigid bar or steering wheel impacts and seat belt loadings and was shown as rate-sensitive, different from THOR dummy abdomens tested in the current study. Silicone abdomen developed by Rouhana et al. (2001) for Hybrid III was found to have an improved biofidelity, but as for THOR dummy, improvements are needed to obtain a more human-like abdominal response so that it can better predict abdominal injuries in car crashes. Various instrumentation and design solutions were considered on different dummies. However, the challenge would also be the definition of a suitable injury criterion.

ACKNOWLEDGEMENTS

The authors would like to sincerely thank Pr. Koshiro Ono (JARI), Bruce Donnelly, Edward Probst (VRTC) for their information and advices while conducting THOR abdomen experiments; and to Craig D. Foster for kindly sharing his results.

The authors would also like to express their appreciation to UNEX staff for its support during the experiments.

REFERENCES

- Child Advanced Safety Project (CASPER), FP7 EC project, Contract No 218564, 2009-2012.
- Cavanaugh J. M., Nyquist GW., Goldberg S. J., King A. I., 1986, Lower Abdominal Tolerance and Response. *Stapp Car Crash Journal*, Vol. 30, p. 41.
- Child Injury Led Design (CHILD), EC project, Contract No G3RD-CT-2002-00791, 2002-2006.
- Child Restraint System for Cars (CREST), EC project, Contract No SMT4-CT95-2019, 1996-2000.
- EEVC, Working Group 12, EEVC Recommendations on the Future of the Harmonised THOR Dummy: Report on the outcome of the Special Workshop on “Harmonisation of THOR – The Advanced Frontal Dummy”, held 4-5 May 2006 at TRL, UK.
- Elhagediab A. M., Rouhana S. W., 1998, Patterns of abdominal injury in frontal automotive crashes. 16th International Technical Conference on the Enhanced Safety of Vehicles, Windsor, Ontario, Canada, No 98-S1-W-26, US Department of Transportation, NHTSA Administration.
- Elhagediab A. M., Hardy W. N., Rouhana S. W., 2010, Development of Three-Dimensional Abdominal Displacement Measurement System for the Frontal Crash Anthropometric Test Device. Sixth World Congress of Biomechanics, Singapore. WCB-A01270-02270.
- Eppinger, R. H., 1976, Prediction of thoracic injury using measurable experimental parameters. 6th International Technical Conference on Experimental Safety Vehicles, Washington DC, US Department of Transportation, NHTSA Administration.
- FID Partners, 2003, Final Publishable Report. European Project GRD1-1999-10559, Contract 1999-RD.10559.
- Foster C. D., Hardy W. N., Yang K. H., King A. I., 2006a, High-Speed Seatbelt Pretensioner Loading of the abdomen. *Stapp Car Crash Journal*, Vol. 50, p. 22.
- Foster C. D., 2006b, Response of the Human Cadaver Abdomen to High-Speed Seatbelt Pretensioner Loading. Thesis Manuscript, Wayne State University.
- Hardy W. N., Schneider L. W., Rouhana S. W., 2001, Abdominal impact response to rigid-bar, seat belt, and airbag loading. *Stapp Car Crash Journal*, Vol. 45, p. 1.

- Ikari T., Kawahara H., 2009, Rear Occupant Protection JNCAP Test. 21st International Technical Conference on the Enhanced Safety of Vehicles, Stuttgart, Germany, No 09-0299, US Department of Transportation, NHTSA Administration.
- Johannsen H., Alonzo F., Goubel C., Schindler V., 2005, Abdominal injuries, injury criteria, injury severity levels and abdominal sensors for child dummies of the Q family. Proceedings of IRCOBI Conference 2005, p. 201.
- Johannsen H., Schindler V., 2007, Development and assessment of a surface force abdominal sensor. 20th International Technical Conference on the Enhanced Safety of Vehicles, Lyon, France, No 07-0365, US Department of Transportation, NHTSA Administration.
- Klinich K. D., Flanagan C. A. C., Nicolson K., Schneider L. W., Rupp J. D., 2008, Abdominal injury in motor-vehicle crashes. UMTRI Report No UMTRI-2008-40.
- Klinich K. D., Flanagan C. A. C., Nicolson K., Schneider L. W., Rupp J. D., 2010, Factors Associated with Abdominal Injury in Frontal, Farside, and Nearside Crashes. Stapp Car Crash Journal, Vol. 54, p. 73.
- Lamielle S., Cuny S., Foret-Bruno JY., Petit P., Vezin P., Verriest JP., Guillemot H., 2006, Abdominal injury patterns in real frontal crashes: influence of crash conditions, occupant seat and restraint systems. 50th Annual Proceedings of Association for the Advancement of Automotive Medicine. October 16-18, 2006, p. 109.
- Lamielle S., Vezin P., Verriest J-P., Petit P., Trosseille X., Vallancien G., 2008, 3D Deformation and Dynamics of the Human Cadaver Abdomen under Seatbelt Loading. Stapp Car Crash Journal, Vol. 52, p. 267.
- Leung Y. C., Tarrière C., Lestrelin D., Got C., Guillon F., Patel A., Hureau J., 1982, Submarining Injuries of 3 Pt. Belted Occupants in Frontal Collisions – Description, Mechanisms and Protection. Stapp Car Crash Journal, Vol. 26, p. 173.
- Martin J-L., Lardy A., Compigne S., 2010, Specificities of rear occupant protection: Analysis of french accident data. Proceedings of IRCOBI Conference 2010, p. 315.
- Moorhouse K. M., Probst E. P., 2007, A repeatability Assessment of the THOR-NT ATD Response and an Evaluation of the Certification Procedures. NHTSA VRTC Report, May 2007.
- Onda K., Matsuoka F., Ono K., Kubota M., Peter M., Youmei Z., 2006, Differences in the Dynamic Responses of the Thor-NT and Thor-FT Dummies. SAE paper No 2006-01-0676, Society of Automotive Engineers.
- Ono Y., Komiyama Y., Takatori O., 2005, Method of evaluating abdominal injury in Japan's child-restraint-system assessment program. 19th International Technical Conference on the Enhanced Safety of Vehicles, Washington D.C., No 05-0292, US Department of Transportation, NHTSA Administration.
- Parent D., Tyrell D., Perlman B., Matthews, P., 2005, Evaluating Abdominal Injury in Impacts with Workstation Tables. Transportation Research Record: Journal of the Transportation Research Board, No. 1908, Transportation Research Board of the National Academies, Washington D.C., 2005, p. 205.
- Rouhana S. W., Elhagediab A. M., Walbridge A., Hardy W. N., Schneider L. W., 2001, Development of a Reusable, Rate-Sensitive Abdomen for the Hybrid III Family of Dummies. Stapp Car Crash Journal, Vol. 45, p. 375.
- Rupp J. D., Schneider L. W., Klinich K. D., Moss S., Zhou J., Perlman M. D., 2001, Design, development and testing of a new pregnant abdomen for the HIII small female crash test dummy. UMTRI final report UMTRI-2001-07.
- Steffan, H., Hofinger, M., Parenteau C., Shah M., Webber J., Darok M., Leinzinger P., 2002, Abdominal responses to dynamically lap belt loading. Proceedings of IRCOBI Conference 2002, p. 315.

THOR Certification Manual, 2005, GESAC Report No GESAC-05-04, Revision 2005.02.

Trosseille X., Le-Coz J-Y., Potier P., Lassau J-P., 2002, Abdominal Response to High-Speed Seatbelt Loading. Stapp Car Crash Journal, Vol. 46, p. 71.

Yaguchi M., Ono K., Masuda M., 2007, Evaluation of biofidelity and repeatability and the influence of different positioning for THOR-NT dummy. 20th International Technical Conference on the Enhanced Safety of Vehicles, Lyon, France, No 07-0286, US Department of Transportation, NHTSA Administration.

Yaguchi M., Ono K., Masuda M., 2008, Biofidelic Responses of the THOR-NT and Hybrid III Based on Component Tests. SAE paper No 2008-01-0520, Society of Automotive Engineers.